

*Proceedings of the*  
*14<sup>th</sup> International Conference on*  
**Management and Innovative  
Technologies**

***MIT 2016***

*Fiesa, Slovenia*  
*5<sup>th</sup> – 7<sup>th</sup> September 2016*

Golden sponsor



Silver sponsors



Razvojni center orojarstva Slovenije

*Proceedings of the*  
*14<sup>th</sup> International Conference on*  
**Management and Innovative  
Technologies**

***MIT 2016***

*Fiesa, Slovenia*  
*5<sup>th</sup> – 7<sup>th</sup> September 2016*

*Editors:*

Joško Valentinčič  
Paul R. Levy  
Izidor Sabotin

Title: Proceedings of the 14th International Conference on Management and Innovative Technologies, MIT 2016

Editors: **Joško Valentinčič**, University of Ljubljana, Slovenia  
**Paul R. Levy**, University of Brighton, UK  
**Izidor Sabotin**, University of Ljubljana, Slovenia

Programme committee: **J. Valentinčič, I. Sabotin**, University of Ljubljana, Slovenia.

Organizers: **Laboratory for Alternative Technologies**, Uni. of Ljubljana, Slovenia  
**Centre for Research in Innovation Management**, Uni. of Brighton, UK

Sponsors: **BFT**, Austria  
**BSH**, Slovenia  
**TECOS**, Slovenia

Design: **J. Valentinčič, I. Sabotin, M. Jerman**, University of Ljubljana, Slovenia.

Publishers: **LAT** - Laboratory for Alternative Technologies, Faculty of Mechanical Engineering, University of Ljubljana, Slovenia.

Note: This is an electronic version of the conference proceedings published only in digital form (PDF format) and can be accessed over specified URLs:  
<http://mitconference.wordpress.com/>  
<http://lab.fs.uni-lj.si/lat/index.php?page=domov&hl=eng>

CIP - Kataložni zapis o publikaciji, Narodna in univerzitetna knjižnica, Ljubljana

005:001.895(082)(0.034.2)

621:502.131.1(082)(0.034.2)

INTERNATIONAL Conference on Management and Innovative Technologies (14 ; 2016 ; Piran)

MIT 2016 [Elektronski vir] : proceedings of the 14th International Conference on Management and Innovative Technologies, Fiesa, Slovenia, 5th-7th September 2016 / [organizers Laboratory for Alternative Technologies, Uni. of Ljubljana, Slovenia [and] Centre for Research in Innovation Management, Uni. of Brighton, UK] ; editors Joško Valentinčič, Paul R. Levy, Izidor Sabotin. - El. knjiga. - Ljubljana : LAT - Laboratory for Alternative Technologies, Faculty of Mechanical Engineering, 2016

ISBN 978-961-6980-17-3 (pdf)

1. Gl. stv. nasl. 2. Valentinčič, Joško 3. Fakulteta za strojništvo (Ljubljana). Laboratorij za alternativne tehnologije 4. Centre for Research in Innovation Management (Brighton)

286562816



*The Editors and the Conference Committee believe that the subject of the papers to be presented are in line with the objectives of the conference, but it is not responsible for any data or any other information dispensed in the Proceedings.*

*All papers have been peer reviewed by the members of Scientific Committee.*

## *Preface*

The MIT Conference first began life in 1995. Since then we have been a bi-annual international gathering of industrial practitioners and academics from different disciplines and from all over the world.

The conference based in Slovenia has brought together a unique dialogue in the fields of management and innovative technologies.

Previous MIT conferences have seen world economic boom and subsequent collapse. Our conferences have explored technological innovation and technology management from multi-disciplinary perspectives. That has been the unique contribution of our previous thirteen conferences – bringing together academics and practitioners from different fields to exchange ideas, knowledge and experience that can impact significantly on cross-disciplinary research and also stimulate innovation in practice.

Human factors, “technosophy” (the wise application of technology) and sustainability have been key areas of interest for many of the conference’s contributors and now, as we announce our call for contributions to the 14th MIT Conference in 2016, in a year of continuing but recovery from global recession, financial and environmental challenges, our conference seems as relevant and important as ever.

In the beautiful setting of Fiesa, Slovenia, bordering with Croatia and Italy and within driving distance of many other countries, we are glad our conference sits as the borderland of different cultures, just as our programme sits at the border of different disciplines, interests and perspectives.

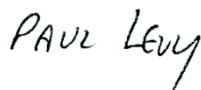
For the second time in a row our conference takes the form of a more interactive conference workshop. Based on feedback from participants who value the presentation of academic work but also seek further interaction around practical themes arising, our conference workshop is designed around dialogue and interaction, still very much rooted in academic research and industrial practice. It is a very compelling and potent mix!

It is our hope that the conference will generate insights that will directly contribute to our emerge from economic crisis, in our respective sectors, industries, economies and as a world community. We welcome case studies and stories, as well as sessions which may lead to inter-disciplinary research.

Joško Valentinčič



Paul R. Levy



Izidor Sabotin





## **International Scientific Committee:**

### **Chairman:**

Valentinčič J., University of Ljubljana, Slovenia

Levy P. R., University of Brighton, UK

### **Academic Members:**

Annoni M., Politecnico di Milano, Italy

Butala P., University of Ljubljana, Slovenia

Carutasu G., Romanian-American University, Romania

Cotet E.C., University Politehnica of Bucharest, Romania

Foldyna J., Institute of Geonics, Czech Republic

Hadar A., University Politehnica of Bucharest, Romania

Herakovič N., University of Ljubljana, Slovenia

Hloch S., Technical University Košice, Slovakia

Jerman M., University of Ljubljana, Slovenia

Kramar D., University of Ljubljana, Slovenia

Lampič G., Elaphe Ltd., Slovenia

Lebar A., University of Ljubljana, Slovenia

Mitrouchev P., University of Grenoble Alpes, France

Museau M., University of Grenoble Alpes, France

Orbanič H., BSH Ltd. Nazarje, Slovenia

Popescu D., University Politehnica of Bucharest, Romania

Pude F., Inspire, ETH Zurich, Switzerland

Sabotin I., University of Ljubljana, Slovenia

Schmid M., Inspire, ETH Zurich, Switzerland

Trieb F., BFT Ltd., Austria

Vrabič R., University of Ljubljana, Slovenia

Zaremba D., University of Hannover, Germany

### **Organizing committee:**

Valentinčič J., University of Ljubljana, Slovenia

Lebar A., University of Ljubljana, Slovenia

Sabotin I., University of Ljubljana, Slovenia

Jerman M., University of Ljubljana, Slovenia

Drešar P., University of Ljubljana, Slovenia

Levy P. R., University of Brighton, UK

Juvan T., Slovenia

# *Content*

## **PREFACE**

### **INVITED KEYNOTE LECTURES TITLES:**

G. Lampič

**Elaphe Propulsion Technologies – From invention to production**

F. Trieb

**Water as a tool – high pressure as passion**

A. Hančič

**Industry 4.0 in toolmaking**

P.R. Levy

**From Science Fiction to Reality**

F. Pude

**Challenges of AWJ technology and new research ideas**

M. Schmid

**Additive Manufacturing - State of the art, Opportunities and Challenges for the future**

### **PAPER SESSIONS:**

**Session A: AWJ machining and manufacturing technologies**

**Chair: Andrej Lebar**

D. Zarembo, P. Heitzmann, L. Overmeyer, L. Hillerns and T. Hassel

**Automatable splicing method for steel cord conveyor belts – Evaluation of water jetting as a preparation process** pp 1 – 7

A. Perc, F. Pude, M. Kaufeld and K. Wegener

**Obtaining the selected surface roughness by means of mathematical model based parameter optimization in abrasive waterjet cutting** pp 8 – 15

J. Klich, D. Klichova, V. Foldyna, P. Hlavacek and J. Foldyna

**Effects of pulsating water jet on aluminium alloy with variously modified surface** pp 16 – 22

V. Foldyna, J. Foldyna, D. Klichova, J. Klich, P. Hlavacek, L. Bodnarova, T. Jarolim and K. M. Kutlakova

**Effects of continuous and pulsating water jet on CNT/concrete composites** pp 23 – 29

N.L. Carutasu, D. Ghiculescu

**High productivity and precision technology and equipment for ultrasonically aided micro-electrical discharge machining** pp 30 – 35

M. Prijatelj, M. Jerman, P. Drešar, H. Orbanić, I. Sabotin, J. Valentinčič and A. Lebar

**Determining focusing nozzle wear by measuring AWJ diameter** pp 36 – 42

**Session B: Virtual manufacturing**  
**Chair: Izidor Sabotin**

C.E. Cotet, C.L. Popa, G. Enciu, A. Popescu and C.E. Stoica	
<b>Material flow digital twinning in the Industry 4.0 paradigm</b>	pp 43 – 49
L.F. Parpala and R.C. Parpala	
<b>Security issues in virtual enterprises</b>	pp 50 – 55
P. Mitrouchev, J.T. Chen, S. Coquillart and F. Quaine	
<b>Length perception in virtual reality environment</b>	pp 56 – 62
D.M. Popa and G.B. Cotet	
<b>Connecting two trends in the scientific community: knowledge sharing and scientific output measuring</b>	pp 63 – 67
G. Carutasu	
<b>Further challenges of eCall service and infrastructure</b>	pp 68 – 72
D. Popescu, D. Laptou, A. Hadar, R. Marinescu and I. Botezatu	
<b>Surgeon-engineer: Can we really collaborate? Yes, we can.</b>	pp 73 – 80
H. Zupan, J. Žerovnik and N. Herakovič	
<b>A hybrid metaheuristics for layout optimization in production cell</b>	pp 81 – 87
R. Vrabič and J.A. Erkoyuncu	
<b>Engineering interaction in multi-reality environments for remote operations and maintenance support</b>	pp 88 – 95

**Session C: Additive manufacturing**  
**Chair: Joško Valentinčič**

P.R. Levy	
<b>The crazy future of 3D printing</b>	
A. Piaget, M. Museau and H. Paris	
<b>Manufacturing Space Homogeneity in Additive Manufacturing – Electron Beam Melting Case</b>	pp 96 – 103
M. Peroša, J. Valentinčič, A. Lebar, M. Jerman, I. Sabotin and P. Drešar	
<b>Compensation of uneven illumination on stereolithography based 3D DLP printer</b>	pp 104 – 110
D. Grguraš, D. Kramar, D. Homar and J. Kopač	
<b>Comparison of optimal technological parameters obtained with two different nozzle sizes in hybrid manufacturing of 3D printing and milling</b>	pp 111 – 121
A. Zupan, J. Valentinčič, A. Lebar and M. Jerman	
<b>Comparison of stereolithography in two modes of illumination with DLP technology</b>	pp 122 – 125

**Conference organizers:**



**Conference sponsors**

**Golden sponsor:**

**BFT, Austria**



**Silver sponsors:**

**BSH, Slovenia**



**TECOS, Slovenia**





## Automatable splicing method for steel cord conveyor belts – Evaluation of water jetting as a preparation process

D. Zaremba<sup>1</sup>, P. Heitzmann<sup>2</sup>, L. Overmeyer<sup>2</sup>, L. Hillerns<sup>1</sup> and T. Hassel<sup>1</sup>

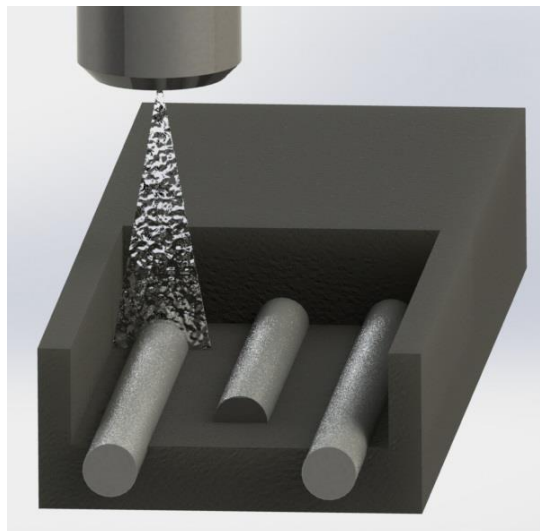
<sup>1</sup> *Institut für Werkstoffkunde (Materials Science), Leibniz Universität Hannover, Germany*

<sup>2</sup> *Institute of Transport- and Automation Technology, Leibniz Universität Hannover, Germany*

### Abstract

The increased demand of mineral resources leads to worldwide application of incessantly longer conveying systems. The length between axes can amount to 15 km and more. Owing to manageable dimensions and weight, appropriate conveyor belts are produced in segments of up to 300 m. Final assembly takes place at the conveyor system, where the multitude of segments is connected to a long conveyor belt. An important point in assembly preparation is the stripping of the steel cords, which is mainly carried out manually using rudimentary techniques. The optimization potential is high, since the adoption of automatable and application-oriented preparation methods can minimize the conveyor downtime and improve the joint quality.

In this study, the application of the pure water jet is investigated, since this selective stripping method offers a lot of potential for automation and the creation of rough surfaces. The objective was to determine if an efficient, homogenous and selective removal of the rubber is possible without damaging the zinc coating of the steel cords. Following a parameter study, the generated kerf geometries and surfaces were investigated. The stripped steel cords and zinc coatings were analyzed through the preparation of micrographs. Concluding, an evaluation about the qualification of water jetting as an automatable method for joint and repair preparation is made.



### Keywords:

Steel cord conveyor belts, splicing method, repair preparation, automation, water jetting

## 1 Steel cord conveyor belt

The belt is one of the most important parts of a conveyor system when it comes to design and investment costs. Due to logistic reasons, the belt can only be transported in segments to the conveyor system, limited by weight or length of the individual segment. The splicing is done directly at the system. In the splice, tensile forces are transferred through the core rubber and not via tension member. This fact makes a splice the weakest point of a conveyor belt. The tension member of a belt can consist of textile fabric or steel cords, depending on the tensile strength of the belt. Steel cord conveyor belts can reach a nominal belt breaking strength up to 10.000 N/mm. Figure 1-1 shows the general structure of a steel cord conveyor belt. [1]

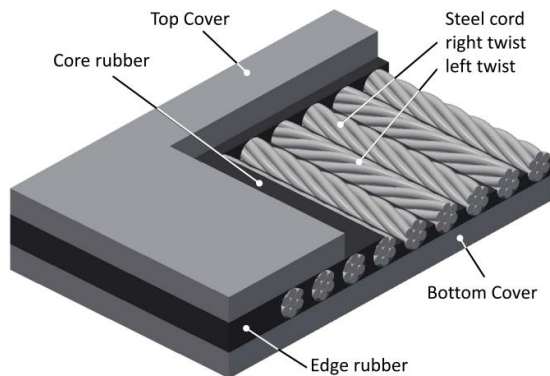


Figure 1-1: Steel cord conveyor belt

The steel cords are covered in core rubber and form the carcass of the belt which is covered by top and bottom cover. The bottom cover transfers the driving forces from drive pulley to the belt. The top cover transports the bulk material and protects the carcass from damages caused by material impacts. The steel cords are right and left twisted and placed alternate next to each. The cords are zinc coated and have a zinc oxide layer on top. Zinc oxide has two effects during the belt fabrication. On the one side, it is a vulcanization accelerator and, on the other hand, it provides the basis for a zinc sulfide layer that occurs during vulcanization process between rubber and steel cords and leads to a better adhesion. [2, 3]

The splicing procedure of a steel cord conveyor belt is performed as follows. First, the splicing area needs preparation. Before assembling the vulcanization press, the new rubber has to be placed into the splice. Then the vulcanization of the splice area completes the splicing procedure. The present preparation process for splicing procedure consists of numerous manually performed steps. The steel cords of both ends of the conveyor belt have to be completely removed from rubber. Therefore, the first step is to remove top and bottom cover with an oscillating cutting edge. To cut the steel cords apart, a stripping machine is used. Then the biggest amount of the core rubber is stripped from the cords with piano wires. As last step, cutting tools are used to remove the remaining amount of rubber and shorten the steel cords to the required length if necessary. Figure 1-2 (A) shows a splicing process. Then the cords have to be placed according to the splice layout, see figure 1-2 (B). Then new core rubber has to be put between the steel cords. The total process is very time consuming due to its low level of automation and considerable number of manual work steps. The splicing quality can be primary defined through the adhesion between steel cords and core rubber. The fact that the zinc oxide layer of the steel cords is responsible for it, the layer must not be damaged during the preparation of the splicing procedure. To avoid damaging the zinc oxide layer is almost impossible due to the removal of core rubber just by cutting tools. [1]

The splicing procedure of a steel cord conveyor belt is performed as follows. First, the splicing area needs preparation. Before assembling the vulcanization press, the new rubber has to be placed into the splice. Then the vulcanization of the splice area completes the splicing procedure. The present preparation process for splicing procedure consists of numerous manually performed steps. The steel cords of both ends of the conveyor belt have to be completely removed from rubber. Therefore, the first step is to remove top and bottom cover with an oscillating cutting edge. To cut the steel cords apart, a stripping machine is used. Then the biggest amount of the core rubber is stripped from the cords with piano wires. As last step, cutting tools are used to remove the remaining amount of rubber and shorten the steel cords to the required length if necessary. Figure 1-2 (A) shows a splicing process. Then the cords have to be placed according to the splice layout, see figure 1-2 (B). Then new core rubber has to be put between the steel cords. The total process is very time consuming due to its low level of automation and considerable number of manual work steps. The splicing quality can be primary defined through the adhesion between steel cords and core rubber. The fact that the zinc oxide layer of the steel cords is responsible for it, the layer must not be damaged during the preparation of the splicing procedure. To avoid damaging the zinc oxide layer is almost impossible due to the removal of core rubber just by cutting tools. [1]

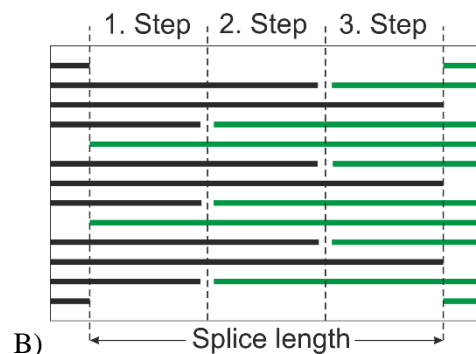


Figure 1-2: A) Preparation process of a steel cord splice [RI-Belt Sud S.R.L]; B) Layout of a 3-step steel cord splice

In this study, the application of the pure water jet is investigated, since this selective stripping method offers a lot of potential for automation and the creation of rough surfaces. The objective was to determine if an efficient, homogenous and selective removal of the rubber is possible without damaging the zinc coating of the steel cords.

## 2 Materials and methods

The investigations were carried out using a segment of an industrial steel cord conveyor belt with a total thickness of  $t = 30$  mm. The test material was in new condition. It was vulcanized using “STG type” primer, rubber strips and cover plates (components manufacturer: “Nilos”). The cover plate had a thickness of  $t = 15$  mm, the diameter of the subjacent zinc-coated steel cords was  $d = 8$  mm. Figure 2-1 shows a sectional view of the test material.



Figure 2-1: Sectional view of the test material

All jetting experiments were carried out using a “Stein Moser WS0707” gantry-style (x, y, z)-guiding machine. The high-pressure pump was a “BFT Servotron 40.37” (max. operating pressure  $p_w = 400$  MPa, max. volume flow rate  $Q_w = 3.8$  l/min). The high-pressure valve applied was a “BFT WJ070060”, modified to include a “Hammelmann” nozzle mount. Three flat-jet nozzles “Hammelmann Type R” with the jet angles  $\alpha_1 = 10^\circ$ ,  $\alpha_2 = 20^\circ$  and  $\alpha_3 = 30^\circ$  were used alongside with sharp-edged round-jet nozzles “Hammelmann Type I”. The nozzle diameter was kept constant with  $d_0 = 0.4$  mm. The nozzle coefficients were specified with  $k_f = 0.67$  for the flat-jet nozzles and  $k_r = 0.70$  for the round-jet nozzle by the manufacturer, respectively. The nozzles allowed for a maximum water pressure of  $p = 300$  MPa. Because of the flexible material behavior of the rubber, the achieved kerf-depth- and surface-roughness values were measured optically using fringe projection technology (equipment manufacturer: “GF Messtechnik”), in five positions each respectively.

For a neutral comparison of the material removal profile and –efficiency, the optimum standoff distance was determined for each jet angle  $\alpha$  to allow a material removal width of  $b = 10$  mm. Following, surface structure and -profile were analyzed. Through different jet disintegration stages are present at the same jet width when using various jet angles, an influence on the material removal profile can be expected. For the round jet nozzle, staggered tool paths were used with variation of the tool path distance. The nozzles with the most promising results were picked for a more detailed parameter investigation, also including multiple material removal iterations. After parameter and procedure optimization, the conveyor belt was stripped down to its steel cords. A micro section was prepared in order to investigate if the formerly applied zinc coating was still intact.

## 3 Results and discussion

Initial experiments showed that the utilized round jet nozzles did not allow a consistent material removal of the belt rubber. Similar to nozzle types used for cutting applications, they generate a coherent and narrow jet with a characteristically high energy density on a small contact area. Although this kind of nozzle is well suited for precise material removal of other composite materials (e.g. CFRP [4]), the elastic flexibility of the rubber effected a bending of the material away from the jet. This resulted in lamellar surfaces, combined with a comparatively low material removal rate. The results obtained using flat-jet nozzles were considerably better. As expected, different surface profiles were generated dependent on the jet angle. While the flat-jet nozzles with  $\alpha_1 = 10^\circ$  and  $\alpha_2 = 20^\circ$  produced a straight surface profile with a consistent surface roughness, the surface profile generated by the nozzle with  $\alpha_3 = 30^\circ$  was accentuated in the edges and less consistent. Through a furthermore lower material removal rate compared to  $\alpha_1 = 10^\circ$  and  $\alpha_2 = 20^\circ$ , the jet angle of  $\alpha_3 = 30^\circ$  did not implicate applicable advantages and was therefore rejected from the following investigations. Figure 3-1 shows a consistent material removal path of a flat jet nozzle with  $\alpha_1 = 10^\circ$  and  $p = 100$  MPa.

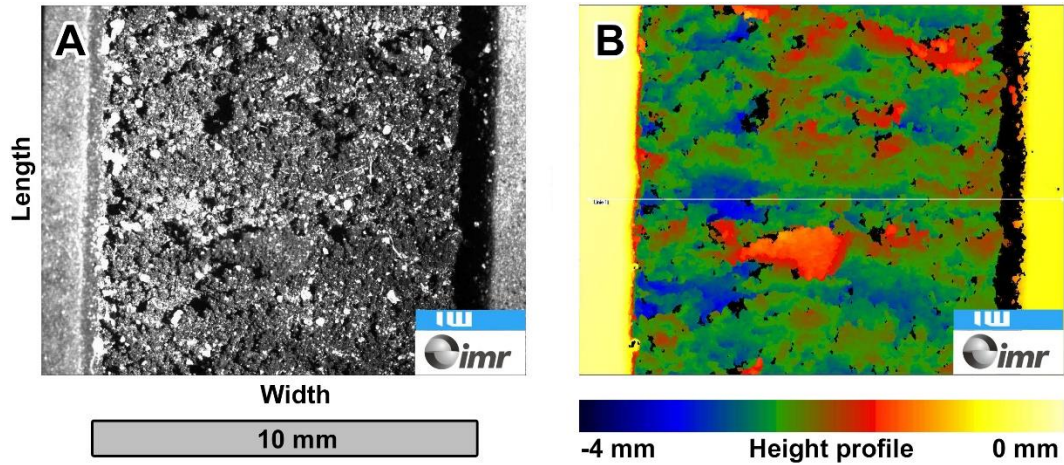


Figure 3-1: Surface topography in camera view (A) and height profile (fringe projection, B) of a material removal path generated by a nozzle with  $\alpha_1 = 10^\circ$  and  $p = 100$  MPa

As displayed in Figure 3-2, achieved kerf depths for  $\alpha_1 = 10^\circ$  were slightly higher than for  $\alpha_2 = 20^\circ$ . Measured surface roughness was significantly higher for the narrower jet angle. Since higher surface roughness goes along with an increased surface area, this can be advantageous when it comes to priming and splicing. Therefore, a higher surface roughness is generally preferable. A noteworthy fact is that the utilized flat-jet nozzles required a higher water volume flow rate than the stated nozzle coefficient of 0.67 would assume. The available water volume flow rate of  $Q_w = 3.8$  l/min was almost consumed at  $p = 150$  MPa ( $\alpha_1 = 10^\circ$ ) and  $p = 200$  MPa ( $\alpha_2 = 20^\circ$ ). For this reason, the stated pressure levels were set as the maximum values for each test series, respectively. As expected for an appropriate parameter study, kerf depth and surface roughness increase with an elongated contact time (smaller feed rate).

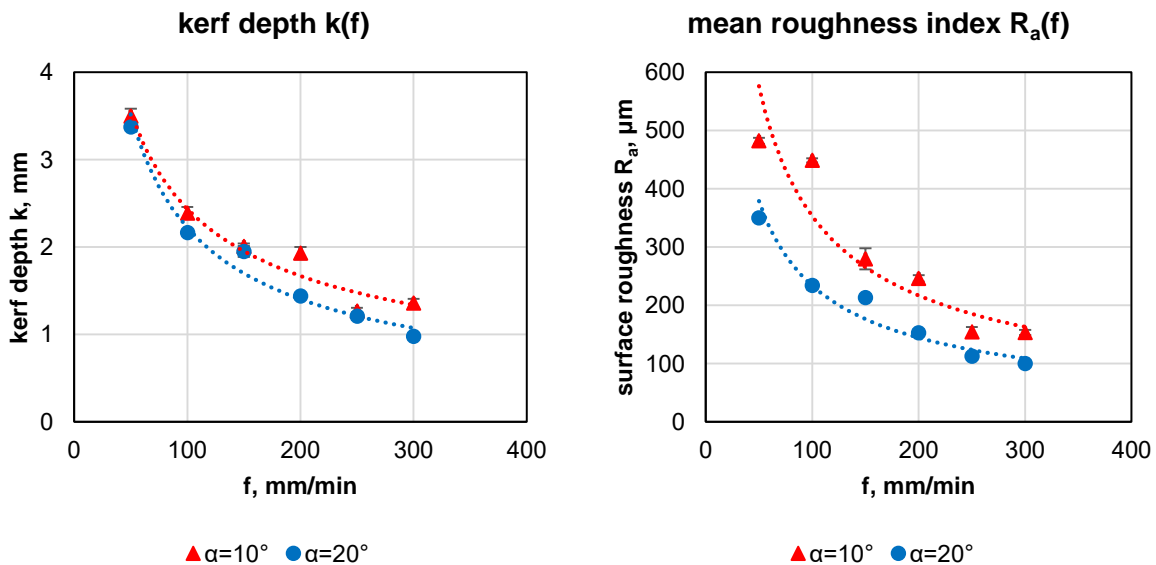


Figure 3-2: Kerf depth  $k$  and mean surface roughness index  $R_a$  compared to the feed rate  $f$  for a kerf width of  $b = 10$  mm

As displayed in Figure 3-3 and Figure 3-4, the achievable kerf depth increases straight proportional to the quantity of iterations for both jet angles. Using the test setup, a total of  $n = 4$  iterations was necessary to completely remove the top cover and strip the steel cords at a feed rate of  $f = 100$  mm/min. For  $\alpha_1 = 10^\circ$  a water pressure of  $p = 150$  MPa was necessary, for  $\alpha_2 = 20^\circ$  a water pressure of  $p = 200$  MPa. In both cases, the real water volume flow rate is expected to be similar close to  $Q_w = 3.8$  l/min, recognizable by the pump's

maximum workload. Furthermore, it was found that the surface roughness remains constant independent of the iteration quantity. The test equipment allowed for maximum surface roughness values of  $R_{a1} = 480.9 \mu\text{m}$  ( $\sigma_1 = 5.3 \mu\text{m}$ ) for  $\alpha_1 = 10^\circ$ ,  $p = 150 \text{ MPa}$  and  $R_{a2} = 465.7 \mu\text{m}$  ( $\sigma_2 = 6.2 \mu\text{m}$ ) for  $\alpha_2 = 20^\circ$ ,  $p = 200 \text{ MPa}$ , respectively. Both jet angles were likewise found suitable for the application, with advantages regarding equipment wear which can be expected for the lower necessary pressure at  $\alpha_1 = 10^\circ$ .

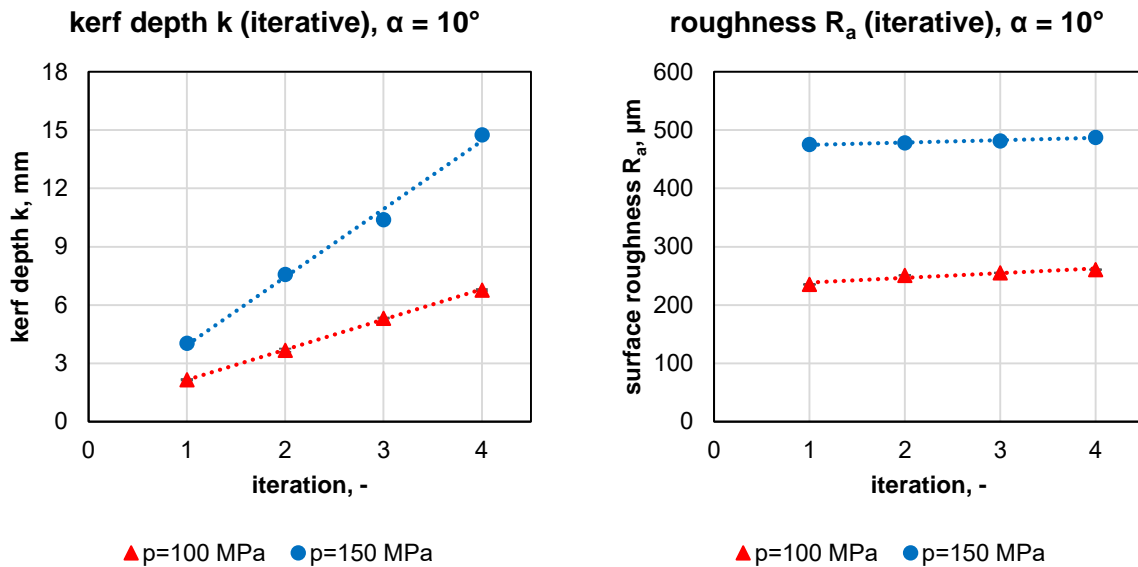


Figure 3-3: Kerf depth  $k$  and mean surface roughness index  $R_a$  compared to water pressure  $p$  for iterative material removal procedure, a jet angle of  $\alpha = 10^\circ$  and a feed rate of  $f = 100 \text{ mm/min}$

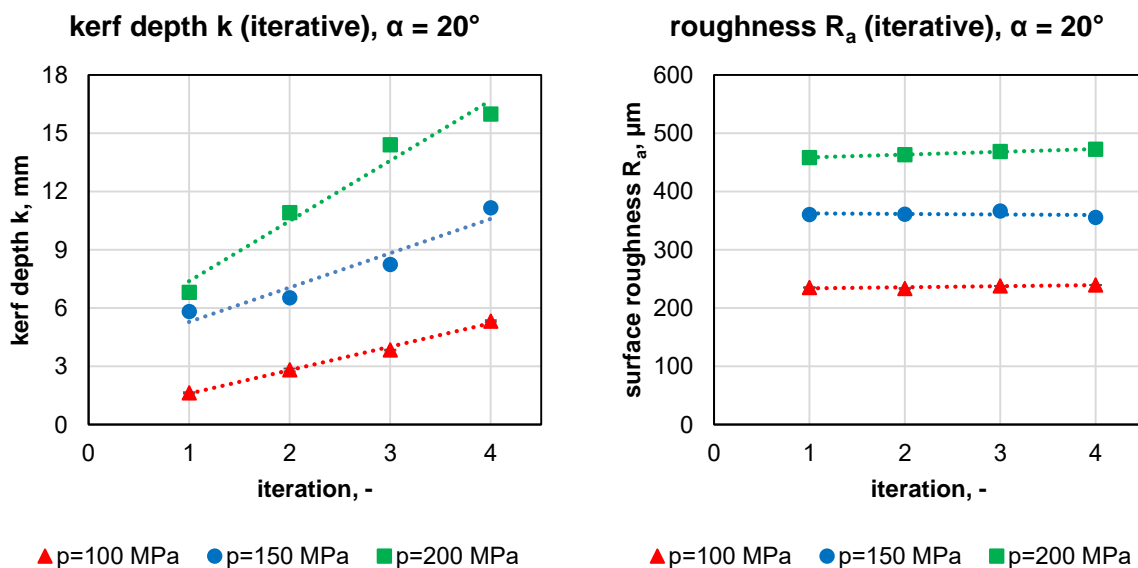


Figure 3-4: Kerf depth  $k$  and mean surface roughness index  $R_a$  compared to water pressure  $p$  for iterative material removal procedure, a jet angle of  $\alpha = 20^\circ$  and a feed rate of  $f = 100 \text{ mm/min}$

Figure 3-5 shows two photographs after removal of the cover plate and stripping the steel cords by water jetting and following drying by compressed air, as well as a micro-section of a single cord wire. It shows that a deep material removal with sharp, orthogonal and plane-parallel edges is possible with the utilized equipment (Figure 3-5 A). The exposed zinc-coated steel cords do not suffer visible damage (Figure 3-5 B). The prepared micro-section of a stripped cord shows that the galvanized zinc coating is still visible on the waterjet-treated

side (Figure 3-5 C). The thinner coating on the opposite side originates from the wire production method (wire drawing); this appearance can also be found on new condition steel cords.

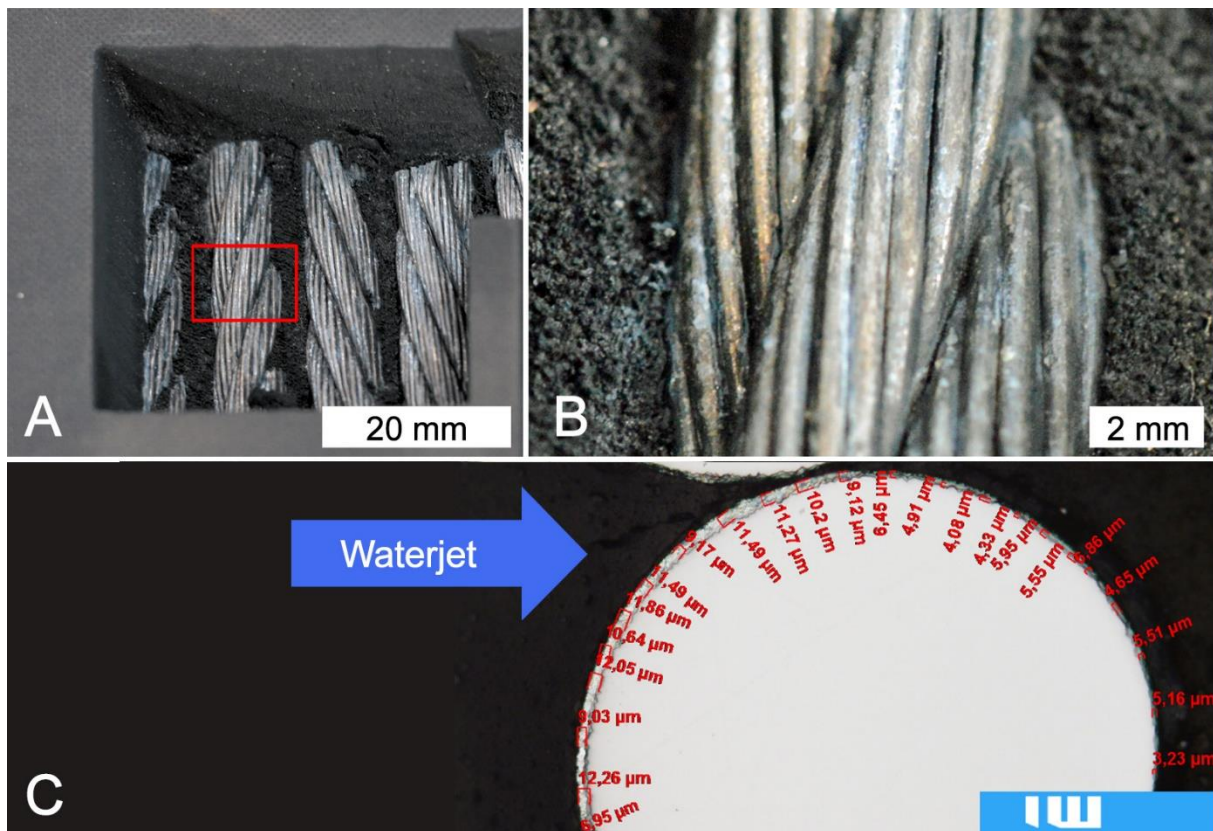


Figure 3-5: Stripped steel cords after iterative removal of the cover plate (A), detail view (B), micro section of a stripped cord with measurements of the zinc coating thickness (C)

#### 4 Conclusions and outlook

Concluded, water jetting is a promising preparation method for the splicing of steel cord conveyor belts that comes along with an excellent potential for automation. Utilizing commercially available pump technology combined with flat-jet nozzles, stripping rubber of the steel cords is easily possible in high quality without visible damage of the zinc coating. The produced rubber surfaces are consistently rough, which comes along with a larger contact surface for following vulcanization processes. Compared to the flat surfaces, which are generated through the conventional preparation techniques as described before, the application of this technology does not only offer a lot of potential to reduce downtime and splicing duration through automation, but also to improve the adhesion quality. The effect on quality and reproducibility of appropriate belt splicing has to be analyzed in further investigations.

Besides the effect on splice quality, the described preparation process offers further improvement opportunities. Material removal rate and surface roughness are further expected to be increased through bigger water volume flow rates, which go along with an increase of hydraulic power. Appropriate technology is available in the market and will be utilized by the authors for further investigations. Considering the behavior of load transmission in a steel cord belt splice, it becomes apparent that it mainly takes place at the lateral cord flanks. Unlike this, the preparation method described in this paper only includes the top- and bottom machining of the belt (cf. Figure 4-1 A). Therefore, future investigations should also include 3D machining processes, cf. Figure 4-1 B. Following the described optimization of the preparation and splicing processes, an application in form of automatable preparation- and splicing machines is likely.

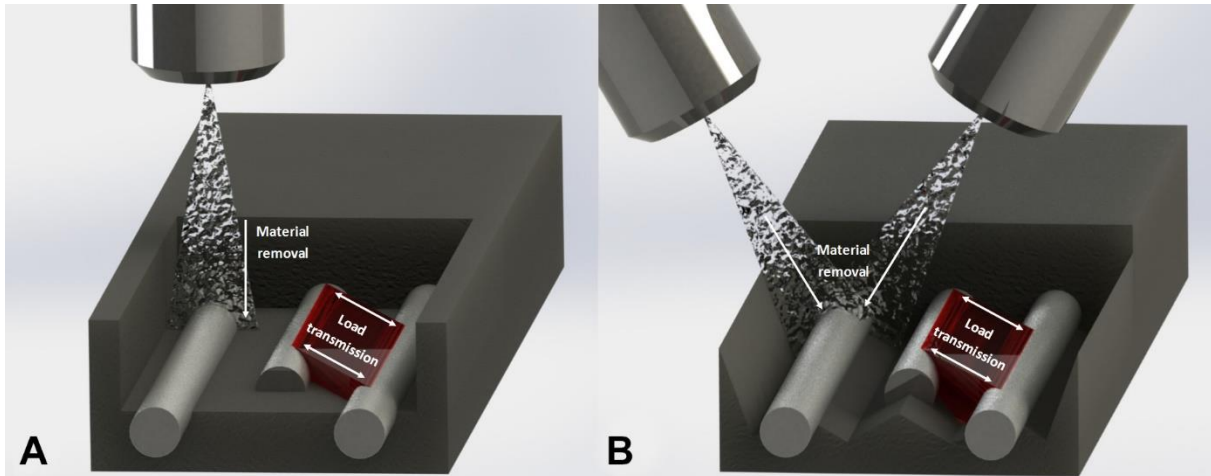


Figure 4-1: Direction of load transmission and material removal for 2D (A) and 3D machining (B)

## 5 Acknowledgements

The authors thank the Institute of Measurement and Automatic Control (IMR) for providing the fringe projection instrumentation and the German Working Group of Waterjet Technology (AWT) for fruitful discussion.

## 6 References

- [1] Ziller, T.; Hartlieb, P.: *Fördergurte in der Praxis – Know How and Know Why*, NILOS GmbH & Co. KG, VGE Verlag GmbH, Deutschland, 2010 – ISBN 978-3-86797-105-8
- [2] Sönksen, H.: *Korrosionsschutz von Seilen als Zugträger in Fördergurten*, Dissertation, Universität Hannover, Fakultät für Maschinenbau, 1987
- [3] Rzymiski, W.; Wolska, B.: *Unkonventionelle Vernetzung ausgewählter Elastomere*, GAK – Gummi Fasern Kunststoffe, Dr. Gupta Verlag, 6/2005
- [4] Zaremba, D.; Wachsmuth, S.; Schneider, P.; Hufenbach, W.; Maier, H. J.; Hassel, T.: *Method for the material-specific repair preparation of carbon fiber reinforced plastic structures*. Proceedings of the 22nd International Conference on Water Jetting, Haarlem/NL, Sept. 3-5, 2014
- [5] Spur, G.; Stöferle, T.: *Handbuch der Fertigungstechnik*. Band 4/1, Abtragen/Beschichten. Carl Hanser Verlag, München, Wien, 1987

# Obtaining the selected surface roughness by means of mathematical model based parameter optimization in abrasive waterjet cutting

A. Perc <sup>1</sup>, F. Pude <sup>1</sup>, M. Kaufeld <sup>2</sup> and K. Wegener <sup>1,3</sup>

<sup>1</sup> Inspire AG, ETH Zürich, Zurich, Switzerland

<sup>2</sup> Institute of Production Engineering and Materials Testing, University of Applied Sciences Ulm,  
Ulm, Germany

<sup>3</sup> Institute of Machine Tools and Manufacturing, ETH Zürich, Zurich, Switzerland

## Abstract

Existing models for predicting the results of cutting by water jet as presented for example in [1, 2, 10, 11] cannot achieve satisfactory results in the wide area of parameter changes, especially for the large number of different materials. This implies the need to conduct extensive research in order to expand the empirical database. One of the methods of determining the effect of process parameters on the controlled process is the Taguchi Method. This method allows to limit the amount of research needed to achieve the desired test results, thereby reducing the time as well as the cost required to carry them out. The Taguchi signal/noise (S/N) ratio enables the assessment of the relevance of the impact of various parameters on the process, which is still not well enough understood.

**Keywords:** abrasive water jet, design of experiment, optimization, cutting, prediction.

## 1 Introduction

In recent years, high pressure water-jet machining has competed effectively with conventional methods of separation of materials. This is mainly because of the wide range of options it offers, including the processing of complex shapes, cutting of a large variety of materials, and its effectiveness under extreme conditions (hazard of fire or explosion, work under water up to a depth of 6000 m, etc.).

Further advantages of the treatment of materials with a high-pressure fluid jet include:

- ability to cut with constant stand-off distance between the working nozzle and machined top surface of the workpieces,
- good surface structure after cutting or surface processing,
- leaves the structure of the cut material thermally unaffected,
- no internal stresses in the cutting zone,
- fluid jet can be operated very easily.

However, the application of a pure fluid jet is not very effective in cutting hard materials such as metals or rocks. The application of solutions for intensifying the erosive abilities of the fluid jet, such as the introduction of a loose abrasive is necessary for improving the effectiveness of the treatment. It should also be noted that the treatment is performed without significant increase in heat, as any heating produced as a result of the friction of the abrasive against the material and the nozzle is immediately counteracted by the water jet.

## 2 Water jet cutting

Cutting by high-pressure water jet is an advanced method of separating materials. Processing materials using a high pressure abrasive water jet is more complex than conventional treatments. High pressure water is



converted to a high speed jet inside a nozzle (Figure 1a.) and flows out of the nozzle at a speed of several hundred meters per second, hits a stream of abrasive particles and accelerates them to high particle speed. Adding dry abrasive to the water jet in a special mixing chamber (Figure 1b) increases cutting efficiency. As a result, it becomes possible to cut almost any material. Typical pressure levels used by the abrasive water jet (AWJ) system range from 400 to 600 MPa. The most commonly used abrasive is garnet as indicated in [12].

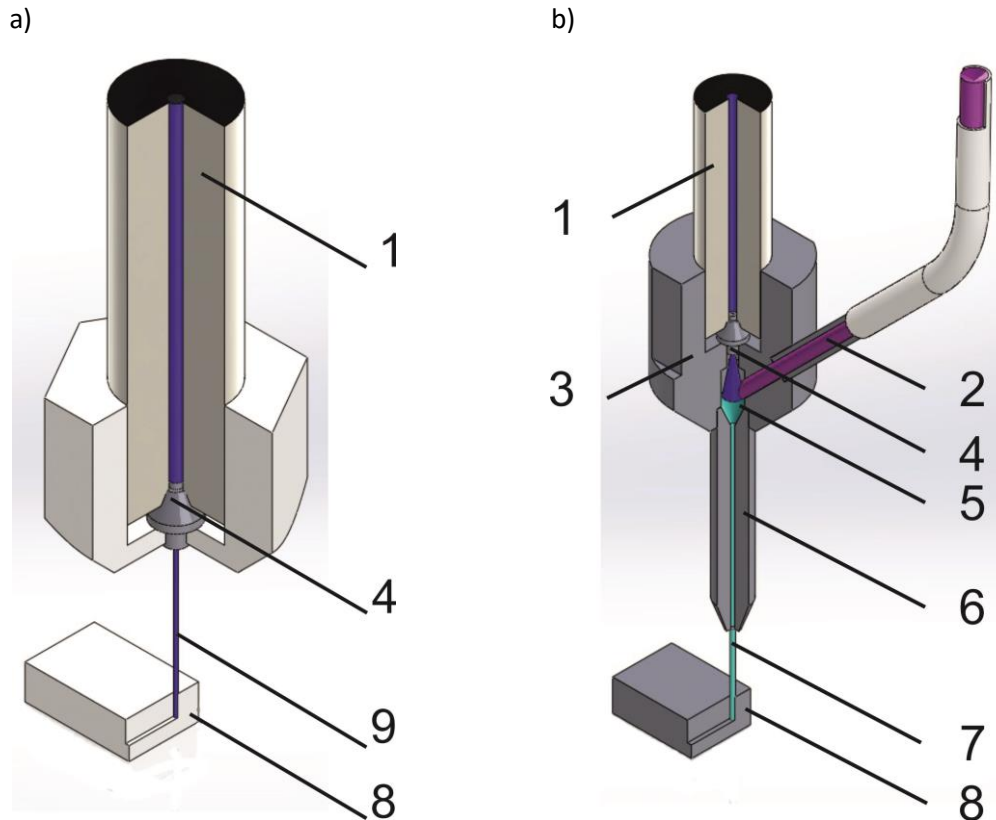


Figure 1: Schematic diagram of: a) water jet cutting and b) abrasive water jet cutting:  
 1. high pressure water inlet, 2. abrasive inlet, 3. cutting head, 4. water nozzle, 5. mixing chamber,  
 6. focussing tube, 7. high speed abrasive water Jet, 8. sample, 9. high speed water jet.

### 3 Materials and Experimental Setup

The study is conducted on the test rig shown in Figure 2 by using a high pressure intensifier (BYPUMP 50APC) presented in Figure 2b. The maximum working pressure is 400 MPa at a flow rate of 5 dm<sup>3</sup>/min. This allows the use of a water nozzle with maximum diameter of 0.4 mm. The cutting head used, as shown in Figure 2a is equipped with a water nozzle with a diameter of 0.28 mm, and a focussing tube with a diameter of 0.76 mm and a length of 75 mm, mounted on 3-axis Siemens Sinumerik 840D CNC machine as can be seen in Figure 2c. The working area is 1000 x 1000 x 400 mm. The machine is equipped with an abrasive feeder from the Swiss company Allfi. During the test garnet (Almandine) 80 mesh is used, from which a sample is presented in Figure 3. The basic properties of this abrasive are presented in Table 1.

The garnet abrasive group contains closely related, isomorphous, minerals that may contain low percentages of elements found in other members of the garnet family. Garnets are isostructural, meaning that they share the same crystal structure.

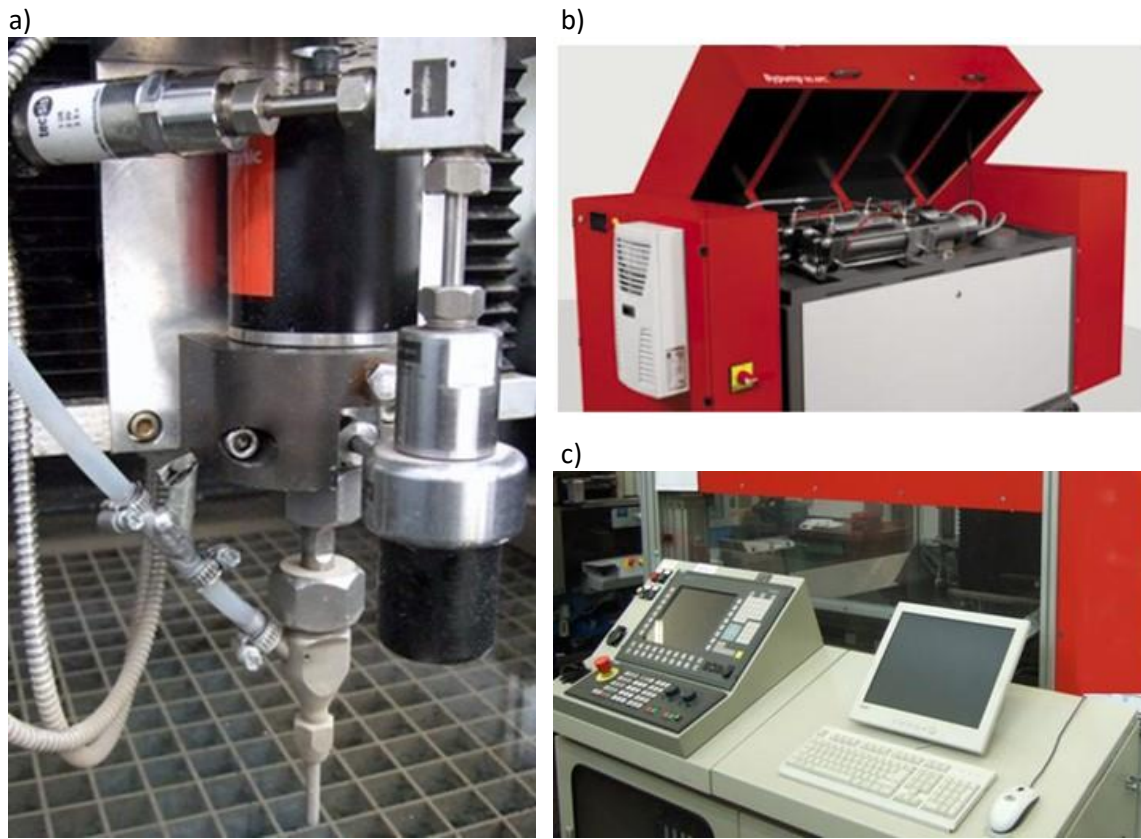


Figure 2: Test rig: a) cutting head, b) high pressure intensifier, c) control module

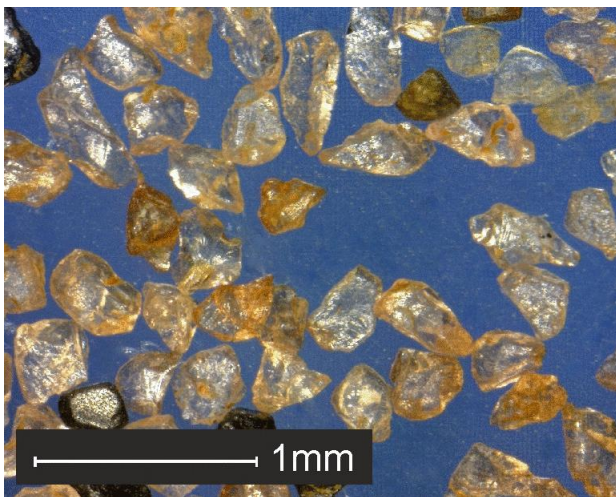


Figure 3. Garnet (Almandine) 80 mesh

Table 1. Garnet (Almandine) properties [7]

Crystal system	cubic
Twining	none
Unit cell	$a = 11.53 \text{ \AA}$
Habit	crystals usually dodecahedrons or trapezohedrons; also in combination or with hexoctahedron; massive; granular
Cleavage	1; $\{110\}$ parting sometimes distinct
Fracture	conchoidal to uneven
Tenacity	brittle
Color	deep red to reddish-brown, sometimes with a violet or brown or brownish black hue

#### 4 The Taguchi Method

The selection of parameters which can produce optimal results is usually a complex process. Typically this requires carrying out a number of tests, and in this way the effect of technological parameters on the properties of the final product can be determined. The Design of Experiment can be shortened by using this method. The planning of such studies is an interdisciplinary science, which lies at the intersection of metrology, applied mathematics, statistics, and computer science, allowing researchers to use the information

the program has provided them with to reduce both the cost and time expended in obtaining the relevant information. This Design of Experiment enables researchers to select the input variables which significantly affect the process observed and can also build a mathematical model of the process and the mathematical relationships between input and output values. Further, it can determine the value of the input quantities which affect the most desired outcome of the process (process optimization), and determine the effect of variation in the size of the input on the variability of the whole process [16].

The Taguchi Method [15] is a technique that provides a systematic and efficient methodology for process optimization and is a useful tool for the design of high quality systems. The Taguchi approach to Design of Experiments is easy for users with less experience of statistical methods to apply, and has therefore gained wide popularity in engineering. It is used for example in [4, 5, 6, 13, 14, 16, 17]. This is an engineering methodology for obtaining optimized products and processes, which are minimally robust and which produce high-quality products with reduced development and production costs. Signal to noise ratio (S/N ratio) and orthogonal matrix are two major tools used in the planning of experiments.

The S/N ratio values can be divided into three categories when the number is continuous:

- nominal is the best,
- smaller is better,
- larger is better.

The Taguchi Method is used to generate a S/N ratio  $\eta$  in order to determine the current scatter of values. The signal (S) is derived from factors which are adjustable or under the control of the user, but noise (N) refers to those factors which affect the signal, but which are beyond the control of the user.

The aim of the design is to enable the selection of the parameters of the experiment (in this case the process), so as to maximize the  $\eta$ . Various S/N indicators can be used according to the researcher's needs [17].

Orthogonal matrix is selected subset of combinations of multiple factors at multiple levels. Taguchi Orthogonal matrix are balanced to ensure that all levels of all factors are considered equally. For this reason, the factors can be evaluated independently of each other despite the fractionality of the design [18].

In abrasive water jet cutting typically aims at achieving the maximal depth of cut and low roughness of the cut surface. Especially during precision cutting low roughness of the cut surface is of paramount importance. In this case the roughness of the kerf's surface should be as small as possible. This is described by the "smaller is better" equation:

$$\eta = -10 \log \left( \frac{1}{n} \sum_{i=1}^n y_i^2 \right) \quad (1)$$

where:

- $n$  is the number of repetitions of measurement,
- $y$  is the current value of the measurement,
- $i$  is the number of variables.

## 5 Optimization and Prediction Procedure

The influence of the selected parameters of abrasive water jet cutting on the accepted optimization criterium – surface roughness of the cutting kerf – is analyzed.

A machining parameter selection process, using the L18 orthogonal array, was applied in this study (table2). This array is chosen because it consists of three control parameters: one (P1) with 6 levels, and the next two (P2 and P3) with three levels, as shown in Table 2.

In this case, the control parameter P1 is represented by the traverse speed, control parameter P2 by the pressure, while control parameter P3 by the abrasive flow rate.

The Minitab16 program is used for the calculation procedure. The variation interval of the selected cutting parameters used under optimization are presented in Table 3.

After conducting research at relevant parameters according to Taguchi array, roughness values were measured for each parameter combination. Roughness was measured according to the three most commonly used methods:  $R_{max}$ ,  $R_z$  and  $R_a$  [3, 8, 9].

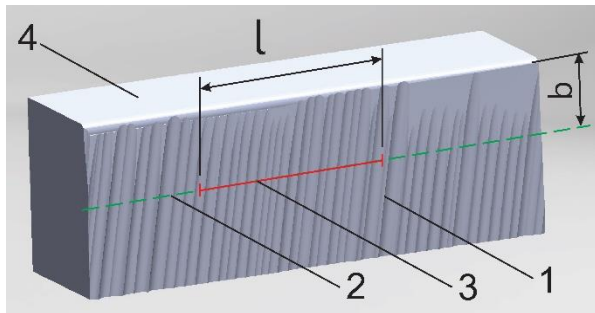


Figure 4. Measurement of roughness:

- 1) cutting surface,
- 2) sampling line,
- 3) sampling length,
- 4) top plane.

Table 2. Orthogonal array L18 for Taguchi design of experiment

Test number	P1	P2	P3
1	1	1	1
2	1	2	2
3	1	3	3
4	2	1	1
5	2	2	2
6	2	3	3
7	3	1	2
8	3	2	3
9	3	3	1
10	4	1	3
11	4	2	1
12	4	3	2
13	5	1	2
14	5	2	3
15	5	3	1
16	6	1	3
17	6	2	1
18	6	3	2

Table 3. Parameters of the cutting process and values of  $\eta$  factor

Traverse speed [mm/min]	Pressure [MPa]	Abrasive flow rate [g/min]	$R_{max}$ [ $\mu$ m]	S/N ( $R_{max}$ ) $\eta$	$R_z$ [ $\mu$ m]	S/N ( $R_z$ ) $\eta$	$R_a$ [ $\mu$ m]	S/N ( $R_a$ ) $\eta$
20	360	700	16	-24.4	13	-22.3	2	-5.4
20	300	550	17	-24.7	14	-23.1	2	-7.0
20	240	300	19	-25.2	16	-24.0	3	-9.2
40	360	700	21	-25.0	13	-22.5	2	-6.6
40	300	550	18	-25.3	15	-23.3	3	-8.2
40	240	300	17	-25.9	16	-24.2	3	-10.4
60	360	550	23	-26.7	20	-25.3	3	-8.9
60	300	300	26	-27.8	20	-25.9	3	-9.9
60	240	700	19	-26.7	16	-25.0	3	-9.8
100	360	300	20	-26.0	18	-24.8	3	-8.3
100	300	700	18	-25.5	15	-23.6	2	-7.0
100	240	550	19	-25.2	17	-24.7	3	-9.8
140	360	550	22	-28.3	17	-25.3	3	-10.6
140	300	300	32	-29.5	19	-25.9	4	-11.6
140	240	700	29	-28.4	20	-25.0	4	-11.4
180	360	300	23	-27.5	20	-26.2	3	-10.4
180	300	700	21	-27.0	18	-24.9	3	-9.0
180-	240	550	24	-26.8	20	-26.1	4	-11.8

To eliminate the influence of rounded cutting edges (Figure 4), the sampling line was set at  $b=1$  mm from the top surface. The sampling length of the measurement is  $l=4$  mm.

Figure 5 presents the calculated dependency terms of the cut of the value of S/N ratios  $R_a$ ,  $R_z$  and  $R_{max}$  coefficients. The impact of individual process parameters on the S/N ratio is similar for all analyzed roughness values. For each roughness coefficient, a maximal S/N ratio is reached at the smallest traverse speed value, which was 20 mm/min. In the case of pressure, the largest value of the S/N ratio is reached at

the highest pressure, which was 360 MPa. This result is obtained for all roughness coefficients. Maximal S/N ratio values are reached for the highest abrasive flow rate (700 g/min), for all roughness coefficients.

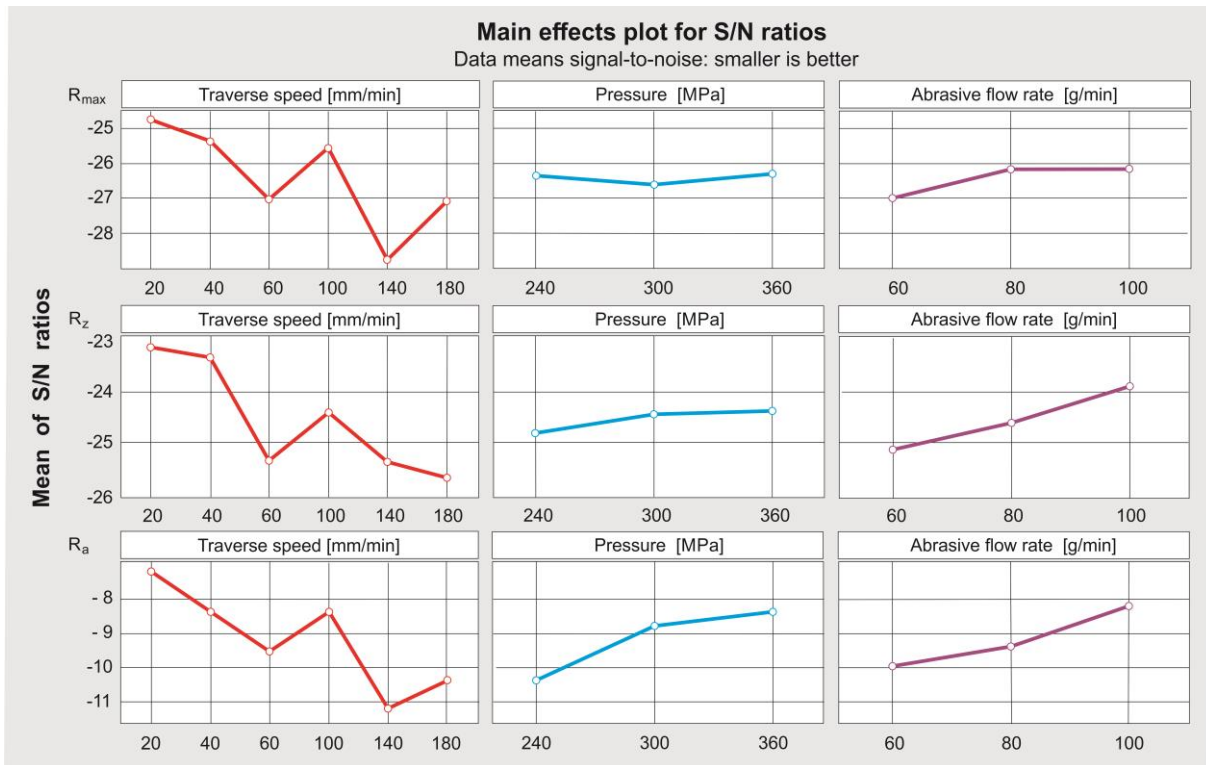


Figure 5. S/N ratio of roughness for each of tested parameters

In Figure 6 are shown the predicted and the measured roughness values reached at optimal cutting parameters: traverse speed = 20 mm/min, pressure = 360 MPa and abrasive flow rate = 700 g/min.

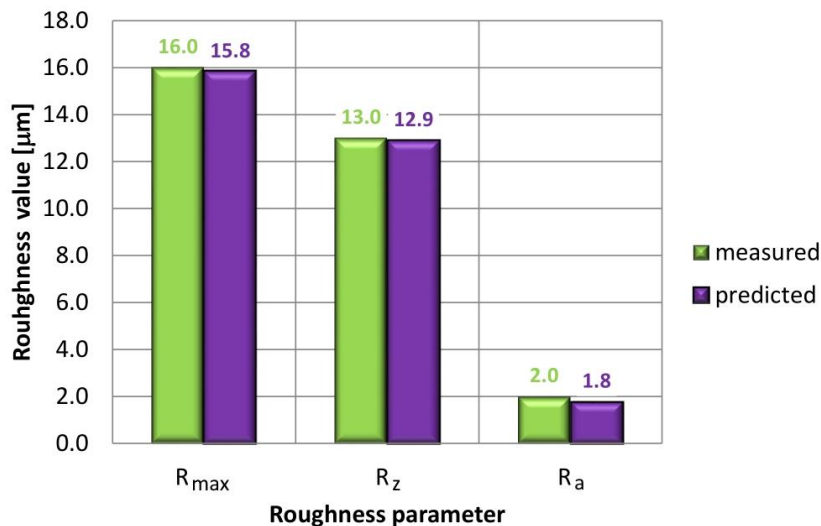


Figure 6. Results of predicted and measured values for different roughness parameters.

Figure 7 shows an exemplary photorealistic shading view and profile generated by machining parameters which were optimal from the roughness point of view. In Figure 7a oblique parallel cutting traces, which are typical for abrasive water jet machined surfaces can be noted.

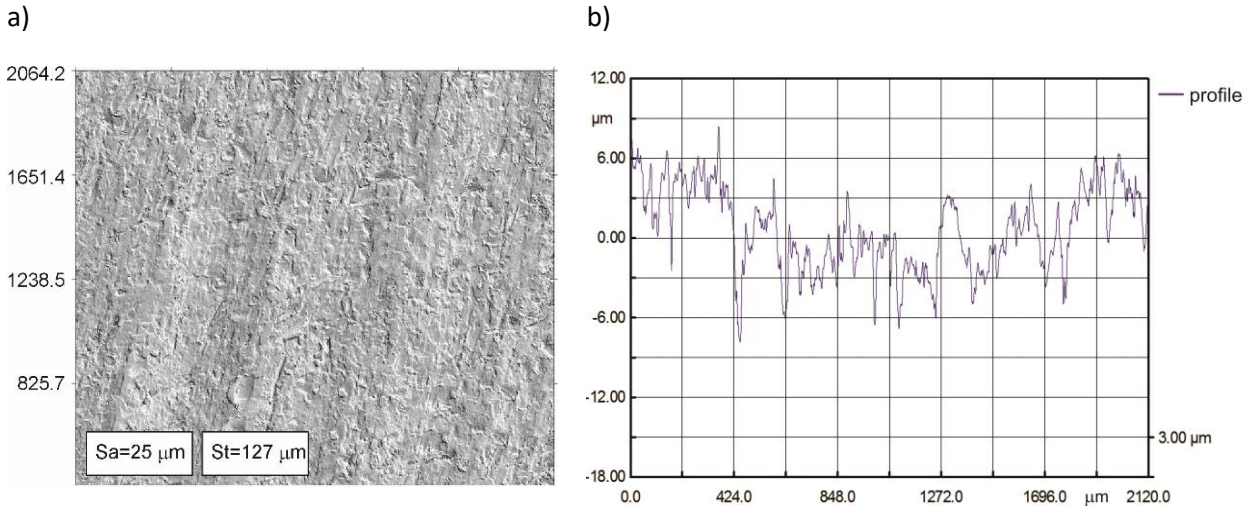


Figure 7. Sample of a cut steel surface at optimal parameters: traverse speed = 20 mm/min, pressure = 360 MPa, abrasive flow rate = 700 g/min, a) photorealistic shading view, b) surface profile of the sample.

A summary of results of measurements and predictions of surface roughness values separately for each of the analyzed factors is shown in Figure 8. The best prediction data is reached for the roughness coefficient  $R_z$ . The deviation value is equal to 0.0355. The worst fit is reached for the roughness coefficient  $R_{max}$ . In this case the deviation is 0.056.

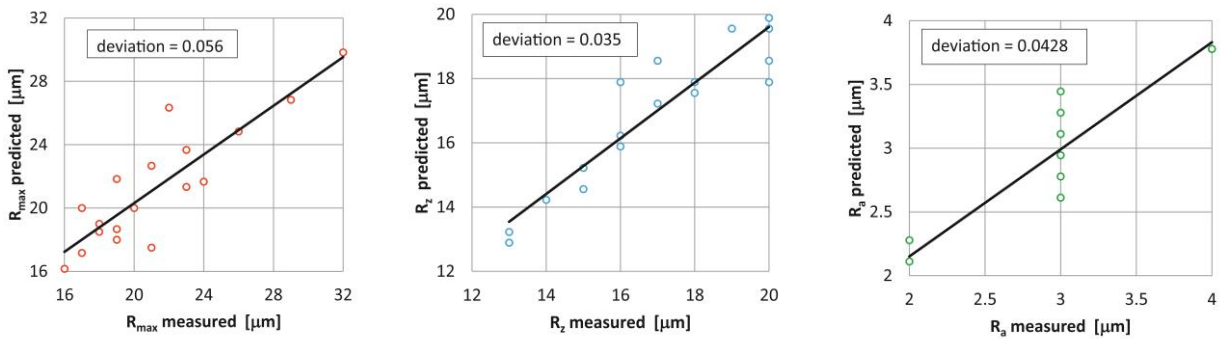


Figure 8. Measured and predicted roughness values of the cutting kerf's surface.

## 6 Conclusions

The application of the Taguchi method allows the determination of the effect of process parameters which significantly affect the test process, and their implementation in a manner most consistent with the assumptions. This enables the user to ignore those factors which have a negligible impact on the results and not on the significance of results. It also reduces the number of needed trials in that it significantly reduces the costs of the experimental work. The method may be particularly useful in planning research into the treatment of new materials regarding which there is insufficient information, about the properties. It may also be important in assessing the significance of the parameters that influence the cutting of new materials and newly developed procedures which are not yet sufficiently understood.

## References

- [1] G. Chomka, J. Chudy: Analysis and Interpretation of Measurements of Surface Machining Effectiveness in Process of Varnish Removal by Water-Ice Jet. In: Technical Gazette, Vol. 20, (5), pp. 847-852.
- [2] Feed Rate Calculator. [Online]. Available: [www.wardjet.com/downloads.html](http://www.wardjet.com/downloads.html) [2014, March 1]
- [3] P. Hreha, S. Hloch: Potential use of vibration for metrology and detection of surface topography created by abrasive waterjet. In: Int. J. Surface Science and Engineering, Vol. 7 (2), pp. 135-150.
- [4] F. Kolahan, H. Khajavi: Modeling and Optimization of Abrasive Waterjet Parameters using Regression Analysis. In: World Academy of Science, Engineering and Technology, Vol. 3, pp. 11-23.
- [5] J. T. Krishankant, M. Bector, R. Kumar: Application of Taguchi Method for Optimizing Turning Process by the effects of Machining Parameters. In: International Journal of Engineering and Advanced Technology (IJEAT), Vol. 2 (1), pp. 263-274.
- [6] D.O. Macodiyo, H. Soyama: Optimization of cavitation peening parameters for fatigue performance of carburized steel using Taguchi methods. In: Journal of Materials Processing Technology 178, pp. 234-240.
- [7] P. Martinec, J. Foldyna, L. Sitek, J. Ščučka, J. Vašek: Abrasives for AWJ cutting. Institute of Geonics, Ostrava, Czech Republic 2002.
- [8] P. Miles, A. Henning:  $R_z$ : A Better Measurement of Abrasive Waterjet Cut Surface Finishes. In: Proceedings of 2013 WJTA-IMCA Conference and Expo. Houston, Texas, USA, paper C2.
- [9] A. Perc: Comparison of abrasive grain disintegration during the formation of Abrasive Water Jet and Abrasive Slurry Injection Jet. In: Water Jetting Looking to the Future Learning of the Past. Fairhurst, M. BHR Group Ltd. Cranfield, UK, pp. 319-328.
- [10] A. Perc: Theoretics of the Abrasive Micrograin Application to High-pressure, Hydroabrasive Waterjet Treatment. In: Proceedings of Management of Innovative Technologies'2005. Piran, Slovenia 2005, pp. 199-204.
- [11] A. Perc: The Simulation Model of High-pressure, Suspension Waterjet Cutting Process with Use of the Artificial Neural Network. In: 2007 WJTA American Waterjet Conference. September 2007, Houston, Texas, USA, paper B-2.
- [12] A. Perc: Investigations of Effectiveness Constructional Steel Cutting with Hydroabrasive, Suspensive Waterjet about Lowered Pressure. In: Proceedings of 2-nd. International Conference on Water Jet Machining WJM 2001. Wantuch, E. (Ed.) Cracow, Poland, pp. 209-218.
- [13] V. Sharma, S.A. Chattopadhyaya, S. Hloch: Multi response optimization of process parameters based on Taguchi—Fuzzy model for coal cutting by water jet technology. In: The International Journal of Advanced Manufacturing Technology, Vol. 56, (9-12), pp. 1019-1025.
- [14] A. Sreenivasa Rao, B. S. Ravinder, A. Seshu Kumar: Parametric Optimization of Abrasive Waterjet Machining for Mild Steel: Taguchi Approach. In: International Journal of Current Engineering and Technology, Special Issue-2 (Feb 2014), pp. 27-30.
- [15] Taguchi, G. Quality engineering in production systems. McGraw-Hill, New York.
- [16] M. Ťavodova, M.: Optimization of abrasive water jet cutting using DoE method. Proceedings of Conference on Water Jetting Technology Water Jet 2015 – Research, Development, Applications. Velké Losiny, Czech Republic 2015, pp. 207-216.
- [17] B. Warcholinski, R. Olik, J. Ratajski, J. Michalski: Application of Taguchi Method to Optimize process Parameters of Gas Nitriding. In: Surface engineering Vol 4/2011, pp. 3-7.
- [18] <http://www.weibull.com/hotwire/issue111/tooltips111.htm> (access 16.07.2016)

# Effects of pulsating water jet on aluminium alloy with variously modified surface

J. Klich, D. Klichova, V. Foldyna, P. Hlavacek and J. Foldyna

*Institute of Geonics of the ASCR, v.v.i, Czech Republic*

## Abstract

The paper deals with the topic of the determination of erosion effects of a pulsating water jet impinging the surface of aluminium alloy samples treated by various techniques (rough and fine milling, planing and rolling). The influence of the initial surface topography on the final topography of the sample exposed to the pulsating water jet was investigated. Erosion of surface layers was analysed and discussed in relation to the traversing velocity of the jet. It was found that initial surface properties have a significant impact on the final topography. Degree of the surface erosion was determined by the measurement of the surface parameter  $Ra$ .

**Keywords:** pulsating water jet, surface topography, material erosion

## 1 Introduction

Over hundred years, researchers have been interested in the interaction of a liquid with a solid. One of the first researchers dealing with this subject was Cook [1] who wrote his article on the surface erosion in 1928. He clearly recognized the importance of the water hammer pressure.

Although the pulsating water jet (PWJ) has been successfully used for several industrial applications, the fundamentals of the technique remains unclear. Pulsating water jet is an extension of the conventional (continuous) jet, consisting of an array of high-speed water pulses. When a pulsating water jet impinges a target, the momentum flux through the nozzle is not transmitted to the target material as a steady force, but as a discontinuous sequence of impacts, creating high momentary stresses in the impingement zone. As a result, the peak pressure acting on the surface is not the stagnation pressure, but the significantly higher water hammer pressure [2].

There are several ways how to create the pulsating water jet as shown, for instance, in [3]. It can be done using mechanical interrupters, self-resonating systems, jets modulation by the piezoelectric magnetostrictive effects, jet disruption by electric discharge, laser based pulsating of water jets, etc. In our case, the system for the generation of acoustic pulsations developed at the Institute of Geonics of the ASCR, v. v. i. was used [4, 5, 6].

The pulsating water jets are generated by sufficiently high pressure pulsations in pressure water in the upstream direction to the nozzle exit. In the nozzle, the pressure pulsations change into velocity pulsations and the jet emerges from the nozzle exit as a continuous jet with variable axial velocity. Owing to the variable velocity, the jet is formed into pulses at a certain stand-off distance towards the nozzle exit (so called forced break-up length of the jet) and it starts acting as a pulsating jet. Exploitation of effects related to the water pulses impingement on solids in the field of the high-speed water jet technology should result in considerable improvement of its performance, better adaptation to progressively more demanding environmental requirements and, consequently, more cost-saving use of the technology from the economical point of view [7].

The objective of the paper is to determine erosion effects of the pulsating water jet impinging the surface of aluminium alloy samples treated by various techniques (rough and fine milling, planing and rolling) and to discuss the influence of the initial surface topography on the final topography of the sample exposed to the pulsating water jet.



## 2 Experimental facility

The facility used for the experiment consisted basically of a high-pressure water supply system, pulsating water jet generator, robotic manipulator for traversing the jet over test samples and optical surface profilometer for the evaluation of surface characteristics of the samples.

The high-pressure water was supplied to the generator of pulsating water jet by a plunger pump able to deliver up to  $65 \text{ l}\cdot\text{min}^{-1}$  of water at the operating pressure up to 160 MPa. The generator was equipped with a commercially available fan nozzle with the equivalent orifice diameter of 2.0 mm and the spraying angle of  $10^\circ$ .

The generator of pulsating water jet was designed for the maximum operating pressure of 150 MPa. It consisted of a piezoelectric transducer vibrating at the operating frequency of about 20 kHz and it was driven by an ultrasonic generator with the maximum output power of 800 W.

Test samples were manufactured from the aluminium alloy known as EN AW 5083 H111. Basic properties of the alloy are given in Tab. 1. Firstly, the abrasive water jet technology was used to cut the samples from 10 mm thick sheet in order to eliminate thermal effects on the properties of samples [8, 9, 10]. Dimensions of the test samples were  $10 \times 60 \times 100 \text{ mm}$  (Fig. 1). Secondly, the samples surface was treated by rough milling, fine milling and planing. One sample remained untreated; its surface was only affected by rolling during the aluminium sheet manufacturing. Parameters of the used technological operations are presented in Tab. 2. Then, surfaces were scanned by an optical profilometer to determine the initial surface roughness of the prepared samples (before their exposition to the pulsating water jet) [11, 12].

Table 1: Basic properties of aluminium alloy EN AW 5083 H111

Chemical composition			Mechanical properties			
Al	Mg	Mn	Yield strength $\sigma_{0,2}$ [MPa]	Tensile strength $\sigma_{Pt}$ [MPa]	Elongation $A_{50}$ [mm]	Hardness
%						Brinell [HB]
94.8	4.5	0.7	125	275	12	75

Table 2: Parameters of technological operations

Surface treatment	Technological parameters
Rough milling	Milling cutter $\varnothing 63 \text{ mm}$ , 12 cutting edges, 360 RPM, traversing velocity $65 \text{ mm}\cdot\text{min}^{-1}$
Fine milling	Milling cutter $\varnothing 63 \text{ mm}$ , 12 cutting edges, 1500 RPM, traversing velocity $470 \text{ mm}\cdot\text{min}^{-1}$
Planing	Planing machine 52 strokes per minute, feed rate 0,12 mm per stroke
Rolling	N/A

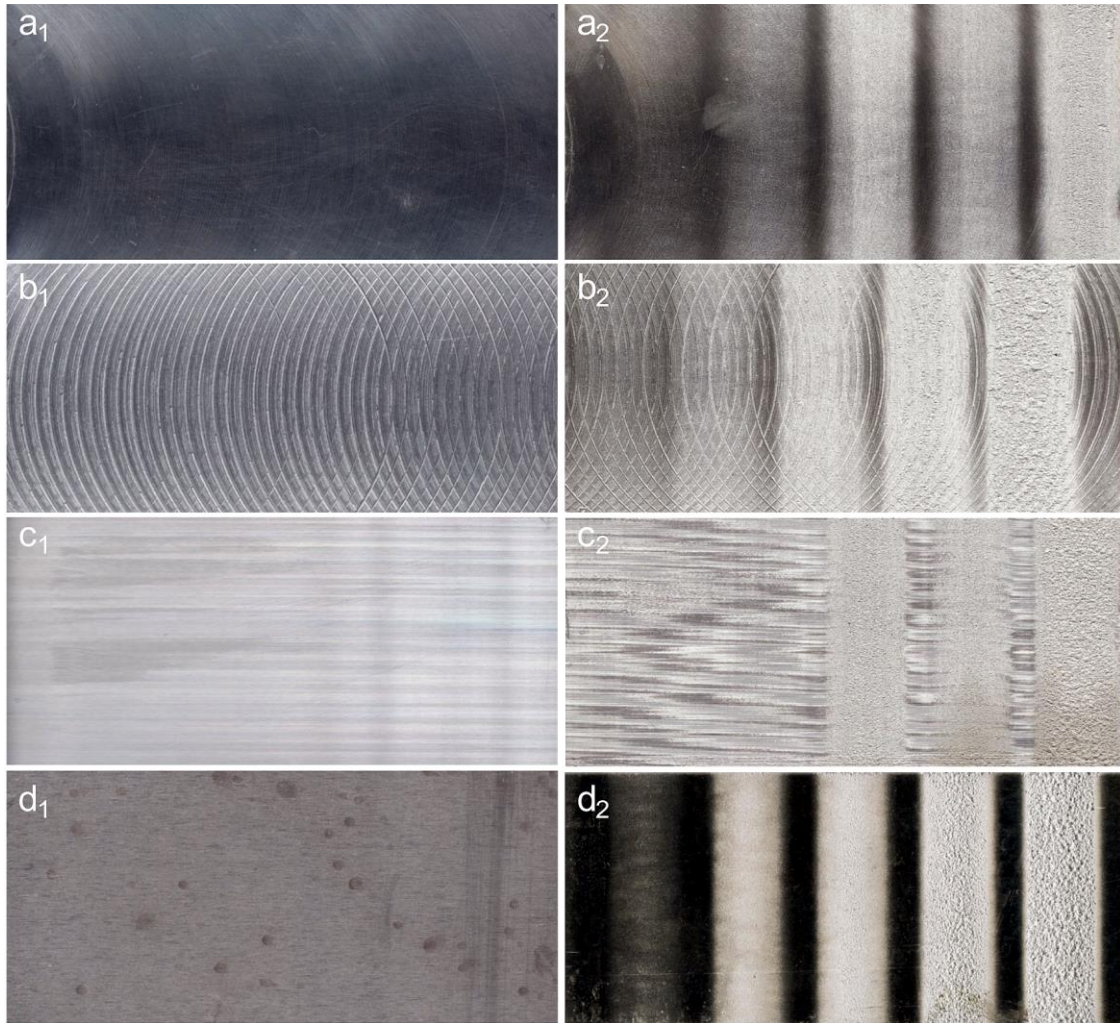


Figure 1: Left column: Appearance of initial surfaces of EN AW 5083 H111 samples after treatment by various technologies a1) fine milling, b1) rough milling, c1) planing, d1) rolling. Right column: Traces formed by PWJ on pre-treated surfaces, a2) fine milling, b2) rough milling, c2) planing, d2) rolling. Traversing velocities: 4; 2; 1; 0.75 and 0.5  $\text{mm}\cdot\text{s}^{-1}$  (from left to right).

### 3 Experimental procedure

To enable to expose the sample surface to the effect of the pulsating water jet, the following testing procedure was developed (Fig. 2). A robotic arm ensured the nozzle movement with an exactly programmed trajectory. During experiments, the traversing velocity of the nozzle was set to 0.5; 0.75; 1; 2 and 4  $\text{mm}\cdot\text{s}^{-1}$ ; the stand-off distance was set to 55 mm. This stand-off distance was determined as optimal for experimental conditions based on previous tests [7]. The angle of incidence was set to  $90^\circ$ .

The tests were performed at the operating pressure of 20 MPa (the corresponding jet velocity was approx.  $180 \text{ m}\cdot\text{s}^{-1}$ ). Pressure pulsations were generated in a pulsating water jet generator at the frequency of 20.09 kHz (the readout displayed by the ultrasonic generator); the amplitude of vibration of the ultrasonic sonotrode tip was set to 7  $\mu\text{m}$ .

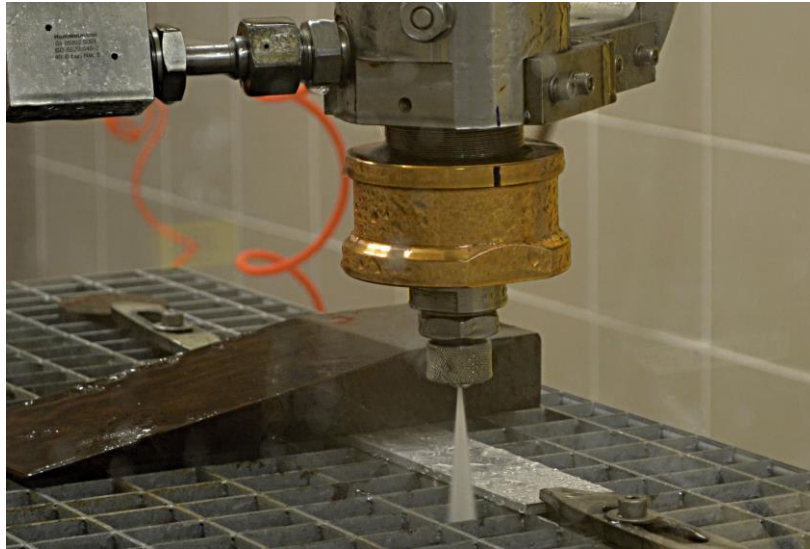


Figure 2: Pulsating water jet method on surface sample.

Each sample was exposed to the action of the pulsating jet in five areas according to a predefined experimental plan based on variations of the traversing velocity of the pulsating water jet (Fig. 1).

Subsequently, the optical profilometer FRT MicroProf was used for the 3D determination of sample surfaces (Fig. 3). Measured data were processed using the SPIP software. Fig. 4 shows the areas of  $40 \times 5$  mm measured on tested surfaces. The distance of measurement points for every tested surface profile was set to  $4 \mu\text{m}$  in y direction and  $250 \mu\text{m}$  in x direction. Then, five profiles in each kerf of the obtained topography were analysed. After averaging, the profile was analysed and the 2D surface parameter Ra was finally determined.

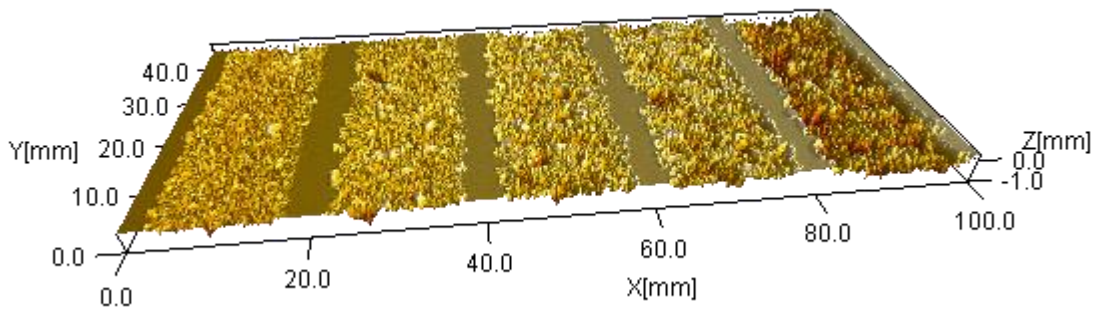


Figure 3: 3D visualization of formed traces on pre-treated (planed) surface.

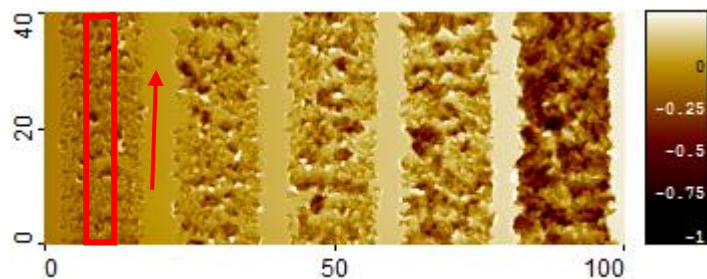


Figure 4: Designation of measured areas and profile direction on pre-treated surface.

## 4 Results and discussion

The values of the parameter  $Ra$  in relation to the traversing velocity of the jet  $v$  and the initial surface treatment of a material are presented in Tab. 3.

Table 3: Parameters of surfaces created by pulsating water jet technology.

Surface treatment	$Ra_{ini}$ [ $\mu\text{m}$ ]	$v$ [ $\text{mm}\cdot\text{s}^{-1}$ ]				
		4	2	1	0.75	0.5
	Before PWJ effect	$Ra$ [ $\mu\text{m}$ ]				
Fine milling	0.9	1.4	1.9	4.5	5.4	23.4
Rough milling	4.5	7.9	9.2	14.7	30.8	60.3
Planing	2.6	4.0	6.8	15.2	21.9	46.6
Rolling	0.5	2.6	7.2	33.2	51.3	74.6

The least roughened initial surface with an average value of  $Ra = 0.5 \mu\text{m}$  was achieved on a surface affected by the rolling technology. This value was measured in a direction perpendicular to the rolling direction. The roughness of  $Ra = 0.9 \mu\text{m}$  was achieved on a fine milled surface. The planing technology showed the roughness of  $Ra = 2.6 \mu\text{m}$  in a direction perpendicular to the direction of the cutter. The roughest surface with the value of  $Ra = 4.5 \mu\text{m}$  was created using the rough milling technology.

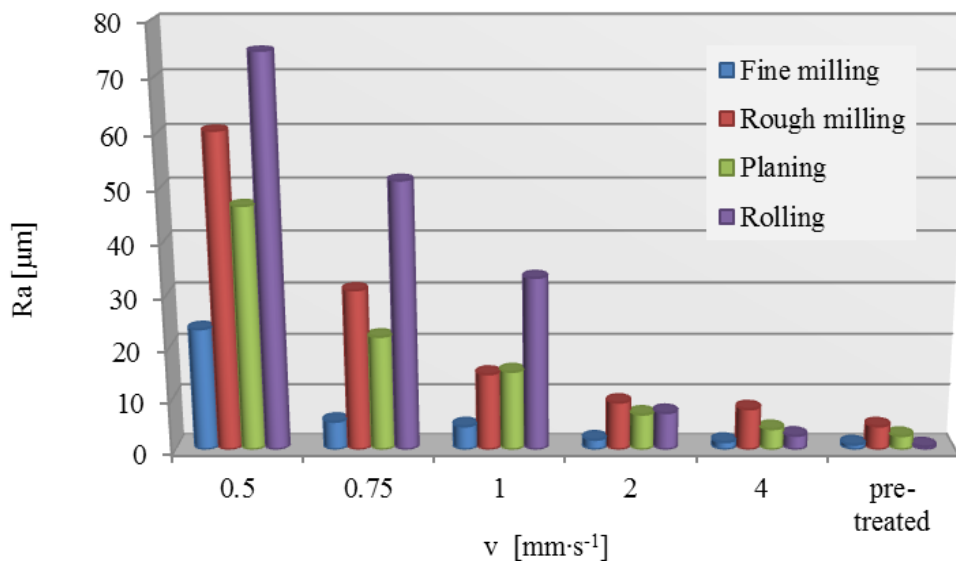


Figure 5: Effect of traversing velocity  $v$  on arithmetical mean of profile  $Ra$ .

Obtained results indicate that the surface pre-treatment of a material has a significant effect on the surface topography after the application of the pulsating water jet (Tab 3). Fig. 5 shows the surface roughness  $Ra$  in relation to the traversing velocity  $v$  on various tested surfaces. It can be observed that at the traversing velocity  $v = 4 \text{ mm}\cdot\text{s}^{-1}$ , the roughness  $Ra$  does not really differ from its initial values. The roughest surface is the rough milled surface, followed by the planed surface, then the rolled surface and finally the surface treated by the fine milling. At the traversing velocity  $v = 2 \text{ mm}\cdot\text{s}^{-1}$ , the PWJ has even stronger effect and roughness order of the rolled surface is changed. At the traversing velocity  $v = 1 \text{ mm}\cdot\text{s}^{-1}$ , the PWJ effect on material surface is very strong and the roughness of the rolled surface increases rapidly. In contrast, the parameter  $Ra$  does not change considerably on both roughly and finely milled surfaces. At the traversing velocity  $v = 0.75 \text{ mm}\cdot\text{s}^{-1}$ , the value of  $Ra$  for fine milled surface is still low. The  $Ra$  value increases significantly in case of other surfaces. At the lowest traversing velocity  $v = 0.5 \text{ mm}\cdot\text{s}^{-1}$ , very large volume removal occurs on every surface. Accordingly, the value  $Ra$  increases significantly on all surfaces.

To compare the roughness of surfaces before and after treatment of the PWJ, the parameter  $Ra_{ratio}$  was used, where  $Ra$  represents the roughness of surface after the PWJ treatment and  $Ra_{ini}$  represents the roughness of initial surface untreated by the PWJ:

$$Ra_{ratio} = \frac{Ra}{Ra_{ini}}. \quad (1)$$

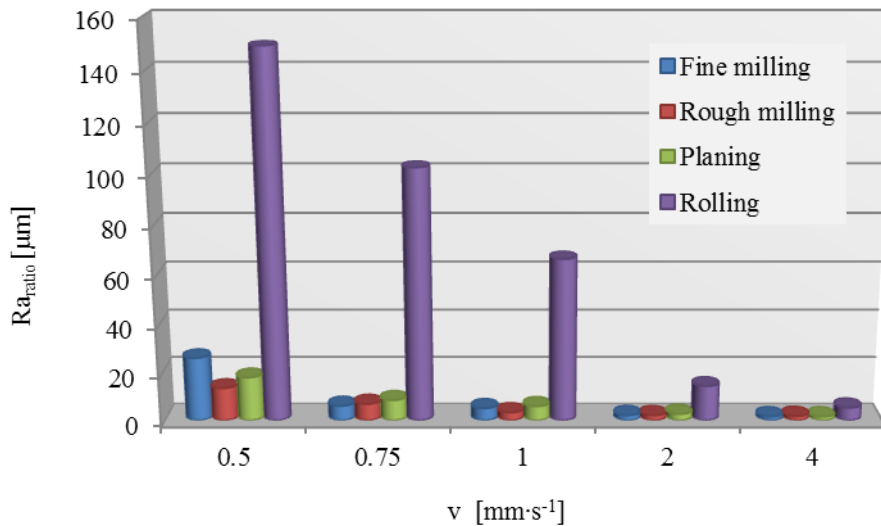


Figure 6: Relative roughness  $Ra_{ratio}$  between original surface and the surface affected by PWJ at different traversing velocity  $v$ .

If we look at Fig. 6 showing the ratio of the roughness  $Ra$  (1) before and after the PWJ action, we can realize that the roughness of the rolled surface treated by the PWJ at the traversing velocity  $v = 0,5 \text{ mm}\cdot\text{s}^{-1}$  has increased 150 times, by other surfaces only approximately 20 times.

The assumptions that surfaces with significant roughness (after rough milling) disrupt the effect of the PWJ and that the radial flow of the liquid on the surface aligns peaks created by rough milling were confirmed. Values of roughness  $Ra$  are very similar to the values of the rolled and milled surfaces before the PWJ action. However, significant difference between these two surfaces occurs after using the PWJ. This could be caused by hardening of the surface layer during milling, which results in its greater resistance to the impact of the PWJ.

## 5 Conclusion

Experimental work oriented on the evaluation of effects of the pulsating water jet on surfaces treated by different technologies shows that the erosion caused by repeated impacts of water pulses depends on the initial conditions of a material surface.

Generally, the highest values of roughness after the pulsating water jet application were achieved on surfaces pre-treated by the rolling and consequent annealing which relieved stresses in surface layer. In contrast, other surface treatments based on various machining methods strengthened surface layers and thereby hindered the jet from easy penetration into the material.

Next steps of the research in this area should be oriented to the study of the influence of the surface layer hardness on the erosion process caused by effects of the pulsating water jet and the investigation of changes of properties of surface layers due to impacts of the water pulses.

## Acknowledgments

Presented work has been supported by the ASCR project No. AV0Z30860518 and by the Ministry of Industry and Trade of the Czech Republic project No. FV 10446 and the project Institute of clean technologies for mining and utilization of raw materials for energy use, reg. No. CZ.1.05/2.1.00/03.0082, supported by the Research and Development for Innovations Operational Programme financed by the Structural Funds of the European Union and from the means of the State budget of the Czech Republic.

## References

- [1] S S. Cook: Erosion by water hammer. Proceedings of the Royal Society, pp. 481-488, London, 1928
- [2] C. Bai, S. Chandra, B. Daniels, B. Ren, W. Yan, A. Tieu, M. Vijay: Abrasive-entrained high-frequency pulsed waterjet: basic study and applications. Proceedings of the 18th International Conference on Water Jetting, pp. 325-336, Gdansk, 2006
- [3] F. W. Bach, A. Schenk, G. Kremer, C. Biskup, O. Meier, M. Fargas, J. Bunte, P. Jäschke: Increase of erosive potential of water jets by laser pulsing. Proceedings of the 18th International Conference on Water Jetting, pp. 357-366, Gdansk, 2006
- [4] J. Foldyna, B. Švehla: Method of generation of pressure pulsations and apparatus for implementation of this method. CZ patent 299 412, 2008
- [5] L. Sitek, J. Foldyna, P. Martinec et al.: Use of pulsating water jet technology for removal of concrete in repair of concrete structures. Baltic journal of road and bridge engineering, pp. 235-242, 2011
- [6] Z. Riha, J. Foldyna: Ultrasonic pulsations of pressure in water jet cutting tool. Technical Gazette, pp. 487-491, 2012
- [7] J. Foldyna, J. Klich, P. Hlaváček et al.: Erosion of metals by pulsating water jet. Technical Gazette, pp. 381-386, 2012
- [8] P. Hreha, S. Hloch, P. Monka, K. Monková, L. Knapčíková, P. Hlaváček, M. Zelenák, I. Samardžić, D. Kozak: Investigation of sandwich material surface created by abrasive water jet (AWJ) via vibration emission. Metalurgija, pp. 29-32, 2014
- [9] P. Hreha, A. Radvanská, J. Cárach, D. Lehocká, K. Monková, G. Krolczyk, A. Ruggiero, I. Samardžić, D. Kozak, S. Hloch: Monitoring of focusing tube wear during abrasive waterjet (AWJ) cutting of AISI 309. Metalurgija, pp. 533-536, 2014
- [10] P. Hreha, A. Radvanská, S. Hloch, V. Peržel, G. Królczyk, K. Monkova: Determination of vibration frequency depending on abrasive mass flow rate during abrasive water jet cutting. International Journal of Advanced Manufacturing Technology, 2014
- [11] G. Krolczyk, S. Legutko: Experimental analysis by measurement of surface roughness variations in turning process of duplex stainless steel. Metrology and Measurement Systems, pp. 759-770, 2014
- [12] S. Wojciechowski, P. Twardowski, M. Wiczorowski: Surface texture analysis after ball end milling with various surface inclination of hardened steel. Metrology and Measurement Systems, pp. 145-56, 2014

# Effects of continuous and pulsating water jet on CNT/concrete composites

V. Foldyna<sup>1,2\*</sup>, J. Foldyna<sup>2</sup>, D. Klichova<sup>2</sup>, J. Klich<sup>2</sup>, P. Hlavacek<sup>2</sup>, L. Bodnarova<sup>3</sup>, T. Jarolim<sup>3</sup> and K. M. Kutlakova<sup>1</sup>

<sup>1</sup> Nanotechnology Centre, VSB-Technical University of Ostrava, 17, listopadu 15/2172, 70833 Ostrava-Poruba, Czech Republic

<sup>2</sup> Department of Material Disintegration, Institute of Geonics of the ASCR, v.v.i., Studentská 1768, 708 00 Ostrava – Poruba, Czech Republic

<sup>3</sup> Institute of Technology of Building Materials and Components, Faculty of Civil Engineering, Brno University of Technology, Veveří 331/95, 602 00 Brno, Czech Republic

\*e-mail: vladimir.foldyna@ugn.cas.cz

## Abstract

This paper presents first results of the study of the resistance of CNT/concrete composite to the action of continuous and pulsating water jets. The experiments oriented at the determination of erosion effects of pulsating and continuous water jets impinging the surface of reference (concrete) and CNT/concrete composite samples were performed. Tested samples were characterized by X-ray diffraction and scanning electron microscope. Samples were exposed to pulsating and continuous water jets at various operating parameters. Erosion effects of pulsating and continuous jets were evaluated in terms of material removal rate. The possible influence of addition of CNTs to the concrete on its resistance to the action of continuous and pulsating water jets is discussed in the paper.

**Keywords:** pulsating and continuous water jet, CNT/concrete composite, surface topography, material erosion

## 1 Introduction

In past years, concrete was used worldwide in the field of civil engineering [1]. The main advantages of cement based composites are ease for construction, room temperature setting, low cost and the ready availability of properties and performance data for design and construction [2]. The major weakness of traditional cement based material is low tensile strength and can be easily crack, which affect durability, safety and strength of concrete structures. Tensile strength of plain concrete is between 2 – 8 MPa [3]. Although many types of fillers were used to improve properties especially toughness of cement based composites. Used fillers increased tensile strength, but has only slight effect on initiation of micro-cracks as a result of volumetric changes due to high autogenous shrinkage stresses and delaying only macro-cracks. There is a big effort to adapt to the flexural and tensile mechanical properties of the matrix in order to improve the fracture and damage resistance of concrete. To deal with disadvantages of reinforcement of cementitious material mentioned above is typically provided at the micro and milli-scale using microfibers and macrofibers. Concrete matrix however exhibit flaws at the nanoscale, where traditional fillers are not effective [4-9].

With spreading of nanotechnology into various technology specializations comes also application in concrete composites. Nanomaterials provide unique multifunction properties due to its size. A new types of reinforced polymers, nanoparticles ( $\text{TiO}_2$ ,  $\text{Fe}_2\text{O}_3$ ,  $\text{SiO}_2$ ) and especially carbon nanotubes (CNTs) are suitable micro-fillers for these composites, because of its high strength at atomic scale [10].

Nanomaterials has these beneficial effects on the microstructure and properties of cement nanocomposites:

- fill in free space between cement grains and prevent flow of water
- form crystalline centers and speeds up cement hydration process
- support creation of small crystals such as  $\text{Ca}(\text{OH})_2$  and uniform agglomeration of C-S-H products
- speed up pozzolanic reactions, which consume  $\text{Ca}(\text{OH})_2$  and produce additional C-S-H gel
- enhance contact area, which increase bonding strength between aggregates and cement compound

CNTs are one of the most promising filler to improve concrete nanocomposite properties. Carbon nanotubes are hexagonal nets formed from rolled up graphene into cylindrical nanostructured tubes. Some of them are ended with fullerene hemispheres. There are two main groups of CNTs: single-walled carbon nanotubes (SWCNTs) and multi-walled carbon nanotubes (MWCNTs). SWCNTs consist from single rolled up graphene sheet and MWCNTs are composed of two or more layers of graphene. MWCNTs are cheaper to prepare so they are used more often than SWCNTs. Moreover, MWCNTs offer better reinforcement in cement composites. Due to their exceptional chemical and physical properties (thermal conductivity, electrical conductivity, low specific weight, and high resistance to corrosion) they have many applications in industry such as: electronic materials, medicine, chemistry [11-13].

Researchers of Institute of Geonics of the Academy of Science of Czech Republic have been studying problematics of water jet for more than two decades. Water jet technology is recommended for removal of surface layers and concrete surface treatment before the repair action by the Ministry of Transport of the Czech Republic. It is not recommended only in Czech Republic, but in many other countries. In the articles we usually compare effect pulsating and continuous water jet on various materials. Disintegration of surface is higher when the structure is damaged and lower strength [14].

## 2 Preparation and characterization of tested samples

### 2.1 Preparation

Concrete was not fully hydrated, hydration was stopped after 9 days and samples were took for characterization by scanning electron microscopy (SEM) and X-ray diffraction (XRD). We were trying to examine if addition of CNTs speed up the hydration process or change the structure in first third of strengthening of concrete, which takes 28 days.

### 2.2 Characterization

#### 2.2.1 X-ray Diffraction

Samples were characterized by XRD patterns measured under CoK $\alpha$  irradiation ( $\lambda = 1.789 \text{ \AA}$ ) using the Bruker D8 Advance diffractometer (Bruker AXS) equipped with a fast position sensitive detector V $\dot{A}$ NTEC 1.

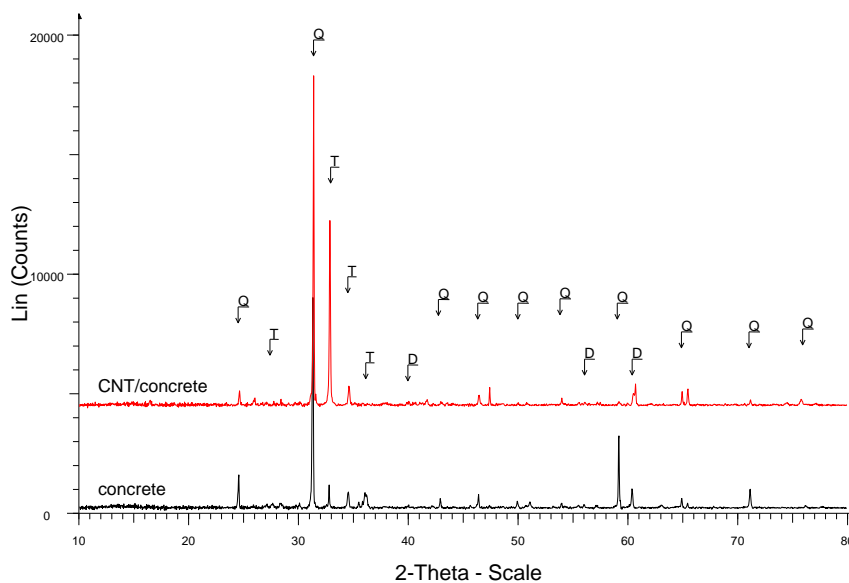


Figure 1. XRD pattern of concrete and CNT/concrete composite. Q – Quartz, D – Dicalcium silicate, T – Tricalcium silicate.

As you can see in Figure 1 Quartz and non-hydrated phases of Portland cement overshadowed the hydrated phases. Tricalcium and dicalcium silicate indicates that concrete was not fully hydrated.



### 2.2.2 Scanning electron microscopy

Samples were also analysed by ASPEX PSEM Explorer in Figure 2 and 3.

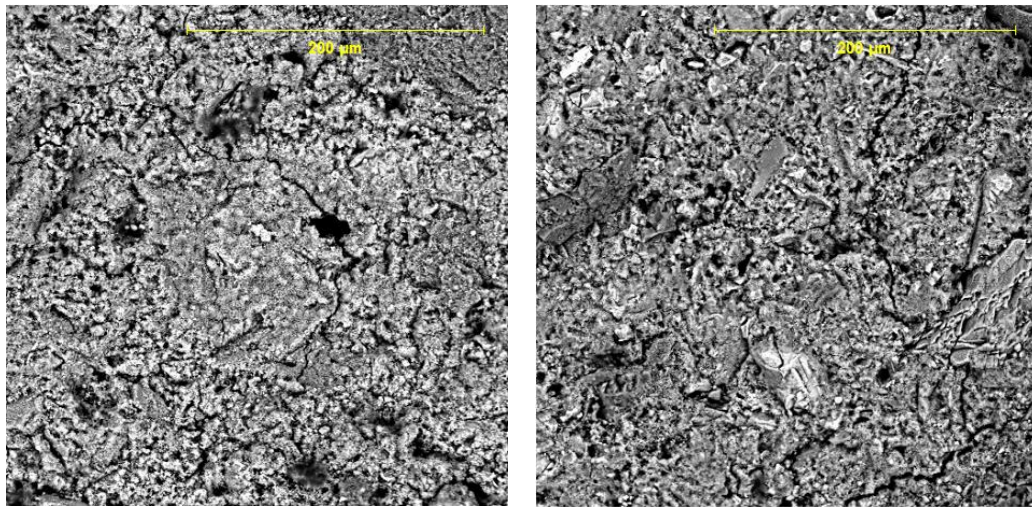


Figure 2. Photograph of concrete (left) and CNT/concrete (right).

There is no big difference we can observe in the structure of concrete and CNT/concrete. Only thing we can see is that concrete was not fully hydrated.

## 3 Experiments

The experiments oriented at the determination of erosion effects of pulsating (PWJ) and continuous (CWJ) water jet impinging the surface of reference (concrete) and CNT/concrete composite samples were performed in the Waterjet laboratory of the Institute of Geonics. Disintegration effects of high-speed water jets were tested and evaluated to compare their effects on CNT/concrete composite and reference samples.

### 3.1 Laboratory equipment and testing conditions

The experimental assembly for water jetting tests consisted of the high-pressure plunger pump Hammelmann HDP 253 (delivering up to  $67 \text{ l}\cdot\text{min}^{-1}$  at the maximum operating pressure of 160 MPa), a pulsating water jet head (with a 20 kHz ultrasonic generator) installed on the arm of the ABB IRB 6640 robot. The PWJ head (high-speed water jet) was moved over the tested sample by the robot using various traversing velocities. The commercially available nozzle StoneAge Attack 0.075" (nozzle diameter  $d$  was 1.90 mm) was used in the experiment to generate both continuous and pulsating jets. Two values of operating pressure  $p$  20 and 40 MPa were used in experiments. Standoff distances  $SOD$  of 25 mm (at 20 MPa) and 35 mm (at 40 MPa) were determined in previous experiments to be optimal for given testing conditions. Traversing velocity  $v_{TR}$  was changed from 10 to  $80 \text{ mm}\cdot\text{s}^{-1}$  during tests at 20 MPa and from 50 to  $160 \text{ mm}\cdot\text{s}^{-1}$  during tests at 40 MPa. Proprietary method of the generation of the pulsating liquid jet based on the generation of acoustic waves by the action of the acoustic transducer on the pressure liquid and their transmission via pressure system to the nozzle (so called acoustic generator of pressure pulsations) was used to generate PWJ. Acoustic generator of pressure pulsations used in experiments generated pressure pulsations at the frequency of about 20 kHz (exact frequency depends on the actual geometrical configuration of the generator), amplitude of vibrations of the acoustic transducer was set to  $7 \mu\text{m}$ . More details on the method of PWJ generation used in the experiments can be found elsewhere [15, 16]. Schematic drawing of the experimental setup is given in Figure 3.

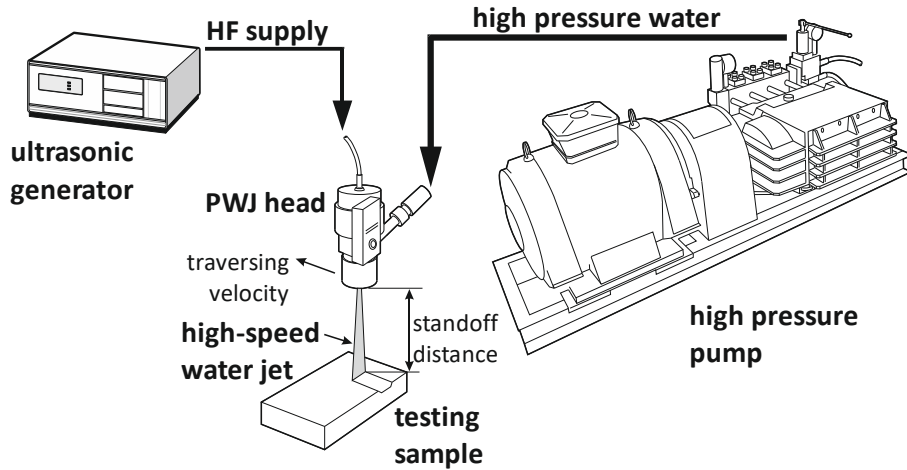


Figure 3. Schematic drawing of the experimental setup.

### 3.2 Experimental procedure

Erosion effects of PWJ and CWJ on CNT/concrete composite and reference (concrete) samples exposed to their action under various operating parameters were evaluated in terms of material removal rate. Grooves created by the action of the jets were measured using MicroProf FRT optic profilometer and 2D and 3D images of grooves were created and the volume of removed material  $V$  was determined using SPIP software. Evaluated length of the groove  $l$  was 20 mm, 56 grooves were processed in total. Subsequently, material removal rate  $\Delta V$  was determined using following formula:

$$\Delta V = \frac{V \cdot v_{TR}}{l} [\text{mm}^3 \text{ s}^{-1}]$$

## 4 Results and discussion

Results of evaluation of erosion effects of PWJ and CWJ on CNT/concrete composite and reference samples are presented in form of graphs in Figures 4 and 5. From obtained data was created 3D views, which you can see in Figures 6 – 9.

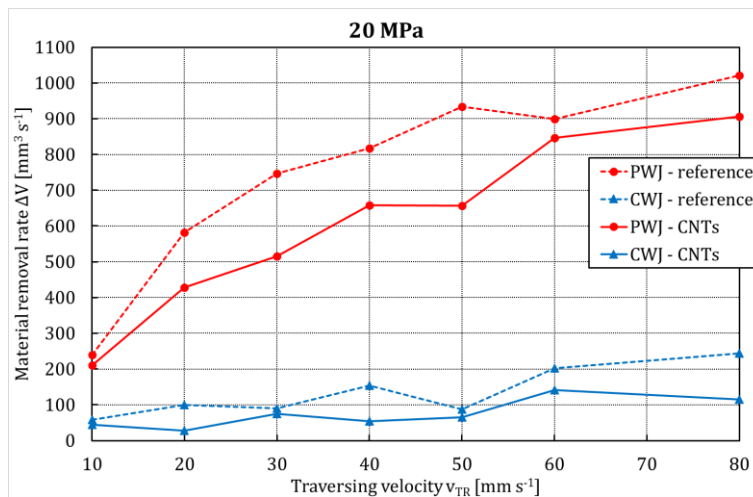


Figure 4. Influence of traversing velocity  $v_{TR}$  on the material removal rate  $\Delta V$  in CNT/concrete composite and reference concrete exposed to CWJ and PWJ generated at 20 MPa.

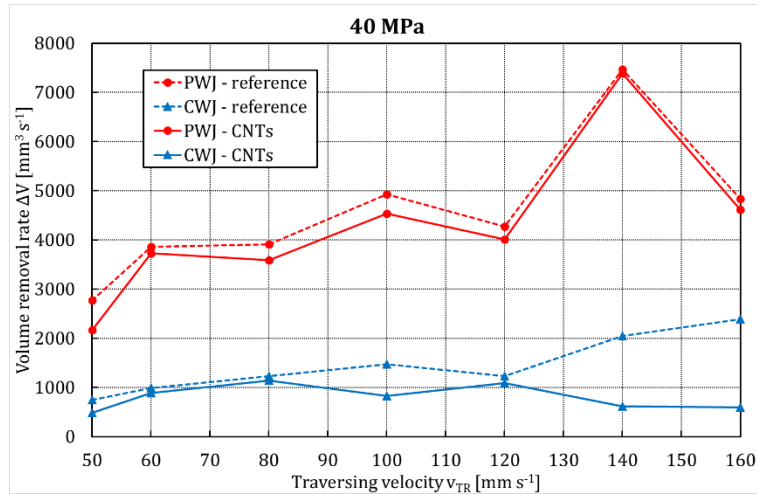


Figure 5. Influence of traversing velocity  $v_{TR}$  on the material removal rate  $\Delta V$  in CNT/concrete composite and reference concrete exposed to CWJ and PWJ generated at 40 MPa.

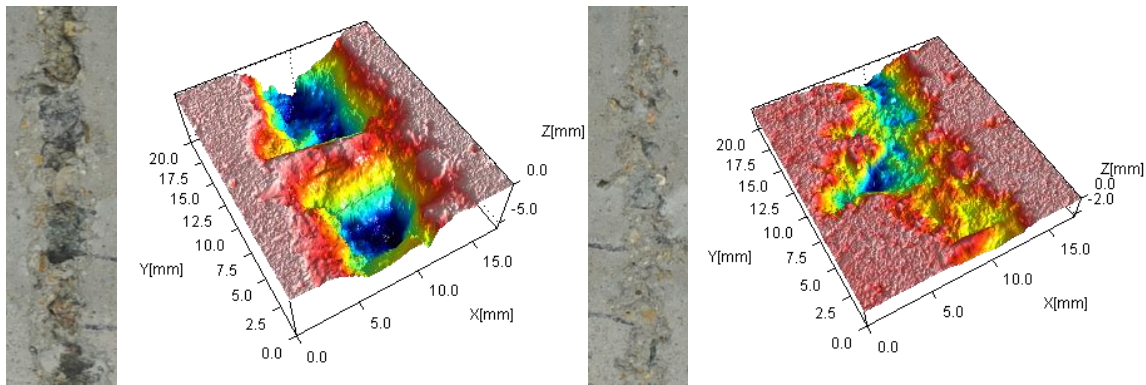


Figure 6. Photograph and 3D view of the groove created by the PWJ (left) and CWJ (right) in reference concrete sample (operating pressure  $p = 20$  MPa, traversing velocity  $v_{TR} = 40$  mm s<sup>-1</sup>).

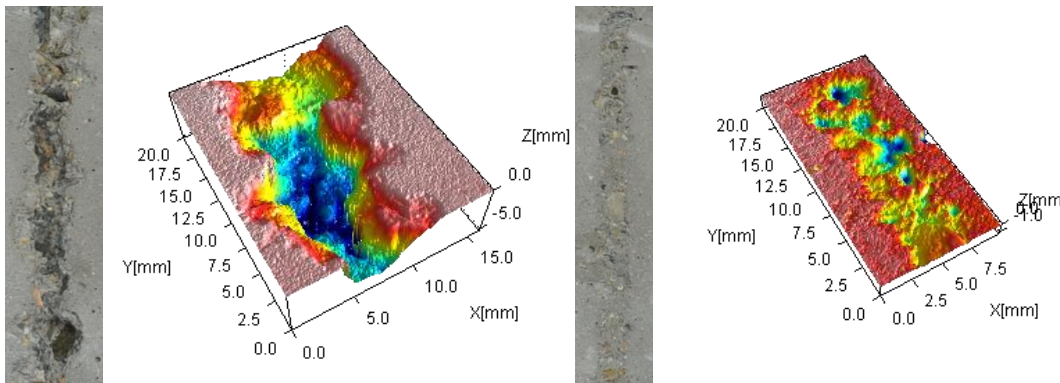


Figure 7. Photograph and 3D view of the groove created by the PWJ (left) and CWJ (right) in CNT/concrete composite sample (operating pressure  $p = 20$  MPa, traversing velocity  $v_{TR} = 40$  mm s<sup>-1</sup>).

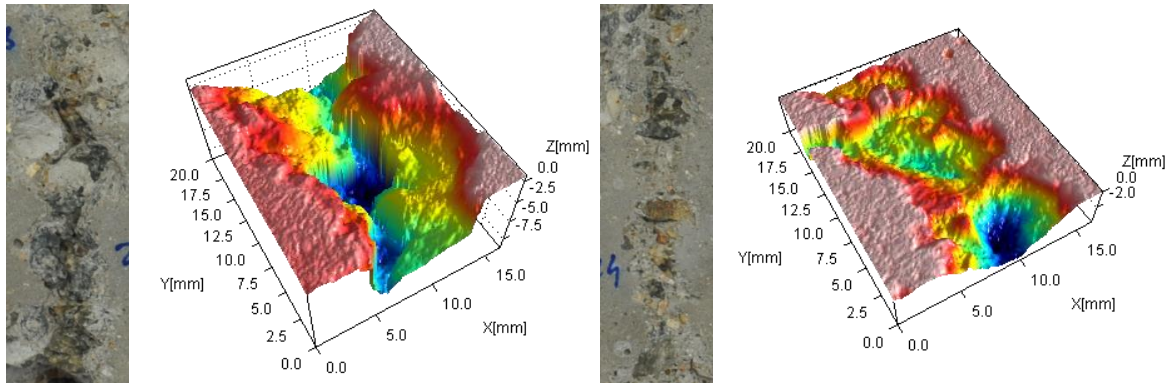


Figure 8. Photograph and 3D view of the groove created by the PWJ (left) and CWJ (right) in reference concrete sample (operating pressure  $p = 40$  MPa, traversing velocity  $v_{TR} = 120$  mm s<sup>-1</sup>)

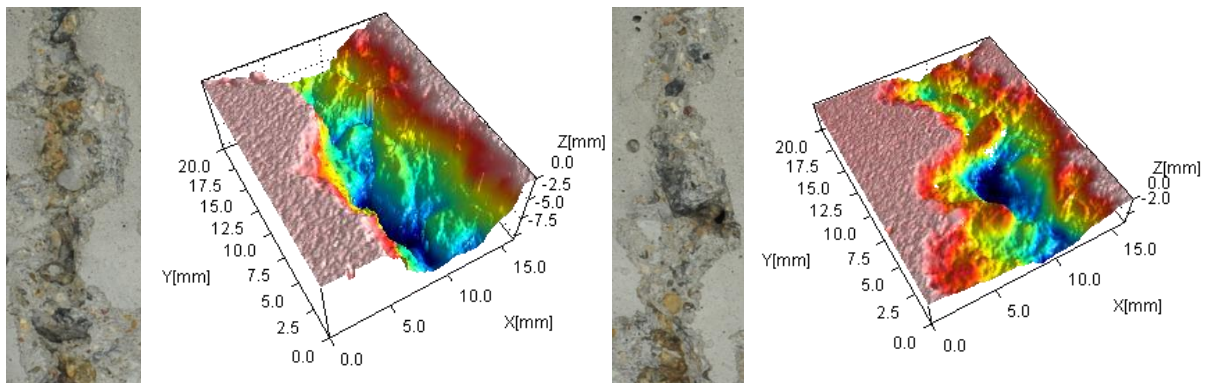


Figure 9. Photograph and 3D view of the groove created by the PWJ (left) and CWJ (right) in CNT/concrete composite sample (operating pressure  $p = 40$  MPa, traversing velocity  $v_{TR} = 120$  mm s<sup>-1</sup>)

## 5 Conclusions

Experimental part aimed on effects of pulsating and continuous water jet showed that erosion depend on traversing velocity and operating pressure. Graphs showed that decomposition by pulsating water jet was higher at all measured traversing velocities and both pressures. Highest volume removal rate 7500 mm<sup>3</sup>·s<sup>-1</sup> was obtained by using traversing velocity 140 mm·s<sup>-1</sup> and pressure 40 MPa. CNTs strengthen the concrete matrix.

The next research should be focused on preparing CNT composites only with Portland cement and not whole concrete. Next evaluation should be done after 28 days, because after nine days of hydration there were not enough hydrated phases to see them by X-ray diffraction.

## 6 Acknowledgement

The work presented in the paper was performed under the support of the project of the Czech Science Foundation “Study of methods of nanoparticles dispersion, determination of conditions for preventing their re-agglomeration for application in cement composites”, reg. no. 15-23219S, the Institute of Clean Technologies for Mining and the Utilization of Raw Materials for Energy Use – Sustainability program, reg. no. LO1406 financed by the Ministry of Education, Youth and Sports of the Czech Republic, and the long-term conceptual development of the research institution RVO: 68145535 and by the Ministry of Education, Youth and Sports of Czech Republic (project reg. no. SP2016/67). The authors are thankful for the support.

## References

- [1] Q. Li, J. Liu and S. Xu: Progress in Research on Carbon Nanotubes Reinforced Cementitious Composites. *Advances in Materials Science and Engineering*. 2015, 1-16. DOI: 10.1155/2015/307435. ISSN 1687-8434. <http://www.hindawi.com/journals/amse/2015/307435/papa>
- [2] J. Foldyna, V. Foldyna and M. Zelenak: Dispersion of Carbon Nanotubes for Application in Cement Composites. *Procedia Engineering*. 2016, 149, 94-99. DOI: 10.1016/j.proeng.2016.06.643. ISSN 18777058. <http://linkinghub.elsevier.com/retrieve/pii/S1877705816311511>
- [3] A. M. Neville and J. J. Brooks: *Concrete Technology*. Longman Scientific & Technical, Harlow, UK, 1987.
- [4] S. Xu and Q. Li: Theoretical analysis on bending behaviour of functionally graded composite beam crack-controlled by ultrahigh toughness cementitious composites. *Science in China, Series E: Technological Sciences*, vol. 52, no. 2, pp. 363–378, 2009.
- [5] V. C. Li and C. K. Leung: Theory of steady state and multiple cracking of random discontinuous fiber reinforced brittle matrix composites. *Journal of Engineering Mechanics*, vol. 118, pp. 2246–2264, 1992.
- [6] N. P. Balaguru and S. Shah: *Fiber-reinforced cement composites*. New York: McGraw-Hill, c1992. ISBN 0070564000
- [7] A. M. Okeil, S. El-Tawil and M. Shahawy: Short-term tensile strength of carbon fiber-reinforced polymer laminates for flexural strengthening of concrete girders, *ACI Structural Journal*, vol. 98, no. 4, pp. 470–478, 2001.
- [8] T. Y. Lim, P. Paramasivam and S. L. Lee: Analytical model for tensile behavior of steel-fiber concrete. *ACI Materials Journal*, vol. 84, no. 4, pp. 286–298, 1987.
- [9] C. Zweben: Tensile failure of fiber composites. *AIAA Journal*, vol. 6, no. 12, pp. 2325–2331, 1968.
- [10] S. Iijima. Helical microtubules of graphitic carbon. *Nature* 1991;354:56–8
- [11] S. KANG, J. SEO and S. PARK: The Characteristics of CNT/Cement Composites with Acid-Treated MWCNTs. *Advances in Materials Science and Engineering*. 2015, 1-9. DOI: 10.1155/2015/308725. ISSN 1687-8434.
- [12] N. Grobert: Carbon nanotubes – becoming clean. *Materials Today*. 2007, 10(1-2), 28-35. DOI: 10.1016/S1369-7021(06)71789-8. ISSN 13697021. <http://linkinghub.elsevier.com/retrieve/pii/S1369702106717898>
- [13] V. Popov: Carbon nanotubes: properties and application. *Materials Science and Engineering: R: Reports* 2004, 43(3), 61-102 [cit. 2016-03-29]. DOI: 10.1016/j.mser.2003.10.001. ISSN 0927796x. <http://linkinghub.elsevier.com/retrieve/pii/S0927796X03001268>
- [14] L. Sitek, L. Bodnarova, J. Valek, M. Zelenak, J. Klich, J. Foldyna a M. Novotny. Effects of Water Jet on Heat-Affected Concretes. *Procedia Engineering*. 2013, 57, 1036-1044 DOI: 10.1016/j.proeng.2013.04.131. ISSN 18777058. <http://linkinghub.elsevier.com/retrieve/pii/S1877705813008643>
- [15] J. Foldyna, B. Svehla: Method of generation of pressure pulsations and apparatus for implementation of this method. US patent No. 7,934,666, 2011.
- [16] J. Foldyna, L. Sitek, J. Scucka, P. Martinec, J. Valicek, K. Palenikova: Effects of pulsating water jet impact on aluminium surface. *Journal of Materials Processing Technology*, 209, 20(2009), pp. 6174–6180.

# High productivity and precision technology and equipment for ultrasonically aided micro-electrical discharge machining

N.L. Carutasu<sup>1</sup>, D. Ghiculescu<sup>1</sup>

<sup>1</sup> *University POLITEHNICA of Bucharest, Romania*

## Abstract

The ultra-miniaturization is the well-known trend that has been developed continuously in high technology areas such as ICT, micro-electronics, micro-optical, automotive, aeronautics, etc. The necessity to process new advanced materials, surfaces whose complexity and accuracy increased permanently, has represented a major challenge for the used technologies. Micro-electroerosion (Micro-Electrical-Discharge Machining -  $\mu$ EDM) assisted by ultrasound ( $\mu$ EDM + US) are able to answer to this challenge. These technologies can achieve micro-surfaces with high precision and complexity in any electrical conductive, difficult or impossible to machine by conventional cutting. The paper presents some aspects of ultrasonic aiding of micro-EDM ( $\mu$ EDM+US) process and equipment. This technology consists in longitudinal oscillations of tool, with a frequency of 40 kHz having several improvements on material removal process in comparison with classic EDM. The first one is an efficient gap flushing and removed particles evacuation. Furthermore, it is obtained a spectacular increase of machining rate due to ultrasonic additional mechanisms of material removal. It is also observed surface quality improvement (roughness and white layer decrease) due to micro-peaks removal through ultrasonic shock waves, oriented parallel to the machined surface. The melted material is removed by hydraulic forces of dielectric that can access the EDM spot because the reduced life time of gas bubble around plasma channel that is ultrasonically collapsed.

**Keywords:** micro electrical discharge machining, ultrasonics, machining rate, surface roughness, precision.

## 1 Introduction

At international level,  $\mu$ EDM has a continuous development with a higher dynamic in South East Asia as it will be presented; some results of  $\mu$ EDM+US were also reported. At Romanian level,  $\mu$ EDM is very rare used only on up-to-date EDM installations, but ultrasonic assistance of microEDM is not all used. If Romanian EDM users should want to resist on the market, it is a *sine qua non* condition to approach this up-to-date evolution of EDM ( $\mu$ EDM+US), which is cost less than nowadays  $\mu$ EDM approaching.

Micro-machining defines the processes that achieve products in the range of 1 to 999  $\mu$ m, according to CIRP committee of Physical and Chemical processes. The present trend of ultra-miniaturization led to  $\mu$ EDM applications, microscopic mechanical components and devices. In this respect, the  $\mu$ EDM technology is helpful for precision machining as well as for microcomponents, filigree structures up to 5  $\mu$ m. A large range of products can be achieved like fuel injector valves, parts and components for medical devices, micro-moulds, stamping tools, micro-electronic parts etc. For this type of EDM, the discharge energy must be minimized and consequently, also the size of the gap at a width of 1  $\mu$ m [1].

The increments of 0.2  $\mu$ m of the feed system, the lowest reported in the state of the art [1], are effectuated gradually by the equipment achieved in the project, after a short delay (sample time), as gap increases. Thus this  $\mu$ EDM requirement is attained.

MicroEDM is considered a very flexible machining process in different variants. Three versions of big industrial applications are micro-die sinking ( $\mu$ -die sinking), micro-wire electrical discharge machining ( $\mu$ -WEDM) and micro-electrical discharge drilling ( $\mu$ -ED drilling). The other  $\mu$ EDM variants with less industrial relevance are micro-electrical discharge milling ( $\mu$ -ED milling), micro-electrical discharge grinding ( $\mu$ -EDG), and micro-wire electrical discharge grinding ( $\mu$ -WEDG).

The  $\mu$ EDM process features two very important bottlenecks as encountered problems (Figure 1):

- $\mu$ EDM is rather slow machining process. The material removal rate is relative low comparing to conditions of EDM occurring at very narrow working gaps (under 5  $\mu\text{m}$ ), characteristic of  $\mu$ EDM, leading to process instability. It is also a serial process (successive discharge). For example, lithography and electrochemical machining have parallel nature making them more productive [2].
- The second bottleneck is shape inaccuracies due to high tool wear. Several solutions to improve machining rate were undertaken. A research direction was to drill multiple holes with multiple electrodes. The pocket-sized EDM permits many clamping systems to be placed on a large part, drilling several holes at the same time. More recently, other attempts to use multiple electrodes at microEDM were reported, obtaining a raise of machining rate [3]. However, the attempt to increase the number of electrode-tools working in parallel does not lead necessarily to proportional augment of machining rate due to increased number of short-circuits and consequently, corresponding retracts of electrode-tool. An optimum number of tools working in parallel to increase machining rate is needed to be found experimentally.

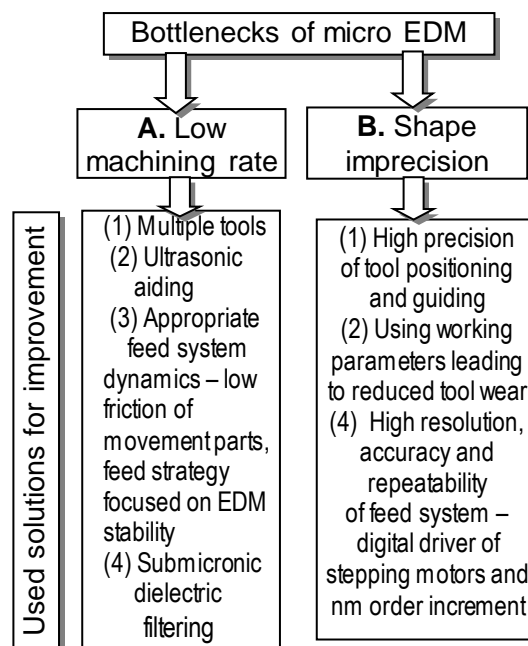


Figure 1: Encountered problems at microEDM and adopted solutions

## 2 Project aims

The project “High productivity and precision technology and equipment for microelectrical discharge machining aided by ultrasonics” aims at achieving an ultra-performing technology and equipment dedicated to micro-die sinking and micro-drilling which can be assembled on any classic electrical discharge machining (EDM) installation, due to its modular conception. The market segment which is targeted by project end products are Micro, Small and Medium Enterprises (SMEs), which execute surfaces with transversal dimensions of 100...999  $\mu\text{m}$  in any electrically conductive material. Commonly, such SMEs have low financial resources and cannot afford buying an up-to-date EDM installation of hundreds EUR, which is not necessarily specialized in microEDM.

The equipment will solve the well-known process instability characteristic to very narrow working gap between electrode-tool and workpiece, which in this case, has only 1...5  $\mu\text{m}$ , determining frequent short-circuits. This inconvenient determines a lot of tool retracts from the working gap and consequently, very low machining rate, poor quality of machined surface, lack of precision etc.

Our technology of ultrasonic aiding of micro-EDM ( $\mu$ EDM+US) consists in longitudinal oscillations of tool, with a frequency of 40 kHz having several improvement actions on material removal process: efficient gap flushing and removed particles evacuation, spectacular increase of machining rate due to ultrasonic additional mechanisms of material removal, surface quality improvement, i.e. roughness and white (melted

and re-solidified) layer decrease due to micro-peaks removal through ultrasonic shock waves oriented parallel to the machined surface, and melted material removed, hydraulic forces of dielectric liquid acting on melted material because the decreased life time of gas bubble around plasma channel that is ultrasonically collapsed.

The equipment comprises a specialized EDM generator of very low pulses energies (ignition voltage  $u_0=90V$ , minimum current  $I=100\text{ mA}$ , pulse time  $t_i=0.1\text{...}2\text{ }\mu\text{s}$ ), ultrasonic generator with automatic control of frequency of 40 kHz, synchronized with EDM generator, a feed system with  $0.2\text{ }\mu\text{m}$  resolution and a filtering unit of dielectric liquid with under  $1\text{ }\mu\text{m}$  finesse rating, ultrasonic chains with vibrating electrode-tool at their ends with amplitude  $A=1\text{...}2\text{ }\mu\text{m}$ , clamping and orientation devices for ultrasonic chains and workpieces with precision of  $1\text{ }\mu\text{m}$ . An optimized technology will result in terms of working parameters aiming at machining rate increase with more than 100%, surface roughness and volumetric relative wear decrease up to 50% in comparison with classic micro-EDM (unaided by ultrasonics) in the same working conditions.

The equipment for micro-EDM aided by ultrasonic longitudinal oscillations of electrode-tool, dedicated to micro-die sinking and micro-drilling in the range of  $100\text{...}999\text{ }\mu\text{m}$ , has high machining rate and precision. It comprises (see Figure 2): low energy EDM pulses generator; ultrasonic generator with 40 KHz automatic controlled frequency, synchronized with EDM generator, feed system of EDM working head with  $0.2\text{ }\mu\text{m}$  resolution, unit for pumping with pressure of 7 MPa, and filtering dielectric liquid with under  $1\text{ }\mu\text{m}$  finesse rating, ultrasonic chains integrating the electrode-tools, orientation and clamping devices for ultrasonic chain and workpiece with  $1\text{ }\mu\text{m}$  precision level.

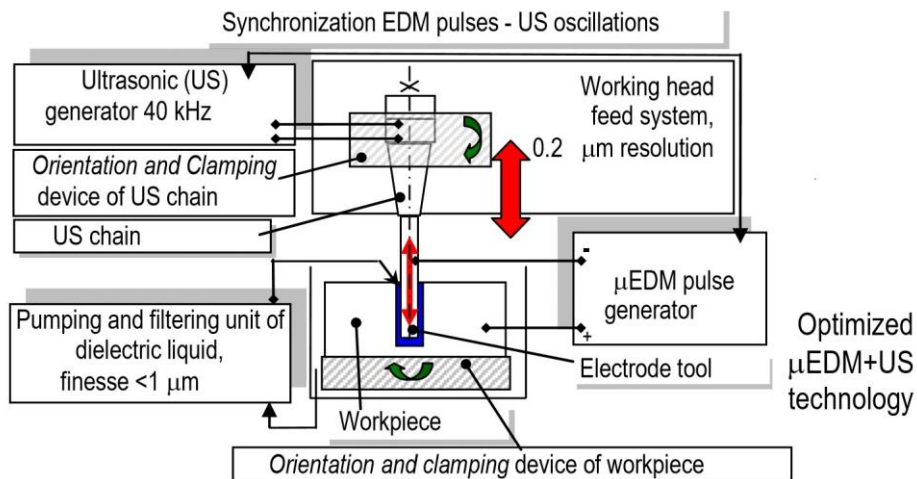


Figure 2: Scheme of ultrasonic aiding microEDM equipment components and technology.

### 3 Project contribution

The results of this project extend the grow of technological performances of EDM+US in the micro-domain comparatively to classic EDM in the same working conditions through decrease of machined surface roughness and relative volumetric wear with up to 50%; increase of machining rate over 100%, approaching different EDM sinking types and  $\mu$ drilling in the range  $100\text{--}999\text{ }\mu\text{m}$ . The  $\mu$ EDM+US dedicated modular equipment can be assembled on any classic EDM machine, decreasing costs of 10 times against acquisition of up-to-date machine. The SMEs market segment is addressed that use EDM, aiming at their performances increase though overtaking strategies - combination between focused costs and differentiation strategies. Compared to classic EDM,  $\mu$ EDM is focused on the following items [4], synthesized in Figure 3:

**Strict control of discharge parameters:** frequency of discharge (pulse and pause time), level of the energy input, (current, voltage and pulse time) - the minimum discharge energy of  $0.1\text{ }\mu\text{J}$  is obtainable in the project frame, assured by a very small material removal at one single discharge and an extremely small gap width, ranging from  $1\text{ to }5\text{ }\mu\text{m}$ , achieved through the gap following strategy mentioned above.

**High precision control of electrodes motion** - At actual installations, the feed is achieved through a servo system with highest sensitivity and positional accuracy of  $0.5\text{ }\mu\text{m}$  on the X, Y and Z axes movement. Our



earlier experiments done on Z axis with 0.5 μm resolution, associated with the following strategy mentioned above, confirmed a good stability of material removal process. The results are expected to be better since the feed system parameters in the project will be superior to the ones from the state of the art, i.e. resolution 0.2 μm, repeatability and positioning precision under 1 μm.

**Requirement concerning the wear of the electrodes and compensation for the wear** - since μEDM operates at very short discharge durations from  $t_i = 10 \text{ ns}$  to  $t_i = 2.5 \text{ μs}$ , the tool electrode is usually charged as the cathode to reduce tool electrode wear [3]. This is explained by the polarity effect, which is also included in famous Van Dijk's model, validated by relatively recent data - overheated material next to EDM spot with 200-300K over the boiling temperature and material removal by sudden boiling after pulse end - the basis of FEM modelling in our previous papers [5-9]; graphite, WC or WCu (very thermally and mechanically resilient) are used for tool electrodes, the relative wear can be over 30%, very visible at machined edges and corners due to increased electric field intensity.

**Improved understanding of μEDM process removal** and the factors that affect it like material properties, thermal conduction of the workpiece, melting and recasting processes, and their effect on the surface finish/integrity - these are our goals in the project frame, and also previously published papers, by undertaking FEM studies at micrometre scale, validated by experimental data concerning material removal mechanism and phenomena from the gap visualized by ultra-speed camera with at least  $10^6$  frames/s; Improved flushing of the gap, evacuation of the removed particles from the process - this is in strong correlation with gap size and working of dielectric unit. Taking into account the gap width of several μm, a filtering capacity under 1 μm is recommended. The issue of dielectric liquid has to be considered too. Dielectric oil with lower kinematic viscosity,  $v \leq 1.8 \times 10^{-6} \text{ m}^2/\text{s}$  (appropriate for μm gap size), is used in the micro-die sinking process. In comparison to dielectric oil, deionized water contributes to a higher surface quality and material removal rate. These could be explained by the following phenomena: water viscosity is lower, allowing the development of the plasma channel and consequently, a lower energy density on EDM spot from machined surface; the water has higher conductivity determining a greater gap size and therefore an improved evacuation of the removed particles from the gap. In order to avoid the secondary effect of electrolysis, negative polarity will be used aiming at achievement of additional anodic dissolution of the workpiece material, and thus increasing the machining rate too.

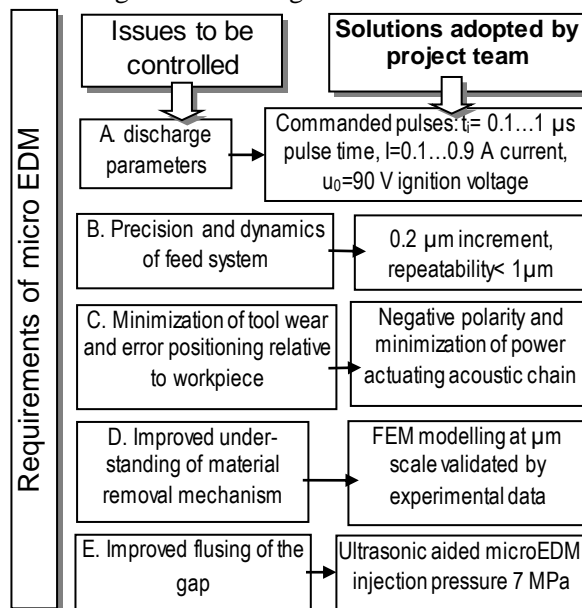


Figure 2: MicroEDM scientific and technical barriers addressed by this project.

#### 4 Conclusions

The equipment dedicated to micro-machining through ultrasonic aided addresses the market segment of SMEs that use electrical discharge machining, but they are not afford to buy an upto-date machine with prices between 200000-400000 EUR, because usually they not have high financial resources. These new machines, which are not necessarily specialized in μ EDM, have some limits of performances in micro field

– the EDM generator does not provide discharges with low energy level, in agreement to this field requirements; reduced capabilities for clamping the electrode-tools with dimensions lower than 0.1 mm on the work head; filtration of dielectric liquid with appropriate finesse dielectric to the size of the working gap, injection pressure of several MPa, needed to exceed the hydraulic resistance caused by reduced section of flowing holes through workpiece, electrode-tool and very narrow lateral and frontal gap etc.

It is estimated that in Romania, there are at least 500 EDM classic machines from Romanian ELER series or second hand ones provided by foreign manufacturers, used by SMEs that apply electrical discharge machining in a large diversity of fields. The equipment dedicated to  $\mu$ EDM+US, project end-product, can be assembled on these machines due to its modular design. The feed system with 0.2  $\mu$ m resolution is assembled on work head, blocking the existing system with lower precision (hydraulic or electro-mechanical); The  $\mu$ EDM and ultrasonic generators are attached, which are synchronized, that supply the machining, respectively the ultrasonic chain; The mobile unit for pumping and filtration of dielectric liquid is attached, having a submicronic filtering capacity, and 7 MPa injection pressure.

The  $\mu$ EDM+US equipment and technology are original and innovative, having several novelty elements at world level, which will be the topics of some patent requests and already granted ones [10-12] such as: orientation and fastening of ultrasonic chains and workpieces with micrometric precision; the generator dedicated to  $\mu$ EDM+US with polluting pulse aiming at generation of pulse trains within ultrasonic semiperiod of dielectric liquid stretching, synchronized with US generator, optimized technology of  $\mu$ EDM+US with two innovative approaches: pulses overlapping on cumulative microjets stage (or delivering in temporal proximity), and previous craters borders removal through the effect of shock waves produced by ultrasonic cavitation parallel to machined surface, consequently growing machining rate with over 100% and lowering surface roughness with up to 50%, in comparison with the classic machining unaided by ultrasonics. The enterprises that will buy the equipment and optimized technology dedicated to  $\mu$ EDM+US could gain competitive advantage against their competitors through protected innovative solutions at Romanian Patent Office.

## Acknowledgment

The presented results were obtained through the projects: Joint Applied Research Project supported by MENUFISCDI, project no. PN-II-PT-PCCA-2013-4-0236, Contract no. 222/2014.

## References

- [1] E. Uhlmann, M. Reohner, M. Langmack: Micro EDM in Qin Yi, Micromanufacturing Engineering and Technology, Elsevier 2010.
- [2] E. Uhlmann, S. Piltz, U. Doll: Machining of micro/miniature die and moulds by electrical discharge machining – recent development, Journal of Materials Processing Technology, Elsevier, 2005.
- [3] K. Takahata, Y.B. Gianchandani: Batch mode micro-electro-discharge machining, Journal of MEMS, pp. 102-110, vol. 11 no. 2. 2002.
- [4] S. Piltz: Grundlagen und Prozessstrategien der Mikrofunktenerosion für die Bearbeitung von Rotationsbauteilen, Fraunhofer IRB Verlag, Stuttgart, 2007.
- [5] D. Ghiculescu, N.I. Marinescu, S. Nanu, Da. Ghiculescu, R. Gonczi: Finite element method study on machined shape influence at ultrasonic aided and not aided microelectrodischarge machining, Nonconventional technology Review, p. 33-40, nr. 3, 2011
- [6] D. Ghiculescu, N. Marinescu, O. Alupeii, N. Carutasu: Finite element modelling of hydraulic mechanical removal mechanism at ultrasonically aided EDM finishing. Nonconventional Technologies Review/Revista de Tehnologii Neconventionale, vol. 19, no. 3, 1 Sep., 2015.
- [7] D. Ghiculescu, N. Marinescu, O. Alupeii, N. Carutasu: Some Issues Regarding Finite Element Modelling of Micro-Electrical Discharge Machining Aided by Ultrasonics. In Key Engineering Materials, pp. 683-688, vol. 651, Trans Tech Publications, 2015.

- [8] D. Ghiculescu, N. Marinescu, T. Klepka, N. Carutasu: On Correlation of Pulses and Tool Elongations at Micro-Electrical Discharge Machining Aided by Ultrasonics. In Applied Mechanics and Materials, pp. 309-314, vol. 809, Trans Tech Publications, 2015.
- [9] Ghiculescu D, Marinescu N, Alupei O, Carutasu N. On influence of workpiece geometry at hydraulic mechanical removal mechanism of ultrasonically aided EDM finishing. Nonconventional Technologies Review/Revista de Tehnologii Neconventionale, vol.19, no.4, 1 Dec., 2015.
- [10] Ghiculescu, D., Marinescu N.I., Nanu, S., Equipment for ultrasonic aiding of electrical discharge machining of microslots, Romanian granted patent, RO-126191. (30.05.2012).
- [11] Ghiculescu, D., Marinescu N.I., Nanu S., Equipment for deep microslots machining through electrical discharge machining aided by ultrasonics, Romanian granted patent, RO-125516 (29.11.2013).
- [12] Marinescu N.I., Ghiculescu, D., Nanu S., Equipment for microholes finishing by electrical discharge machining aided by ultrasonics. Romanian granted patent, RO-1269381 (30.07.2015).

# Determining focusing nozzle wear by measuring AWJ diameter

M. Prijatelj<sup>1</sup>, M. Jerman<sup>1</sup>, P. Drešar<sup>1</sup>, H. Orbanic<sup>1</sup>, I. Sabotin<sup>1</sup>, J. Valentinčič<sup>1</sup> and A. Lebar<sup>1,2</sup>

<sup>1</sup> *University of Ljubljana, Faculty of Mechanical Engineering, Slovenia*

<sup>2</sup> *University of Ljubljana, Faculty of Health Sciences, Slovenia*

## Abstract

Abrasive water jet (AWJ) cutting is a very versatile technology, but is limited by a relative poor accuracy. The main problem is that the diameter of jet is unknown, as there is no device on the market that would enable quick and easy measurement of diameter. With such instrument the diameter could be regularly measured, nozzle wear monitored and the offset adjusted. This would greatly improve quality control of the process and accuracy of the cut. This paper investigates the usage of the through beam laser sensor for monitoring jet diameter and nozzle wear. Experiments were conducted on five differently worn nozzles, with two different water pressures, with and without abrasive. Results show that sensor is capable of monitoring the jet diameter and nozzle wear, but is very susceptible to spraying of the jet and abrasive sticking to screens of the sensor. Results also show that jet diameter correlated better with the diameter of focusing nozzle, when taking measurements without the abrasive.

**Keywords:** optical measurement, laser measurement, abrasive water jet, nozzle diameter, jet diameter

## 1 Introduction

Abrasive water jet (AWJ) technology utilizes a high pressure stream of water to accelerate abrasive particles, which then erode a narrow line in stock material. Main advantages of this technology are the ability to cut virtually all materials and no heat affected zone, while disadvantages are mainly related to relatively poor accuracy, which is usually between 0.05 mm and 0.1 mm [1]. Source of poor accuracy lies in geometrically non-defined and flexible tool which bends as it cuts and brakes-up as it enters the atmosphere. Result of jet brake-up is tapered and striated cut, which can be partially solved by tilting the cutting head. The other problem is determining jet diameter, since radius of the jet is used as tool offset during programme setup. Tool offset is currently set as radius of a new nozzle. This means that parts cut with new nozzle can achieve accuracy of  $\pm 0.08$  mm, but as the nozzle wears and diameter increases the accuracy drops. The other method for determining offset, is by cutting a test piece and measuring dimensions of that piece. The new offset is then calculated from the measured dimensions and the one required[2]. This method is both time consuming and produces waste material. Another problem is uneven nozzle wear [3] which means that at some point offset can no longer be adjusted and nozzle has to be replaced.

For industrial applications, a quick and easy to use instrument for measuring jet diameter is needed. An instrument that measures jet diameter prior to the machining and displays correct offset would improve accuracy of the cut and provide a better quality control. Several instruments for measuring the jet diameter have already been developed. Orbanic et. al. [4] measured AWJ diameter by passing cutting head over a load cell while AWJ was on. The device determined the diameter by measuring the force of the jet on the load cell at a constant feed rate. Problem with this device is the wear of the measuring probe which distorts further measurements on the same spot of the probe. Folkes and Li [5] measured the jet diameter using optical instruments. First sensor was a non-contact LED micrometre which projects a parallel line on the surface of the jet and with a CCD camera then measures the contour it forms on the surface. The second sensor used a narrow beam laser that detected a change in intensity as the AWJ passed across the beam. The diameter was calculated by using constant feed rate and a time difference between changes in intensity. It is questionable whether it is possible to measure AWJ diameter using a through beam laser, which is an optical instrument for measuring hard tools. Such a method could be used to monitor nozzle wear, adjust its offset and determine when nozzle needs to be replaced.

## 2 Experimental setup

### 2.1 Measuring instrument

The instrument used for measuring jet diameter was Keyence digital display compact laser through beam sensor LX2-V10W series (Keyence, JP). Sensor was designed to measure a diameter or a gap between objects and works using a shadowing method. On one side the line laser emits light and on the other side the receiver measures the amount of light passed through an obstacle. Controller then calculates the amount of received light and displays percentage. If there is nothing between laser and receiver the value is 100 %. If there is an object between the laser and receiver the amount of light decreases and controller displays the percentage of light that object covers, as shown in Figure 1.

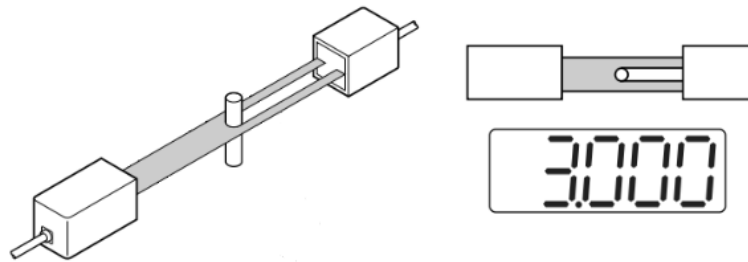


Figure 1: Keyence sensor. [6]

Sensor uses 5 mm wide laser beam with the wave length of 780 nm and repeatability of 10  $\mu\text{m}$ . The controller has an analog voltage output that was connected to Arduino Uno microcontroller (Arduino LLC, USA) in order to store and process the acquired data.

In order to avoid getting damaged by water, it was enclosed in waterproof casing, like shown in Figure 2.

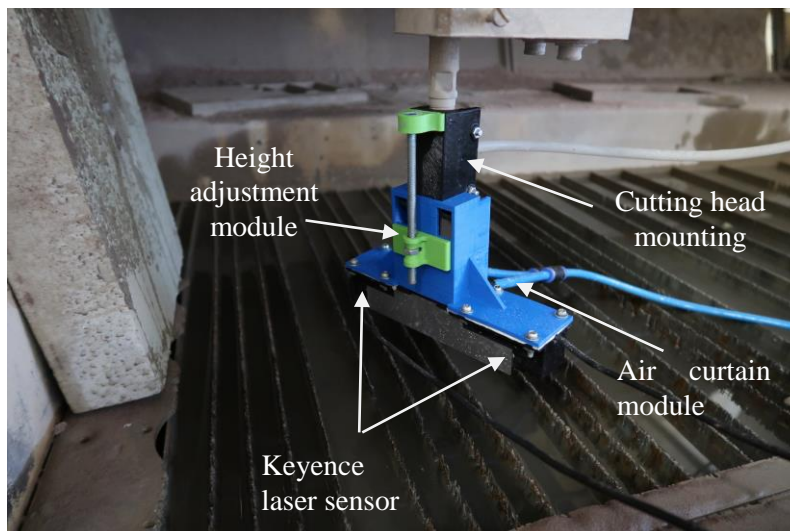


Figure 2: Waterproof casing designed to protect laser sensor from water.

### 2.2 Casing

The casing was designed to fit firmly onto the cutting head while enabling height adjustment of the sensor. This is achieved with threaded rod and a nut. By turning the nut, the sensor is then raised or lowered in order to measure the jet diameter at the desired distance from the focusing nozzle.

Both, the sensor transmitter and receiver were kept in boxes that are sealed by transparent screen, made out of 1 mm thick acrylic glass on one side. The effect of this material on measurements, was tested by measuring the calibration blocks. Sensor characteristic is shown in Figure 3 **Error! Reference source not found.**

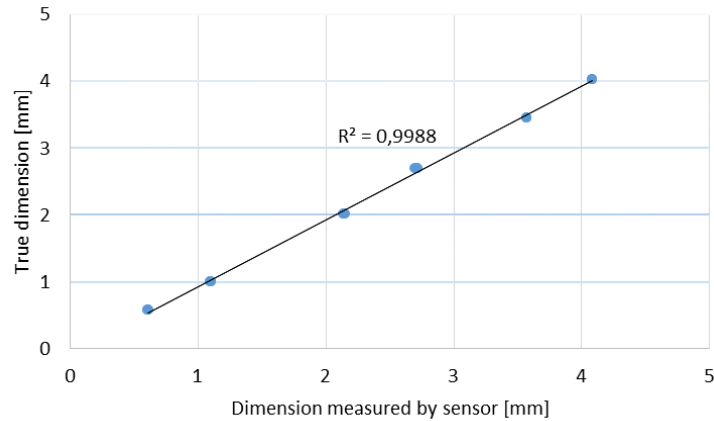


Figure 3: Sensor calibration characteristics.

During the initial tests some droplets landed on screens of either laser transmitter or receiver due to the jet spray or its splash back from the catcher tank. This caused a significant distortion of the measuring results, so a module that creates a air curtain barrier and a splash guard were designed. Air curtain module creates a stream of air at around  $20^\circ$  angle away from jet, to prevent interaction between jet and air. Splash guard was designed to prevent the back splashing of water onto the screens, while enabling air from air curtain module to escape. Air curtain module and splash guard are shown in Figure 4.

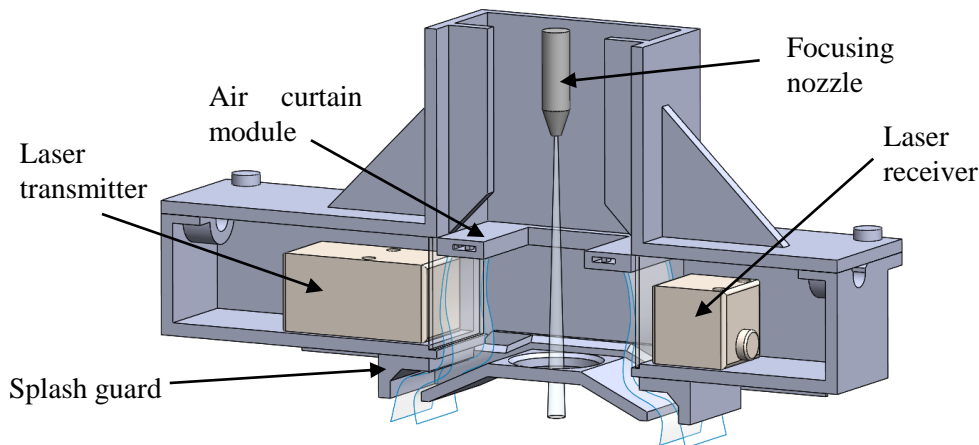


Figure 4: Cross section of casing showing air curtain and splash guard.

### 2.3 Measuring the focusing nozzle diameter

In the experiment, five focusing nozzles were used, each with different wear. Two nozzles were 0.76 mm in diameter when new and three were 1.02 mm in diameter when new. Length of all nozzles was the same and was 76.20 mm. Before the experiment the diameters of the focusing nozzle were measured. Using a Mitutoyo microscope (Mitutoyo, JP) designed for observing tool wear, surface quality, etc. The microscope was equipped with a 2.0 Mega-pixel CCD camera and a software tools MoticImages Plus 2.0 to process the acquired pictures and measure the diameter of the nozzles. Positioning accuracy of the microscope table was 0.001 mm. nozzles were observed under 30 x magnification with illumination from above. The diameter was measured by selecting three points on the inner edge of the nozzle, from which the programme then calculated the radius. For every nozzle, the diameter was measured at least four times. The number of measurements depended on the nozzle wear. The more the nozzle is worn, the more times it was measured. Images of nozzle diameters are shown in **Error! Reference source not found.** and average diameters are shown in Table 1.

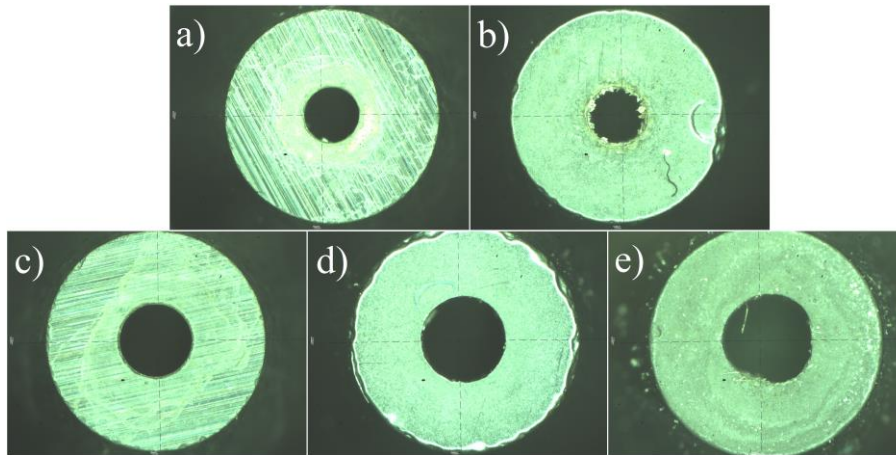


Figure 5: Images of focusing nozzles taken with Mitutoyo microscope: a) 0.76 mm new, b) 0.76 mm old, c) 1.02 mm new, d) 1.02 mm old, e) 1.02 mm very old.

Table 1: Average focusing nozzle diameter measured with the microscope.

Nozzle diameter (new) [mm]	Average nozzle diameter [mm]
0.76 new	0,832
0.76 old	0,904
1.02 new	1,095
1.02 old	1,301
1.02 very old	1,364

From the images we can see that when the nozzle is new the hole is almost perfectly round, but as the wear starts to increase the roundness slowly decreases. Figure 5c shows why, at some point, increasing the offset is no longer an option and the nozzle has to be replaced. That is also the reason why monitoring the nozzle wear is of great importance for a good quality control.

#### 2.4 Experimental procedure

Measurements were conducted on Omax 2652A machine (Omax, USA), equipped with the Ecotron 403 high pressure water pump (BFT GmbH), capable of reaching pressures of 400 MPa. Experiments were conducted at water pressures of 200 MPa and 275 MPa, using the orifice diameter of 0.3 mm. Measurements were done with and without the abrasive, for which the garnet mesh 80# was used. The jet diameter measurements were taken at the exit from the focusing nozzle. Experimental setup is shown in Figure 6.

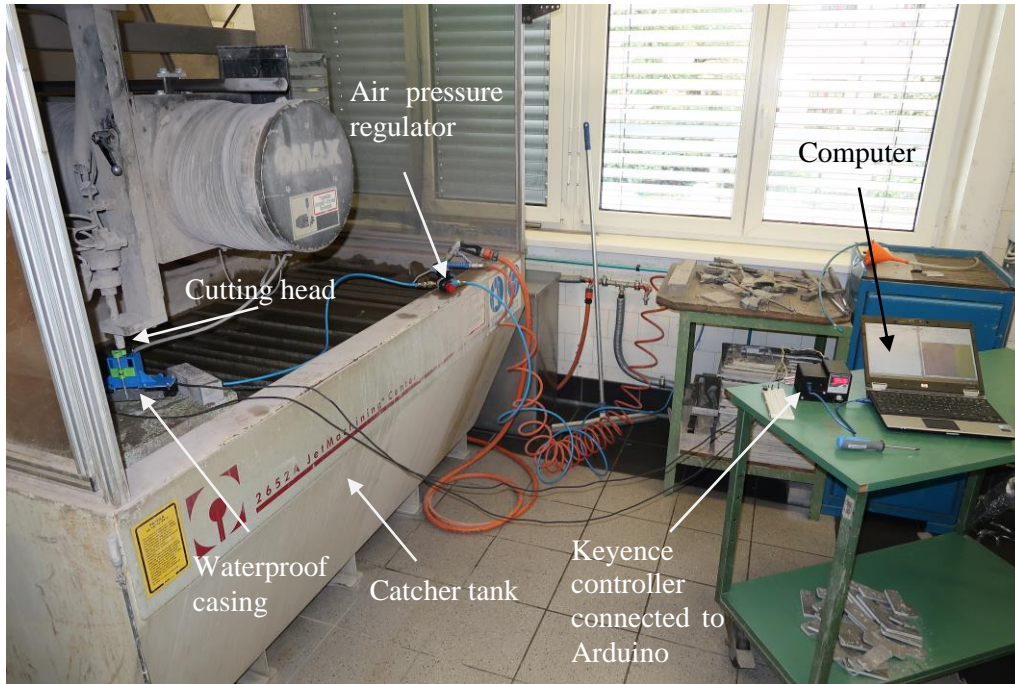


Figure 6: Experimental setup

Firstly the nozzle is mounted onto cutting head and then the casing was mounted onto cutting head. By turning the nut on the back of the casing, the sensor was raised until it reached the tip of the nozzle. After turning the jet on, the microcontroller then read the values from sensor and converted them into values between 0 and 1023. Collected data was then copied to Microsoft Excel and processed so that it was transformed into mm and corrected by calibration. Three measurements were taken for each setup combination.

### 3 Results

Arduino programme was set to measure the jet diameter for 3 s with a frequency of 100 Hz. Purpose of this test was to determine whether it is possible to get a reliable measurement in a short time and to see the effect of abrasive. Figure 7 shows measurements obtained by the device. Measurements are labelled as new focusing nozzle diameter - type of jet - test number (for example 0.76 WJ 1 means that measurement involves focusing nozzle 0.76 mm in diameter, without abrasive and is the first repetition).

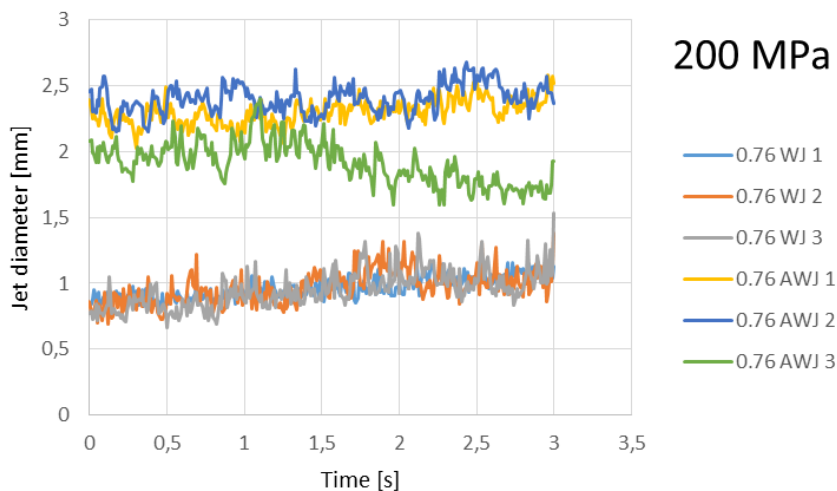


Figure 7: Results from measurements using a new 0.76 mm focusing nozzle at 200 MPa of water pressure.



From Figure 7 we can see that measurements without abrasive are relatively stable, have a good repeatability and correlate better with measurements taken with microscope, while measurements with abrasive do not. The reason lies in spraying of the jet. In case without abrasive, spraying involves only water which does not stick to acrylic glass very well and is quickly blown off by air curtain module. When using abrasive, tiniest particles of abrasive, dissolved in water droplets tend to stay on acrylic glass and are not effectively blown away by air curtain module. As the dirt accumulates, measurements become more and more unreliable. 0.76 AWJ 1 and 0.76 AWJ 2 are close together, while 0.76 AWJ 3 is off. This type of behavior was also observed in the rest of the measurements, so AWJ tests were discarded. Figure 8 shows measurements when the pressure was 275 MPa. From Figure 7 and Figure 8 we can see that jet diameter oscillates quite significantly, which is why measurements can't be as accurate as measurements of solid tools.

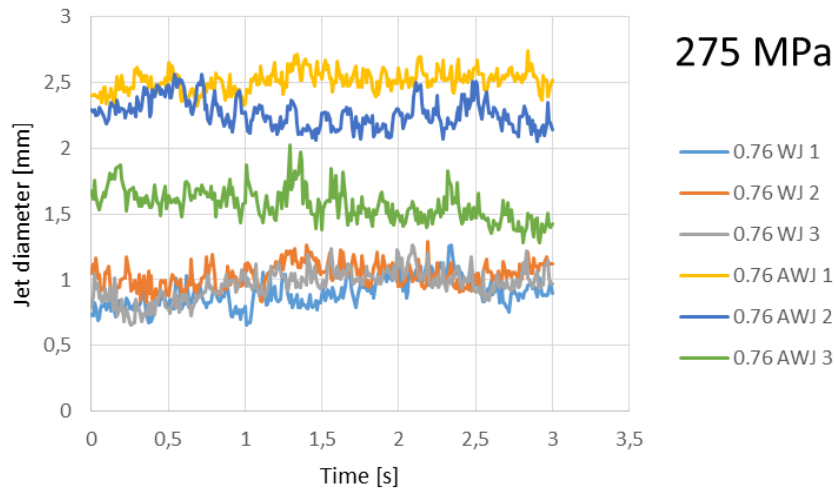


Figure 8: Results from measurements using a new 0.76 mm focusing nozzle at 275 MPa of water pressure.

Results from all measurements are shown in Figure 9 and Figure 10. Blue dots represent measured jet diameter values and orange squares represent measured focusing nozzle diameters. Experiments show that pressure has significant effect on correlation between jet diameter and nozzle diameter. Measurements done with 200 MPa are, on average, off by 0.18 mm, while measurements done with 275 MPa are, on average, off by 0.10 mm.

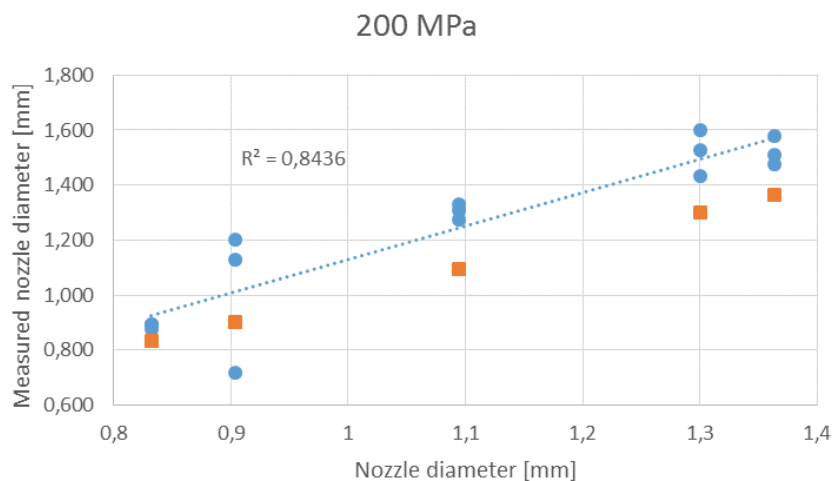


Figure 9: Results from all measurements at 200 MPa of water pressure.

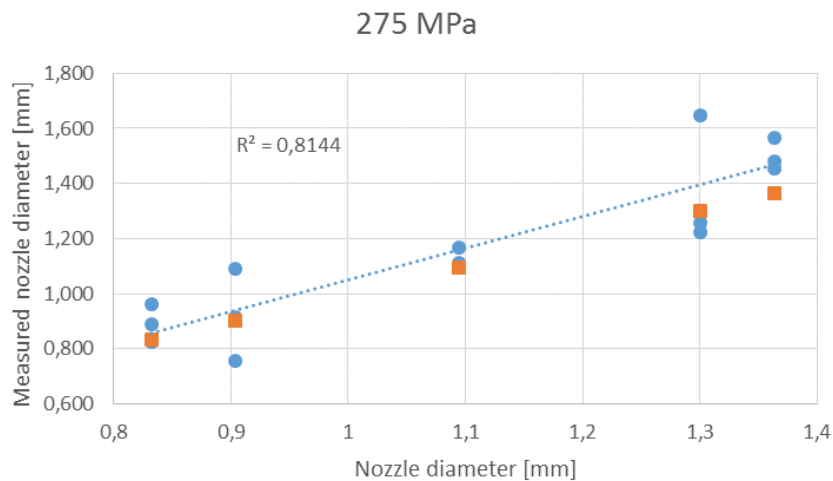


Figure 10: Results from all measurements at 275 MPa of water pressure.

#### 4 Conclusions

In this paper the usage of through beam sensor for measuring the jet diameter and determining the focusing nozzle diameter was analyzed. Results show that there is better correlation between jet diameter and focusing nozzle diameter at high water pressures (difference is on average 0.1 mm) and when not using abrasive. Main problem of accuracy is that, as the jet sprays, dirt accumulates on the screens of the instrument and measurements become distorted. Air curtain module and splash guard were effective, but not enough to completely eliminate cleanliness problems. Solving this would also include adding a cleaning module and applying a hydrophobic coating to screens. Before every measurement, screens would then first be cleaned, instrument calibrated and only then measurement done. This would eliminate cleanliness problems and provide much more stable and reliable measurements. At this stage in research the instrument is not yet reliable enough to be used for industrial purposes. Future research will also include study of orifice diameter effect on diameter of jet and adding pressure measurement to device to monitor clogging of the nozzle.

#### 5 Acknowledgement

The authors are grateful to all members of Laboratory for alternative technologies for all advice and guidance during the making of this research.

#### 6 References

- [1] OMAX Corporation, "Learn about waterjets.". Available: <https://www.omax.com/learn/waterjet-cutting>.
- [2] WaterJets.org, "waterjets.org - The most complete waterjet resource on the web - Measuring kerf and tool offset." [Online]. Available: [http://www.waterjets.org/index.php?option=com\\_content&task=view&id=186&Itemid=54](http://www.waterjets.org/index.php?option=com_content&task=view&id=186&Itemid=54).
- [3] M. Nanduri, D. G. Taggart, and T. J. Kim, "The effects of system and geometric parameters on abrasive water jet nozzle wear," *Int. J. Mach. Tools Manuf.*, 2002.
- [4] H. Orbanić, M. Junkar, I. Bajsić, and A. Lebar, "An instrument for measuring abrasive water jet diameter," *Int. J. Mach. Tools Manuf.*, 2009.
- [5] F. H. Trieb, "Waterjet cutting in Austria – history and actual status."
- [6] S. Electroblotting, "Instruction manual," *Packag. (Boston, Mass.)*, vol. 2, 1993.

# Material flow digital twinning in the Industry 4.0 paradigm

C.E. Cotet<sup>1</sup>, C.L. Popa<sup>1</sup>, G. Enciu<sup>1</sup>, A. Popescu<sup>1</sup> and C.E. Stoica<sup>1</sup>

<sup>1</sup> *University Politehnica of Bucharest, Romania*

## Abstract – use style Normal

The authors agreed with the thesis that in industrial engineering success depends on adopting the new digital industrial technologies that are collectively known as Industry 4.0. Therefore, the research presented in this paper was based on a need analysis study from May 2016 provided by Boston Consulting Group (BCG) to assess how quickly this fourth wave of technological advances is gaining momentum in Germany and the US and to inventory the major arisen problems. Our paper presents a solution for some of the problems identified by BCG using a digital twinning centred algorithm developed by the authors to optimize the material flows in the industrial engineering area. The accent is put on exploring different possibilities to use this algorithm based on virtual modelling and simulation to increase productivity and profit in various manufacturing architectures. In the first part the paper describes the theoretical model used in the proposed digital twinning based algorithm. The second part focuses on the specific applications in industrial engineering material flow management (MFM). The main topics of this main section are: digital twinning for diffused and concentrated manufacturing architectures including virtual modelling of the manufacturing architecture structural elements, MFM simulation algorithm, diagnosis and optimization for manufacturing architectures using this algorithm.

**Keywords:** digital twinning, Industry 4.0, simulation algorithm, virtual modelling.

## 1 Need analysis and state of the art

In March 2016, BCG conducted an online survey of companies and their progress toward Industry 4.0. The survey's participants included executives and operations management personnel of 312 German and 315 US companies with revenues of more than \$50 million [1]. The survey's goal was to evaluate the extent of companies' progress in implementing Industry 4.0, understand what their management considers to be the major challenges, and identify how implementation could be more efficient. One of the major challenges identified was to accelerate the introduction of digital technologies, thereby reducing costs, increasing flexibility, and accelerating the speed of manufacturing. The algorithm proposed in this paper is based on digital technologies, accelerating the speed of material flow to promote productivity gains of the manufacturing architecture. At the most basic level, the algorithm is centred on a digital twin of the manufacturing architecture (MA). We performed a literature review for this area [2], [3], [4] and we identified various existing solutions describing digital twinning for every structural element of the MA. Simple analytics applied by individual products to their own data reveal basic insights. The solution we propose is innovative because it shifts from this level to a digital twin of the entire manufacturing architecture, where all the structural elements of the MA are not only smart but also connected products. We use this MA virtual prototype to increase productivity by monitoring and controlling material flows. This technology stack is made up of multiple layers, including new product hardware, embedded software and connectivity. Manufacturing goes beyond production of the physical object, because operating a smart connected MA requires a supporting cloud-based system. More sophisticated analytics, applied to product data that has been pooled into a lake with data from external and enterprise sources, unearth deeper insights. For example, a work point can detect a potentially dangerous malfunction, shut down other equipment that could be damaged and direct maintenance staff to the problem. As well as CAE use the virtual prototype of the product provided by CAD, material flow digital twinning uses the virtual prototype of the MA. In both cases the primary goal is to have diagnose of the behaviour in exploitation in order to improve the performance. However, in material flow management we can also increase productivity by eliminating material flow concentrators, as we describe below.

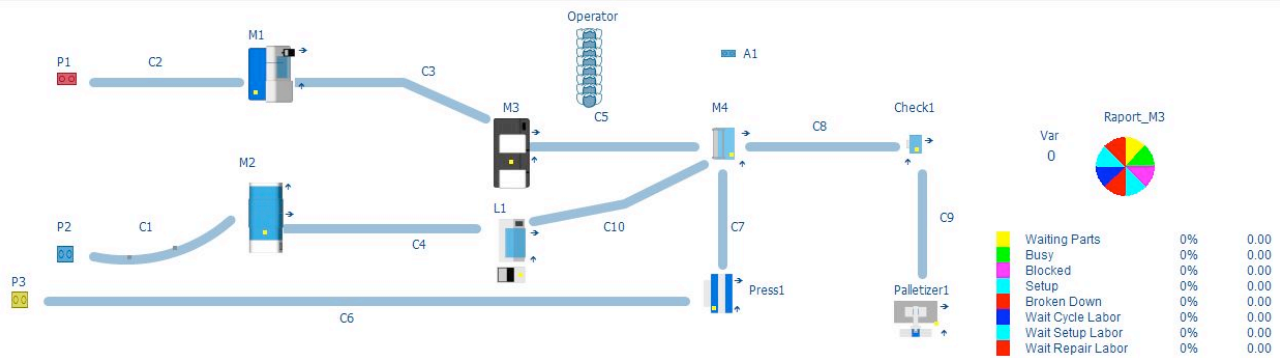


Figure 1: A manufacturing architecture virtual prototype.

## 2 Theoretical model of a manufacturing architecture digital twin

Our optimization algorithm is based on material flow theory MFT. The most comprehensive MFT description embraces the concepts of physical distribution and logistics and refers as well to the flow of macroscopic and microscopic elements [5]. From the seven major theories under the MFT [5] we are interested only in material flow engineering and industry theory. In this context we define here MFT as a support theoretical system for modelling, simulating, diagnosing and behaviour prognosis of material flow.

Also for the same area of interest in industrial engineering, we define the material flow as a group of mobile entities whose trajectories are determined by a generic associated architecture. This associated generic architecture is structured as a group of physical objects interacting with the material flow by a set of constraints determining the material flow trajectories. There are two kinds of interactions between the generic associated architecture (GAA) and the material flow trajectory. The structural elements of the GAA set bound to the material flow trajectories. The structural GAA elements determine the material flow trajectories by their movements.

More details about those interactions manufacturing architectures for industrial engineering applications are given further in this chapter. Considering our approach to MFT, the classification of the material flow is based on the mobile entities nature: We define discrete material flow when the mobile entities are distinct and countable. We define continuous flow when the mobile entities are not distinct and not countable. We define hybrid material flow when the mobile entities are distinct but not countable.

In order to clarify this classification, we could illustrate each category as follows: parts moving on a conveyor represent a discrete material flow, liquids streaming in pipes represent a continuous flow, and sand on a conveyor represents a hybrid material flow. The modern manufacturing constraints should produce highly customizable and innovative products; continuously increase their quality and decrease the time-to-market and costs in order to gain competitive advantages. All these determined a focus on optimizing the manufacturing systems starting early from their design phase by using MFT and specific simulation software tools. Depending on product characteristics and production type, several classical architectures of manufacturing systems (assembly line, flexible manufacturing system, flexible manufacturing cell, job shop, etc.) can be deployed in a factory. These architectures can be analysed in conjunction MFT applications and specific algorithms in the material flow management area, and optimized based on mathematical and virtual modelling [6]. To optimize a material flow one should focus on maximizing or minimizing specific parameters according with their nature (for instance, cost is a minimizing parameter, while productivity is a maximizing parameter). One of the main methods is based on identifying the points where the material flow is slowed down or even blocked (flow concentrators or bottlenecks) and finding solutions to eliminate such problems with or without modifying GAA. Such methodology uses the virtual model of GAA and flow simulator software application, which is meant to simulate the evolution and the material flow behaviour in time.

The algorithm developed by us using MFT (applicable independent of the flow nature, but nevertheless used mainly in industrial engineering) and used to optimize the GAA consists in the following steps:

1. Modelling GAA using flow simulator specific elements and establishing the material flow trajectories inside the GAA.
2. Simulating the material flow of this initial model and run a GAA performances diagnosis.
3. Identifying flow concentrators and the solutions to eliminate them, and modifying GAA model accordingly.
4. Simulating the material flow for the modified GAA model and run a new performance diagnosis.
5. Validating the financial investment by quantifying the increased performances.

There are several different kinds of simulations necessary in this algorithm, further an overview of these categories being presented. According to their velocity in material flow simulation, we use:

- Accelerated simulation - used to generate quick GAA performance diagnosis reports.
- Decelerated simulation - used to detail the critical events that could generate a flow concentrator.
- Real time simulation - used to experimentally validate the material flow performances.

According to their duration in material flow simulation, we use:

- Determined simulation - with a critical event generating the end of the simulation.
- Undetermined simulation - with no such a critical event.

Despite of restricting the field, the engineering and industry oriented MFT approach presented here covers however different area oriented applications: optimizing city traffic or building evacuation, packaging sorting and distribution, increasing manufacturing productivity and avoiding crowded areas in airports, designing the layout of recycling lines being some of these.

In a very comprehensive view, material flow management (MFM) in industrial engineering comprises optimization techniques for procurement, usage, handling, transformation and disposal of physical mobile entities like tools and parts in manufacturing architectures [6]. The area of MFM applications in this acceptance is wide and implies modules of MFT out of previous MFT presented selection. Therefore, we will refer here at MFM in a restricted acceptance, as a set of simulation and optimization rules for the industrial projects duration and costs using a virtual manufacturing architecture model.

This MFM algorithm for optimizing manufacturing architectures performances should be adapted to the specific requirements of two categories. We define a manufacturing architecture as a set of structural elements interacting such as to contribute at a product manufacturing. We recognize here four main structural elements (work points, transport systems, transfer systems, buffers) and two auxiliary structural elements (mobile entities and human resources) for a manufacturing architecture. For each one of these categories, establishing a manufacturing architecture for a product or a family of products involves designing and structuring the relationships between structural elements, processes, procedures and human resources, that is both defining these elements, placed and acting in a specific layout, as well as the material and information flow between them.

We agree to define the role of the structural elements as follows. The work points (machine tools, assembly points...) are the structural elements covering all the technological stages necessary for the part manufacturing. Transport systems (conveyors, AGVs, RGVs...) are moving the mobile entities between the long distance situated structural elements. The transfer systems (robots and manipulators) are orienting and fixing the mobile entities, making as well the connection between near structural elements. Buffers are storing the mobile entities for a limited period of time. The mobile entities are parts and tools. The human resources are involved in two postures: operational (acting like a worker) and monitor (supervising the activity of the manufacturing architecture).

The advances in computer-aided design (3D CAD software) made possible the creation and use of databases containing parameterized virtual models of all the structural elements that can be included in a manufacturing systems. These databases are made available by producers (being already included in software applications, such as RobCAD from Siemens or Quest from Dassault Systems) and their items can be put together in order to form a virtual model of a manufacturing system. This virtual model should precisely reproduce the real system structural elements, in terms of overall dimensions and reciprocal positions and placement in the layout, being essential in designing and optimizing the manufacturing architecture.

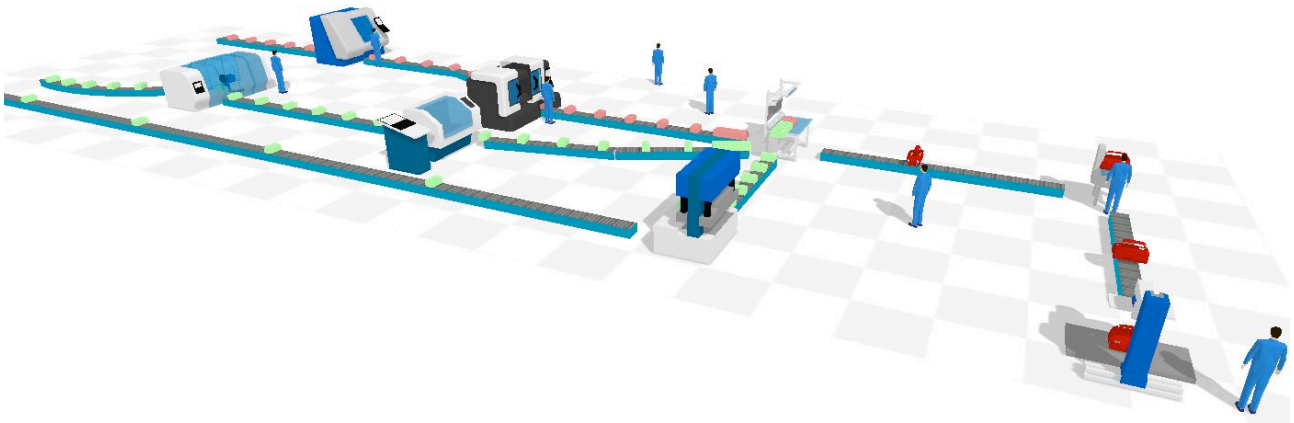


Figure 2: A material flow digital twin.

The modifications in the manufacturing architecture needed after different simulation runs are easy to perform due to the parameterization of the virtual models, therefore decreasing the total optimization time. Moreover, simulations made at the manufacturing system level can use as input simulations data obtained at the machine/process level [7]. The modelling and simulation algorithms for optimizing manufacturing architecture using MFM are different according with two main categories as follows. First we define diffused manufacturing architectures as systems with more than two work points connected by transport & transfer systems and using deposits at local or system level. We define then concentrate manufacturing architectures as systems based on a single work point surrounded & assisted by transport, transfer & deposit facilities [7].

In a work post, one or several operations/activities can take place using processes and machines [8]. In an attempt to decrease the overall production time, there are approaches which consider eliminating the transport & transfer times between work posts by combining in a single machine, two (or more) manufacturing processes. As known, the manufacturing processes can be classified as: subtractive – involving material removal (such as milling, drilling, turning/lathing, etc.), additive – involving material addition layer-by-layer (stereo lithography, fused deposition modelling, selective laser sintering, etc.) and with material distribution (injection molding, forming, casting, etc.). In the hybrid manufacturing work post, additive and subtractive processes can be combined [9] within a single machine, completely computer-controlled, in order to benefit of the advantages of each technology, such as complex geometry, controlled geometry, functional graded material parts – for additive fabrication, and high precision and surface quality or very good mechanical properties – for subtractive fabrication. From the point of view of the MFT, these hybrid manufacturing systems, currently gaining more interest and importance, are considered as concentrate architecture, and can modelled and optimized accordingly.

### 3 A manufacturing architecture and the material flow digital twin

MFM in industrial engineering customizes for manufacturing architectures the step-by-step GAA optimization algorithm previously presented. Everything starts here with some preliminary steps referring to the virtual prototype used for the design of the new product (CAD – Computer Aided Design) that should be produced using the manufacturing architecture. This virtual prototype is used then to simulate the functional behaviour of the product in order to identify potential design flaws (CAE – Computer Aided Engineering). If the results of CAE simulations are satisfactory then the next step is generating the succession of technological operations needed to obtain the product, as well as the associated manufacturing processes simulations (CAM – Computer Aided Manufacturing). If one of the simulated operations could not be realized, a return to the previous steps is necessary to redesign the part. When these iterations are over, the outcomes are defined: product design, bill of material, manufacturing operations plan for each component of the product and for the whole assembly, the required machines, devices and tools and their characteristics, and the work points and their successions in the production line [10]. The main MFM steps are starting from this point and are based on all the above information, as follows. A preliminary manufacturing architecture virtual modelling is done with the necessary parameters for the work points, buffers, the transport and transfer systems. The trajectories of the mobile entities (parts and tools) are established. For this preliminary architecture virtual prototype, the material flow is simulating for a performance diagnosis report.

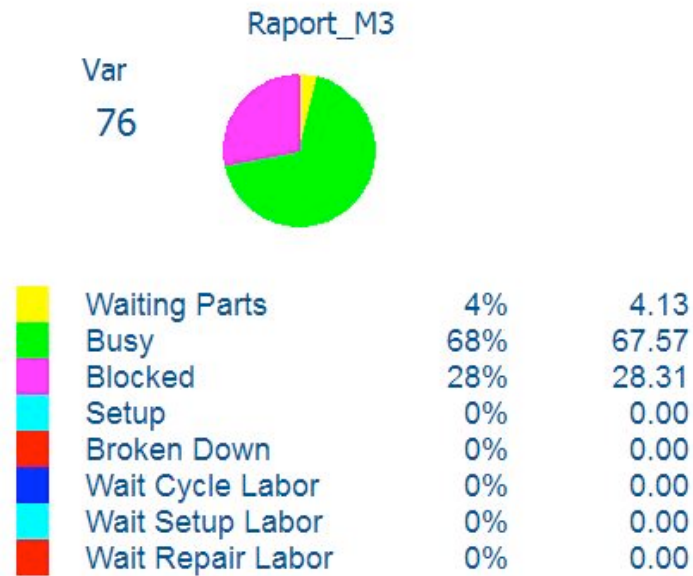


Figure 3: Initial performance diagnosis report.

Using this report the flow concentrators could be identified. There are two kinds of solutions for eliminating these concentrators by modifying the manufacturing architecture. Functional remodelling potentiates the manufacturing architecture performance by modifying the structural elements layout or functional parameters but is not introducing or eliminating structural elements. Technological remodelling allows manufacturing architecture changes also when structural elements should be added or removed.

After functional or technological remodelling, another material flow simulation is performed for quantifying the increasing performance of the optimized manufacturing architecture.

The last stage is the profit validation based on the comparison of the investment in optimizing the manufacturing architecture and the gain from the increased system performance. When designing the layout of manufacturing system, virtual models of different structural elements can be used, while in simulating the material flow in the manufacturing architecture, data from processes simulations can constitute input parameters. In this context of using data from different types of applications for defining and optimizing GAA, data compatibility and data portability issues should not be neglected when choosing the software tools for supporting the optimal definition of a manufacturing architecture.

In dealing with MFT applied to manufacturing systems, one should consider using a specific algorithm for optimizing the associated architecture by modelling and then simulating the material flow trajectory within the system. This algorithm, detailed in the previous section, offers a structured modality to increase the productivity and profit in manufacturing architectures in order to respond to different requirements.

The main benefits of our optimization algorithm are as follows.

- Improving performances analysis by developing new measuring tools.
- Integrating CAM and material flow simulation.
- Integrating engineering knowledge in MFM.
- Integrating MFM with ERP (Enterprise Resource Planning) applications.

Current needs and practice in industrial engineering determined us to adapt the general MFT and to develop specific algorithms for diagnosis and optimization for manufacturing architectures using MFM.

As can be noticed, our approach, although restrictive to industrial projects, can be however used to accommodate the advances in digital fabrication and the development of new manufacturing processes/technologies, thus responding to the current trend of mass-customization as a paradigm shift from mass production.

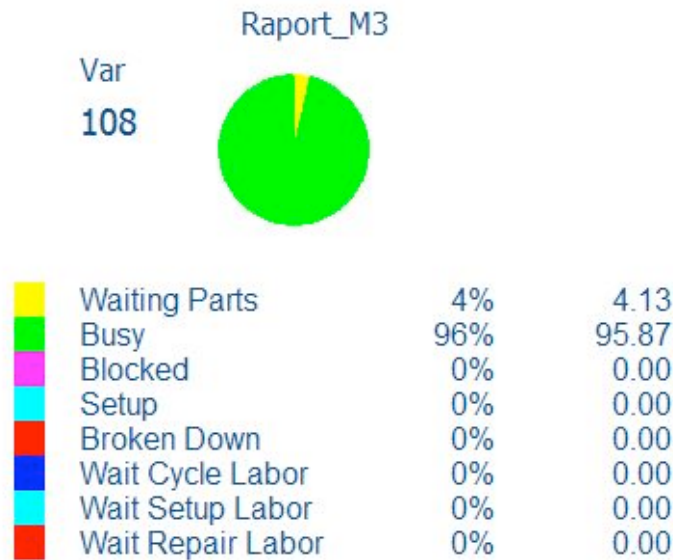


Figure 4: Optimized performance diagnosis report.

#### 4 Conclusion

Considering the field of research described in this paper the main interest is concerning the new elements introduced by this industry 4.0 paradigms in material flow simulation. In the engineering phase, 3-D simulations of products, materials, and production processes are already used, but in this new approach proposed by our optimization algorithm, simulations will be used more extensively in plant operations and cloud as well. The virtual prototype of the manufacturing architecture becomes a part of the manufacturing plant design. The digital twin of the material flow will use this MA virtual prototype to provide diagnose and optimization of the system performances in different manufacturing scenarios based on simulations including machines, products, and humans. One could not only test and optimize the machine settings for the next product, but also compare the real and the digital twin performing parameters during manufacturing, thereby generating new scenarios and increasing quality and productivity as well. Also, if only some of a manufacturer's sensors and machines are now networked and make use of embedded computing organized in a vertical automation pyramid (in which sensors and field devices with limited intelligence and automation controllers feed into an overarching manufacturing-process control system), our solution based on material flow digital twinning will introduce some changes. More devices including even unfinished products will be enriched with embedded computing and connected to communicate and interact both with one another and with centralized controllers, as necessary. Smart and connected structural elements require a rethinking of the MA design. At the most basic level, product development shifts from largely mechanical engineering to true interdisciplinary systems engineering. All smart, connected structural elements, from work points to transport systems, share three core elements: physical components (such as mechanical and electrical parts); smart components (sensors, microprocessors, data storage, controls, software, an embedded operating system, and a digital user interface); and connectivity components (ports, antennae, protocols, and networks that enable communication between the structural element and the MA cloud, which runs on remote servers and contains the MA's external operating system). Manufacturing goes beyond production of the physical object, because operating a smart connected MA requires a supporting cloud-based system [3]. In this new industrial engineering paradigm, the material flow management use Internet of things to establish trajectories of mobile elements, cybersecurity & the cloud to process safely big data, additive manufacturing and autonomous robots as structural elements, augmented reality and simulation for horizontal and vertical management system integration.



## References

- [1] M. Lorenz, D. Kupper, M. Rüßmann, A. Heidemann, A. Bause: Time to accelerate in the Race toward Industry 4.0, BCG, May 2016, <https://www.bcgperspectives.com>
- [2] M. Rüßmann, M. Lorenz, P. Gerbert P, M. Waldner, J. Justus, P. Engel, M. Harnisch: Industry 4.0: The Future of Productivity and Growth in Manufacturing Industries, 2015, <https://www.bcgperspectives.com>
- [3] M.E. Porter, J.E. Heppelmann: How Smart, Connected Products Are Transforming Companies, Harvard Business Review, October 2015, 1-19, HBR.org
- [4] M.E. Porter, J.E. Heppelmann: How Smart, Connected Products Are Transforming Competition, Harvard Business Review, November 2014, 1-24, HBR.org
- [5] S. Xu: The concept and theory of material flow. *Information Systems Frontiers*, 10(5), 601-609, ISSN: 1387-3326 print, 1572-9419 online, doi: 10.1007/s10796-008-9113-4, 2008.
- [6] C.E. Cotet, D.Popescu: Material Flow Management in Industrial Engineering, in Encyclopedia of Information Science and Technology, Category: Industrial Engineering, Third Edition, Editor Mehdi Khosrow-Pour, Published in the United States of America by Information Science Reference (an imprint of IGI Global), pp. 3786 – 3794, ISBN 978-1-4666-5888-2 (hardcover) -- ISBN 978-1-4666-5889-9 (ebook) -- ISBN 978-1-4666-5891-2 (print & access), 2014.
- [7] D. Popescu, D. Anania, C.E. Cotet, & C. Amza, C: Fully automated liquid penetrant inspection line simulation model for increasing productivity. *International Journal Simulation Modelling*, 12(2), 82-93, ISSN online: 1740-2131, ISSN print: 1740-2123, 2013
- [8] C. Wang, X.B. Liu, G.Z. Zhao, & K. O. Chin: Multi-Objective Integrated Production Planning Model and Simulation Constrained Doubly by Resources and Materials, in: International Journal of Simulation Modelling IJSIMM, volume 13, no. 2, pp.243-254, ISSN 1726-4529, 2014.
- [9] J.K.S. Nagel & F.W. Liou: Chapter 11. Hybrid Manufacturing System Design and Development. In *Manufacturing System*, F.A. Aziz (Ed.), (p.223-246), Publisher InTech, ISBN 978-953-51-0530-5, 2012
- [10] C.E. Cotet, C.L. Popa, G. Enciu, A. Popescu, T. Dobrescu: Using CAD and flow simulation for educational platform design and optimization, *International Journal Simulation Modelling*, vol. 15, number 1, March 2016, ISSN 1726-4529 pp. 5-16, DOI:10.2507/IJSIMM12(2)2.225, 2016

# Security issues in virtual enterprises

L.F. Parpală<sup>1</sup> and R.C. Parpală<sup>1</sup>

<sup>1</sup> *University POLITEHNICA of Bucharest, Romania*

## Abstract

Even from the start of internet, security has been an issue. Nowadays, considering the continuous growth of the internet and internet applications, security issues are more complex. For the virtual enterprises the challenges are even bigger if we keep in mind the fact that a virtual enterprise needs to open its private network for the partners and is continuously accessed through the internet by the costumers. There are new solutions that have to be developed in order to keep all the data safe. Another challenge is the cloud computing which enables partner's collaborative working, but comes with big problems form the security point of view. The security challenges that are associated with unauthorized cloud use are well documented. Shadow cloud services and assets can lead to various issues such as data leaks, unknown vulnerabilities, and wasted resources. In this paper we will discuss all these issues and the solutions for each of them. We will focus this research on the database security, which is a key component of all cloud collaboration solutions.

**Keywords:** security, databases, virtual enterprises, cloud computing.

## 1 Introduction

As the National Institute of Standards and Technology, USA defined, cloud computing is a model for enabling ubiquitous, convenient, on-demand network access to a shared pool of configurable computing resources (e.g., networks, servers, storage, applications, and services) that can be rapidly provisioned and released with minimal management effort or service provider interaction. This cloud model is composed of five essential characteristics, three service models, and four deployment models. [1]

An example of a cloud computing network architecture is presented in figure 1.

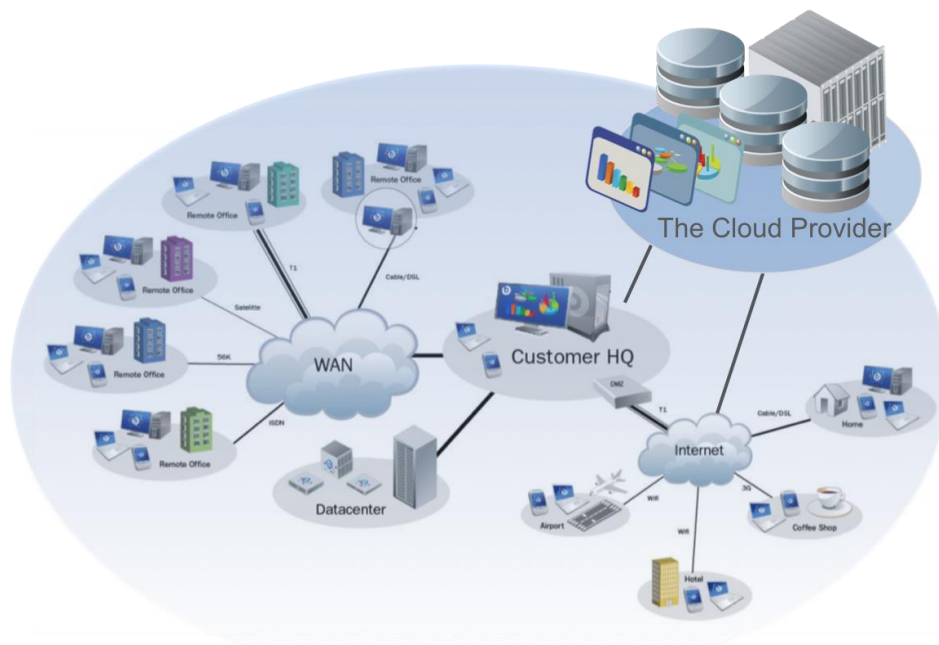


Figure 1 Architecture of a cloud computing network

The essential characteristics of cloud computing are:

Cloud computing is an on-demand self-service, which means that a consumer can unilaterally provision computing capabilities, such as server time and network storage, as needed automatically without requiring human interaction with each service provider.

Also, cloud computing allows broad network access. This way, capabilities are available over the network and accessed through standard mechanisms that promote use by heterogeneous thin or thick client platforms (e.g., mobile phones, tablets, laptops, and workstations).

The provider's computing resources are pooled to serve multiple consumers using a multi-tenant model, with different physical and virtual resources dynamically assigned and reassigned according to consumer demand. There is a sense of location independence in that the customer generally has no control or knowledge over the exact location of the provided resources but may be able to specify location at a higher level of abstraction (e.g., country, state, or datacenter). Examples of resources include storage, processing, memory, and network bandwidth.

Capabilities can be elastically provisioned and released, in some cases automatically, to scale rapidly outward and inward commensurate with demand. To the consumer, the capabilities available for provisioning often appear to be unlimited and can be appropriated in any quantity at any time.

Cloud systems automatically control and optimize resource use by leveraging a metering capability at some level of abstraction appropriate to the type of service (e.g., storage, processing, bandwidth, and active user accounts). Resource usage can be monitored, controlled, and reported, providing transparency for both the provider and consumer of the utilized service.

The three Service Models are:

**Software as a Service (SaaS).** The capability provided to the consumer is to use the provider's applications running on a cloud infrastructure. The applications are accessible from various client devices through either a thin client interface, such as a web browser (e.g., web-based email), or a program interface. The consumer does not manage or control the underlying cloud infrastructure including network, servers, operating systems, storage, or even individual application capabilities, with the possible exception of limited userspecific application configuration settings.

**Platform as a Service (PaaS).** The capability provided to the consumer is to deploy onto the cloud infrastructure consumer-created or acquired applications created using programming languages, libraries, services, and tools supported by the provider.<sup>3</sup> The consumer does not manage or control the underlying cloud infrastructure including network, servers, operating systems, or storage, but has control over the deployed applications and possibly configuration settings for the application-hosting environment.

**Infrastructure as a Service (IaaS).** The capability provided to the consumer is to provision processing, storage, networks, and other fundamental computing resources where the consumer is able to deploy and run arbitrary software, which can include operating systems and applications. The consumer does not manage or control the underlying cloud infrastructure but has control over operating systems, storage, and deployed applications; and possibly limited control of select networking components (e.g., host firewalls).

And the Deployment Models are presented below:

**Private cloud.** The cloud infrastructure is provisioned for exclusive use by a single organization comprising multiple consumers (e.g., business units). It may be owned, managed, and operated by the organization, a third party, or some combination of them, and it may exist on or off premises.

**Community cloud.** The cloud infrastructure is provisioned for exclusive use by a specific community of consumers from organizations that have shared concerns (e.g., mission, security requirements, policy, and compliance considerations). It may be owned, managed, and operated by one or more of the organizations in the community, a third party, or some combination of them, and it may exist on or off premises.

**Public cloud.** The cloud infrastructure is provisioned for open use by the general public. It may be owned, managed, and operated by a business, academic, or government organization, or some combination of them. It exists on the premises of the cloud provider.

**Hybrid cloud.** The cloud infrastructure is a composition of two or more distinct cloud infrastructures (private, community, or public) that remain unique entities, but are bound together by standardized or proprietary technology that enables data and application portability (e.g., cloud bursting for load balancing between clouds).

## 2 Threats of the virtual enterprises security

A virtual enterprise is a temporary alliance of enterprises that come together to share skills or core competencies and resources in order to better respond to business opportunities, and whose cooperation is supported by computer networks. [2]

### 2.1 Cloud computing security threats

Cloud computing is one of today's most exciting technologies due to its ability to reduce costs associated with computing while increasing flexibility and scalability for computer processes. During the past few years, cloud computing has grown from being a promising business idea to one of the fastest growing parts of the IT industry. IT organizations have expressed concern about critical issues (such as security) that exist with the widespread implementation of cloud computing. These types of concerns originate from the fact that data is stored remotely from the customer's location; in fact, it can be stored at any location. Security, in particular, is one of the most argued-about issues in the cloud computing field; several enterprises look at cloud computing warily due to projected security risks. The risks of compromised security and privacy may be lower overall, however, with cloud computing than they would be if the data were to be stored on individual machines instead of in a so - called "cloud" (the network of computers used for remote storage and maintenance).[3]

### 2.2 Database security threats

Databases are one of the most compromised assets according to the 2014 Verizon Data Breach Report. The reason databases are targeted so often is quite simple: they are at the heart of any organization, storing customer records and other confidential business data. But why are databases so vulnerable to breaches? One reason is that organizations are not protecting these crucial assets well enough. [4]

The top ten database security threats are:

1. Excessive and Unused Privileges - when someone is granted database privileges that exceed the requirements of their job function, these privileges can be abused.
2. Privilege Abuse - users may abuse legitimate database privileges for unauthorized purposes.
3. Input Injection (Formerly SQL Injection) – There are two major types of database injection attacks: SQL Injection, that targets traditional database systems, and NoSQL Injection, that targets Big Data platforms. SQL Injection attacks usually involve inserting (or “injecting”) unauthorized or malicious statements into the input fields of web applications.
4. Malware – Cybercriminals, spies use advanced attacks that blend multiple tactics, such as spear phishing emails and malware, to penetrate organizations and steal sensitive data.
5. Weak Audit Trail – Automated recording of database transactions involving sensitive data should be part of any database deployment. Failure to collect detailed audit records of database activity represents a serious organizational risk on many levels.
6. Storage Media Exposure – Backup storage media is often completely unprotected from attack. As a result, numerous security breaches have involved the theft of database backup disks.
7. Exploitation of Vulnerable, Misconfigured Databases – It is common to find vulnerable and unpatched databases, or discover databases that still have default accounts and configuration parameters. Attackers know how to exploit these vulnerabilities to launch attacks against the organization.
8. Unmanaged Sensitive Data – Many companies struggle to maintain an accurate inventory of their databases and the critical data objects contained within them.

9. Denial of Service – Denial of Service (DoS) is a general attack category in which access to network applications or data is denied to intended users. The motivations behind DoS attacks are often linked to extortion scams in which a remote attacker will repeatedly crash servers until the victim meets their demands.
10. Limited Security Expertise and Education – Internal security controls are not keeping pace with data growth and many organizations are ill-equipped to deal with a security breach. Often this is due to the lack of expertise required to implement security controls, enforce policies, or conduct incident response processes.

### 3 Solutions for the virtual enterprises security

Figure 2 presents a solution for cloud computing security from VMware adapted for virtual enterprises.

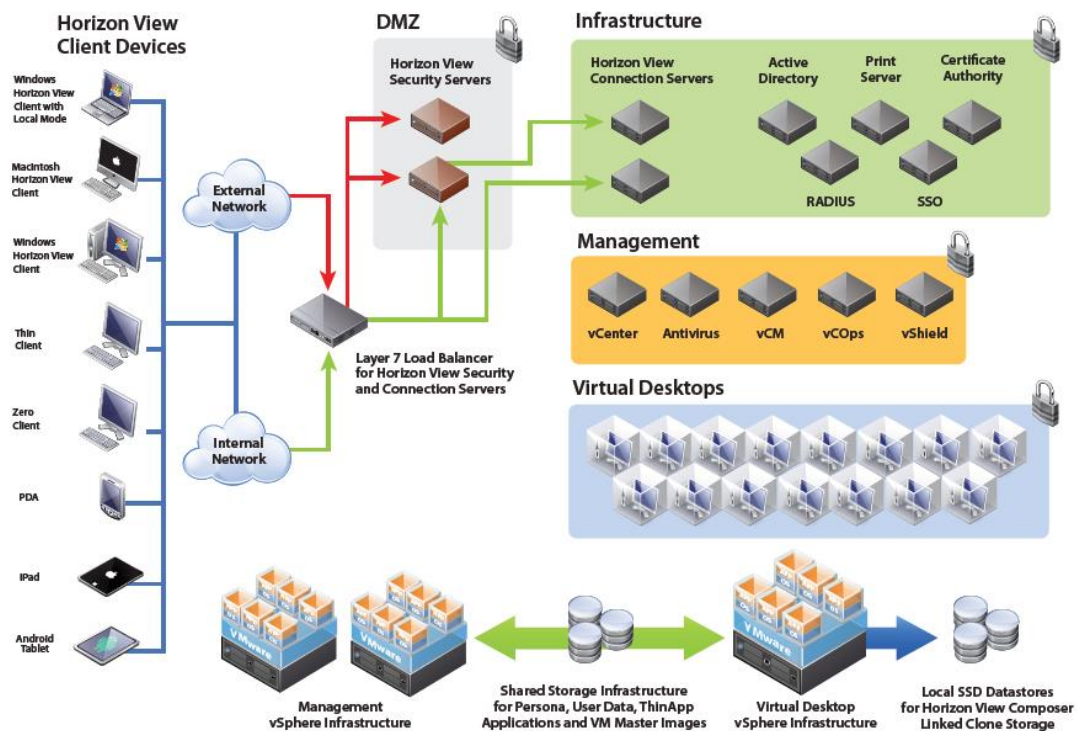


Figure 2 Cloud computing for virtual enterprises

Today’s workforce is no longer tethered to traditional stationary desktops. New devices have proliferated companies of all sizes. Workers are increasingly mobile, and more than 60 percent of enterprise firms and 85 percent of SMB organizations are looking to initiate Bring Your Own Device (BYOD) programs. But while end users are embracing these trends, IT departments, faced with tight budgets, are struggling with how to best support and manage these new devices while protecting corporate data as it is accessed across networks and locations. This is why finding a secure, streamlined and more cost-effective way to manage end users across devices and locations has become a top priority for so many customers today.

By virtualizing desktop and using a validated architectural design, organizations can now have unparalleled desktop and application access across devices and locations. With the VMware Horizon Mobile Secure Workplace, processes are automated and efficient, data is secure and the total cost of ownership is reduced by as much as 50 percent. And because this solution ties desktop environments to user identities instead of devices, end users are free to access their data and applications from any qualified device, whether in the office or halfway around the world.

The Mobile Secure Workplace is specifically built to meet the needs of organizations looking to securely support end users across devices and locations. It combines VMware and ecosystem products and services to meet the necessary requirements for supporting security, rapid and automated provisioning and mobile access across devices.

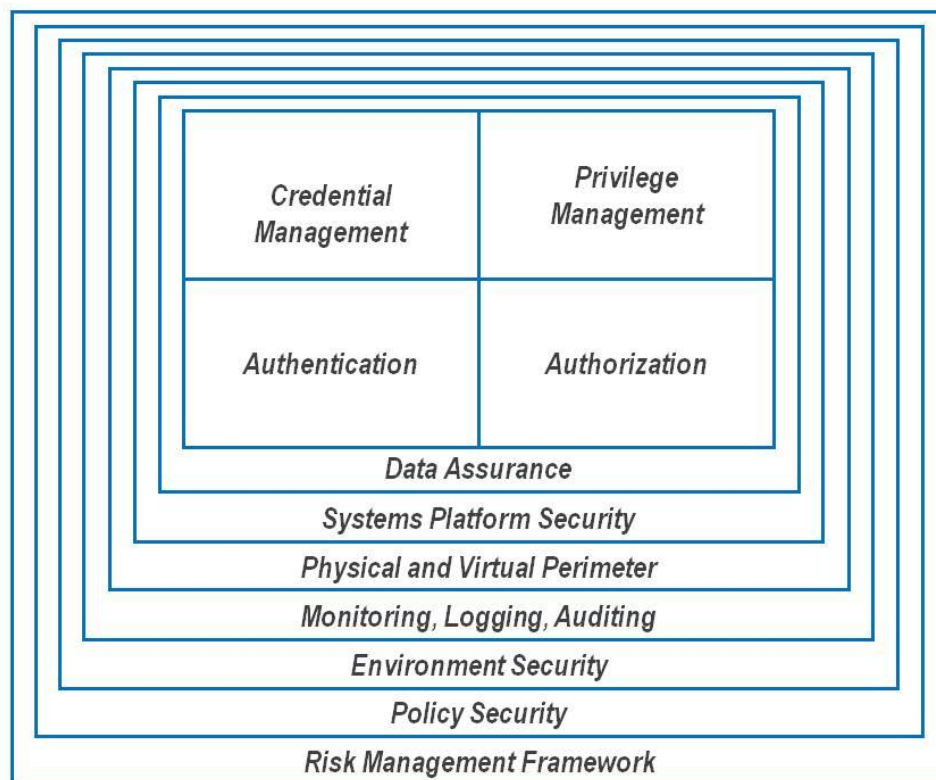


Figure 3 An example of a security model

In figure 3 is presented an example of a security model. This model includes:

**Unified Credential Management:** Issuing of admin, operations, and end-user identities for access to virtual components and applications

**Privilege Management:** Definition and assignment of resource access privileges and roles for infrastructure components and applications.

**Authentication:** Validation of identities (admin, operations, and end-user on the basis of credentials.

**Authorization:** Privilege-based granting of access to protected virtual infrastructure resources to authenticated users.

**Data Assurance:** Confidentiality, integrity, and availability of data at rest, in transit, and in use

**Systems and Platform Security:** Controlling the operation of the application, hardening the VM, the O/S, application server software

**Physical and Virtual Perimeters:** Hardening of networks against eavesdropping, penetration and data leakage; intrusion detection

**Monitoring, Logging, Auditing, Reporting:** recording of infrastructure configuration, management events and policy changes. Security of the logging, auditing, and reporting environment

**Environment Security:** Protection and recoverability of physical infrastructure and system-level assets

**Policy Security:** Protections and controls over policy metadata and processes that define, enforce, and report on virtual security operating environment

**Risk Management Framework:** Framework and process for determining inherent risk, security controls, and residuals

## 4 Conclusions

The main benefits of cloud computing are:

1. Flexibility - Cloud-based services are ideal for businesses with growing or fluctuating bandwidth demands.
2. Disaster recovery - Businesses of all sizes should be investing in robust disaster recovery, but for smaller businesses that lack the required cash and expertise, this is often more an ideal than the reality. Cloud is now helping more organisations buck that trend.
3. Automatic software updates - The beauty of cloud computing is that the servers are off-premise and out of sight. Suppliers take care of them for you and roll out regular software updates, including security updates.
4. Capital-expenditure Free - Cloud computing cuts out the high cost of hardware.
5. Increased collaboration - When the teams can access, edit and share documents anytime, from anywhere, they're able to do more together, and do it better. Cloud-based workflow and file sharing apps help them make updates in real time and gives them full visibility of their collaborations.
6. Work from anywhere - With cloud computing, with an internet connection one can be at work. And with most serious cloud services offering mobile apps, there are no restrictions by which device the work will be done.
7. Document control - Before the cloud, workers had to send files back and forth as email attachments to be worked on by one user at a time.
8. Security - Lost laptops are a problem but the loss of the sensitive data inside it is an even bigger problem. Cloud computing gives greater security when this happens
9. Competitiveness - Moving to the cloud gives access to enterprise-class technology, even for small business.

In conclusion, a good cloud solution with a strong security is just what a virtual enterprise might need.

## References

- [1] Peter Mell, Timothy Grance: The NIST Definition of Cloud Computing
- [2] L. M. Camarinha-Matos, H. Afsarmanesh: The Virtual Enterprise Concept. In Networking Industrial Enterprises IFIP TC5 WG5.3 / PRODNET Working Conference on Infrastructures for Virtual Enterprises (PRO-VE'99) October 27–28, 1999, Porto, Portugal, Springer, ISBN 978-1-4757-5499-5 ISBN 978-0-387-35577-1.
- [3] Farzad Sabahi: Cloud computing security threats and responses. In IEEE 3rd International Conference on Communication Software and Networks (ICCSN), 27-29 May 2011, ISBN 978-1-61284-486-2
- [4] Top Ten Database Security Threats. Imperva white paper, 2015

# Length perception in virtual reality environment

P. Mitrouchev<sup>1</sup>, J.T. Chen<sup>1,2,3</sup>, S. Coquillart<sup>2</sup> and F. Quaine<sup>3</sup>

<sup>1</sup> Univ. Grenoble Alpes, CNRS, G-SCOP, 38000 Grenoble, France

<sup>2</sup> INRIA-LIG Montbonnot, 38334 Saint-Ismier, France

<sup>3</sup> Univ. Grenoble Alpes, GIPSA-Lab, CNRS, 38000 Grenoble, France

## Abstract

Today simulation platforms in Virtual Reality Environment (VRE) play a very important role during the initial design phase of products throughout the Product Life-Cycle (PLC). However, current simulation platforms do not offer the necessary information and versatility required for a complete perception process in simulation and evaluation. This paper deals with a new method for measuring the influence of Virtual Reality on the perceived length of an object (e.g. a bar). The method is based on the assessment of the length of a part by the subject, with two sources of visual information. The first one is the screen of the VRE where the movements are displayed, with different coefficients  $C_{eb} = (\text{object length displayed on the screen}) / (\text{length of the arm's movement})$ . The other source is a set of two crossed meters (measuring tapes) situated on the wall behind the subject. The method is validated by a set of experimental tests performed in a Virtual Reality Environment. The results show that subjects are more likely influenced by the movement of the arm rather than the length of the arm displayed on the screen. Moreover, the length's perception of subjects is modified when moving direction changes (horizontal or vertical) or when putting/placing a meter (measuring tape) in the subject's field of view. The horizontal bar or the meter (measuring tape) leads them to choose lengths closer to what they are seeing on the screen, than when the bar is vertical or without meter. The proposed method provides the feasibility to integrate the visual perception into length evaluation via VRE when performing disassembly operation simulations for instance.

**Keywords:** Virtual Reality Environment, Disassembly sequences simulation, Distance perception, Length evaluation

## 1 Introduction

Virtual Reality (VR) is a trendy issue and is nowadays applied in a lot of fields such as: industry, science, estate agency, video games and others. Nonetheless, it could be certainly improved with the advent of nowadays' technologies. Real effects of the VR on a human are not actually well known and the comprehension of these effects could be beneficial for Human/VR interaction. Many studies have especially a closer look on the influence of VR on human's perceptions. A novel pseudo-haptic approach for simulation of force fields called HEMP – *Hand-displacEMent-based Pseudo-haptics* was introduced in [1]. The main idea of the authors was to provide haptic-like sensations by dynamically displacing the visual representation of the user's hand. Other approaches follow comparable strategies of modulating given force sensations through vision [1]. A stiffness feeling, for instance, was simulated by linking a perturbed visual feedback with a force sensor in [2]. Other work [3] demonstrated that a torque impression can be induced by employing a force input device combined with a virtual torsion spring.

In [4] it was shown that subjects estimated the weights of objects with equal mass based on their apparent visual size (Charpentier's size-weight illusion). That means, the larger the object appeared, the lighter it was perceived. Similar works on weight perception of objects were recently carried out in INRIA Institute from Rennes [5].



Dozens of studies dealt with perception aim. Let mention some principal human perceptions they dealt with, such as:

- the flavor and the olfaction [6] from Tokyo University on olfactory perception of food,
- the hearing [7],
- stiffness perception [8, 9]
- volume perception [4],
- distance perception [10].

Others perceptions have to be analyzed. We are interested in studying the influence of VR on length perception. This investigation could allow this technology to be improved and learn more about the interaction between the human and the VR.

In this context, a new method for quantification the influence of the visual weed-back on the length perception of an object (part) is presented in this paper. The present work provides a new way to estimate the length of a mechanical part (here a bar) in VRE. This estimation may be an aid for designers allowing them to assess ergonomic gesture evaluation. Thus, the results of this study may be useful for designers, for instance, allowing them to evaluate difficulties of Assembly/Disassembly operations, in a virtual environment in the initial phase of a product's design.

The remainder of the paper is structured as follows. Section 2 presents the new method for length perception in VRE. Then the experimental tests performed in a VRE are presented in Section 3. After that, the results are presented and discussed in Section 4. Finally, conclusion and future work are suggested in Section 5.

## 2 Method

The proposed method for distance evaluation/perceptions deals with the influence of the visual weed-back on the length perception of an object (part). It is based on two sources of visual information: the screen (visual feed-back) for comparison the perceived length and two meters (rulers or measuring tapes) for visual estimation.

For this purpose the coefficient  $C_{eb}$  defined as:  $C_{eb} = (\text{object length displayed on the VRE screen}) / (\text{length of the arm's movement in the real physical environment})$  is calculated. The object length displayed on the VRE screen is variable, however, the length of the arm's movement in the real physical environment is constant. The method consist in comparing the distances while moving a part of a mechanical assembly in horizontal and/or vertical directions. Thus, we want to value two criteria which are the influence of the bar's orientation and the influence of the two measuring tapes. The screen of the VRE is in front of the subject. The two measuring tapes (two crossed meters) are bonded on the wall behind the subject. The method consists in estimating the perception for the length of the part by comparing the results from these two sources: screen and meters.

## 3 Experimental tests

In order to prove the proposed method, a series of experiments were carried out in a VRE. The task consisted of moving a ring (weight, 0,5 kg) along a beam (bar), in a restricted vertical/horizontal space with bottom-up/up-down, and left-right/right-left movements. As previously mentioned, the experiment's goal is to assess the virtual reality's influence on humans' perception of the length.

### 3.1 Equipment

The tests were performed in the virtual reality environment in GINOVA Lab at Grenoble INP (National Polytechnic Institute). The environment consists of (Fig. 1): VIRTUOSE 6 D35-45 haptic device with force

feedback, stereoscopic screen, 3D glasses and two crossed measuring tapes (meters, rulers). Two computers have been used as well: one to control the object displayed on the screen (Catia V5 environment) and another one to stock/record the results.

The software used to generate the simulation environment is IFC (Interactive Fitting for CATIA), which is a CAAV5- based plug-in for CATIA V5TM for interactive simulations. The weight of the component was simulated by the gravity environment in CATIA and the virtual objects in the software are constrained by a gravity field. The force feedback, during collisions, is sent to the haptic device.



Figure 1: Virtual reality environment equipment.

### 3.2 Subjects

Nine subjects (five males and four females) all right-handed, aged 20–57 years, were involved in the experiments. During a first survey subjects declared not exerting intensive muscle efforts during a 24-h period. All participants reported no history of problem in the upper limbs and eyes.

After a short explanation about the aim of the experiment, subjects were able to test the haptic arm in order to be familiar with. One experiment lasted roughly *1h and 15min* per subject. Another survey is fulfilled at the end of the experiment in order to know whether subjects were tired, what the goal of the experiment in their view was, and what their opinion (they thought) were about it.

### 3.3 Presentation of the experiment

The experimental place remained as silent as possible in order to avoid loss of concentration from the subject. The subject, face the screen, uses only his handwriting arm to move the haptic arm (Fig. 2). On the screen, the subject can observe the mechanical assembly composed by a bar and a ring. The bar is in horizontal or vertical position and along it the subject can move the ring with the arm. Ring's rotations are blocked with the software. The subject is free to move the ring along the bar as he wants: bottom-up/up-down movements when the bar is vertical, and left-right/right-left movements when the bar is horizontal). Then, he/she gives a value, trying to assess the length of the bar. The values are recorded in a database.

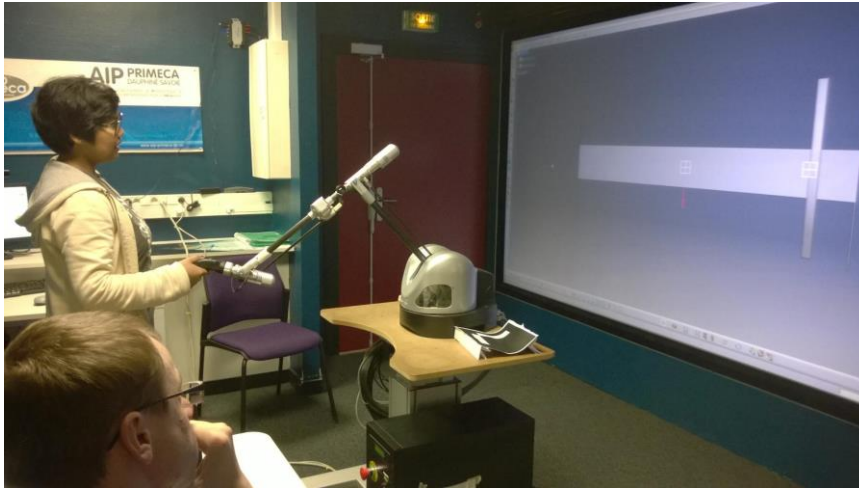


Figure 2: Subject perceiving horizontal length.

Afterwards, the subject turns back and can see the two crossed measuring tapes on the wall behind him/her: one vertical and one horizontal (Fig. 3). With this second source of information, he/she tries to assess again the length/distance. The subject is free to give again or not a value of the perceived distance.

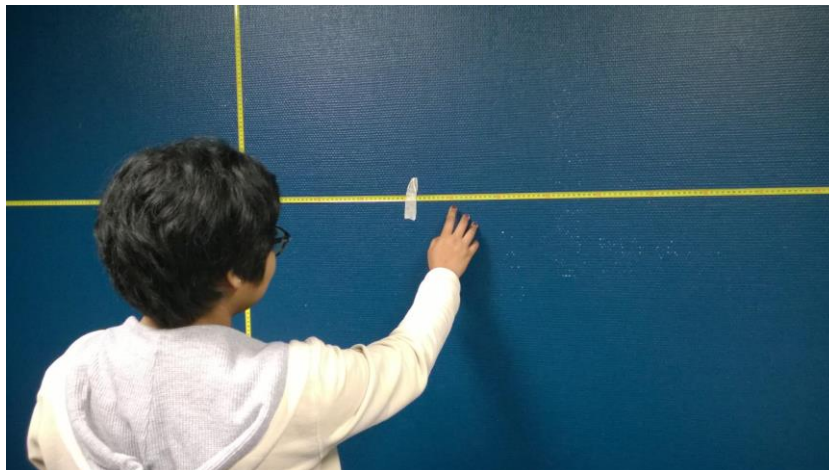


Figure 3: Subject estimating the length with ruler (measuring tape).

Before assessing the next value (next trial in the experiment), we change the bar's length displayed on the screen. Yet, the arm's movement remains the same and the subject ignores it. All in all there is sixty-four tests divided in two parts. The thirty-two first tests are realized when the bar is vertical and the thirty-two others with a horizontal bar. The length's perception is tested for eight different length. For each test, as previously said, a coefficient defined as:  $C_{eb} = (\text{bar's length displayed on the screen}) / (\text{length of the arm's movement})$  is calculated which will serve as a reference for comparison the tests between them. The experiment allows us to assess whether the subject is influenced visually by what he/she is seeing or based on what he/she touches, that is to say, depending on the race of the arm. Moreover, we want to value the two criteria which are the influence of the bar's orientation and the influence of the two measuring tapes.

### 3.4 Expected results

We expect that subjects will assess intermediary values between the length of the bar displayed on the screen and the length of the arm's movement. We assume also that the measuring tape will influence their visual perception. Finally, we suppose that results for the horizontal bar will be closer of the length seen (displayed) on the screen because a human have the habit to look from left to right as if he/she was reading. Note that other kinds of reading/writing such as: Hebrew and Arabic (from right to left), Chinese (up-down) ... are not considered in this study.

### 4 Results and discussion

With the experiment, we note the length assessed by the nine subjects, with and without measuring tapes (meters). All in all, we have  $64 \cdot 2 = 128$  length values per subject. First, we take the average value of the nine subjects for each test, separately with and without ruler (measuring tapes, meters). Then we chart the results: there is a chart of averages without measuring tapes (Fig.4) and a chart of averages with measuring tapes (Fig.5). The idea is to plot the point clouds of the collected perceived lengths depending on the  $C_{EB}$  coefficient. The higher the coefficient is, the longer the length of the bar on the screen is. We have made scatter plots of the perceived length in function of the coefficient  $C_{EB}$ . The higher  $C_{EB}$  is, the longer the bar displayed on the screen is. Coefficient  $C_{EB}$  varies from 0,3 to 3,6 for the experiments without ruler and from 0,5 to 6,1 for the experiments with ruler. Furthermore, in order to have a sharper analysis, when the bar displayed is horizontal plots are green and when it is vertical plots are yellow. The blue line represents the length of the bar displayed on the screen for each coefficient  $C_{EB}$ . The orange one represents the length of the arm's movement for each coefficient  $C_{EB}$ .

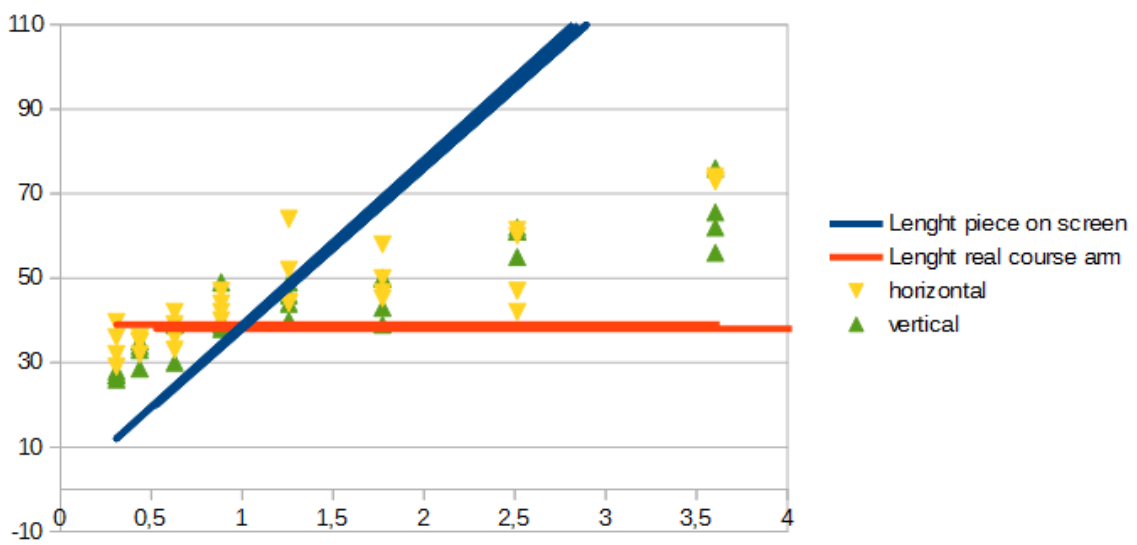


Figure 4: Average perceived length (cm) without ruler according to  $C_{EB}$  coefficient.

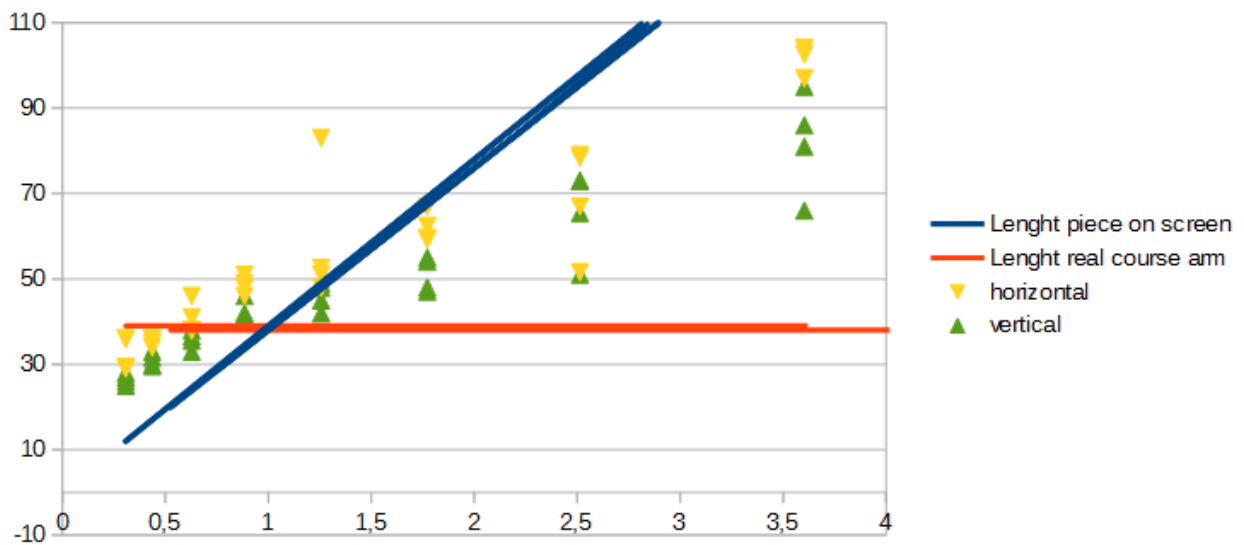


Figure 5: Average perceived length (cm) with ruler according to  $C_{EB}$  coefficient

From the figures, it is seen that subjects are influenced both by the bar on the screen and the stroke of the arm. To go further, the subjects are more influenced by the stroke of the arm than by the screen. Indeed, in any case, the standard deviation between the length on the screen and the average length assessed by subjects

is higher than the standard deviation between the length of the arm's movement and the average length assessed by the subjects (Table 1).

Table 1: Results of standard deviation [cm]

Relative to the length of the bar on the screen				Relative to the length of the stroke of the arm			
without meter	with meter	vertical bar	horizontal bar	without meter	with meter	vertical bar	horizontal bar
56,7	46,5	29,8	67,0	14,8	24,7	17,2	23,2

This result can be disturbing when it is compared to others studies on the influence of virtual reality on perceptions. In fact, the flavor [6], the olfaction [6], the stiffness perception [8, 9] and the spatial representation [7] are all mostly influenced by the sight (visual).

In our opinion, while assessing lengths, the association of the VR with the physical movement (i.e. the arm's movement) could be an exception among perceptions. In addition, we observe that, results (values) with the help of measuring types are higher. When subjects are looking at measuring types, they assess what they have seen on the screen and not the real motion of the arm. Indeed, the bar displayed on the screen and the two measuring types are assessed by the sight (visual), contrary to the arm's movement.

Finally, when the bar displayed on the screen is horizontal, subjects are much more influenced by their sight (what they are seeing) than by the arm's movement. This trend is emphasized when subjects use measuring types. It approves what we assume on the habit of a human to read from left to right (this was the case with the subjects involved in the experiments).

A qualitative analysis of the surveys fulfilled by subjects after performing the tests gives us further information. Out of the nine subjects, three said that they have been more influenced by what they felt with the arm, two have been more influenced by the screen, and the other four have been more influenced by the two factors, which is consistent with what has been measured. Finally, three of the nine subjects felt tired during the experiment. They were physically tired because they were standing during all the experiment and mentally tired because they were confused all along the experiment, due to the confusion of their brains receiving conflicting information by the two sources of data (information).

## 5 Conclusion and future work

Some limitations of the available techniques for human's perceptions stimulated this research on length perception (evaluation). This paper introduces a new method to quantify the influence of the visual feedback on the length perception of an object in Virtual Reality Environment.

Based on the proposed method for distance estimation, an application for virtual simulation is developed. The results of the performed VRE experiments show that subjects are more likely influenced by the movement of the arm rather than the length of the arm displayed on the screen, while quantifying the length of a part.

However, at this stage, the work has some limits. The first one deals with the relatively small number of subjects, which leads to an uncertainty of the results. Secondly, we wanted to improve the "random" aspect of the experience; alternating e.g. random vertical and horizontal bars. Unfortunately it is technically impossible to work with two simultaneous simulation files with Haption. In fact, the Haption unit from CATIA V5 is not designed to modify an object while it is manipulated. In addition to increase the amount of subjects and develop an appropriate haptic unit for the experiment, we can give some indications to improve the experiment.

Future work will focus to change the length of the arm's movement from one test to another. Thus, the race covered by the arms could have changed from one test to another, so that the subjects do not realize that the movement of the arm was still the same. It would have been also possible to perform the tests separately for the screen and the arm, in order to get a baseline for the experience.

At last, our analysis could be more precise by using statistics skills. Furthermore, we would improve the randomization of the different tests of our experiment by switching between verticals bar and horizontal bar.

**Acknowledgement:** This work has been partially supported by the LabEx PERSYVAL-Lab (ANR--11-LABX-0025) » (<http://www.persyval-lab.org/index.html>) and the European Community's Research Infrastructure Action - grant agreement VISIONAIR 262044 - under FP7/2010.-2015. (<http://www.infra-visionair.eu/>). We would like to thank Miss. Clémence CHALONY and Mr. Florian SCHMIDT for their involvement in the experiments.

## References

- [1] A. Pusch, O. Martin, S. Coquillart: HEMP – Hand-Displacement-Based Pseudo-Haptics: A Study of a Force Field Application, IEEE Symposium on 3D User Interfaces, 2008, 8-9 March, Reno, Nevada, USA, 978-1-4244-2047-6/08/\$25.00 ©2008 IEEE
- [2] A. Lécuyer, S. Coquillart, A. Kheddar, P. Richard, P. Coiffet: Pseudo-Haptic Feedback : Can Isometric Input Devices Simulate Force Feedback”, In Proceedings of the IEEE Virtual Reality 2000 Conference, Washington, DC, USA, 2000.
- [3] A. Paljic, J.-M. Burkhardt, S. Coquillart: Evaluation of pseudo-haptic feedback for simulating torque: a comparison between isometric and elastic input devices, HAPTICS '04, Chicago, USA, 2004.
- [4] D. J. Murray, R. R. Ellis, C. A. Bandomir, H. E. Ross, Charpentier P: On the size-weight illusion, In Perception & Psychophysics 61(8), 1999.
- [5] D.A. Gomez., F. Argelaguet, A. Olivier, M. Marchal, F. Multon, A. Lecuyer: Toward Pseudo-Haptic Avatars: Modifying the Visual Animation of Self-Avatar Can Simulate the Perception of Weight Lifting, IEEE, 654-661, 2014.
- [6] T. Tanikawa, M. Hirose: A Study of Multi-modal Display System with Visual Feedback, IEEE, 285-292, 2008.
- [7] K. Nguyen, C. Suiedy, I. Viaud-Delmony, O. Warusfe: Spatial audition in a static virtual environment: the role of auditory-visual interaction, IRCAM, 1-11, 2009.
- [8] N. Gurari, K. Kuchenbecker, A. Okamura: Stiffness Discrimination with Visual and Proprioceptive Cues, Pen Librairies, 121-126, 2009.
- [9] M.A. Srinivasan, G.L. Beauregard, D.L. Brock: The impact of visual information on the haptic perception of stiffness in a virtual environment, ASME, 555-559, 1996.
- [10] V. Interrante, L. Andersonand, B. Ries: Distance Perception in Immersive Virtual Environments, Revisited, IEEE, 3 -11, 2006.

# Connecting two trends in the scientific community: knowledge sharing and scientific output measuring

D.M. Popa<sup>1</sup> and G.B. Cotet<sup>1</sup>

<sup>1</sup> *University Politehnica of Bucharest, Romania*

## Abstract

In this paper we look at two present day trends from the scientific community: the push for open and free knowledge sharing under the form of open access papers and data bases and the evenly strong movement for measuring and quantifying research output.

The digitalization of knowledge has made it possible to store and measure the research results of diverse entities, such as individual researchers, departments, universities and even fields of study taken as a whole. The “scientific output” of a scholar is now easily and readily measured, compared and ranked against the results of others and numerous tools for facilitating such measuring and comparing are now openly available. More and more researchers stop to look at this dynamic picture of the scientific community’s outputs. We take a look at this growing trend and we review the scientific approaches analysing the results of the scientific community in a self-reflexive exercise. We also compare some of the available online tools that facilitate this trend for knowledge quantification.

**Keywords:** scientific collaboration, knowledge sharing, measurement.

## 1 Introduction

The digitalization of scholarship [1] has facilitated the mapping of scientific research and the specific measuring of research output. It seems that everyone and everything is now being measured, compared and ranked. Entities being measured range from individual researchers, university departments, universities, to countries and even research fields taken as a whole. Therefore, not only do researchers have to stay up to date with the discoveries in their fields, but they also have to keep track of research measuring instruments used in their fields in order to best promote their work. Scholars still live in a publication and citation driven culture, where citations are a base for formal rewards and this can lead to citation stress [2]. In addition to this, scholars also have to be present on social networks dedicated to researchers. Social networks such as ResearchGate make it easier for researchers to see who has read their work, not only who has cited their work in other indexed journals or books. On this background, the discussions about open access to articles, databases and knowledge in general have taken up an important place in the academic debate. While many agree that there are benefits in open knowledge sharing, scholars still face a dilemma: If I share before I publish, how will this affect my future H-index, consequently my chances of faster advancement, tenure, receiving other research grants etc.? Fear of nonreciprocal or opportunistic behaviour also stays in the way of open and free knowledge sharing. Part of the dilemma lies in the question “If I share first, how can I know that others will also share?”

This is why in the present article we look at these two trends from the present day scientific community: the push for open and free knowledge sharing under the form of open access papers and data bases and the evenly strong movement for measuring and quantifying research output. In a holistic perspective, openly sharing knowledge leads to scientific progress. From the view point of the “giver” open knowledge sharing has both incentives and disincentives. The incentives are that open knowledge sharing, open access (either of data or research output) can lead to higher citation rates and the consolidation of one’s reputation. But the “giver” faces a number of disincentives for sharing his research data. First of all, sharing is time and money consuming. Some of the most mentioned fears of scholars (identified in studies presented in the following sections) include the fear that others will publish first, that others will misinterpret the data and that they will

not give due credit to the creator of the data when using it. But as we will try to show in the following, open sharing can be a base for reputation building.

## 2 Knowledge sharing

The network society [3] is also present in the academic world. Scholars want to make their results known to others in their field, want to know what breakthroughs were made by others in their field and want to collaborate with others in research activities. With the help of the Internet, digital tools for knowledge sharing are now freely available to scholars who wish to make their research known to the world and who wish to stay informed about the state of the art in their field. Platforms such as Mendeley [4], PubMed [5], Meta [6], F1000 [7], ResearchGate [8] etc. help researchers to keep themselves informed about subjects of their choice and stay connected to their research network.

This enriched and Internet facilitated exchange of ideas leads to the advancement of knowledge. Open and free knowledge sharing could speed up this process. Thus, at a macro level, knowledge sharing leads to the progress of science, but a mismatch between the greater interest and the individual one has been observed, mismatch that halts the open sharing of knowledge [9]. At a micro level, open knowledge sharing can be seen as a form of social exchange. In a social exchange, unlike economic exchange, the price for the offered good is not asked at the moment of the transaction, but rather the giver expects a future return, that is not necessarily tangible [10]. Other researchers have also seen in the scholarly world a form of social exchange [11] or a form of reputation economy [12].

Researchers [9] who wished to know what the interest about data sharing in the academic community was made a literature review of papers about practices in data sharing by searching for the phrase *data sharing* in some of the most used databases in the academic world for article indexing. We followed this example and made a few inquiries in the Web of Science (WoS) [13] database and the Google Scholar (GS) [14] database in order to see how many articles have already been published about data sharing, open access, and bibliometric in general. The results are presented in Tables 1 and 2. An observation to be noted here is that when searching in WoS for the phrase *open access* in the topic field, the results list includes articles that are published in the open access system but do not actually speak about open access.

Table 1. Number of articles in WoS and GS when searching in the article title for:

Searched phrase in the title of indexed articles	Number of results in Web of Science	Number of results in Google Scholar
Open access	3626/3028*	13400
Data sharing	2934/1104*	4440

\*the second figure indicates search results for the exact phrase.

\*where only one figure is given it indicates the search results for the exact phrase.

When searching Google Scholar for articles with the exact phrase *open access* in the title, we get about 13400 results, after excluding patents and citations. When searching Google Scholar for articles with the exact phrase *data sharing* in the title, we get about 4440 results, after excluding patents and citations. This stands to show that researchers are quite inquisitive and responsive to the trends that develop in their own community, engaging in self-reflexive exercises about the status-quo and the desired state of things.

Table 2. Number of articles in WoS when searching in the topic of the article for:

Searched topic	Number of results in Web of Science
Open access	24146
Data sharing	111387/4795*

\*the second figure indicates search results for the exact phrase.

\*where only one figure is given it indicates the search results for the exact phrase.



Researchers are therefore interested in the topic of data sharing and open access, however there remain a few disincentives that stop researchers from openly sharing their research data. The most common reasons that researchers name when asked about why they do not openly share their research data are: too much time and effort [9], [15], the right to publish first or competitive misuse [9], fear of misinterpretation of data and of lack of recognition [9], [15]. Based on a survey of researchers from Germany, studies [12] found that researchers across the investigated disciplines (agriculture, engineering, social sciences, humanities, human science, natural science) rank the stimulants for sharing and the reasons for not sharing almost in the same order. Another interesting reported find by [15] is that research-intensive staff will more likely share data in a shorter time period in comparison to teaching-intensive staff. This is because teaching-intensive staff has less time to focus on research and publication due to teaching assignments. They therefore need more time to publish and they most likely publish at longer time intervals, therefore the time it takes to extract all benefits from their data is longer. Despite the existing disincentives, studies [16] have shown that sharing detailed research data lead to increased citation rate. Therefore, openly sharing could lead to higher citation rates, higher impact and influence scores and a stronger academic reputation, all of these being desired elements in the scholarly world. Open data sharing could lead to increased dissemination and also to increased social impact of research. Data sharing can be a new alternative impact meter for the work of a scholar, as presented in the following.

### 3 Measuring research output

The current academic main stream control tool for research output is the Web of Science database but numerous other alternatives have been introduced. Following the increase in the available tools for monitoring and measuring research output, numerous scientists published comparative analyses of these tools, describing advantages and disadvantages for each [17] [18]; [19]. An alternative, free and open for the large public impact meter is Google Scholar and many articles have analysed the comparative advantages and disadvantages of WoS and GS. Because publication culture differs across disciplines [17] the subsequent citation sources in these disciplines also differ. For example, in some research fields like Arts and Humanities or Social Sciences it is more likely that books will be published [20], [21] in comparison with fields from technical research fields. Consequently, a higher percentage of books in these areas will be cited. According to researchers [21] these fields are underrepresented in the Web of Science database. A similar conclusion has been drawn about the field of Anthropology, based on the output of Dutch scholars [17]. As these researchers [17] conclude, for such research fields, Google Scholar can be a promising source for measuring research output. In this case, in comparison with WoS, Google Scholar was found to be more suitable for indexing the research output, despite still existing problems with the database of Google Scholar, such as duplicates false-positive citations and the fact that “the construction of the dataset and the calculation of indicators are more transparent in the WoS than in GS”.

How preoccupied are scholars with these new alternative measuring instruments? If we considered the number of published papers on this subject, the answer would be “quite a lot.” When searching Google Scholar for articles with the exact phrase Google Scholar in the title, we get 1670 results, after excluding patents and citations (Table 3).

Table 3. Number of articles in WoS and GS when searching in the article title for:

Searched phrase in the title of indexed articles	Number of results in Web of Science	Number of results in Google Scholar
Google Scholar	170	1670
Web of Science	266	1210
Bibliometric	2269	5270

When searching Google Scholar for articles with the exact phrase *Web of Science* in the title, we get about 1210 results, after excluding patents and citations. An observation here is that some results in GS are in fact either print screens or pdf documents showing articles indexed in the WoS database and not articles about the WoS database. The general problem of the indexing of non-scientific works (among others) in Google

Scholar is also underlined by [18]. In the Web of Science database, all searched phrases receive smaller values. The results count is much higher in WoS when the search phrase is completed in the topic field and not in the tile field (Table 4).

Table 4. Number of articles in WoS when searching in the topic of the article for:

Searched topic	Number of results in Web of Science
Google Scholar	5033
Web of Science	10799
Bibliometric	5455

Collaboration in research output (articles) is also measured in databases by the number of co-authors (in some cases we also see a “top co-authors” description), as is international collaboration (authors affiliated to institutions in different countries). An example of such an analysis can be found in the work of [21] where, with the help of digital maps the authors show in a graphical manner the web of international and institutional collaborations in the field of Digital Humanities. Other scholars [22] developed such maps by “using millions of abstracts from MEDLINE” in order to show the network connections between authors, articles, methods diseases and chemicals. Google Scholar also offers metrics for articles. The Publish or Perish software retrieves and analyzes academic citations based on the results found in Google Scholar [23]. The interdisciplinary nature of collaboration is however more difficult to measure based on research output without detailed, targeted data analysis.

The arrival of other alternative tools for measuring research output led to the development of *altmetrics*. Altmetrics could for example measure the online impact of a researcher’s work, under forms less traditional than articles and books [19]. One such online alternative is the Altmetric platform [24]. The Platform Altmetric collects and measures online conversations about scholarly content, making it easier for researchers to know who is talking about their work. A comparison of 15 of these new available tools and alternative impact metrics is presented in the work of Wouters & Costas (2012) and the authors conclude that most of the tools are suitable for individual assessment rather than aggregated levels. This is why the authors named these instruments ‘technologies of narcissism’ [19]. However, if perfected, these alternative measuring instruments could in time turn into more official control mechanism and data sharing could be one of them.

#### 4 Conclusion

Altmetrics could help reputation building and lead to current day formal recognitions. Therefore, researchers should not completely neglect these alternative metrics, because a better online presence could in time have an impact on main stream performance indicators. However, critics say that these alternative metrics do not have the benefits of the classical peer review process and that social “noise” doesn’t automatically equal scientific impact. Also, in very specialized fields, scientific output is targeted to a limited number of specialists who have the specialized field knowledge. The previous mentioned tools can be seen as the infrastructure of the scientific community. Along with their spread come the questions: “How much time should a researcher dedicate to learning how to best use this infrastructure?”, “What is the reasonable time period a researcher should dedicate to these technologies of narcissism?”, “Will their use modify the research and publication behaviour of scholars?”, “How many redundant measuring tools are there/ will there be?”, “Will data sharing become an impact meter for the scholarly work?”.

#### References

- [1] C.L. Borgman. *Scholarship in the Digital Age: Information, Infrastructure, and the Internet*. The MIT Press. 2007.

- [2] J. K. Tijdkink, S. de Rijcke, C. H. Vinkers, Y. M. Smulders, P. Wouters. Publicatiedrang en citatiestress. De invloed van prestatie -indicatoren op wetenschaps beoefening. In Ned Tijdschr Geneesk. 2014;158:A7147. 2014
- [3] M. Castells. The Rise of the Network Society. Wiley, 2000.
- [4] <https://www.mendeley.com/> Accessed August 2016
- [5] <https://www.ncbi.nlm.nih.gov/pubmed> Accessed August 2016
- [6] <http://meta.com/> Accessed August 2016
- [7] <http://f1000.com/> Accessed August 2016
- [8] <https://www.researchgate.net/> Accessed August 2016
- [9] B. Fecher, S. Friesike, M. Hebing: What Drives Academic Data Sharing?. In PLoS ONE 10(2): e0118053. doi:10.1371/journal.pone.0118053. 2015(a)
- [10] P. Blau: Exchange and power in social life, New York Wiley, 1964.
- [11] T. P. Liang, C.C. Liu, and C.H. Wu: Can Social Exchange Theory Explain Individual Knowledge-Sharing Behavior? A Meta-Analysis. In ICIS 2008 Proceedings. Paper 171, 2008
- [12] B. Fecher, S. Friesike, M. Hebing, S. Linek, A. Sauermann: A Reputation Economy: Results from an Empirical Survey on Academic Data Sharing. In DIW Berlin Discussion Papers. IMPRESSUM, 2015
- [13] Web of Science: <http://apps.webofknowledge.com> Accessed 2<sup>nd</sup> September 2016
- [14] Google Scholar: <https://scholar.google.com/>. Accessed 2<sup>nd</sup> September 2016
- [15] Tenopir C, Allard S, Douglass K, Aydinoglu AU, Wu L, et al. (2011) Data Sharing by Scientists: Practices and Perceptions. PLoS ONE 6(6): e21101.
- [16] H.A. Piwowar, R.S. Day, D.B. Fridsma: Sharing Detailed Research Data Is Associated with Increased Citation Rate. In PLoS ONE 2(3): e308. doi:10.1371/journal.pone.0000308. 2007
- [17] A. Prins, R. Costas, T. van Leeuwen, P. Wouters: Using Google Scholar in research evaluation of humanities and social science programs: A comparison with Web of Science data. In Research Evaluation, 1–7, Oxford University Press, 2016.
- [18] J. de Winter, A Zadpoor, D. Dodou: The Expansion of Google Scholar Versus Web of Science: A Longitudinal Study. In Scientometrics, 98, 1547–65, 2014. DOI: 10.1007/s11192-013-1089-2.
- [19] P. Wouters, R. Costas: Users, Narcissism and Control. Tracking the Impact of Scholarly Publications in the 21st Century. SURFfoundation, 2012
- [20] B. Wellman, D. Dimitrova, Z. Hayat, G. Ying Mo, L. Smale: Networking scholars in a networked organization. In Contemporary Perspectives on Organizational Social Networks Research in the Sociology of Organizations, Volume 40, 479- 497, Emerald Group Publishing Limited, 2014
- [21] A. Salah, A. Scharnhorst, S. Wyatt: Analysing an Academic Field through the Lenses of Internet Science: Digital Humanities as a Virtual Community. In Tiropanis et al (Eds) Internet Science. Second International Conference, INSCI 2015, Brussels, Belgium, May 27-29, 2015, Proceedings pp 78-89, Springer International Publishing, 2015.
- [22] F. Shi, J. G. Foster, J. A. Evans. Weaving the fabric of science: Dynamic network models of science's unfolding structure. Social Networks 43 (2015) 73–85. Published by Elsevier B.V. 2015
- [23] A.W Harzing: Publish or Perish, available from <http://www.harzing.com/pop.htm>, 2007. <http://www.harzing.com/resources/publish-or-perish> Accessed August 2016
- [24] <https://www.altmetric.com/> Accessed August 2016

# Further challenges of eCall service and infrastructure

G. Carutasu<sup>1</sup>

<sup>1</sup> *Romanian-American University, Romania*

## Abstract

The approaching deadline for eCall service implementation for new cars in 2018, raises a series of technical and logistic issues. The eCall service, part of iCar initiative, aims to reduce the road fatalities and severity injured person reduction, for post-crash situations. The eCall service consists into an In Vehicle System (IVS), which will be delivered mandatory on new cars, starting with 2018, able to transmit, in case of an car accident, the necessary data for 112 emergency system. The IVS transmit relevant information, as accident coordinates, type, model, colour, owner using a data message, using Public Land Mobile Network (PLMN). The data packet is treated as an emergency call using a flag discriminator under the form of Minimum Set of Data and carried to nearest Public-Safety Answering Point (PSAP) managed by emergency organizations. After MSD is resolved by 112 systems and relevant information is displayed to 112 operators. After 20 seconds, the 112 system initiates a voice call-back to the source of MSD. The IVS now is used as regular cellular, the operator getting contact with the car driver. If the operator cannot establish a connection and identify the severity of the crash, will dispatch a standard emergency team. However, the eCall can be triggered also manual, pressing a button installed in the car, if the driver is suffering a heart attack or is witness of another accident. In this paper are debated further challenges of eCall implementation, given by adapting the service to specific types of vehicles, like two wheels' vehicles, heavy goods vehicles, dangerous goods transportation and long distance vehicle transports. The results presented were obtained into iHeERO project, financed by European Commission and previous research.

**Keywords:** Intelligent Transport Systems, emergency systems, eCall, iCar

## 1 Introduction

In 2004, European Commission started the e-Safety plan, aiming to reduce road crash fatalities. This plan is part of a larger initiative called Intelligent Car Solution i2010. The e-Safety plan was to cover all phases regarding road accidents: *exposure, crash avoidance, injury reduction* and *post-crash* situations.

The concept of Intelligent Transport Systems (ITS) was introduced by e-Safety, considering the implementation of IT&C on-board of vehicles to reduce or avoid the accidents and consequences limitation. As part of iCar promoted systems, eCall offers the possibility of accident advertising to PSAP, using an automatic sequence of data and voice call, from incident car to PSAP and backwards.

In Figure 1 is presented the eCall service chain. When an accident occurs, the on-board eCall system module, called IVS initiates a data transmission under the form of MSD, containing references regarding time of accident, place, car involved or some additional information. The MSD is carried by MNO through PLMN and treated as emergency call, using the emergency flag. The MSD arrives to PSAP and it is presented to PSAP operator. To link the car details, like: color, manufacturer, owner etc. the Vehicle Identification Number (VIN) is used. After the MSD is received, the PSAP initiates a call to the vehicle implied in the accident to gather additional information to size the emergency team that will be dispatched on the crash site.

The IVS contain an GNSS module, who offers the position of the accident, embedded in MSD. The IVS contains also an In Band Modem to connect the IVS to PLMN. A full description of IVS was given in [1], using the standard given specifications.

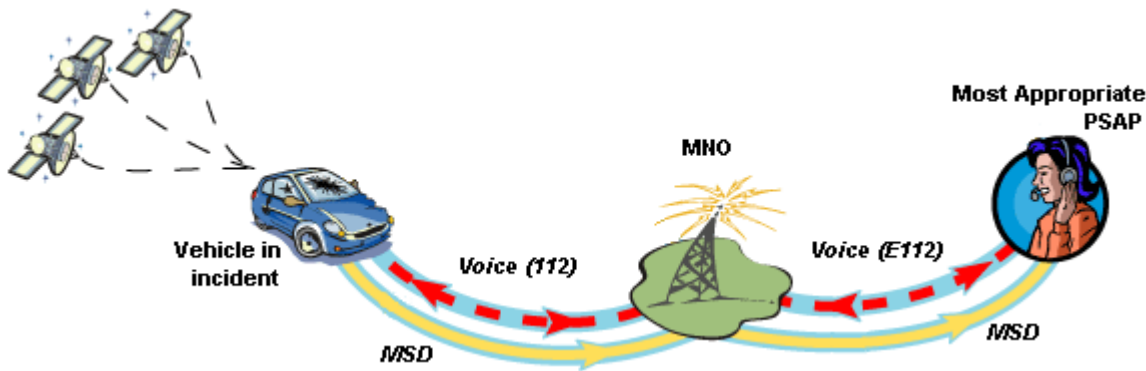


Figure 1: eCall service chain. [2]

It is estimated, accordingly to the European Commission studies, that more than 2 500 lives will be saved each year using the eCall service on full deployment. The implementation of the eCall faced a series of delays, but now it has been scheduled to be operational starting with 2018.

2

## 2 Previous work and eCall barriers

### 2.1 HeERO projects

After e-Safety plan approval, the Forum assembled around e-Safety initiates in 2004 a Memorandum of Understanding (MoU) for Realisation of Interoperable In-Vehicle eCall. This was one of the first steps towards an integrated and interoperable service among European Union. The design and implementation of such service demanded a strong support from EC and European Parliament, formalized as Directives or approved legislation.

As part of the design and implementation, it faced several barriers, opposing to a large and harmonized adoption of eCall. The efforts were concentrated over PSAP upgrade, from state members, in order to be able to operate eCalls. The first sustainable initiative of EC was to fund HeERO project. It begun in 2011, with a three years' duration, HeERO concerning the pan-European in-vehicle emergency call service "eCall".

The main objective of HeERO was to create the necessary infrastructure and fully demonstrate the eCall operability. A list of secondary objectives was aimed also, by the consortium organized in nine pilot sites, one for each country (Croatia, Czech Republic, Finland, Germany, Greece, Italy, The Netherlands, Romania and Sweden). This list covered interoperability and cross border continuity, harmonization across Europe, by implementing available eCall standards, infrastructure upgrades and recommendation for future implementations.

The second HeERO project - HeERO 2, with two years' duration, started on 2013. New 6 countries (Belgium, Bulgaria, Denmark, Luxembourg, Spain and Turkey) have joined to HeERO infrastructure. Also, from the consortium made part also associate partners, without EC funding but granting HeERO expertise.

The preliminary results of Harmonized eCall European Pilot (HeERO) reported by Romanian pilot site in [3]. The implementation of eCall in reported case supposes to route all eCalls to Bucharest, as central PSAP having eCall functionality with a backup situated in Brasov county. It must to be said that Romania has 41 PSAPs, one for each administrative areas (counties). The preliminary call, carrying the MSD is routed from the MNO to Telecom network and presented to nearest PSAP. Because of flag discriminator the signalizes an ecall, the call is routed to Bucharest PSAP. The emergency scenario supposes that after the MSD is resolved and presented in Bucharest to be transferred to nearest PSAP. The same pilot site is presented in [4], revealing a succession of over on thousand live tests performed by Special Telecommunication Service (STS) in Romania in 2012. The STS operates the emergency call unit service in Romania. The tests were made using two different IVSs, having test, automatic or manual triggering condition. Also, the operational tests covered different kind of landscapes and roads: urban, rural, highways and mountain areas. The goal of the study was to measure the availability of the service and two KPIs: one being the time spent between eCall initiation and MSD presentation to PSAP and second, the duration of voice channel blocking by MSD.

They used two scenarios, with and without eCall discriminator flag. The discriminator flag signalizes to MNO operator that present call is an emergency call. The flag was introduction was necessary because, before eCall, the usual direction of an emergency call was from caller to PSAP and not backwards. The reported results showed an over 92% availability of the service and KPI 1 from 23s in urban area to 33s in mountain and for KPI 2 with 14s in urban area and 18s for the mountain section. The study revealed that the availability of the service is strictly correlated to MNO performance in the tested area, with poor values in mountain area. Also, if the flag discriminator isn't properly configured by MNO the MSD is routed to a wrong PSAP (without eCall function) and presented to the operator as silent call.

## **2.2 eCall barriers**

Starting from the eCall definition, this is an automatic call triggered by in vehicle sensors in case of an accident. In [5], the authors evaluate the perspective of automatic triggering of eCall, based on UK case study. The study is built using data collected in the period 2000 and 2010 of car road accidents in UK. They assumed two automatic triggering conditions. First, when the frontal or lateral airbag is committed. The second automatic triggering situation occurs when any airbag is activated. According to the study, only 20 % of total injuries (including fatalities, serious and slight injuries) might be reported, using first condition. In case of second automatic triggering condition, if uses any airbag as input, the sensitivity will rise up to 65%, with even higher values (85%) in case of fatal and serious injuries. Furthermore, the study presumes that eCall service is working without failure. Anyway, the authors couldn't recommend a single triggering condition. The sensors group that trigger the automatic emergency call service remains on car manufacturer choice.

Even if the main purpose of eCall is to save lives, by reducing the intervention time of rescue teams by a proper localization, other issue that may arise is the cost effectiveness. In [6], are presented some business models for aggregating data obtained as a results of an accident. The first one, is theft prevention in case of false car crush, when the owner reports accidents to insurance companies to recover unrealistic damages. So, the insurance company might compare the real accident data with the reported ones. The second, to point into a GIS application, the spot of accidents and to offer alternative routes for drivers. The third, is to use accident data to study various security measures impact, or filtering by car manufacturer, car model etc. Integrating eCall data to Traffic Management Center (TMC) is a must, for proper using of data in real time, conducting to efficient traffic management measures in real time. Nowadays, because of wide spreading of smartphone application, the drivers use in most cases, for unknown destination, the routing application that can point accidents place in real time using on-line connection. Furthermore, the TMC offers, on institutional site the position of major accidents.

The eCall limitation to data and voice communication, using mandatory an MNO number to register into the network, due to security reasons, might be exceeded by using IoT technology. In [7], the NEXES project is presented, proposing an extended concept of emergency message content, including video calls, multimedia messages from smartphone applications, social media, Voice-over-IP (VoIP) or real-time text (RTT). Although, defining Next Generation of Emergency Services is an undergoing process, some reference architectures being published as position papers by various actors involved in the field (e.g. EENA). Anyway, it should be emphasized the gap between today communication facilities (e.g. voice call, MMS, enhanced content from apps etc.) and the ones that emergency services approved to work with. There are only recognized as such the voice calls. So, even it was started almost ten years ago, the eCall it isn't ready yet, having a wide range of issues. Otherwise, it cannot be expected that such complex systems needed to be implemented, in order to assure the services described above, to be available very soon.

The implementation of smartphone in preventing accidents, is seen by [8] in a different way. The authors found a direct link between phone usage on driving and the car accidents. So, they proposed a "smart car system", where the vehicle speed is limited during calls. They also designed an automatic system for text messaging that contains data about the accident, being sent to emergency and, so called "victim guardians". The proposal of IVS replacement might offer a starting choice in case of old vehicles. If the eCall system is mandatory from 2017 and the European Commission expects to have a critical mass in 2020 and a full deployment in 2030, the older vehicles couldn't benefit the service. In that sense, using a smartphone connected to the car, prepared with various sensors that will automatic trigger the eCall, represents a bigger market than new car sells market for IVS vendors.

### 3 iHeERO updates

The core members of HeERO projects, together with new ones, covering eleven countries (Bulgaria, Cyprus, Czech Republic, Finland, Germany, Greece, Ireland, Italy, Portugal, Romania and Slovenia) formed a new consortium that initiates the iHeERO project. The consortium includes 58 commercial partners and counts 26 Associated Partners. The project budget is over 30 mil. EUR and it covers funding for the period 2015-2018.

The issues addressed by the iHeERO (“I” for “infrastructure”) continue the efforts of HeERO1 and HeERO2, regarding the necessary PSAP infrastructure to realise Pan-European eCall preparation for the new member states [9]. The new items on objectives list are: eCall deployment for special vehicles (HGV, Dangerous Goods, Distance Coaches), two wheeled vehicles and PSAP Conformity Assessment.

The issue of special vehicles in emergency situation is quite important to size the proper rescue team. For instance, in case of an accident, where a truck carrying living animals is involved, the dispatch of the animals is a priority. Differing from this situation, in case of Dangerous Goods, it is very important that fire-fighters to be equipped with proper extinguisher gear, suitable for the chemicals transported. There are several notorious accidents, occurred after the car crash, by explosion of inflammable materials, because fire-fighters weren’t aware of the cargo content in real time.

Also, the severity of the accident could be seized knowing how many persons are potentially involved. In case of Distance Coaches, the passengers number might be transmitted in optional fields of MSD. The eCall for two wheeled vehicles, addressed before by [10], differ from a common eCall, because of triggering system. If in case of common eCall the trigger could be the airbag, in case of two wheels’ vehicle is no longer an option.

All the aspects presented above, includes particularities of eCall. The special vehicles require an eCall content update for each transport, to include the type and the size of the goods carried or the number of the person who travel on long distances. For the two wheeled vehicles, the triggering systems (including vehicle and helmet or body part) is different for a standard implementation.

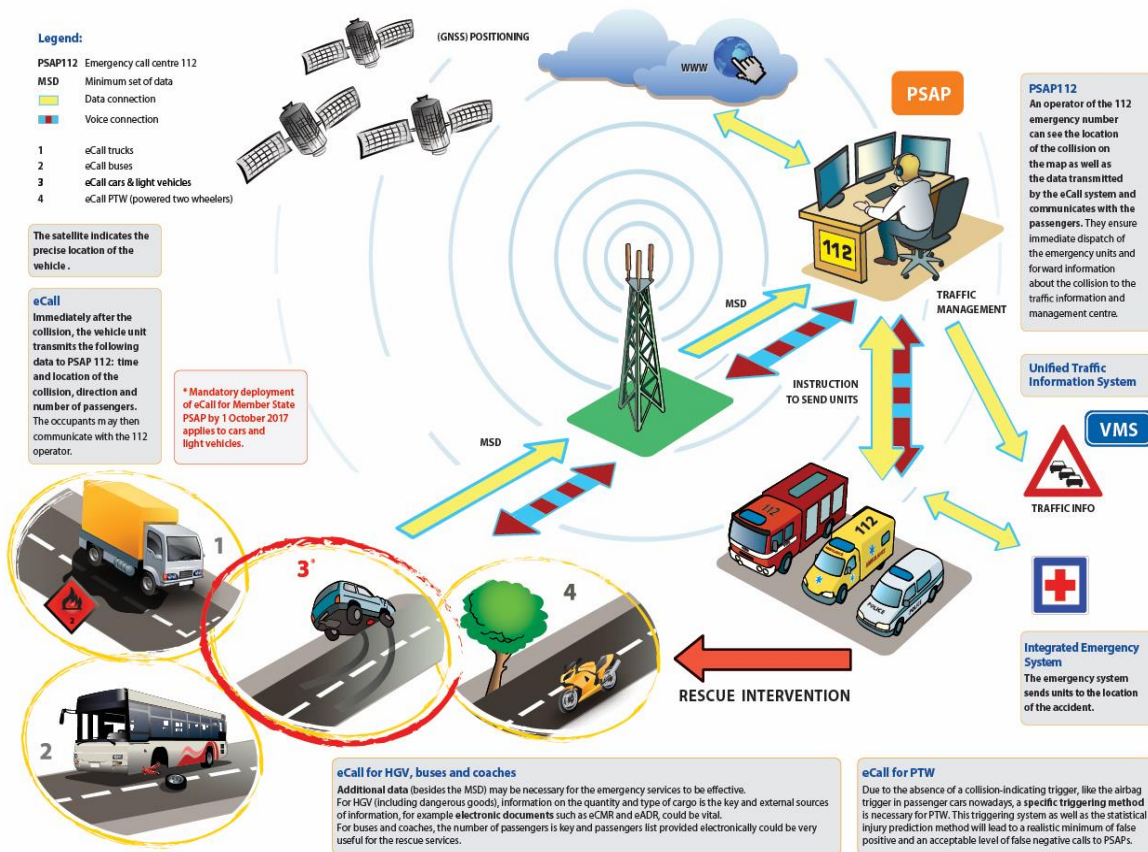


Figure 2: iHeERO description. [9]

## 4 Conclusions

Even eCall started as an initiative for increasing road safety, nowadays it needs to address new challenges. The continuous development of personal telecommunication devices, like smartphones, tablets, laptop shows that the PSAP have to be upgraded in order to be able to receive unstandardized calls (not using MNO or PSTN) and to be treated as emergency call. There are situations when the MNO access isn't available but it is possible an wifi connection. Also, because of recent terrorist attacks, it became obvious the link between the emergency call to other security systems (like CCTV, satellite image etc.).

The interoperability with similar systems should be also a priority. The ERA GLONASS service was tested from the period of HeERO project but still need further attention. This interoperability shows its importance when people travel between EU and Rusia or a vehicle is bought and used outside of EU. The link of actual PSAP with multimedia messages from various sources, forms the foundation for Next Generation of Emergency Service, still encountering a serious gap between the PSAP approved types of incoming calls and the personal communication devices. The EC launched in 2014 a series of funding line under H2020 RIA that hope to fill the gap.

## Acknowledgement

The article presents the activity of iHeERO project funded by the EC. I would like to thank to previous HeERO coordinator, Mr. Andy Rooke. The author was part of HeERO1 project and now is working on iHeERO project as team leader of Romanian-American University partner.

## References

- [1] G. Căruțașu, Cz. Botezatu, C. P. Botezatu: Current status for eCall post-crash vehicle safety system in Europe, in Proceedings of 10th International Conference of Inovative Technologies, MIT, 27-29 Sept., Fiesa –Slovenia, pp. 35, 2009
- [2] European Commision: eCall save lives. Digital market. Available at <https://ec.europa.eu/digital-single-market/en/ecall-time-saved-lives-saved>
- [3] D. Dumitrescu, A. Grososiu, R. Ropot, V. Roșu, G. Ristea, G. Căruțașu: Solution for eCall implementation at national level within the HeERO project – Romania case study, Paper EU-00407, The 19th ITS World Congress, 22-26 Oct., Vienna, 2012
- [4] D. Dumitrescu, Gh. Oncioiu, R. Ropot, Al. Mohora, G. Ristea, G. Căruțașu: eCall operational tests in the live system implemented in Romania, 9th ITS European Congress, Dublin, Ireland, TP 0092, 4-7 Jun., 2013
- [5] M. Seidl, J. Carroll, R. Cuerden: eCall–Defining Accident Conditions for Mandatory Triggering of Automatic Emergency Calls. In 24th International Technical Conference on the Enhanced Safety of Vehicles (ESV), Gothenburg, Sweden, 2015.
- [6] G. Căruțașu, C. P. Botezatu, Cz. Botezatu: Business models for extending of 112 emergency call center capabilities with e-call function insertion, Analele Universității din Oradea, Științe economice Tom XIX, pp. 1195-1199, Dec., 2010
- [7] M. Manso, B. Guerra, C. Carjan, A. Jigman, A. Amditis, E. Sdongos, D. Donaldson: The Application of Telematics and Smart Devices in Emergencies: Use Cases in Next Generation Emergency Services. In 2016 IEEE First International Conference on Internet-of-Things Design and Implementation (IoTDI) pp. 289-292, Apr 4, IEEE, 2016
- [8] V. Kate, A. Karnavat, T. Ahirrao, S. Holkar: Smart Car System. International Journal of Innovative Research and Development, vol. 4, issue 2, 28 Feb., 2015
- [9] iHeERO Official Website. Available at <http://iheero.eu/about-iheero/>
- [10] S. Candefjord, L. Sandsjö, R. Andersson, N. Carlborg, A. Szakal, J. Westlund, B.A. Sjöqvist: Using Smartphones to Monitor Cycling and Automatically Detect Accidents: Towards eCall Functionality for Cyclists. In International Cycling Safety Conference 2014, 18-19 November 2014, Göteborg, Sweden, 2014.



# Surgeon-engineer: Can we really collaborate? Yes, we can.

D. Popescu<sup>1</sup>, D. Laptoiu<sup>2</sup>, A. Hadar<sup>1</sup>, R. Marinescu<sup>2</sup> and I. Botezatu<sup>2</sup>

<sup>1</sup> *University POLITEHNICA of Bucharest, Romania*

<sup>2</sup> *Colentina Clinical Hospital of Bucharest, Romania*

## Abstract

Currently, the development of customized surgical guides is hampered by the difficulty of quantifying and translating surgeon requirements in terms of engineering specifications, in the context of a complex workflow dictated by patient personalization, as well as of a complicated communication between physician and engineer. Therefore, there is a strong need to find computer-aided solutions for bridging the gap between surgeons' ideas and needs and their practical materialization. Our research is focused on developing an intelligent collaborative online platform for the design and manufacturing of customized guides for orthopedic surgery. The platform is intended to support surgeon-engineer cooperation and information sharing in developing patient-specific surgical guides. It offers tools, which enhance the surgeon-engineer online collaboration, and tools, which allow inferring surgeon intents by using structured questionnaire adapted to the surgical intervention type and anatomical zone. Questionnaires' answers support capturing, filtering and defining the design intents using an inference engine. Several case studies for designing and manufacturing osteotomy guides are presented for illustrating platform main functionalities and current stage of implementation.

**Keywords:** customized surgical guides, collaborative design, communication, additive manufacturing.

## 1 Introduction

Worldwide an increased importance is given to personalized medicine and to the fact that nowadays the innovation in creating customized medical products, as well as in keeping a good market position can only be accomplished by a synergetic physicians-engineers approach, aiming at bridging the gap between medical needs and their practical materialization as new customized devices and healthcare services [1]. Collaboration and communication are here the golden words for developing modern medical products and for supporting new and innovative ideas in this field.

During the last decade the research in the medical sector has been focused towards personalizing healthcare, reducing medical expenses, improving patients' quality of life, democratizing the access to quality medical care, remotely monitoring patients' health status, developing new medical devices, materials, treatments or methods of clinical investigations [2-3]. All these objectives could not and cannot be entirely achieved in the absence of the considerable advances from the areas of robotics, nanotechnologies, additive manufacturing (AM), virtual reality, augmented reality, haptic simulators, medical informatics, embedded tracking technologies, sensors and wearable technologies, advanced medical data visualization and processing or intelligent decision support systems. Nor can they be fulfilled in the absence of doctors-engineers cooperation for developing cost effective and innovative solutions for a large range of medical specialties and applications such as virtual surgical training, personalized medical devices design and manufacturing, smart patient e-monitoring, diagnosis or intelligent rehabilitation, for supporting medical decisions, improving the quality and reliability of medical diagnosis and treatment, increasing the accuracy of surgical interventions or for offering access to professional healthcare systems/devices for patients in remote locations, for improving knowledge and skills in shorter times and at lower costs.

However, although this interdisciplinarity has many benefits, for the patient in the first place, there are also aspects that hamper the cooperation between doctors and engineers. The medical and engineering fields have

different practical approaches and research perspectives, different regulations, requirements and constraints, goals, evaluation and performance criteria etc. The professional language (terminology) is also a barrier for a good communication. Studies presented in literature [4-7] show that, indeed, the communication problems have a negative impact on innovation in the field, different solutions being proposed in order to overpass the aforementioned barriers and to find and implement methods, software tools, visualization and simulation applications that can support and improve the competences of all actors involved.

In this context, we are developing a platform (POIGO – figure 1), which enhances the information sharing, and the communication between doctors and engineers for the design and manufacturing patient customized surgical guides. It integrates medical and engineering knowledge database, different sets of computer aided tools, software applications and medical modeling methods, facilitating the collaborative design process mandatory for this type of application. The surgical guides' design process uses specific information about patient anatomy, which obviously imposes an individual solution for each patient/clinical case. In this context, there is a need for a knowledge-based support system to assist the surgeon and the engineer in establishing the guide design by processing CT scanning data, reconstructing the 3D anatomical model of the patient, establishing the number and placement of anatomical landmarks necessary for a correct and unique positioning of the guide on patient bone structure. The proposed online platform implements the above mentioned working protocol, facilitating the cooperation surgeon-designer and supporting communication based on contextual suggestive 3D models/images, in the same time allowing the quantification of surgeons needs and their translation into design specifications.

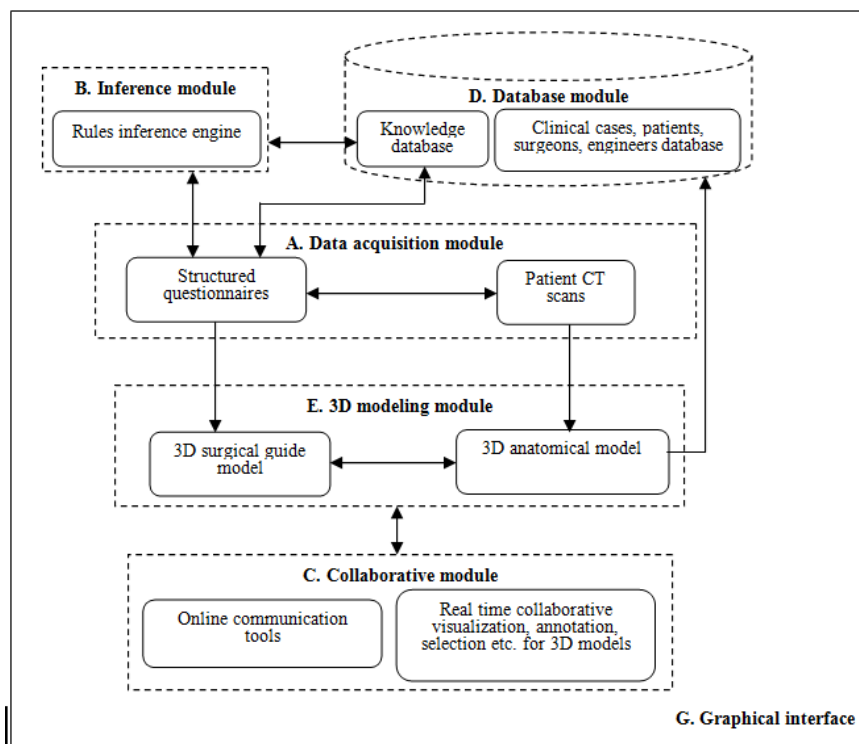


Figure 1: Schematic of POIGO platform: modules and data flow

## 2 Patient-specific surgical guides

Patient-specific surgical guides are used as physical aids in certain surgical procedures (pedicle screw placement, osteotomies for correcting long bones deformities, osteotomies for distal radius intra-articular malunions, osteotomies for total knee or hip arthroplasty, corrective osteotomies for malunited fractures of upper extremities, etc.), guiding the surgeon when performing precise drilling or cutting operations (fig.2) [8]. The advantages offered by using this guides are: safety by decrease of x-ray exposure for patient and medical team, lower intervention cost and increase of surgical accuracy.

The workflow for designing and manufacturing these guides is the same regardless the type of surgery:

1. Patient CT scanning data acquisition, attention being paid to respect the specific scanning protocol for this type of applications;
2. Reconstructing the 3D model of the anatomical area/areas of interest using a dedicated medical modeling software (such as Mimics, 3Doctor, Osirix, Amira, etc.) and exporting the model as .stl file;
3. Importing the .stl file of the anatomical model in the Reverse Engineering application of 3D CAD software such as Imageware (Siemens, NX), Digitized Shape Editor (Dassault Systemes, CATIA), etc. and reconstructing the surface or solid model of the patient bone structures;
4. Selecting zone from the surface or solid model of patient bone structures for supporting the guide (landmarks), and establishing the tools (drills, cutting saw blades) trajectories;
5. Designing the guide based on tools trajectories, landmarks and the supporting surfaces from the patient bone structure;
6. Establishing guide material and manufacturing method – most of the time the guide is fabricated from plastic material which can be sterilized at low-temperature, using AM technology (Stereolithography, Fused Deposition Modeling or Selective Laser Sintering). Moreover, the guide can include metallic sleeves for eliminating the risk of producing plastic debris that come in contact with patient during surgery;
7. Manufacturing the guide – usually, both the guide and physical model of patient bone structures of interest are manufactured using AM in order to check the fit between them before the real surgery;
8. Using the guide after sterilization.

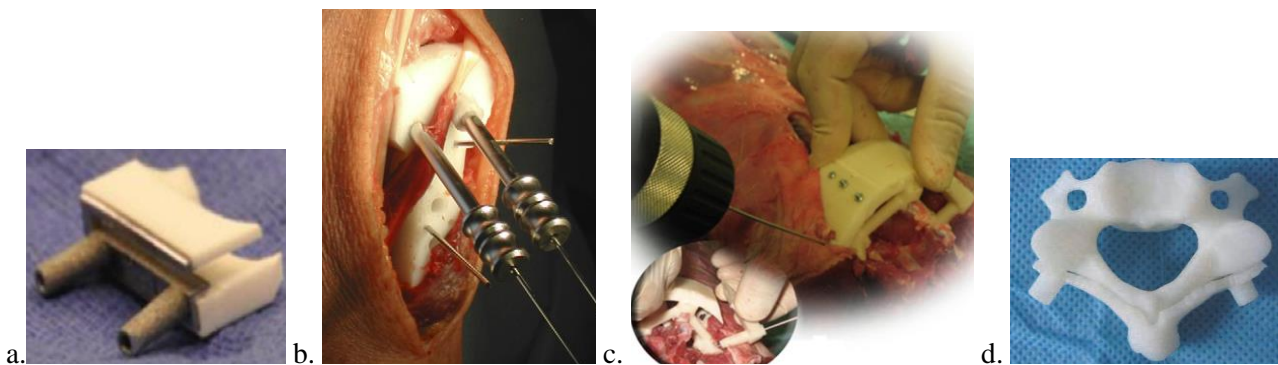


Figure 2: Examples of patient specific surgical guides from literature: a. DeWouters [9], b.Kunz [10], c. Ferrari [11], d. Lu [12]

An example of such a workflow is illustrated in figure 3 for the design and manufacturing of an osteotomy guide needed for correcting a complex femur deformity. In the ‘traditional approach’ of this workflow, the surgeon and engineer separately perform their own tasks, and they collaborate by sitting in front of the same computer, discussing and selecting different zones on the patient anatomical virtual model.

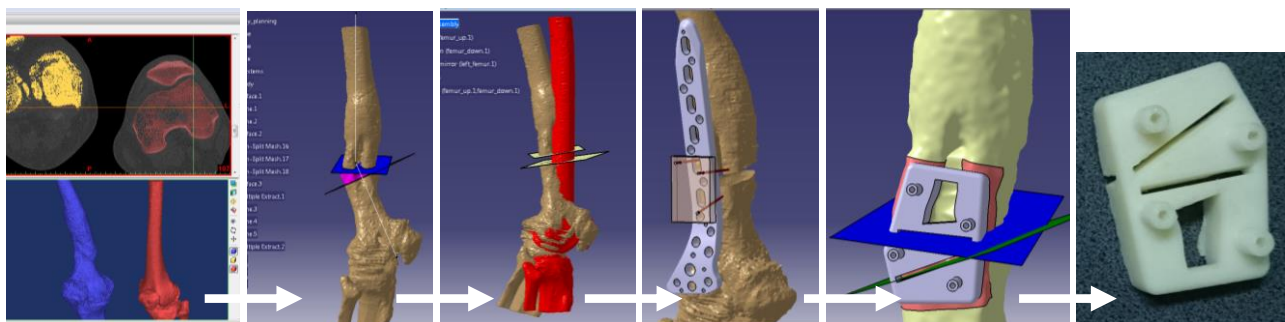


Figure 3. Design and manufacturing osteotomy guide for correcting femur deformity

### 3. POIGO platform

In the process of design and manufacturing patient-specific surgical guides, the collaborative steps are the most complicated ones because they require communication, visualization and annotation of the virtual model. CT files and medical case description can be sent by email, but surgeon and engineer should meet face-to-face for working on the virtual anatomical model on engineer's computer. This last requirement heavily limits the cooperation and the access to these medical tools for surgeons in remote locations. Moreover, during face-to-face working session, several information should be available on spot (similar case studies presented in literature, data sheets with technical specifications of different surgical tools, designs of surgical guides from literature and practice, medical information, manufacturing processes, manufacturing materials data sheets, etc.), which it is not possible most of the time because it implies searching and accessing lots of data – a time consuming task.

A software solution currently available, SurgiCase Connect (Materialise, Be), offers tools that can help surgeons to collaborate in the guides' design process. However, this application still relies on communication using emails and phone conversations and it is not providing contextual information, which can support design and manufacturing decisions.

In this context, in order to eliminate the aforementioned advantages, we proposed POIGO platform. This platform implements a new approach for design and manufacturing patient specific guides for orthopedic surgery. The surgical needs are structured using different sets of questions adapted to the intervention type. The answers to these questionnaires will support capturing design intents, as correctly and complete as possible. In this purpose, an inference engine is developed and implemented in the platform. Rules, which corroborate medical knowledge and design, material and manufacturing specifications, are set in order to be used as input for the inference engine. Moreover, the platform integrates communication tools between surgeon and engineer needed for solving as conflicting design criteria or for eliminating unfeasible designs from early stages. These tools are specific to web communication, but include also a collaborative 3D viewer for .stl files that offers the possibility to visualize the guides' designs, measure their geometrical features, select point and surfaces.

In POIGO, the tasks mentioned in section 2 are modified as presented in figure 4, being performed by surgeon, platform, engineer and in a collaborative manner by surgeon and engineer.

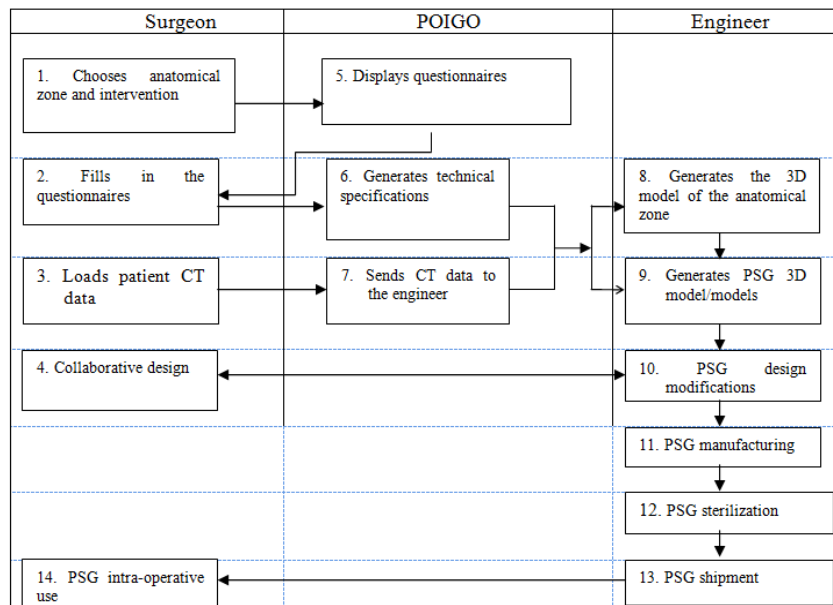


Figure 4: Design and manufacturing flow for PSGs using POIGO platform [13]

Sets of structured questionnaires (fig.5) are defined for the following anatomical zones: spine, arm/shoulder, forearm/wrist/hand and thigh/tibia/foot.

Along specific software tools for modeling and analyzing the guides, the platform integrates an expert system and a knowledge database which contains information regarding the type of orthopedic surgical

procedures which can benefit the use of patient specific guides (e.g. for trauma surgery as inserting pedicle screws in vertebrae, or knee, hip and for orthopedic surgery as inserting plates for osteotomies around the knee or applying guides for different steps in arthroplasty, etc.), morphometry data, clinical specifications, guiding devices already used in practice or presented in literature. This information is available online and it can be contextually accessed by the surgeon while filling the questionnaire regarding the patient specific guide, in order to have a better understanding of different possible options. This way the surgeon corroborates the data from literature with the specific clinical case, operation technique and elaborates a list of requirements expressed in a medical language. Based on this list, the support system provides the designer structured documents in which are described: the main functions of the devices, the design constraints, overall dimensions, material specifications, etc. Moreover, the patient specific CT/MRI data can be uploaded by the surgeon on the online platform and then used by the designer for generating the 3D model of the interest area and for creating the virtual prototype of the device.

POIGO - Screen 1	POIGO - Screen 2	POIGO - Screen 3	POIGO - Screen 4	POIGO - Screen 5	POIGO - Screen 6	POIGO - Screen 7		
Anatomic zone	Specific anatomic zone	Diagnosis	Intervention type	Load CT	Guide type	Fixation (plate, screws, K-wires etc.)		
	4.1. Thigh	4.1.1. Degenerative deformity 4.1.2. Post-traumatic deformity 4.1.3. Malformative deformity 4.1.4. Other - Engineer contact	4.1.1.1. Osteotomy 4.1.1.1. Osteotomy 4.1.1.1. Osteotomy		same as 4.3.1.1.1 same as 4.3.1.1.1 same as 4.3.1.1.1			
4. Thigh/Tibia/Foot	4.2. Tibia/Knee	4.2.1. Degenerative deformity 4.2.2. Post-traumatic deformity 4.2.3. Malformative deformity 4.1.4. Other - Engineer contact	4.2.1.1. Osteotomy 4.2.1.1. Osteotomy 4.2.1.1. Osteotomy		same as 4.3.1.1.1 same as 4.3.1.1.1		selection boxes, pop-up menus	3D viewer selection of points, select support surfaces for drill guide, select points, directions for screws, select points, directions for K-wires
						4.3.1.1.1.1. Screws	number, producer, type, diameter, length	
						4.3.1.1.1.2. K-wires	number, diameter, length	
						4.3.1.1.1.3. Fixation plates	number, producer, type	
		4.3.1. Degenerative deformity	4.3.1.1. Osteotomy	Load CT	4.3.1.1.1. Drill guide 4.3.1.1.2. Cutting guide			
						4.3.1.1.2.1. Saw blade	producer, type, dimensions	
	4.3. Foot (Hindfoot/Midfoot/Forefoot)		4.3.1.2. Fusion	Load CT				
		4.3.2. Post-traumatic deformity	4.3.2.1. Osteotomy 4.3.2.2. Fusion	Load CT Load CT	same as 4.3.1.1.1			
		4.3.3. Malformative deformity	4.3.3.1. Osteotomy	Load CT	same as 4.3.1.1.1			
		4.3.4. Other - Engineer contact	4.3.3.2. Fusion	Load CT				

Figure 5: Structured questionnaire for POIGO platform

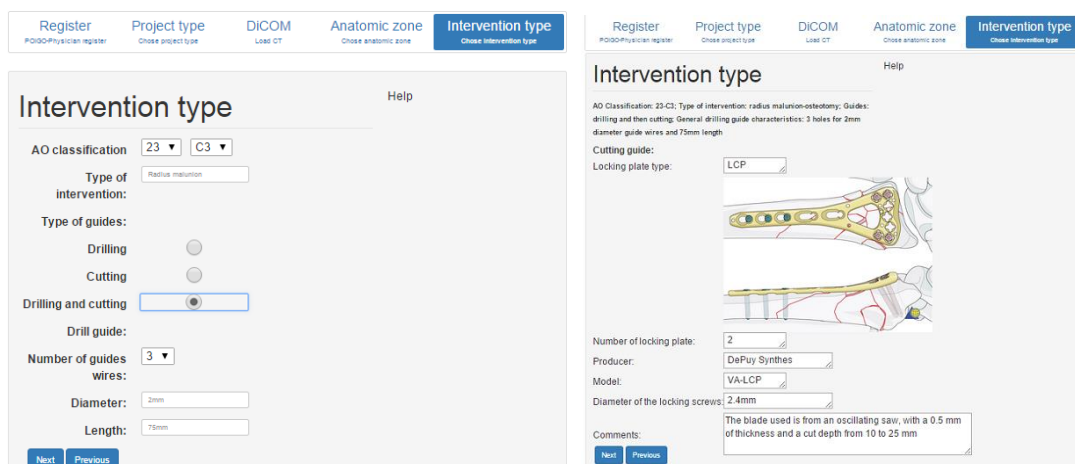


Figure 6: Structured questionnaire printscreens in POIGO

At the moment, structured questionnaires for forearm/wrist/hand (fig.6) and thigh/tibia/foot are implemented. A version called POIGOLite is available at: <http://app-poigo.osf-demo.com/> for reconstructing 3D anatomical models based on patient CT data and, if required, for building also the 3D physical model of the anatomical zone of interest by using Fused Deposition Modeling process.

As communication tools, currently are implemented: new case alert (sent by the platform to an engineer or to a list of engineers registered in the platform) and surgeon-engineer chat. The implemented 3D viewer allows, for the moment, only visualizing the 3D model of the anatomical zone of interest and/or the 3D model of the surgical guide.

#### 4. Case studies

Using the current functions implemented in the platform, several tests based on real patient cases and their CT scanning data were developed. For each case, replica of patients' bone structures and osteotomy guides were manufactured. Each case study allowed us to better define the questionnaires and to understand surgeons' needs, to learn more about the surgeon-engineer communication, to investigate sources of misinterpretations due to professional languages differences, to identify and solve implementation problem or to establish a detailed requirements lists for a real-time collaborative 3D viewer.

**Case study 1:** 72 years old woman that addressed Colentina Clinical Hospital with pain and deformation due to a fracture of the wrist. Clinical and radiological examination showed radius malunion. CT investigation was performed and information was gathered regarding inclinations of fragments, slope and position of carpal bones. Also, based on CT scans, the 3D model of the wrist was reconstructed and using the information provided by surgeons, cutting directions and lengths were established on the virtual model. A cutting guide with two slots accommodating the saw blades and three hollow cylinders for guiding wires was designed and manufactured (fig.7 a). The guide includes the negative of the surfaces (fig.7 b), selected by surgeon, on which the guide should be placed in a stable and unique position. Due to the fact that only the visualization tool was available for 3D viewer, the selection of surfaces and points was made by face-to-face discussions with the surgeon. However, this case study allowed testing the hand/wrist questionnaire structured flow and the reports generated by the platform based on surgeon answers. These reports present in a technical manner the information provided by surgeon when filling in the questionnaire. Also, the availability of contextual information was tested.

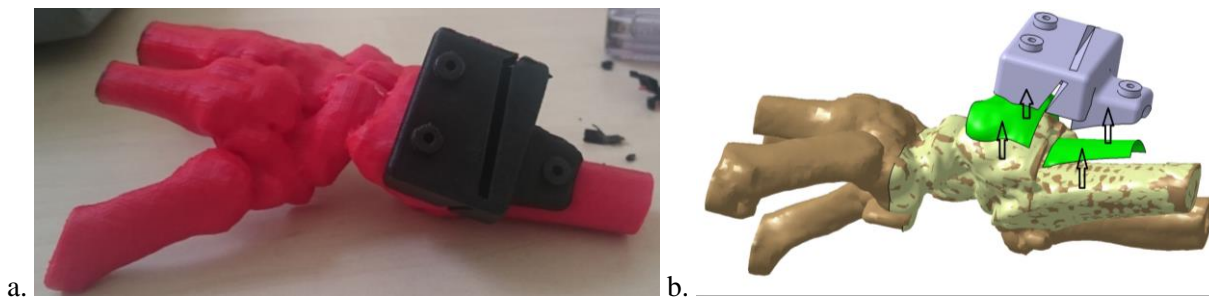


Figure 7: Osteotomy guide for correcting radius malunion (a. physical prototypes, b. surface extraction for guide design)



Figure 8: Images with different designs of osteotomy guides

**Case study 2:** 55 years-old active male with deformity of the femoral bone, secondary to an old complicated fracture of the distal third of the right femur, required a multi-planar corrective osteotomy of femur. With a valgus-producing osteotomy, a small wedge of bone should be removed to improve bone contact at the osteotomy site. As in case study 1, CT data were used for reconstructing the anatomical bone structure of the patient (see also fig.3). Three guides with different designs were modeled, manufactured (fig.8) and evaluated (using Likert based scale questionnaires) by surgeons for: ease of placement and accurate placement. The collaboration during these guides' design process allowed engineer to establish important design rules related to minimal guide thickness, cutting sleeves dimensions' range for saw blade guiding, range of dimensions for contact area between bone and guide etc. Also, for this case study, lessons were learned regarding communication using 2D images sent using online means, when 3D tools were in fact

needed for rotating the model and visualizing the cutting planes' positions. Therefore, this case study was very useful for establishing the requirements for the collaborative 3D viewer:

- Allows real-time collaborative visualisation of 3D models on surgeon and engineer computers or iPads;
- Allows 3D models' manipulation, measuring and performing annotating and selecting points;
- Allows the selection of different anatomical zones from the 3D models;
- Has the capability to manipulate large .stl files.

**Case study 3:** male patient with foot deformity caused by diabetes complications (Charcot osteoarthropathy) required multi-planar osteotomy, removal of osseous prominences and bones' repositioning and fixation with screws. Reconstruction of patient foot was made based on CT data (fig.9) and two osteotomy guides were designed. Due to a highly complex bone structure, special attention had to be paid to the inaccuracies introduced by the reconstruction process (.dicom to .stl model) and reverse engineering process (.stl to surface model). The structured questionnaire for foot intervention was tested step by step. Also, for this case study two guides with cutting slots were initially designed, but at surgeon request design' modifications were made for both guides, the slots being replaced with hollow cylinders placed in line at 5mm distance one from another (fig.10). This design modification was discussed also by face-to-face communication, the surgeon explaining this requirement by presenting to the engineer a new case study from literature [14]. This emphasizes the need to permanently update contextual information in the platform so that novelties in the field to be used in the design and manufacturing process.



Figure 9: Charcot foot replica

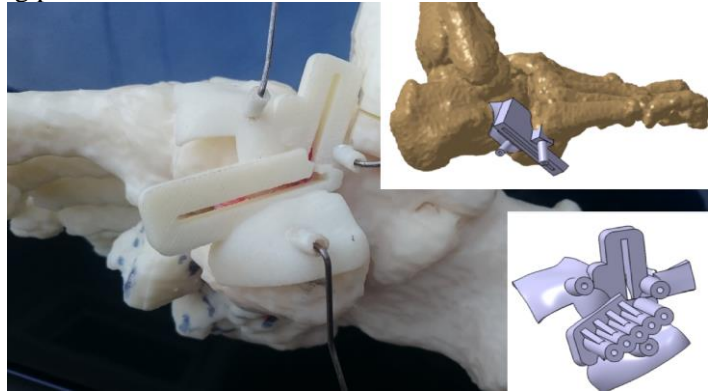


Figure 10: Osteotomy surgical guides

## 5. Conclusions and further work

Orthopedic surgery has continuously developed emphasizing the cognitive and technical register of the therapeutic activity. The technical nature of surgical interventions and specialization of knowledge, have structured this field of healthcare and especially in top surgical specialties as orthopedic reconstructive and spinal surgery. They necessitate the collaboration of technical professions, medical and engineering within hospital technical platforms. Health professions, as a whole, are facing a growing demand for mastery of imaging techniques, quality and safety. The specialization of activities, the complexity of devices and approaches, work intensification and flow (patients, caregivers, surgeon, engineer) results in delegating tasks previously performed by doctors alone and the creation of new applications with the use of internet. Furthermore, devices and equipment used pose new problems of operation, maintenance, selection, adaptation to standards that sometimes are close to engineering sciences than medicine.

Design and manufacturing surgical guides is a complex task requiring a tight and permanent cooperation between surgeon and engineer. Until now, this cooperation was based on face-to-face discussions and work on the virtual models of bone structures and guides using engineers' computer and application. This limits the spread of these surgical devices, despite their proved advantages. Thus the idea to develop an online collaborative platform for enhancing the collaboration during the design and manufacturing process by using new tools: questionnaires for supporting translating surgeons' requirements in design and manufacturing specification and 3D collaborative viewer for visualizing, measuring, selecting points and surfaces.

Therefore, the answer to the question: Surgeon-engineer: can we really collaborate? is: Yes, we can, now by using also POIGO platform.

Three case studies are presented in this paper, each of them being focused on different aspects related to platform functions, questionnaires and platform reports. Also, several design issues were tackled while

working on these case studies, the most important being related to anatomical model reconstruction accuracy, range of dimensions for hollow cylinders and slots, guide thickness, stability vs. number of K-wires and support surfaces area etc. Communication aspects were also analyzed for identifying potential sources of misunderstanding or misinterpretation. Working on the same 3D model in real-time is considered the best solution for overcoming some of these problems.

Further work will be focused on developing the 3D viewer and on implementing new structured questionnaires for other anatomical regions. Then, the work will be focused on testing and optimizing the beta version of the platform for obtaining the final version. Working scenarios based on previously developed case studies will be used for piloting the platform. Real tests will be performed using the platform and feedback from users will be collected and analyzed.

## Acknowledgements

The work has been funded by the Partnerships in Priority Areas Programme – PN II of MEN – UEFISCDI, through the Agreement 5/2014.

## References

- [1] T. Beck et al: Knowledge engineering for health: a new discipline required to bridge the "ICT gap" between research and healthcare, *Hum Mutat.* 2012, 33(5):797-802
- [2] P.Y. Hsueh, et al: Next Generation Wellness: A Technology Model for Personalizing Healthcare, *Healthcare Information Management Systems*, 355-374, 2016, Springer
- [3] Chen, I-M et al. Personalized biomedical devices & systems for healthcare applications, *Frontiers of Mechanical Engineering*, 2011, Volume 6, Issue 1, pp 3-12,
- [4] O. Hisarciklila et al.: User-designer collaboration in the design process of surgical instruments: new aspects for annotation as a communication tool, *International Conference on Engineering Design, ICED'09 24 – 27 August 2009, Stanford University, Stanford, USA*
- [5] O. Hisarciklilar, et al.: Reducing the “Information Gap” Between Synchronous and Asynchronous Co-operative Design Phases. *Virtual Concept '06*, 2006, Cancun, Mexico
- [6] R. Rasoulifar et al.: Integrating an expert user in design process: how to make out surgeon needs during a new surgical instrument design. *International Symposium Series on Tools and Methods of Competitive Engineering (TMCE)*, 2008 Izmir, Turkey
- [7] S. Aubry, et al: Knowledge integration for annotating in virtual environments. *International Journal of Product Development*, 2007, 4, 533-546
- [8] D. Popescu, D. Laptoiu: Rapid prototyping for patient-specific surgical orthopaedics guides: A systematic literature review. *Proceedings of the Institution of Mechanical Engineers, Part H: Journal of Engineering in Medicine*, 2016, 230(6), 495-515
- [9] S. De Wouters et al: Patient-specific instruments for surgical resection of painful tarsal coalition in adolescents. *Orthopaedics & Traumatology: Surgery & Research*, 2014, 100, 423–427
- [10] M. Kunz et al: Image-guided distal radius osteotomy using patient-specific instrument guides. *J Hand Surg Am*, 2013, 38(8), 1618-24
- [11] V. Ferrari et al: An optimal design for patient-specific templates for pedicle spine screws placement. *Int J Med Robot*, 2013, 9(3), 298-304
- [12] S. Lu et al: Application of a novel patient-specific rapid prototyping template in orthopedics surgery, in *Advanced Applications of Rapid Prototyping Technology in Modern Engineering*, 2011
- [13] D. Popescu et al: Workflow for Additive Manufacturing of an Individualized surgical template, *Journal of Proceedings in Manufacturing Systems*, 2015, 10(3), 131-140, 2015
- [14] P. Frnstahl et al: Complex Osteotomies of Tibial Plateau Malunions Using Computer-Assisted Planning and Patient-Specific Surgical Guides, *J. Orthop. Trauma*, 2015, 29(8), e270-6



# A hybrid metaheuristics for layout optimization in production cell

Hugo Zupan<sup>1</sup>, Janez Žerovnik<sup>1</sup>, Niko Herakovič<sup>1</sup>

<sup>1</sup> *University of Ljubljana, Faculty of Mechanical Engineering, Askerceva 6, 1000, Ljubljana, Slovenia*  
*E-mail: hugo.zupan@fs.uni-lj.si; niko.herakovic@fs.uni-lj.si*

## Abstract

Multistart local search heuristics Remove and Reinsert that is based on a simple schedule constructing heuristics is tested for the arrangement of machines in production cell. The result of the optimization lowers the transport cost of the process enormously, which is obvious from the research results of this paper. The implementation within a Plant Simulation software is compared to the build-in genetic algorithm.

**Keywords:** Layout optimization, Remove and Reinsert algorithm, iterative improvement, discrete event simulation, optimization, production cell

## 1 Introduction

In the discussions about the “Factories of the Future” [1] one of the main objectives is to find the way to effectively manage unnecessary wastes in production. The contemporary manufacturing practice is therefore very often based on different production theories like Lean production, Just in Time, Kanban and Pull systems, based on the Toyota production system (TPS) etc., as well as on supply chain and overall equipment efficiency (OEE) optimization [2], [3], [4], [5], [6], [7]. The Lean system has become even a reference model for optimizing production and general performance of larger companies as well as SMEs [8], [9], [10]. Therefore some research works focus in simulation of production processes as well as in material flow and batch quantity optimization [11], [12], [13]. For this reason, the traditional layout of workshop machinery is transformed into more production cells, which is also one of the goals of lean production [14]. For the formation and optimization of the cells, there has been proposed a variety of different methods [15], [16], [17], [18], [20], [21], [22]. In addition to those methods in recent years the usage of method simulation with discrete events is increasing [23], [24], [25].

It is well known that using discrete event simulation or virtual factory is very effective tool for “what-if” scenarios, for every type of production system [26], [27]. In our case we have transformed a possible real production system with all the features and limitations into the simulation model. The idea is that the metaheuristics proposes an initial and iteratively improved arrangement of machines in production a cell while the discrete event simulation performs “what-if” scenario for each proposed arrangement thus providing the quality measure of the arrangement. This process is repeated until the metaheuristics can no longer provide better arrangement of machines.

The rest of this short contribution is organized as follows. In the section II., the metaheuristics RaR is outlined and its operation is illustrated with an example in Section III. Results of the first experiments are given in Section IV and concluding remarks in Section V.

## 2 The metaheuristics RaR

The proposed metaheuristics is called RaR algorithm. The idea (algorithms were given various names) was successfully applied to the probabilistic traveling salesman problem (PTSP) [28], the asymmetric traveling salesman problem (ATSP) [29] and to the classical resource-constrained project scheduling problem (RCPS) [30]. The basic idea of the heuristics is very simple, and this may be a reason for good results. It may be rather surprising that a simple heuristics outperforms much more complicated metaheuristics such as are for example the genetic algorithms, but we believe that this phenomena is not that much unexpected - see [31] and the references there.

RaR can be regarded as a hybrid metaheuristics that consists of two phases: generating an initial solution, and iterative improvement. In the first phase, a solution is usually constructed in a way to solve a sub-

problem optimally first, and then inserting the remaining machines, not unlike the well-known heuristics arbitrary insertion for TSP does [32]. The iterative improvement phase, roughly speaking, removes some of the machines from the current cell, and reinserts them back into the cell in arbitrary order. The arrangement of machines is known to be equivalent to the traveling salesman problem (TSP). Adaptations and modifications used for successful application to the problem studied here are explained in some detail below.

Here, we assume that the initial solution is given (or it is just a random arrangement of machines) and focuses on the iterative improvement phase.

In the inner repeat loop, a subset of  $m$  machines is selected, and an optimal permutation of these  $m$  machines is found by exhaustive search. It should be noted that, contrary to RaR applied to some other problems, the machines which are not selected are not removed, only their relative position is frozen. After the optimal permutation of the selected  $m$  machines is found, these machines are, one by one, removed and reinserted into the solution into the best position, keeping all other relative positions of machines fixed. The loop is repeated until there is no improvement, and then the position of selected  $m$  machines is changed. First, the  $m$  machines at positions  $1...m$  are chosen, then the positions  $2...m+1$ , and finally the positions  $n-m+1...n$  are regarded.

### The RaR Algorithm

```

S ← initial Schedule (M1, M2, ..., Mn)
repeat
  S'' ← S
  w = 1 (position from which the permutation starts)
  x = 0
  repeat
    repeat
      S' ← S
      1. Choose (w ... w+m-1) machines from S and start with permutation on initial
         state w
      2. Check every solution for every combination from permutation table
      3. Choose the best solution and place it in the S
      4. If permutation found better solution than S' then x = 0
    begin (if x = 0)
      P ← Optimum of first step (S)
      Y = m + w (m - number of machines processed with permutation)
      while Y < n (number of all machines) do
        P' = P
        q = 1
        repeat
          P'' ← Insert the machine from place Y on place q
          q = q + 1
        until q = Y
        Find the best solution (P'')
        P ← Choose (P'')
        Y = Y + 1
      endwhile
    end
    S ← Choose (P)
  until S' /= S
  w = w + 1
  x = 1
until w > n - m
until S'' /= S

```

### 3 Problem instance

The heuristics has been tested on a realistic example. To the best of our knowledge, there are no benchmark instances in the literature; we plan to generate a dataset of several instances for a more extensive experiment with results to be reported in the full paper.

We have a production process with 10 work places where operations are carried out. The plan is to produce 20 orders. For each order, the technology procedure and the sequence of operations are known. Raw material goes from material storage and the finished products are stored in the products storage. Orders require different operations. The transport cost between orders is assumed to be 1 per meter.

Machines are distributed in a circle with the same distance between neighbourhood machines (see Figure 1). Based on the input data (technology, quantity, material flow, costs of transportation) we designed a simulation model. The simulation illustrates the current state of production cells and covers all its properties in a selected point of time.

Output data simulation includes:

- the intensity of the material flow between the machines,
- costs of transport and
- Sankey chart.

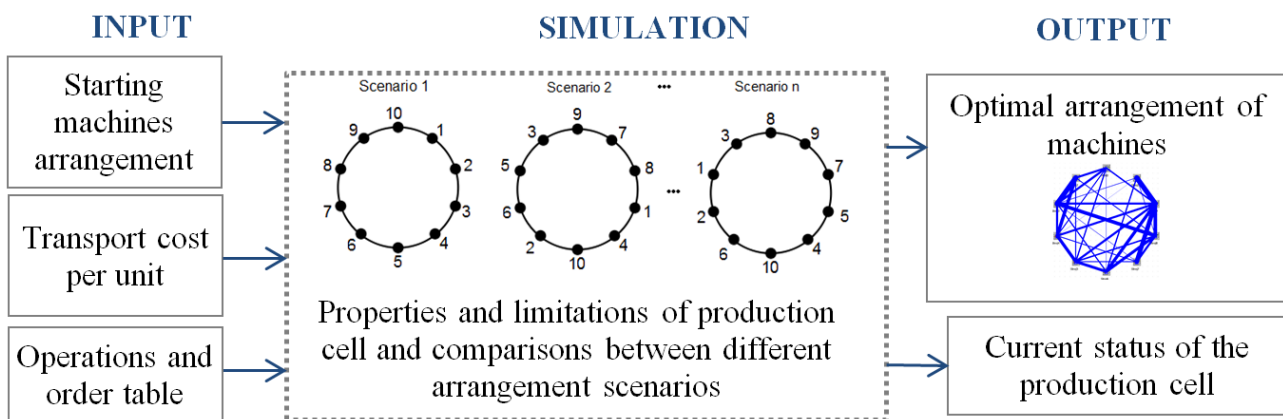


Figure 1. Logical scheme of production cell model.

We briefly outline the operation of the algorithm on the instance. The first step is using the permutation table. The idea is that from the whole instance, which has  $n$  machines, we take  $m$  machines ( $m < n$ ; we use 5) and optimize them using all possible combinations, which are enshrined in the permutation table. We do this by finding the best arrangement of where the chosen  $m$  machines are permuted and the other  $n-m$  machines' relative positions do not change. We continue by considering the machines that were fixed in the first step. One by one, these machines are removed from the arrangement and reinserted, this time without changing relative positions of all other machines.

In our case we have initial schedule of 10 machines (**M1, M2, M3, M4, M5, M6, M7, M8, M9, M10**). Then we choose the first  $m$  (5 in our case) machines and find their permutation with minimal cost. If there is more than one best permutation, the first is taken. In our case, the optimum after first step is: (**M2, M1, M3, M5, M4, M6, M7, M8, M9, M10**).

In the second step we start with inserting the other machines into the optimum solution so far. In particular, here we choose the machine  $M6$  and insert it before the machine  $M2$ , before the machine  $M1$  etc. and end with the insertion of it before machine  $M4$ . Thus we have 6 candidate solutions – the one before inserting and for all 5 inserted possibilities. We choose the combination that gives us the best solution, in this case (**M2, M1, M3, M6, M5, M4, M7, M8, M9, M10**) and continue by reinserting the next element – machine  $M7$ . We insert machine  $M7$  into 6 possible positions, before machine  $M2$ ,  $M1$  etc. and end with the insertion of it before  $M4$  and take the best solution which becomes the initial state before reinserting the machine  $M8$ .

We do this until we reach the last insertion of the last machine (in our case the machine  $M_{10}$ ). The best solution of this second step is (**M2, M1, M7, M3, M9, M10, M6, M5, M4, M8**).

When we finish the step 2 we repeat the algorithm by using the best solution we got so far.

The algorithm repeats these two steps until it can no longer find an improvement.

After finding an arrangement for which no improvement was found by selection the first  $m$  machine, the procedure repeats by selecting the machine on positions 2, ...,  $m+1$ , until no improvement is possible. Then the selection shifts to 3, ...,  $m+2$ , and so on, until the last selection of machines on positions  $n-m+1$ , ...,  $n$ .

#### 4 Computational results

The algorithm was tested at the possible realistic instance. We had 20 orders and 10 machines in production cell. We compared the algorithm with the genetic algorithm, which is already installed in the Siemens programming environment Plant Simulation [33]. The results are as follows:

##### Characteristics of the genetic algorithm (GA):

- 30 generations, size of generation: 100.

Table 1: The results of GA and RaR algorithm.

Algorithm	Total time	... for finding best solution	Quality of the best solution
GA	1 min 52 s	43 s	29593,5 €
RaR	1 min 1 s	15 s	29593,5 €

From the results we see that RaR algorithm finds a very good solution in a relatively short time compared to GA. The great advantage of RaR algorithm is that there is not necessary to store large amounts of data, since the algorithm works sequentially, and in almost every step takes only best solution and discards the others.

In Figure 2 the Sankey chart is presented for the optimal arrangement of machines. Machines that have more of material flow are closer together so there are lower transport costs.

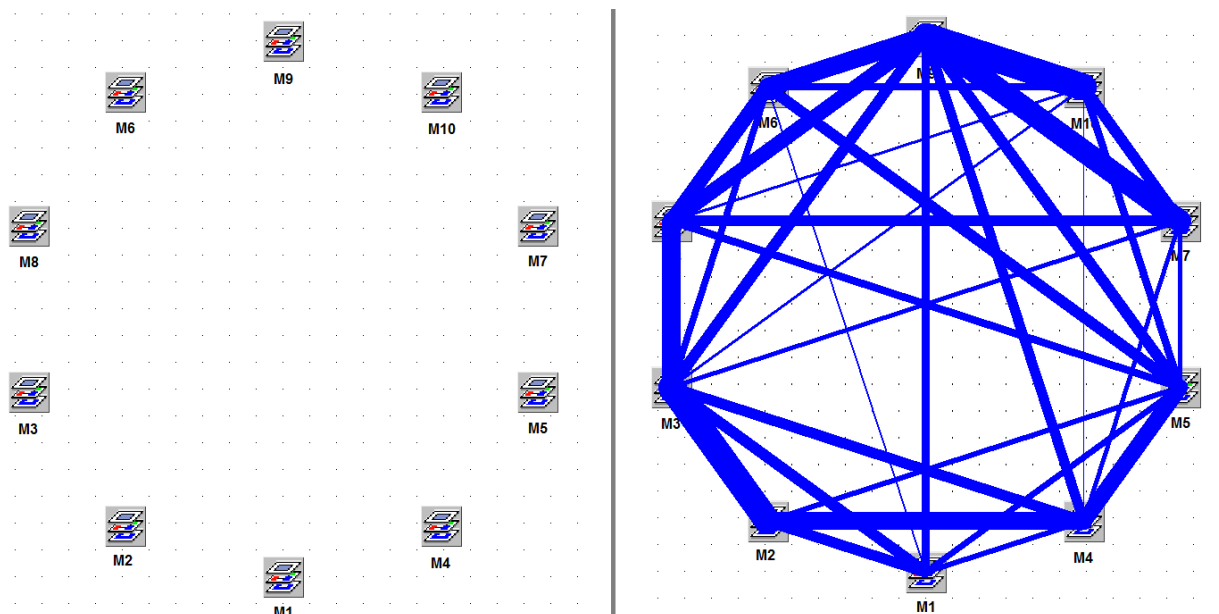


Figure 2: Sankey chart for best arrangement of machines in production cell.

According to the tests that have been carried out (even those that are not described in here), we can say that the RaR algorithm works very well and reliably and in short time gives good solutions.

## 5 Conclusion

This paper proposes Remove and Reinsert (RaR) heuristics for the problem of arrangement of machines in the production cell. It minimizes the expected transport costs within a reasonable amount of calculation time.

For executions of different “what-if” scenarios of the initial schedules, the discrete event simulation (DES) software – Technomatix Plant Simulation was used. A comparison of RaR algorithm with Genetic Algorithm which is built-in module in Technomatix Plant Simulation software showed that RaR algorithm finds same optimal solution in shorter time compared to the Genetic Algorithm.

We also calculated the maximal transport cost for our case and the maximal transport cost we got was 43101,7 € which represents 45,6 % inferior combination compare to best solution.

In the real cell production the orders and amount of orders is changing, so this could be the effective tool for a cell planner to check once in a while if there is a need for the rearrangement of machines in the production cell.

In our future work, further experiments will be conducted to shorten the calculation time of getting the optimal solutions from the RaR algorithm.

## References

- [1] Automatica – Accompanying Program: Smart factory, 6th international Trade Fair for Automation and Mechatronics, Munich, 2014, June 3-6.
- [2] R. Uzsoy, and L.A. Martin-Vega, Modeling Kanban Based and Demand-pull Systems: A Survey and Critique, *Manufacturing Review*, 3, 1990, pp.155-160.
- [3] J.K. Bandyopadhyay, “Implementing Just-In-Time Production and Procurement Strategies,” in *Journal of Management*, Vol. 12(1), 1995.
- [4] C.C. Huang and A. Kusiak, “Overview Of Kanban Systems,” in *Int. J. Computer Integrated Manufacturing*, 9:3, 1996, pp.169-189.
- [5] W.J. Hopp and M.L. Spearman, *Factory Physics: Foundations of Manufacturing Management*, Mcgraw-Hill, New York, 2001.
- [6] B. Buchmeister, D. Friscic, B. Lalic and I. Palcic, “Analysis of a Three-Stage Supply Chain with Level Constraints,” in *International Journal of Simulation Modelling*, Vol. 11(4), 2012, pp.196-210.
- [7] A.J. Kootanaee, K.N. Babu and H.F. Talari, “Just-in-Time Manufacturing System: From Introduction to Implement,” *International journal of Economics, Business and Finance*, Vol. 1(2), 2013, pp. 07-25.
- [8] B. Lyonnet, M. Pralus and M. Pillet, “A Push-Pull Manufacturing Strategy: Analytical Model in the Screw Cutting Sector,” in *Proceedings of the World Congress on Engineering, WCE 2010*, Vol. III, London, U.K.
- [9] D. Powell, J. Riezebos and J.O. Strandhagen, „Lean production and ERP systems in small- and medium-sized enterprises: ERP support for pull production,” in *International Journal of Production Research*, Vol. 51(2), 2013, pp. 395-409.
- [10] I. Belekoukias, J. A. Garza-Reyes and V. Kumar, “The impact of lean methods and tools on the operational performance of manufacturing organisations,” *International Journal of Production Research*, 2014
- [11] N. Herakovic, P. Metlikovic and M. Debsvec, “Motivational Lean Game to Support Decision between Push and Pull Production Strategy” in *International Journal of Simulation Modelling*, Vol. 13(4), 2014, pp. 391-526.
- [12] M.S. Dordevic, N.D. Zrnic, M.R. Milicevic and V.V. Miskovic, “Information and material flow modeling in system of parts regeneration in multi-level supply system,” *Technical Gazette*, Vol. 20, No. 5, 2013, pp.861-869.

- [13] T. Berlec, J. Kusar, J. Zerovnik and M. Starbek, "Optimization of a Product Batch Quantity," in *Strojniski vestnik – Journal of Mechanical Engineering*, Vol. 60(1), 2014, pp. 35-42.
- [14] B.N. Shishir Bhat, "Cellular Manufacturing – The Heart of Lean Manufacturing." In *Advances in Production Engineering & Management* (3): 2008, pp. 171-180.
- [15] Y. Crama and M. Oosten, "Models for machine-part grouping in cellular manufacturing." In *International Journal of Production Research* (34): 1996, pp. 1693-1713.
- [16] K. Shanker and A.K. Agrawal, "Models and solution methodologies for the generalized grouping problem in cellular manufacturing," in *International Journal of Production Research* (35): 1977, pp. 513-538.
- [17] B. Adenso-Diaz, S. Lozano, J. Racerob and F. Guerrerob, "Machine cell formation in generalized group technology," in *Computers & Industrial Engineering* (41), 2001, pp. 227-240.
- [18] Z.P. Fan, Y. Chen, J. Mab and Y. Zhu, "Decision support for proposal grouping: a hybrid approach using knowledge rules and genetic algorithms." in *Expert Systems with Applications* (36): 2009, pp. 1004-1013.
- [19] T. Berlec, P. Potocnik, E. Govekar, and M. Starbek, "A method of production fine layout planning based on self-organising neural network clustering," in *International Journal of Production Research* (52), 2014, pp.7209-7222.
- [20] Z. Pirmoradi, G. Gary Wang and T.W. Simpson, "A review of recent literature in product family design and platform-based product development," T.W. Simpson, J.R. Jiao, Z. Siddique and K. Hölttä-Otto (Eds.), *Advances in product family and product platform design*, Springer, New York, 2014, pp. 1-46.
- [21] R. Logendran, "Impact of sequence of operations and layout of cells in cellular manufacturing," in *International Journal of Production Research*, Vol. 29(2), 1991, pp. 375-390.
- [22] M. Solimanpur, P. Vrat and R. Shankar, "Ant colony optimization algorithm to the inter-cell layout problem in cellular manufacturing," in *European Journal of Operational Research*, Vol. 157(3), 2004, pp. 592-606.
- [23] P. Savory and R. Williams, "Estimation of cellular manufacturing cost components using simulation and activity-based costing," in *Journal of Industrial Engineering and Management*, Vol 3(1), 2010, pp. 68 – 86.
- [24] M. Debevec, M. Simic and N. Herakovic, "Virtual factory as an advanced approach for production process optimization," in *International journal of simulation modelling*, Vol. 13(1), 2014, pp. 66-78.
- [25] S.N. Samy, T. AlGeddawy and H. ElMaraghy, "A granularity model for balancing the structural complexity of manufacturing systems equipment and layout," in *Journal of Manufacturing Systems*, Vol. 36, 2015, pp. 7-19.
- [26] H. Eskandari, M.A. Rahaee, M. Memarpour, E. Hasannayebi and S.A. Malek, "Evaluation of different berthing scenarios in Shahid Rajaee container terminal using discrete-event simulation," in *Simulation Conference (WSC)*, 2013 Winter.
- [27] M. Debevec and N. Herakovic, "Management of resources in small and medium-sized production enterprises" in *Iranian journal of science and technology*, Vol. 34(B5), 2010, pp 509-520.
- [28] J. Zerovnik, "A Heuristics for the Probabilistic Traveling Salesman Problem", *Proceedings of the International Symposium on Operational research 1995 (SOR'95)*, (V.Rupnik, M.Bogataj, eds.), Slovenian Society Informatika, Ljubljana 1995, 165-172.
- [29] J. Brest and J. Zerovnik, "An approximation algorithm for the asymmetric traveling salesman problem," in *Ricerca Operativa*, Vol. 28, 1999, pp. 59-67.
- [30] I. Pesek, A. Schaerf and J. Zerovnik, "Hybrid local search techniques for the resource-constrained project scheduling problem" in *Lect Notes Comput Sci* 4771: 2007 pp. 57-68.

- [31] J. Zerovnik, “Heuristics for NP-hard optimization problems : simpler is better!?” V: IPAVEC, Vesna Mia (ur.), KRAMBERGER, Tomaz (ur.). Pre-conference proceedings of the 11th International Conference on Logistics & Sustainable Transport 2014, Celje, Slovenia, pp. 19-21 June 2014. Celje: Faculty of Logistics.
- [32] D.J. Rosenkrantz, R.R. Stearns and P.M. Lewis, “An Analysis of Several Heuristics for the Traveling Salesman Problem,” in SIAM J. Comput. 6: 1977, pp. 563-581.
- [33] Tecnomatix Plant Simulation, Siemens PLM Software.  
<http://www.emplant.de/english/fact%20sheet%20plant%20simulation.pdf> [accessed on 5/11/2015]

# Engineering Interaction in Multi-Reality Environments for Remote Operations and Maintenance Support

R. Vrabič<sup>1</sup>, J.A. Erkoyuncu<sup>2</sup>

<sup>1</sup> *Department of Manufacturing Systems and Control, University of Ljubljana, Slovenia*

<sup>2</sup> *Operations Excellence Institute, Cranfield University, United Kingdom*

## Abstract

Modern approaches to engineering practice, product realisation, and lifecycle management, such as globally distributed supply networks, product-service systems, and through-life engineering services, call for remote support of operations and maintenance. Traditionally, remote interaction is facilitated by video and voice communication using personal computers and is therefore inherently limited to the two dimensions of the computer screen. Technologies such as augmented reality and virtual reality can be used to add the third spatial dimension to remote interaction and, moreover, augment or diminish the possibilities for interactivity with the environment based on requirements and context. The paper studies engineering interaction in multi-reality environments and presents a conceptual framework for remote task specification, execution, and monitoring. A proof of concept is presented, highlighting the potentials of the approach for remote operations and maintenance support.

**Keywords:** remote maintenance, Virtual Reality, Augmented Reality.

## 1 Introduction

Digital tools and environments are widely used in today's product, service, and system development and operations support. Developing, analysing, testing, and simulating in the digital saves both time and resources. As a consequence, concepts such as Computer-Aided Applications (CAx), Digital and Virtual Factory [1], [2], Digital Twin [3], Industrial Internet of Things [4], and Cyber Physical Systems [5] are becoming well established, both in theory and in engineering practice. Augmented and virtual reality are two technologies which will play a major role in future digital engineering.

Augmented reality refers to imposing digital data on a real-world view, providing additional information and thus augmenting the perception of reality. An important aspect of the technology is the ability to track objects of interest, providing a reference frame for augmented information display. This is achieved by either marking the objects or by so-called markerless tracking which uses scanned 3D geometry of the objects or advanced image processing techniques for their recognition. As demonstrated in the paper, this can be used to translate the 3D information from the real to the digital world.

In the last decade, augmented reality has matured to be an innovative and effective solution. Successful use cases and demonstrations can be found in various domains, ranging from medical, military training, tele-robotics, entertainment, maintenance, to manufacturing. Augmented reality helps to solve some of the critical problems; to simulate, assist, and improve manufacturing processes before or as they are being carried out [6].

Virtual reality, in contrast to augmented reality, replaces the real world with a virtual one. The user is then immersed into the virtual world by using 3D glasses or a head-mounted display. Tracking systems are used to track the position of the user and his interaction interfaces (e.g. a 3D joystick) in order to accurately position the user's viewpoint of the virtual world and facilitate interaction. Both augmented and virtual reality have been proposed for various engineering applications.

The design of products is one of the engineering domains that has seen a lot of applications of augmented and virtual reality. Mostly, they have been used to provide a more intuitive interface between humans and CAD environments [7] or, in the case of augmented reality, for visually presenting the product in its intended environment, e.g. overlaying dashboards on real car body mock-ups at the early stage of development [8]. Interesting ideas for interaction for design applications can be found in [9], where the authors present how a



3D model can be created in a virtual environment, and in [10] where the authors present a method for creating new designs by combining the real and the virtual. Collaborative environments for design have been developed and demonstrated for a case of augmented reality collaborative design using gestures [11], a case of multiple users simultaneously working on a geometrical model [12], and [13], where the distributed design process combines the real with an augmented environment. Another domain in which augmented and virtual reality have been extensively studied is the domain of remote assembly and maintenance support [14]–[18].

The paper studies engineering interactions in a multi-reality environment consisting of the real, augmented reality, and virtual reality ones. Mixed-, dual-, and multi-reality environments are discussed. It is shown how the state of the digital world can be synchronised over the network to facilitate remote interaction and collaboration. Atomic engineering actions are defined, providing a framework for engineering interaction. Extensions of the approach are discussed. An implementation of the framework is illustrated. The potential uses of the approach for remote maintenance support are discussed.

## 2 Mixed-, Dual-, and Multi-Reality

A general classification of digital environments is proposed by Milgram et al. [19]. The classification is based on the notion that different environments exhibit different ratios of virtuality, ranging from the real world to the completely virtual one. This virtuality continuum is shown in Figure 1.

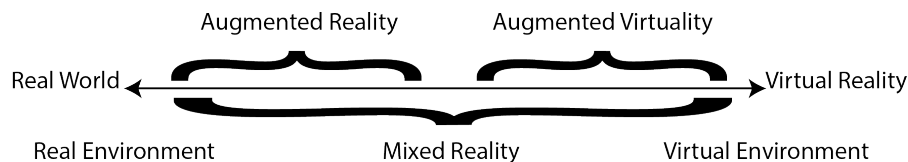


Figure 1: The virtuality continuum, adapted from [19].

Some authors have proposed to add mediality in addition to virtuality as one of the axes. If virtuality considers the type of the environment the user is interacting with, mediality deals with the amount of distortion, either augmentation or diminishment of information, to the environment. Computer-mediated reality thus refers to the ability to add to, subtract information from, or otherwise manipulate one's perception of reality. For example, a welding mask is a simple tool for diminishing the field of view and the intensity of the light the user experiences and is therefore considered to mediate the reality. On the other hand, augmented reality overlays computer generated information on the projection of reality, thereby augmenting the user's experience by providing additional information.

Several concepts were introduced where multiple environments co-exist. One such concept is the dual reality, which states that the virtuality continuum need not be discrete and that sensor networks can facilitate the seamless merger of the real and the virtual, creating an environment that is spread over the virtuality continuum. Dual reality is defined as an environment resulting from the interplay between the real world and the virtual world, as mediated by networks of sensors and actuators [20]. While both worlds are independent and complete on their own, the principle of dual reality postulates that they, in one way or another, mutually influence each other. The data from the real world is captured via sensor networks and, in turn, the state of the virtual world is updated accordingly. The virtual world then allows for immersive exploration and simulation of scenarios. In principle, this works bi-directionally – the state of the simulated sensors in the virtual world can be reflected back in the real one.

The related concept of multi-reality [21] is defined as presenting different worlds in one understandable interface. Using multi-reality, the same objects are presented in parallel. For example, in a remote maintenance scenario, a stereoscopic live view could be used together with a 3D CAD model to present a user interface capable of presenting the complex information required for the execution of the remote maintenance task.

The paper explores the idea of multi-reality in a distributed environment, in which the parallel presentation of the objects takes place at different locations. The key research questions are related to the synchronisation of the objects' state, the presentation of the objects, and the interaction with the objects in an engineering context. The next section reviews the ways of interaction with 3D computer generated environments in context of the multi-reality environments.

### 3 Interactivity in Distributed 3D Computer Environments

The interaction with 3D computer generated objects in multi-reality environments presents several challenges. On the desktop, the interaction with 3D space is limited to the 2D screen, keyboard, and mouse. In augmented reality, the interaction must be detected by analysing the video stream with methods of image processing and object recognition. In virtual reality environments, the interaction is facilitated by 3D controllers (joysticks) and haptic feedback. This section introduces the basic concepts used in computer graphics and defines the key interaction mechanisms in these environments.

#### 3.1 3D Transformations in Computer Graphics

An arbitrary point in 3D space  $(x, y, z) \in \mathbb{R}^3$  can be expressed in homogeneous coordinates as  $(x, y, z, 1) \in \mathbb{R}^4$  on the plane in  $\mathbb{R}^4$ . This enables the translation, scaling, and rotation of the point using single matrix multiplication.

A translation can be seen as an addition of a vector to the point which can be expressed in homogeneous coordinates as  $(x, y, z, 1) \rightarrow (x + t_x, y + t_y, z + t_z, 1)$  and can be computed as shown in Equation 1.

$$\begin{bmatrix} 1 & 0 & 0 & t_x \\ 0 & 1 & 0 & t_y \\ 0 & 0 & 1 & t_z \\ 0 & 0 & 0 & 1 \end{bmatrix} \begin{bmatrix} x \\ y \\ z \\ 1 \end{bmatrix} = \begin{bmatrix} x + t_x \\ y + t_y \\ z + t_z \\ 1 \end{bmatrix} \quad (1)$$

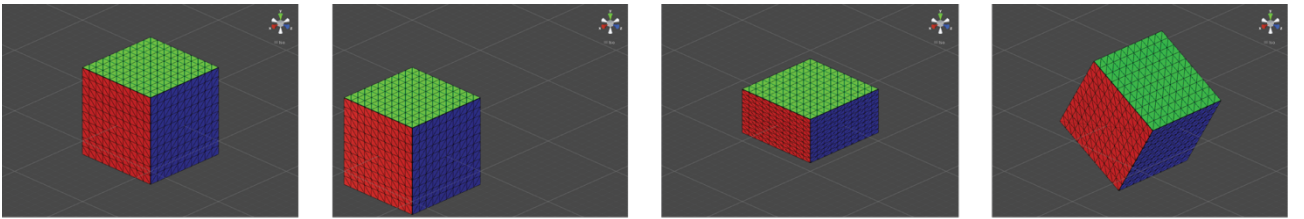
Similarly, scaling of an object can be seen as the multiplication of each of the object's point coordinates with a scalar  $(x, y, z, 1) \rightarrow (s_x x, s_y y, s_z z, 1)$ , resulting in the computation shown in Equation 2.

$$\begin{bmatrix} s_x & 0 & 0 & 0 \\ 0 & s_y & 0 & 0 \\ 0 & 0 & s_z & 0 \\ 0 & 0 & 0 & 1 \end{bmatrix} \begin{bmatrix} x \\ y \\ z \\ 1 \end{bmatrix} = \begin{bmatrix} s_x x \\ s_y y \\ s_z z \\ 1 \end{bmatrix} \quad (2)$$

For rotation in 3D coordinates, the axis of rotation needs to be specified. The rotation matrices for rotations around  $x$ ,  $y$ , and  $z$  axes for the angle  $\theta$  are shown in Equation 3.

$$R_x = \begin{bmatrix} 1 & 0 & 0 & 0 \\ 0 & \cos(\theta) & -\sin(\theta) & 0 \\ 0 & \sin(\theta) & \cos(\theta) & 0 \\ 0 & 0 & 0 & 1 \end{bmatrix} R_y = \begin{bmatrix} \cos(\theta) & 0 & \sin(\theta) & 0 \\ 0 & 1 & 0 & 0 \\ -\sin(\theta) & 0 & \cos(\theta) & 0 \\ 0 & 0 & 0 & 1 \end{bmatrix} R_z = \begin{bmatrix} \cos(\theta) & -\sin(\theta) & 0 & 0 \\ \sin(\theta) & \cos(\theta) & 0 & 0 \\ 0 & 0 & 1 & 0 \\ 0 & 0 & 0 & 1 \end{bmatrix} \quad (3)$$

Application of the affine transformations to a unit cube is illustrated in Figure 2.



a) No transformation.

b) Translation for 1 unit along the x axis.

c) Scaling to 0.5 along the y axis.

d) Rotation for 30 degrees around the x axis.

Figure 2: Application of affine transformations to a unit cube.

The transformations, i.e. the translations, the scaling, and the rotations, can be combined by simply multiplying the individual transformation matrices. Note that the order of multiplication is important; translating an object and rotating it around an axis is not the same as rotating it around the axis and then translating it.

A useful alternative for representing rotations in 3D space is offered by quaternions, which are an extension of complex numbers. Quaternions can be represented as coordinates, or as a scalar-vector pair, as shown in Equation 4.

$$q = (w, x, y, z) = (w, \vec{v}); w, x, y, z \in \mathbb{R}; \vec{v} \in \mathbb{R}^3 \quad (4)$$

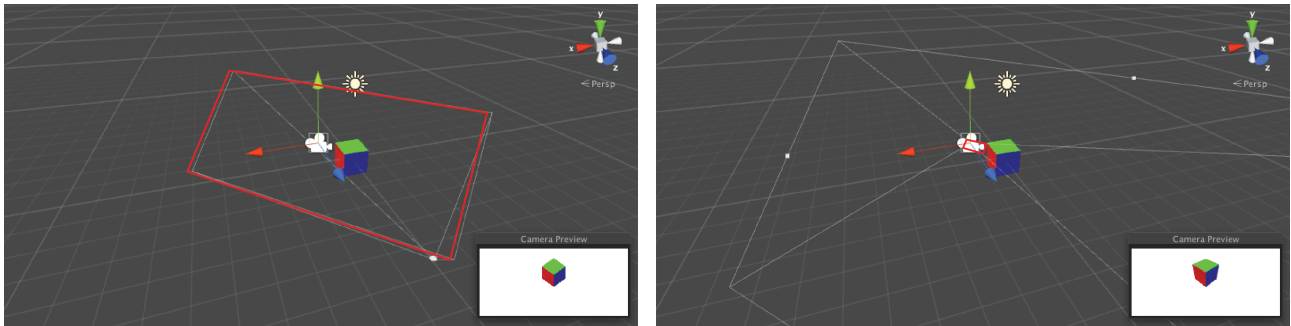
There exists a one-to-one transformation between transformation matrices and quaternions, meaning that any rotation can be expressed using either. The advantage of using quaternions for computer graphics is related to their lesser computational needs for expression of intermediary states between two rotations which makes them particularly useful for animations. Equations 5-7 present some important formulations from the quaternion algebra which hold true for unit quaternions; quaternion inversion is the same as conjugation (Equation 5), the formula for 3D rotation of vector  $\vec{p}$  by quaternion  $q$  (Equation 6), and that applying consecutive rotations (first  $q_1$  and then  $q_2$ ) is equivalent to quaternion multiplication (non-commutative) (Equation 7).

$$q^{-1} = q^* \tag{5}$$

$$p' = qpq^{-1}; p = (0, \vec{p}) \tag{6}$$

$$q' = q_2q_1 \tag{7}$$

Typically, the 3D positions of the objects have to go through two additional transformations, a projection transformation and a transformation from the projection to the 2D computer screen. In the case of virtual reality environments, this happens for each viewpoint – each eye. The main types of projections, i.e. the orthographic and the perspective projection, are shown in Figure 3.



a) Orthographic camera projection

b) Perspective camera projection

Figure 3: Orthographic and perspective camera projections.

Orthographic projection is used when it is important to keep the relative distances between the points meaningful on the 2D view plane, i.e. to keep the ability to measure the relative distances by using the projection. In practice, however, perspective projection is more common, because it gives a realistic effect of the distance, i.e. the objects that are further away seem smaller. Figure 4 shows a scene in which the camera is in the origin and rotated towards the positive z axis.

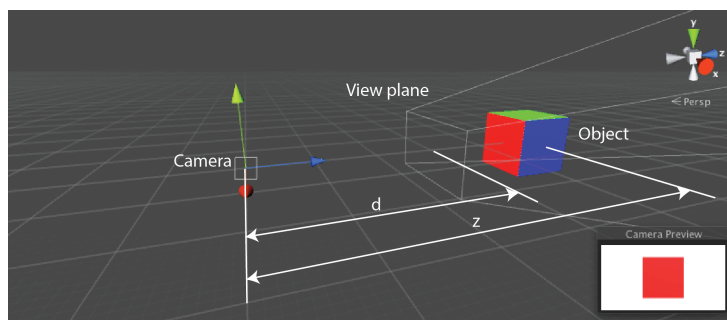


Figure 4: Perspective projection.

The perspective transform for the case in Figure 4 is shown in Equation 8.

$$\begin{bmatrix} 1 & 0 & 0 & 0 \\ 0 & 1 & 0 & 0 \\ 0 & 0 & 0 & 0 \\ 0 & 0 & \frac{1}{d} & 0 \end{bmatrix} \begin{bmatrix} x \\ y \\ z \\ 1 \end{bmatrix} = \begin{bmatrix} x \\ y \\ 0 \\ \frac{z}{d} \end{bmatrix} \Rightarrow \begin{bmatrix} x \frac{d}{z} \\ y \frac{d}{z} \\ 0 \\ 1 \end{bmatrix} \tag{8}$$

The  $x$  and  $y$  coordinates are scaled by  $\frac{d}{z}$  when projected to the view plane in this scenario.

### 3.2 Interaction with Objects in 3D Space

Mechanisms of interaction are influenced by the dimensionality of the user interface. On the 2D computer screen, they primarily consist of a camera moving mechanism which is commonly implemented as the first-person-movement style and the mechanism for interacting with 3D objects using the mouse and the keyboard. Typically, the mouse interaction is implemented by casting a ray through the clicked point on the view plane and detecting collisions between the ray and the 3D objects, which is commonly known as ray casting. Once the collision is detected, either an object that can manipulate the transformation of the clicked object is spawned (commonly referred to as a gizmo), or the object is moved by dragging the mouse as if moved by the ray on a fixed distance from the camera. This interaction mechanism using a gizmo is shown in Figure 5.

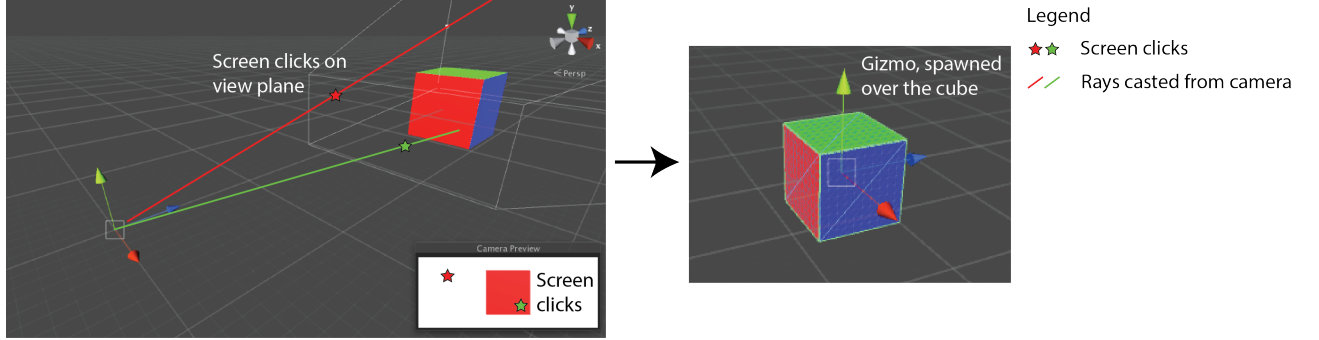


Figure 5: Mouse interaction using a gizmo.

The movement of the object by mouse dragging can be described in an iterative formula shown in Equation 9, in which a unit vector  $\hat{u}$  is scaled to the distance between the object and the camera, rotated towards the ray cast by the new mouse position, and offset by the position of the camera.

$$\vec{p}'_{object} = \vec{p}_{camera} + q_{ray} \cdot (|\vec{p}_{object} - \vec{p}_{camera}| \cdot \hat{u}) \quad (9)$$

The rotation of the object can be updated to be the relative rotation of the ray, as shown in Equation 10.

$$q'_{object} = q_{ray}^{-1} \cdot q'_{ray} \cdot q_{object} \quad (10)$$

In augmented reality environments, the 3D scene, i.e. the positions and rotations of the objects, must be detected through image processing, object detection, and object tracking algorithms. The key transformation is the transformation from pixel coordinates of the video stream to 3D object coordinates. Since pixel sizes and corresponding optical transformations depend on the video camera hardware, the absolute scale cannot be determined from the video alone. A clever solution is to measure the real life tracked objects (or markers) and devise a transformation of real-world to computer-generated-world units. Another way of doing this is through a calibration process. The problem can be described as the inverse of the problem described in Figure 4 and Equation 8. An example of determining the camera position from the size of the markers is shown in Figure 6.

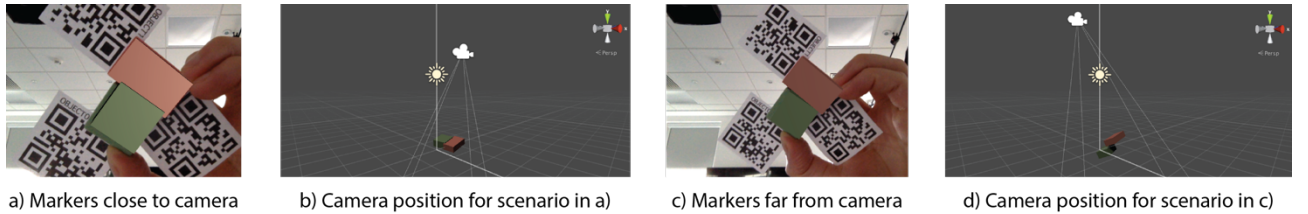


Figure 6: The relation between marker size and camera position. One of the markers is used to mark the origin of the coordinate system.

A common way of interaction in virtual reality systems is using a 3D joystick instead of a mouse. The joystick has a different position than the camera. Equations 9 and 10 have to account for that, as shown in Equations 11 and 12.

$$\vec{p}'_{object} = \vec{p}_{joystick} + q_{ray} \cdot (|\vec{p}_{object} - \vec{p}_{joystick}| \cdot \hat{u}) \quad (11)$$

$$q'_{object} = q_{ray}^{-1} \cdot q'_{ray} \cdot q_{object} \quad (12)$$

### 3.3 Synchronisation of Distributed Multi-Reality Environments

Synchronising the state of an object across the network is vital in distributed multi-reality environments. Several things need to be considered: who is the owner of each of the objects, because multiple owners could break the synchronisation of the object's state; is the object local or global, i.e. is it displayed in all of the environments or just the owner's; and what mechanisms should be applied when interacting with the objects. The topic will herein be discussed in a case of a mixed-multi-reality-environment consisting of a desktop, augmented reality, and virtual reality ones.

Since the augmented reality environment is used to detect real-world objects, it should also be the owner of their digital counterparts. This means the augmented reality environment should have the authority to spawn and to destroy the digital objects. Manipulation of the objects can only be done in the real world. Since the real world objects are transformed into the digital by means of augmented reality, desktop and virtual reality environments can only work on clones of those objects. Whatever action is performed on the objects, can then be reflected by spawning new objects for which the authoritative environment is the spawning one. This does not exclude that other environments can interact with these objects, as it can be done using remote procedure calls or by providing additional state variables and synchronising them over the network. The authoritative environment should also make sure that either the transformation (location, scale, rotation) or the rigid body associated with the digital object are synchronised.

## 4 Engineering Task Specification

This section takes into account the aforementioned concepts of multi-reality systems and interactivity in computer generated environments and presents a framework for the specification of engineering tasks and actions. A task is defined as a graph of actions  $A$  and predecessor-successor relationships  $P$  between the actions.

$$T = (A, P); \forall (a_p, a_s) \in P: \{a_p, a_s\} \subset A \quad (13)$$

Actions are considered to be effects which map the starting state to an end state of an object. The states of the objects are described by their position  $\vec{p}$ , rotation  $q$ , geometry  $g$ , material  $m$  which denotes the object's physical parameters and appearance, other object-specific information  $i$ , and time of the state  $t$ , as shown in Equations 14 and 15.

$$o(t) = (\vec{p}, q, g, m, i); o \in O \quad (14)$$

$$a: o(t) \mapsto o'(t'); t' \geq t \quad (15)$$

Table of atomic actions useful in engineering environments is presented in Table 1.

Table 1: Definitions of engineering actions of multi-reality interactivity.

Action	Inputs	Outputs
<b>move</b>	$o(t)$	$o(t + t_{move}): \vec{p} \mapsto \vec{p}'; \vec{p} \neq \vec{p}'$
<b>rotate</b>	$o(t)$	$o(t + t_{rotate}): q \mapsto q'; q \neq q'$
<b>process</b>	$o(t)$	$o(t + t_{process}): \{g, m\} \mapsto \{g', m'\}$
<b>inspect</b>	$o(t)$	$o(t + t_{inspect}): i \mapsto i'$
<b>store</b>	$o(t)$	$o(t + t_{store})$
<b>create</b>	$\emptyset$	$o(t)$
<b>destroy</b>	$o(t)$	$\emptyset$
<b>assemble</b>	$o_1(t), o_2(t)$	$o(t_{assemble}): o = o_1 + o_2$
<b>disassemble</b>	$o(t)$	$o_1(t + t_{disassemble}), o_2(t + t_{disassemble})$

The atomic actions are connected to one another through predecessor-successor relationships, enabling the construction of an action graph in which the output object of the predecessor is the input object of the successor action. Figure 7 shows an example of an action graph, describing the handling and the processing of object the  $o_1$ , subsequent assembly with another object  $o_2$ , and final storage of the assembled object.

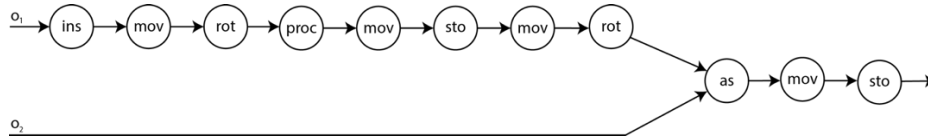


Figure 7: An example of an action graph describing a task.

## 5 Proof of Concept

The feasibility of the concept is tested. The application is programmed in Unity 5.3.4 game engine, using Vuforia library for augmented reality and a wall display with an ART tracking system for virtual reality.

Figure 8 illustrates the move action implementation in an example scenario of manipulation of cuboid objects. The three environments are used by different stakeholders; the augmented reality by the operator performing the task, the desktop by the expert giving instructions, and the virtual reality for remote monitoring of task execution. Figure 8a shows the real world view. The objects and the origin of the coordinate system are marked with QR code markers. Figures 8b shows a screenshot of a mobile application which uses augmented reality to detect the objects and superimposes their digital counterparts. These are then synchronised with the virtual reality and a desktop control application, shown in Figure 8c and 8d. The move action is specified through the control application, which shows the top-down view of the scene (Figure 8e). The action is visualised in both virtual reality (Figure 8f) and augmented reality (Figure 8g). Upon completing the action on real objects, the visualisation of the move action is deleted as shown in Figure 8h.

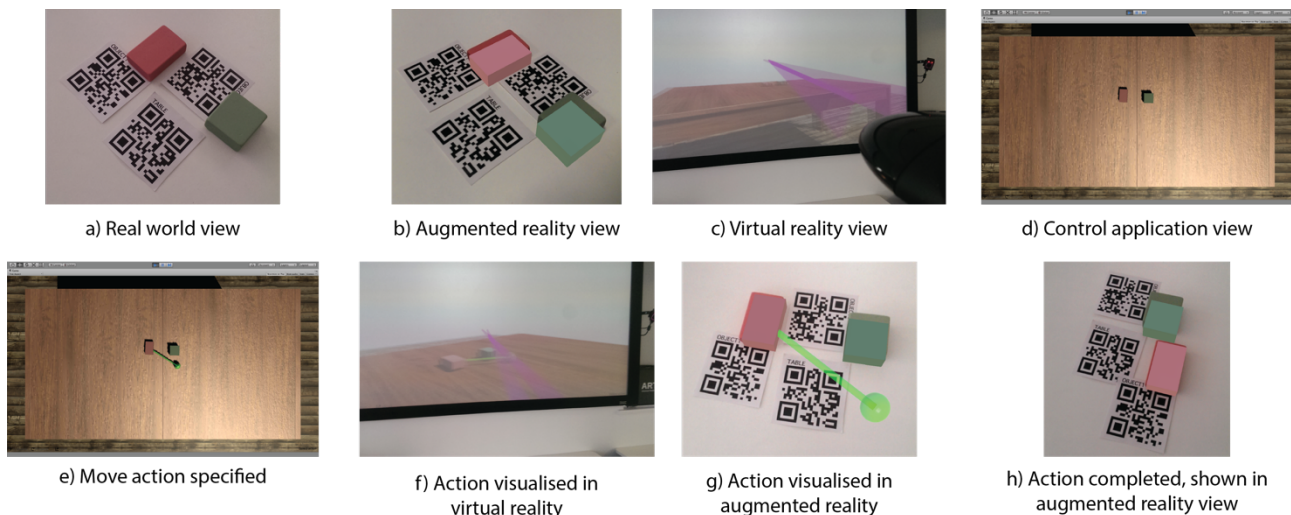


Figure 8: Implementation of the move action in multi-reality.

## 6 Conclusion

The paper presents an overview of engineering interaction possibilities in multi-reality environments by describing the basics of 3D interaction in computer environments and describing example approaches of its implementation on the desktop, in augmented reality, and in virtual reality. A framework defining the atomic engineering actions is presented. The proof of concept shows the applicability of the approach in a remote task specification, execution, and monitoring scenario, and illustrates its potential for remote operations and maintenance support.

The paper is a step towards a foundational framework for engineering applications in mixed- and multi-reality environments. Future work is needed for a full implementation of the concept and demonstrations in real life scenarios of remote operations and maintenance support.

## References

- [1] A. Caggiano, F. Caiazzo, and R. Teti, Digital Factory Approach for Flexible and Efficient Manufacturing Systems in the Aerospace Industry, *Procedia CIRP*, vol. 37, pp. 122–127, 2015.
- [2] W. Terkaj, T. Tolio, and M. Urgo, A virtual factory approach for in situ simulation to support

- production and maintenance planning, *CIRP Ann. - Manuf. Technol.*, vol. 64, no. 1, pp. 451–454, 2015.
- [3] E. H. Glaessgen and D. S. Stargel, The Digital Twin Paradigm for Future NASA and U.S. Air Force Vehicles, *53rd AIAA/ASME/ASCE/AHS/ASC Struct. Struct. Dyn. Mater. Conf. 20th AIAA/ASME/AHS Adapt. Struct. Conf. 14th AIAA*, no. April, pp. 1–14, 2012.
- [4] L. Da Xu, W. He, and S. Li, Internet of things in industries: A survey, *IEEE Trans. Ind. Informatics*, vol. 10, no. 4, pp. 2233–2243, 2014.
- [5] L. Monostori, Cyber-physical production systems: Roots, expectations and R&D challenges, *Procedia CIRP*, vol. 17, pp. 9–13, 2014.
- [6] A. Y. C. Nee, S. K. Ong, G. Chryssolouris, and D. Mourtzis, Augmented reality applications in design and manufacturing, *CIRP Ann. - Manuf. Technol.*, vol. 61, no. 2, pp. 657–679, 2012.
- [7] R. Stark, J. H. Israel, and T. Wöhler, Towards hybrid modelling environments - Merging desktop-CAD and virtual reality-technologies, *CIRP Ann. - Manuf. Technol.*, vol. 59, no. 1, pp. 179–182, 2010.
- [8] J. Fründ, J. Gausemeier, C. Matysczok, and R. Radkowski, Using Augmented Reality Technology to Support Automobile Development, *Lect. Notes Comput. Sci.*, no. 3168, pp. 289–298, 2005.
- [9] H. Perkunder, J. Israel, and M. Alexa, Shape Modeling with Sketched Feature Lines in Immersive 3D Environments, *Proc. Seventh Sketch-Based Interfaces Model. Symp.*, pp. 127–134, 2010.
- [10] L. X. Ng, S. K. Ong, and A. Y. C. Nee, Arcade: A simple and fast augmented reality computer-aided design environment using everyday objects, in *Proc. of the IADIS Int. Conf. Game and Entertainment Technologies 2010, Part of the MCCSIS 2010*, 2010, pp. 227–234.
- [11] J. Rekimoto, Transvision: A Hand-Held Augmented Reality System For Collaborative Design, *Proc. Virtual Syst. Multimed.*, pp. 85–90, 1996.
- [12] K. Smparounis, K. Alexopoulos, V. Xanthakis, M. Pappas, D. Mavrikios, and G. Chryssolouris, A Web-based platform for collaborative product design and evaluation, *Mech. Eng.*, pp. 35–56, 2011.
- [13] S. K. Ong and Y. Shen, A mixed reality environment for collaborative product design and development, *CIRP Ann. - Manuf. Technol.*, vol. 58, no. 1, pp. 139–142, 2009.
- [14] B. J. Nelson, A Virtual Reality Teleoperator Interface for Assembly of Hybrid MemS Prototypes, in *Detc98 / Mech-5836 Design Engineering*, 1998, pp. 1–7.
- [15] S. J. Henderson and S. K. Feiner, Augmented Reality for Maintenance and Repair (ARMAR), *Distribution*, p. 62, 2007.
- [16] P. Gurevich, J. Lanir, B. Cohen, and R. Stone, TeleAdvisor: A versatile augmented reality tool for remote assistance, *Proc. 2012 ACM Annu. Conf. Hum. Factors Comput. Syst. - CHI '12*, no. January, p. 619, 2012.
- [17] M. L. Yuan, S. K. Ong, and a. Y. C. Nee, Augmented reality for assembly guidance using a virtual interactive tool, *Int. J. Prod. Res.*, vol. 46, no. 7, pp. 1745–1767, 2008.
- [18] A. Gomes De Sá and G. Zachmann, Virtual reality as a tool for verification of assembly and maintenance processes, *Comput. Graph.*, vol. 23, no. 3, pp. 389–403, 1999.
- [19] P. Milgram, H. Takemura, a Utsumi, and F. Kishino, Mixed Reality ( MR ) Reality-Virtuality ( RV ) Continuum, *Syst. Res.*, vol. 2351, no. Telemanipulator and Telepresence Technologies, pp. 282–292, 1994.
- [20] J. Lifton and J. A. Paradiso, Dual reality: Merging the real and virtual, *Lect. Notes Inst. Comput. Sci. Soc. Telecommun. Eng.*, vol. 33 LNICST, pp. 12–28, 2010.
- [21] J. Gruen, T. Gerber, and T. Herfet, *Multi-reality interfaces - Remote monitoring and maintenance in modular factory environments*, vol. 14, no. PART 1. IFAC, 2012.

# Manufacturing Space Homogeneity in Additive Manufacturing – Electron Beam Melting Case

A. Piaget, M. Museau and H. Paris

*Univ. Grenoble Alpes, CNRS, G-SCOP, 38 000 Grenoble, France*

## Abstract

This paper focuses on the homogeneity of the manufacturing space of the EBM (Electron Beam Melting) technology. An Arcam AB A1 machine is used as tool for experimentations, with titanium (Ti-6Al-4V) as material. The objective of this study is to show the correlation between workpieces geometrical deformations and their position in the manufacturing space. Results show that the position on Z-axis does not affect quality, but there is a strong link in the Z-plane: significant defects appear near the manufacturing space boundaries. First manufactured layers are deformed in the vicinities of the manufacturing space edges. Up to 3mm of material loss and 8mm of dimensional deformation are measured. Further analyses point that this phenomenon is particularly related to a sintering variation in the powder: there are up to 3% density difference from the centre to borders. To avoid the problem, reduction of the manufacturing space and a supporting strategy are proposed. Defects can also be removed by implementing thermal insulation on the machine or by modifying the beam operation.

**Keywords:** Quality Management, Additive Manufacturing, Electron Beam Melting, Manufacturing Space Homogeneity.

## 1 Introduction

The additive manufacturing technologies have become essential tools for modern industry [1][2]. Among the different additive manufacturing technologies, EBM (Electron Beam Melting) is able to manufacture a wide range of metallic parts (massive, topologically optimized, lattice structure) [3] [4]. Compared to SLM (Selective Laser Melting), the EBM technology is still poorly studied [5]. However, there is a strong need to further master this technology. Aeronautic, spatial and also medical fields are particularly interested in mastering the quality provided by this process [6][7][8][9].

In order to control the quality, without destruction of manufactured parts, test specimens are manufactured simultaneously [10]. By testing those specimens, information about the quality of manufactured parts is obtained. Most of the time, specimens are arranged in the edges of the manufacturing space. A question arises about the homogeneity of the manufacturing space. Indeed, heterogeneity could lead to errors in the manufacturing and control processes. This key point that is not addressed in the literature, is the topic of this paper.

The problem is approached by studying the geometrical deformation which is the main defect. Previously, several parts showed defects when they were manufactured within certain areas of the manufacturing space. Thus, there is a need to characterise this space and its heterogeneity, and the way it impacts on the manufactured parts. These characteristics are related to the machine used (described below), but the experimental method can be applied to other machines.

In the next part, the context of the study and the experimentation are exposed. The type of deformation and measures are presented. Secondly, the possible sources of this defect are analyzed. We also show the impact they may have on manufactured parts. Finally we conclude about the dangers of this phenomenon and the prospects for resolution.

## 2 Defect identification

### 2.1 Context

The Arcam AB A1 machine [11] [12] uses an electron beam to melt powder (Figure 1). The powder from the hoppers is spread over a platform in 50µm thick layers with a rake. The electron beam sinters the whole of



the introduced powder. This increases the thermal and electrical conductivity. Then it locally melts the powder to manufacture the desired geometry. The platform finally goes down of the thickness of a layer and this cycle can be repeated.

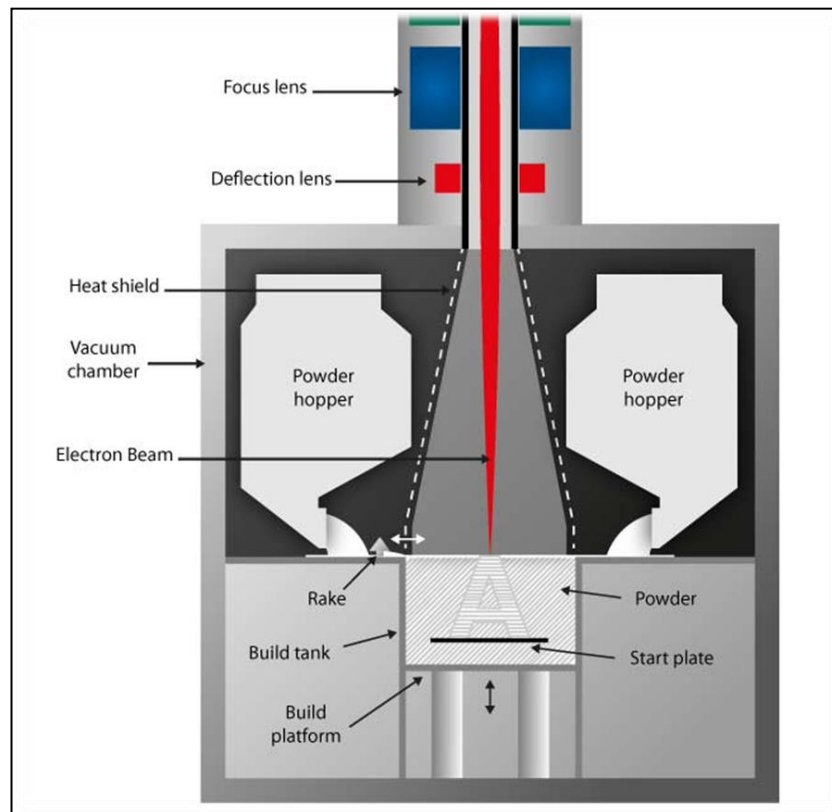


Figure 1: Arcam EBM systems, schematic architecture [11]

In order to qualify the geometric defect, some parameters have to be chosen. Ti-6Al-4V powder from Arcam AB is used for the study. Vayre [13] shown that Arcam AB standard parameter set is well balanced for printing several kind of geometry (lattice structures, massive workpieces...) at the same time. Thereby, this parameter set<sup>1</sup> is kept for the whole experimentation. Otherwise, workpieces will be built without any supporting strategy. Indeed, EBM technology doesn't necessarily involve a supporting strategy to build workpieces [14]. Based on Vayre [15], there is no need to add support to the experimental workpieces (described in the section below) because of the experimented workpieces thinness. Hereafter, evidence that supports aren't necessary to manufacture these workpieces is provided.

For the experimentation, the largest manufacturing space available with the machine is needed. But the manufacturing space is limited by the use of software<sup>2</sup> that reduce the initial manufacturing space (200\*200\*180) to 195mm in length, 195 in width and 180 in height.

## 2.2 Experimentation

The first objective of this study is to evaluate the impact of the position in the manufacturing space on the final workpiece geometry. Indeed, deformations are observed on several workpieces made by EBM. In order to show and identify this phenomenon, the following experimentation is realized.

The principle is to build one workpiece at different locations in the manufacturing space. Then, differences and defects can be observed and correlated to the location. Two kinds of workpieces have been selected for the test (Figure 2). The first one is a massive workpiece. The second one is a lattice structure. Thus, those workpieces represent the two kinds of geometry cases encountered.

<sup>1</sup> Arcam theme melt 50 $\mu$ m for TA6V

<sup>2</sup> Magics (Materialise), Build Assembler (Arcam AB)

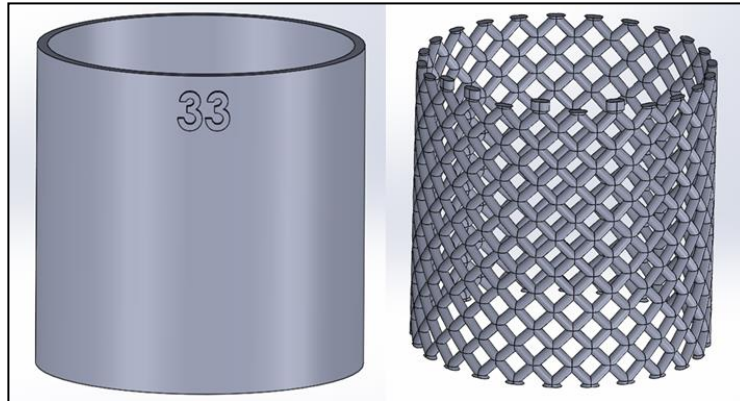


Figure 2: Experimentation workpieces, massive (left) and lattice structure (right).

The height and the diameter of the pipes are 30mm. The thickness of the wall for the massive pipe and of the beam for the lattice one is 1mm. Inside each pipe, two other pipes with different diameters ( $\varnothing 20\text{mm}$  and  $\varnothing 10\text{mm}$ ) are integrated to the experimentation in order to have different thermal conditions. Indeed, the  $\varnothing 10\text{mm}$  workpiece always has a  $\varnothing 20\text{mm}$  and a  $\varnothing 30\text{mm}$  pipes for neighbours while the  $\varnothing 30\text{mm}$  workpiece has a number of neighbours depending on its position.

The experimentation consists in testing 25 locations of the manufacturing space. Grouped by three, workpieces will be repeated on each locations of a unique altitude of the manufacturing space in order to avoid scan length problems [16]. By measuring each workpieces, defects are characterized and linked to the location.

Observations show that the defect appears in first layers. Therefore, the lower part of the workpieces is analysed and that is the reason why the workpieces are represented upside down later in the document. The measurement protocol for the massive workpiece uses a three-dimensional optical control machine<sup>3</sup> in order to measure deformation on the first manufactured layer. This layer is controlled at 24 points (every 15 degrees) distributed all along the surface. The result of a measure is the height of the controlled point with a  $2\mu\text{m}$  precision. From this, we recovered the difference between the nominal height and the measured one (Figure 3, left).

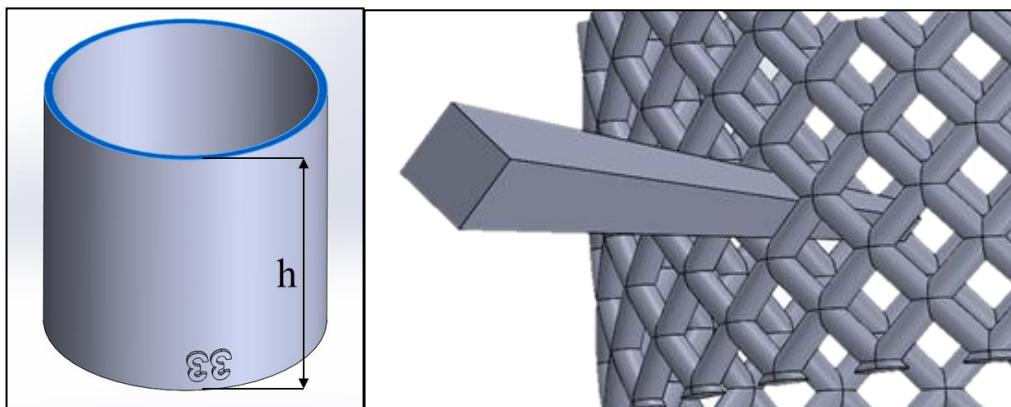


Figure 3: Representation of the measurement processes: massive (left) and lattice (right) workpieces

Measuring the first layer deformation does not provide information on the deformation of the following layers. With the lattice structure, the target is to measure the defect spread through several layers. Consequently, the measurement protocol has to be adapted. A tool has been created to control the external geometry of the lattice pipe (Figure 3, right). This way, we may have information about the defect on the pipe: its angular position and altitude.

<sup>3</sup> Used machine : Vertex, <https://www.microvu.com/>

### 2.3 Results

Measures are presented in a radar chart in order to represent the size and the angular position of the defect. So, in the diagrams, the more a point is far from the middle, the more the defect is important. As shown in Figure 4, defect occurs on some workpieces (on both pictures, the left workpiece fits the CAD model and the right includes a deviation from the model). The defect is materialized in two forms: material loss and geometric deformation. Lattice structures show both failure (Figure 4): between the well-shaped and the defective workpiece, deformations are observed in first layers (missing) and in diamond meshes (misshapen).

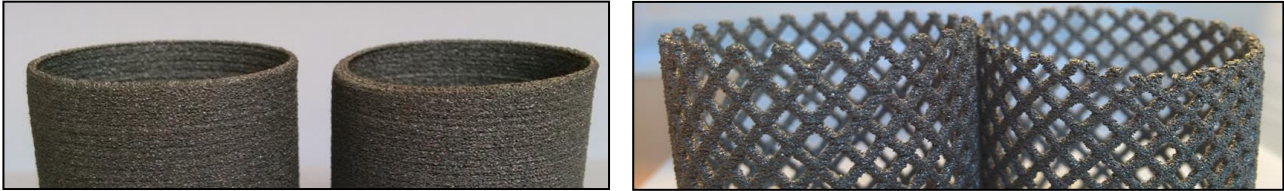


Figure 4: massive (left) and lattice (right) workpieces placed upside down

Figure 5 presents the results for the massive workpiece. From these results, occurrences of defects on nearby workpieces of borders are observed. Furthermore, the defect is more critical as the point observed on a workpiece is close to the borders. The biggest gap measured between the nominal and the manufactured surface is 3mm high. Whereas, for the inner workpieces, measured defects are smaller than 0.8mm. But this fact corresponds with the 50µm roughness owned by the material resource [16].

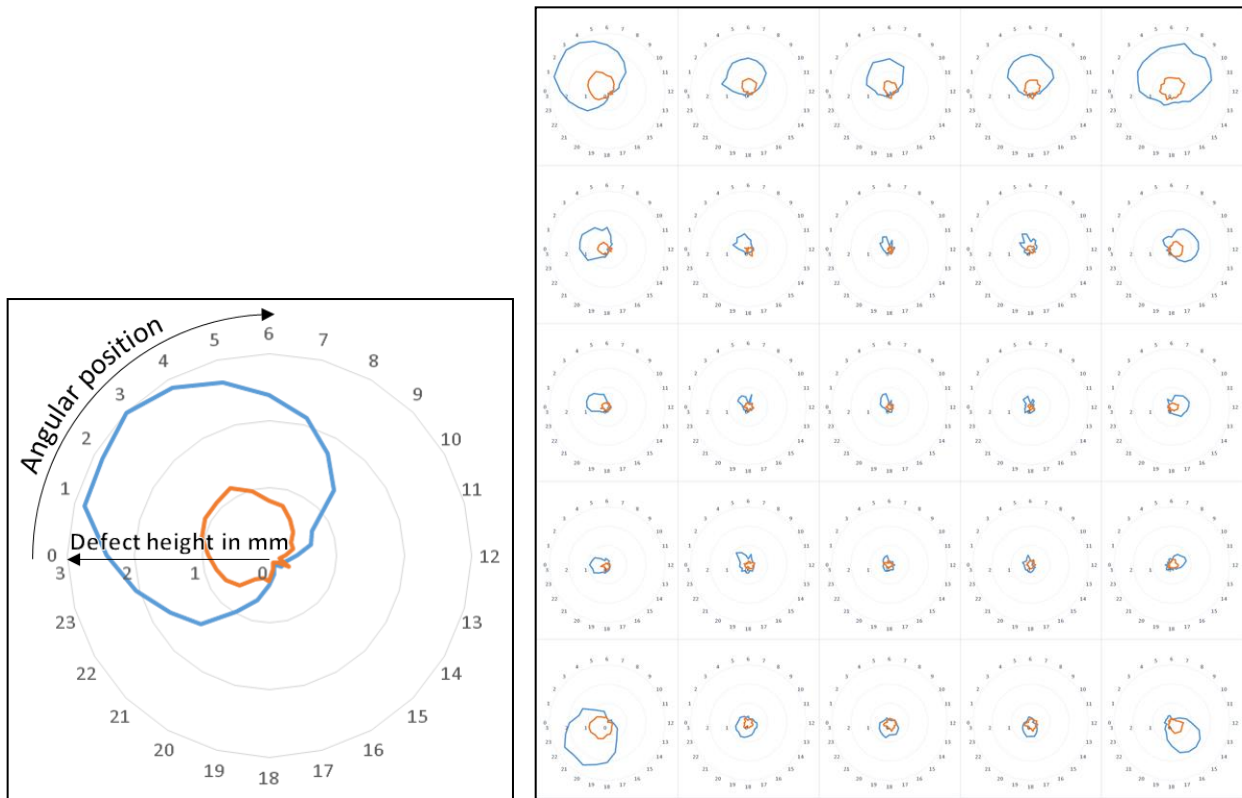


Figure 5: Example and defect cartography of the massive workpieces (blue: Ø30mm, orange: Ø20mm).

Figure 6 presents results for the lattice workpieces in numbers of defective cells, for an angular position and starting from the bottom of a workpiece. The same conclusion can be drawn as there is no defect in the inner workpieces and the external workpieces have an outwardly directed defect. In addition, the highest measured defect is 8mm high from the first layer.

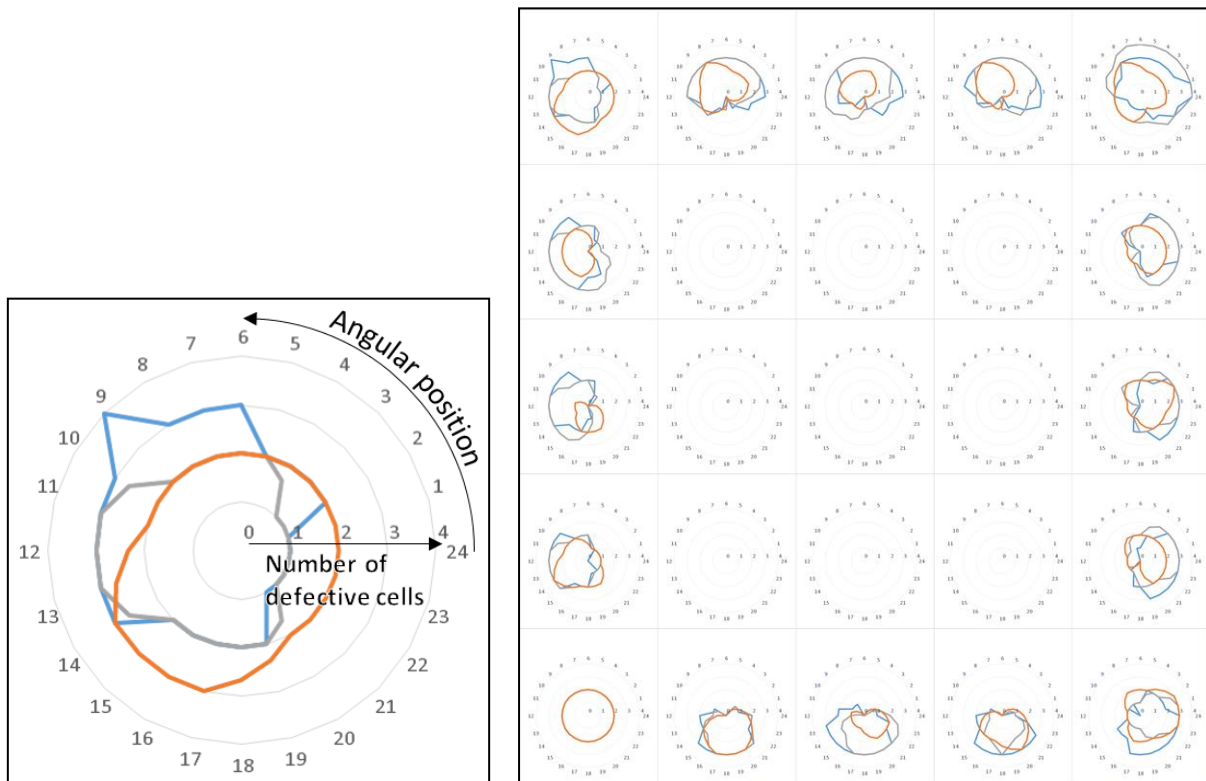


Figure 6: Example and defect cartography of the lattice workpieces (blue: 30mm, orange: 20mm, grey: 10mm).

Another interesting point is that a group of workpieces (located at the bottom right in Figure 6) has undergone a 2mm mechanical shifting. The 3 curves are overlapping because workpieces cells are all affected in the same way. What is interesting in this point is that it brings other elements to explain and understand the sources and consequences of the deformation phenomenon, although this shifting is not repeatable. Figure 7 is a photography that shows the encountered problem. This shifting is in the movement direction of the rake.

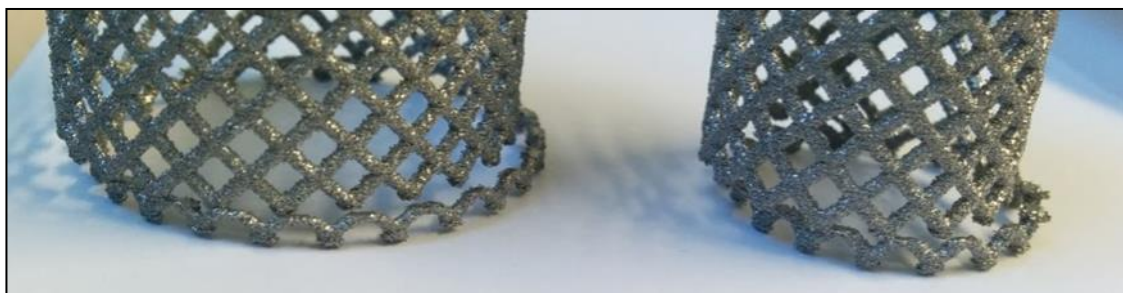


Figure 7: Photography of the 2mm mechanical shifting (Ø30mm on left, Ø20mm on right).

Finally, observations and measures show that only the workpieces near the borders of the manufacturing space are reached by the defects. In corners, the defect reaches its highest value: the maximal height of the defect is 8mm from the first layer. Those defects are significant enough to justify a thorough study with the aim to master and avoid this problem.

### 3 Phenomenon Analysis

#### 3.1 Hypothesis

To explain the phenomenon, several hypotheses have been expressed. First, the electron beam hypothesis has been selected. Indeed, to reach borders, the electron beam has to undergo an important deflection that leads to change the shape of the beam from a circle to an ellipse. The energy broadcasted to the powder is lower as

the surface of transmission gets bigger. It generates a decrease in the temperature that prevents the melting of the powder. This decrease might explain the location of the defect and the defect type also.

The second hypothesis concerns the workspace in the machine. At the borders of the manufacturing space, next to the sintered powder, there are cold powder and the metal enclosure that might absorb the energy of the sintered powder and thereby generate a loss of temperature. As TA6V is a bad thermal conductor [8], this phenomenon might just take place at the border between the sintered powder and the cold powder. Lowering temperature locally leads to the same conclusion as the electron beam hypothesis.

A third hypothesis arises from the mechanical shifting (Figure 7). As a portion of the workpiece has been moved in the rake direction, this hypothesis involves the rake: when the rake spreads the powder out, it can move the matter underneath by the thrust applied on the powders. That might cause deformation and matter loss in the workpiece.

The first and the second hypothesis might explain the difference between the workpieces but they don't solve the matter shifting. On its side, the third hypothesis elucidates the shifting but there is no reason for the non-homogeneity of that phenomenon.

The hypothesis we kept is a combination of the previous ones: the contact area of the electron beam is circular in the powder bed center, but away from the center, it becomes elliptical and provides less energy to the powder. In addition, the energy leaks with the proximity to cold powders and metal enclosure. This makes the sintering of the powder weaker near the borders. Then, the rake passage might easily move the poorly sintered powder and the molten material suspended in the powder. This might lead to a loss of material as well as deformation for the manufactured parts. In addition, the sintering weakness modifies the thermal conductivity, the cooling of the manufactured parts is no more homogeneous and it generates additional deformation.

### 3.2 Analysis

In order to validate the hypothesis, an analysis of the sintered powder is made. This analyse was conducted with an X-ray microtomography machine. The machine is able to reconstruct a 3D model of the studied sample with voxels. This reconstruction aims to display and measure the size of the necks binding in the sintered powder. A difference of necks size between the powders in the centre and in the periphery of the manufacturing space would indicate a significant difference of the sintering [19].

The samples of powders are one centimetre side cube. This size allows observation of a large number of powder grain that limits the impact of defects in the powder. Due to the titanium opacity to X-ray, getting a  $1\mu\text{m}$  resolution with titanium parts requires more power than supplied by the machine [18]. Resolution has been reduced to  $5\mu\text{m}$  in order to provide a clear tomography of the samples. Despite a clear tomography, it becomes impossible to measure necks because of the resolution. However, [19] show there is a link between density and sintering progress with spherical powders. Thereby, measuring density permits comparison of the two samples sintering.

Table 1: Porosity measured from the tomography reconstruction

Samples	Centre	Periphery
Porosity (%)	37.84	41.29
Standard Deviation (%)	1.36	1.92

Table 1 presents the results of the analysis. With more than 3% difference, assumptions about the difference of sintering are justified. Indeed, according to OLMOS [19], 3% are significant enough to make a difference of sintering. This difference impacts the powder stiffness and its heat conductivity. This generates a harmful heterogeneity in the manufacturing space that might have bad effects on manufactured parts [20].

## 4 Conclusion

The observed defect has an impact on geometry of manufactured parts with EBM technology. According to their position, parts may undergo geometric deformation and matter loss. It can be inferred from this study that the manufacturing space is heterogeneous.

In the worst case, the 8 first millimeters are affected by this defect. The closest defect to the center is 86mm distant from the center. The more the defect is far from the center, the more important it is. With this information, a first strategy can be used to bypass the defect. Indeed, creating supports 8mm (or more) long all along the first layer permits to transfer the defect from the part to supports. A manufacturing space reduction to an 86mm radius cylinder can also be a solution to avoid the defect apparition. Those 2 strategies have been validated with the workpieces.

As well, modification could be made to change the machine operation and more precisely the electron beam. By bringing more energy, the powder sintering would be homogenized. Improve the insulation of the powder bath with the machine will also limit the energy loss.

## References

- [1] I. Gibson, D. Rosen, B. Stucker: Development of Additive Manufacturing Technology. Additive Manufacturing Technologies, pp 19-42, 2015.
- [2] W. Gao, Y. Zhang, D. Ramanujan, K. Ramani, Y. Chen, C. B. Williams, C. C. L. Wang, Y. C. Shin, S. Zhang, P. D. Zavattieri: The Status, Challenges, and Future of Additive Manufacturing in Engineering. Computer-Aided Design 69, pp 65-89, 2015
- [3] N. Hrabe, and T. Quinn: Effects of Processing on Microstructure and Mechanical Properties of a Titanium Alloy (Ti-6Al-4V) Fabricated Using Electron Beam Melting (EBM). Materials Science and Engineering: A, V. 573, 20 June 2013.
- [4] N. Novak, M. Vesenjak, Z. Ren: Auxetic Cellular Materials – a Review. Journal of Mechanical Engineering 62, pp 485-493, 2016.
- [5] S.L. Sing, J. An, W. Y. Yeong, and F. E. Wiria: Laser and Electron-Beam Powder-Bed Additive Manufacturing of Metallic Implants: A Review on Processes, Materials and Designs. Journal of Orthopaedic Research, October 2015.
- [6] S. Daneshmand, C. Aghanajafi: Description and Modeling of the Additive Manufacturing Technology for Aerodynamic Coefficients Measurement. Journal of Mechanical Engineering 58, pp 125-133, 2012.
- [7] J. M. Waller, B. H. Parker, K. L. Hodges, E. R. Burke, and J. L. Walker: Nondestructive Evaluation of Additive Manufacturing. National Aeronautics and Space Administration, November 2014.
- [8] G. Budzik, J. Burek, A. Bazan, P. Turek: Analysis of the Accuracy of Reconstructed Two Teeth Models Manufactured Using the 3DP and FDM Technologies. Journal of Mechanical Engineering 62, pp 11-20, 2016
- [9] V. Petrovic, J. V. Haro, J. R. Blasco, and L. Portolés: Additive Manufacturing Solutions for Improved Medical Implants. Metal-Processing Research Institute AIMME, Valencia, Spain, 2012.
- [10] CCT MAT – STR, CNES: PRINTtemps de la Fabrication Additive. Toulouse, June 2016
- [11] Arcam AB: Creating New Opportunitites in Design and Production. [www.arcam.com/wp-content/uploads/justaddbrochure-web.pdf](http://www.arcam.com/wp-content/uploads/justaddbrochure-web.pdf), 2016
- [12] Arcam AB: Arcam A1, the Future in Implant Manufacturing. <http://www.arcam.com/wp-content/uploads/Arcam-A1.pdf>, 2010
- [13] B. Vayre: Conception pour la Fabrication Additive, Application à la Technologie EBM. PhD Thesis, Univ. Grenoble Alpes, 2014.
- [14] A-F. Obaton, A. Bernard, G. Taillandier, J-M. Moschetta: Fabrication additive: Etat de l'Art et Besoins Métrologiques Engendrés. Rev. Franç. Métr. N°41, 2016.

- [15] B. Vayre, F. Vignat, and F. Villeneuve: Identification on Some Design Key Parameters for Additive Manufacturing: Application on Electron Beam Melting. *Procedia CIRP* 7, pp. 264 – 269, 2013
- [16] A. Safdar: A study on Electron Beam Melted Ti-6Al-4V. Lund University, 2012.  
<http://lup.lub.lu.se/record/2543181>, accessed august 2016.
- [17] J. A. Slotwinski, E. J. Garboczi, P. E. Stutzman, C. F. Ferraris, S. S. Watson, and M. A. Peltz: Characterization of Metal Powders Used for Additive Manufacturing. *Journal of Research of the National Institute of Standards and Technology*, Volume 119, 2014.
- [18] C. Thiery: Tomographie à Rayons X. *Techniques de l'Ingénieur*, 10 December 2013.
- [19] L. Olmos: Etude du Frittage de Poudres par Microtomographie in situ et Modélisation Discrète. PhD Thesis. Institut National Polytechnique de Grenoble - INPG, 2009.
- [20] C.-M. Zou, Y. Liu, X. Yang, H-W. Wang, and Z-J. Wei: Effect of Sintering Neck on Compressive Mechanical Properties of Porous Titanium. *Transactions of Nonferrous Metals Society of China*, Volume 22, Supplement 2, December 2012, Pages s485-s490.

# Compensation of uneven illumination on stereolithography based 3D DLP printer

M. Peroša, J. Valentinčič, A. Lebar, M. Jerman, I. Sabotin and P. Drešar

<sup>1</sup> University of Ljubljana, Slovenia

## Abstract

Uneven illumination on the working space of a stereolithography based 3D DLP printer results in bad printing quality. In this paper a process to reduce the unevenness of illumination is presented. The first part presents the method used to capture an image of the DLP projector illumination. The presentation of image acquisition is followed by image processing where the procedure of creating a mask from the previously acquired image is shown. With the mask applied to the DLP projector another image of its illumination was taken and analysed. The results from the tests presented in this paper demonstrated that the method used successfully reduced the uneven illumination.

**Keywords:** uneven illumination, stereolithography, DLP, mask, 3D printing, additive manufacturing

## 1 Introduction

Additive manufacturing (AM) is a formal expression for what used to be called rapid prototyping technology (RP). This technology is used in a variety of industries for rapid creation of a prototype or basis model. From this further models are produced, which contribute to the development of the final product. Recently, users of rapid prototyping technology came to the conclusion that the term "rapid prototyping" is inappropriate, since the technology is already used for other purposes, such as the production of final products [1].

There are numerous ways to classify AM technologies. A popular approach, which is shown on **Error! Reference source not found.**, is to classify the AM technologies into groups, depending on the type of the input material [1].

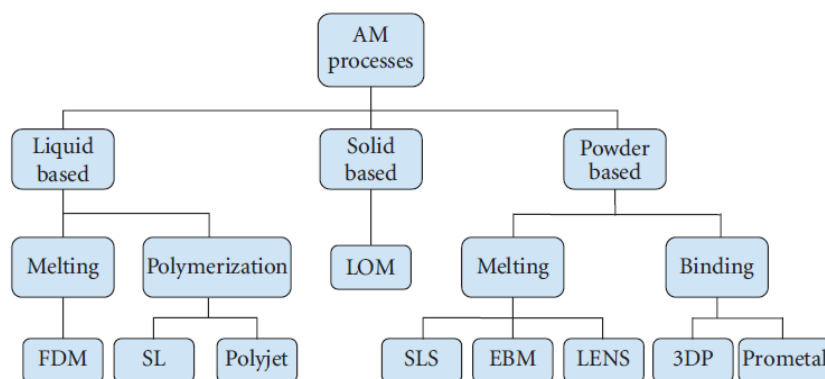


Figure 1: Classification of AM technologies [2].

This article is focused on a liquid-based AM technology, more specifically on stereolithography (SL).

### 1.1 Stereolithography

Stereolithography (SLA) is a liquid-based AM process, from which 3D parts are made by curing a photosensitive polymer with an ultraviolet (UV) laser source. The process starts with the creation of a CAD model, which is then converted into an STL format and sliced into layers using the appropriate software. The UV laser is then used to solidify the resin on specific regions of each layer [2], [3].



Nowadays, various types of light sources can be used to cure photopolymers, including gamma rays, X-rays, electron beams, UV and visible light. UV and visible light are the most commonly used [3].

The configuration of the SLA machine depends on the light source used. In our case we used a mask projection or layer-wise configuration. This kind of configuration uses a large radiation beam that is patterned by another device, for example a Digital Micromirror Device (DMD) [3]. A scheme of an SLA machine with mask projection configuration is shown on Figure 2 **Error! Reference source not found.**

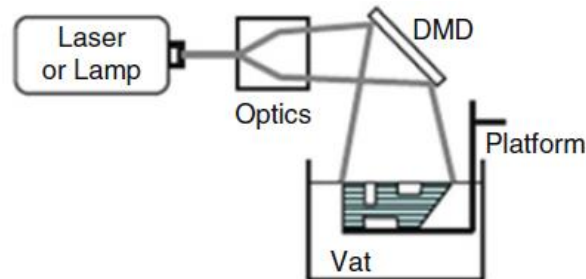


Figure 2: Schematic of an SL machine [3].

## 1.2 Definition of the problem

With the constant lowering costs of components used to build a 3D printer, the popularity of homemade SL based 3D printers has significantly increased in the last years. The custom built stereolithographic 3D printers, made by enthusiasts, usually use a digital light processing (DLP) projector to irradiate entire layers at one time. In our case the same configuration was used.

When we performed the preliminary testing prints on our custom built 3D DLP printer, we noticed, that on certain locations of the printing area the test pieces were not entirely printed. Since we didn't find any relevant scientific articles on the topic we looked on the stereolithography enthusiasts community forums if anybody else had encountered similar problems. With the help from the community forums we have identified a probable cause for the incomplete testing prints. The cause was the lack of uniformity in the DLP projector's illumination [4].

Uneven illumination results in a narrower printing area and poor printing quality. Our objective was to improve the printing area and printing quality by reducing the DLP projector's uneven illumination. A method was mentioned on the community forums [5]. The method, which is described in this article uses a mask to improve the DLP projector's illumination and printing quality. A mask is a layer, which is applied on a projecting image. The mask allows us to control the transparency on different areas of the projecting image separately.

## 2 Experimental setup

### 2.1 3D DLP printer

The 3D printing machine that was used in this paper is shown on Figure 3. It consisted of a digital light processing (DLP) projector as a light source, capable of projecting entire layers at one time. The configuration used was bottom-up, which means that the projector was placed under the vat, illuminating the bottom of the vat.



Figure 3: Custom built 3D DLP printer used in experiments.

In this case we used a DLP projector Acer P1500, which had 1920x1080 native resolution and 3000 lumens brightness.

## 2.2 Image capturing and processing

A testing site to capture the DLP projector illumination was set up. The site consisted of a computer, connected to the DLP projector, a box on which a white image was projected and a camera, used to capture the image. The camera was a Canon 30D with 50 mm lens, 1/125 s shutter speed and f/4.5 aperture. The testing site is shown on Figure 4.

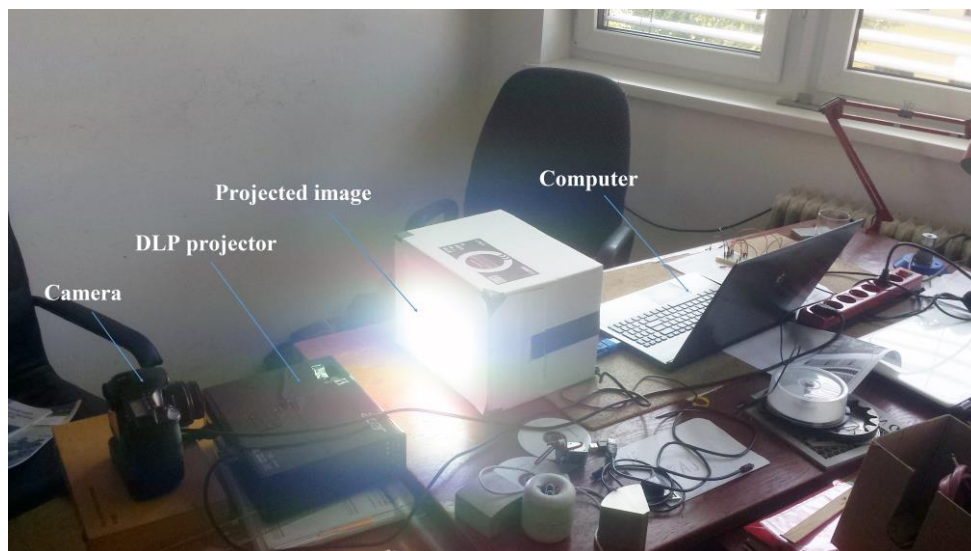


Figure 4: Testing site for image capturing

The captured image had borders that were used to focus the camera as shown on Figure 5. The image was modified for a better presentation of areas with lower illumination.

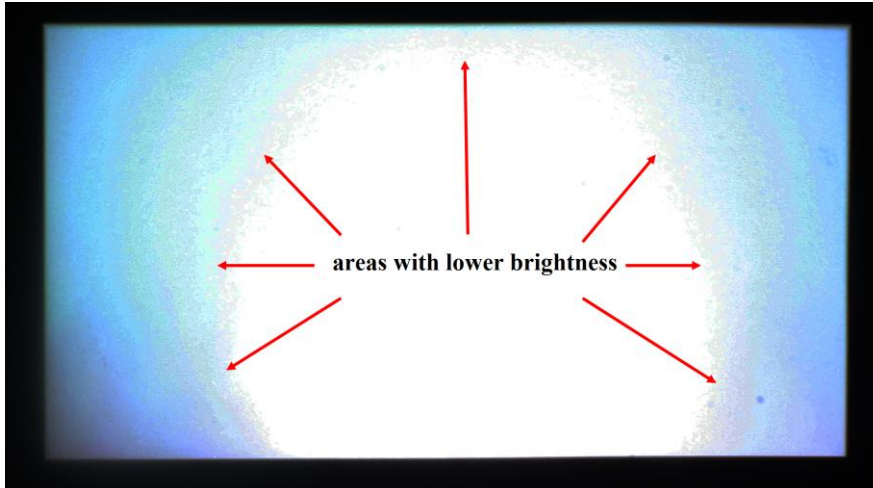


Figure 5: Captured image of the DLP projector illumination.

In the next steps the borders were cropped. The cropped image was then resized to 1920x1080 resolution and converted to a greyscale 8-bit png format, which is needed for image processing.

### 2.3 Creating a mask

The next step in creating a mask was to invert the image. This means that the value of each pixel was subtracted from the brightest value, which is 255. The result was a dark image. Finally a 50% transparency was set by changing the alpha channel value of each pixel on the dark image. The result was a grey image that was used as a mask. The used mask is shown on Figure 6.



Figure 6: A mask produced by a described technique, used to eliminate the uneven illumination.

The resizing, image conversion, image inversion and transparency setting were performed with a Microsoft Visual studio C++ written program.

## 3 Image analysis

An image of the DLP projector illumination with the mask applied was captured and a comparison with the image without mask was performed. The results of the comparison are presented with histograms and its appropriate images on Figure 7 and Figure 8. The brightness was altered to facilitate the comparison.

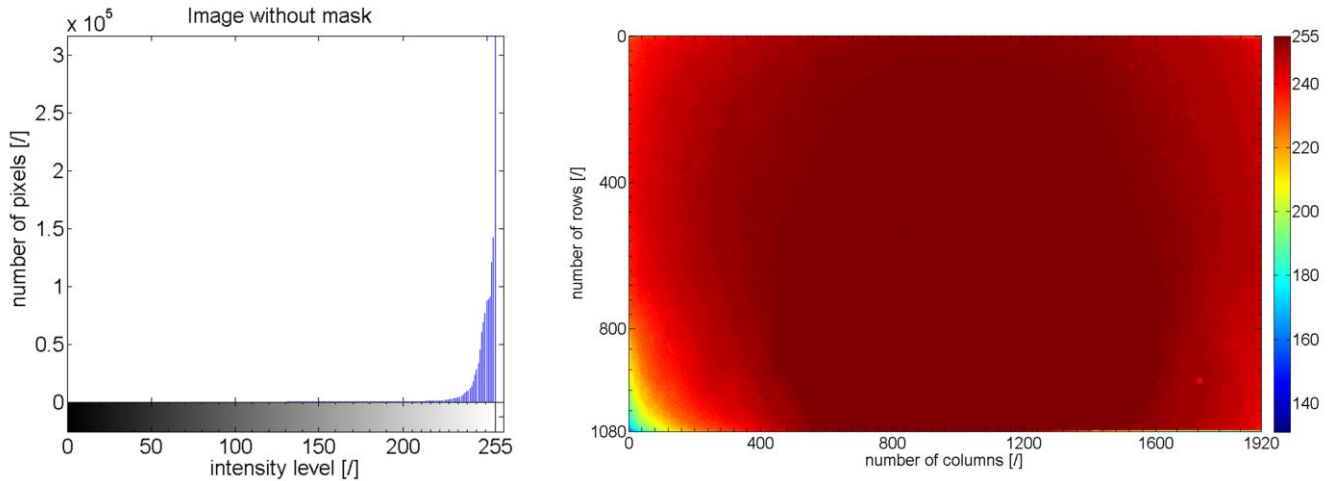


Figure 7: Image without mask.

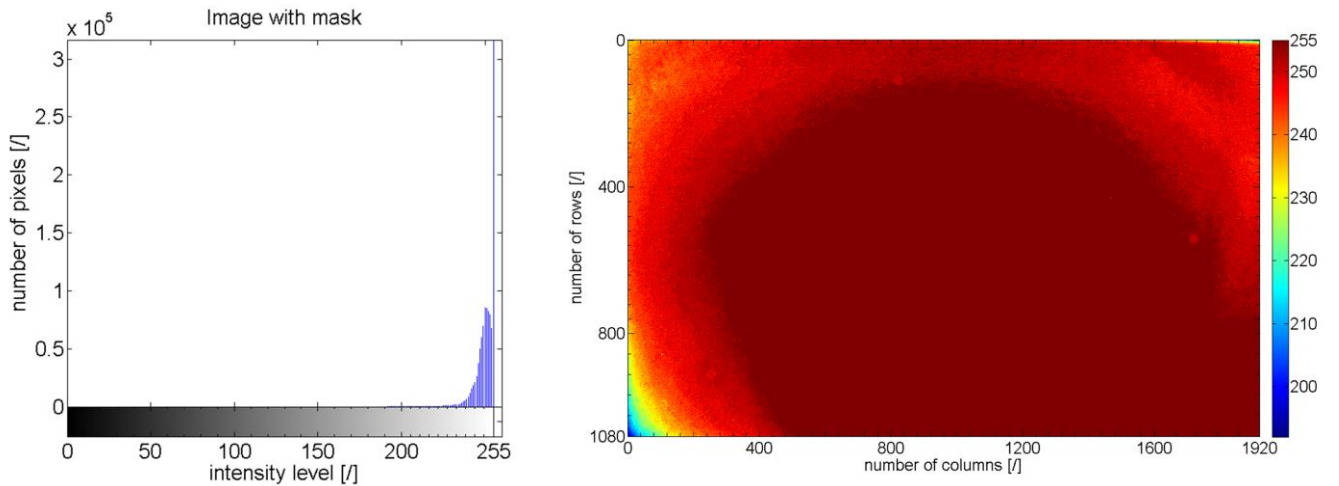


Figure 8: Image with mask applied.

The results from Figure 7 and Figure 8 show a reduction in the number of pixels with intensity level lower than 255, which means that the applied mask is working, but not as good as expected. An additional improvement to the mask was needed in order to additionally reduce the number of pixels with intensity level lower than 255.

#### 4 Mask improvement

To improve the mask the image of the DLP projector illumination with the mask applied, was subtracted from a scalar of 255 (the brightest value). The result was a matrix of pixel intensity variation between the image with the mask applied and an ideally white image (each pixel with intensity level 255). The matrix of pixel intensity variation was then summed with the existing mask.

An image of the DLP projector with the improved mask was taken and analysed. If compared with histograms on Figure 7 and Figure 8, the histogram of the improved mask on Figure 9 shows a greater reduction in the number of pixels with intensity level lower than 255, which means that the uniformity of the DLP projector illumination was improved.

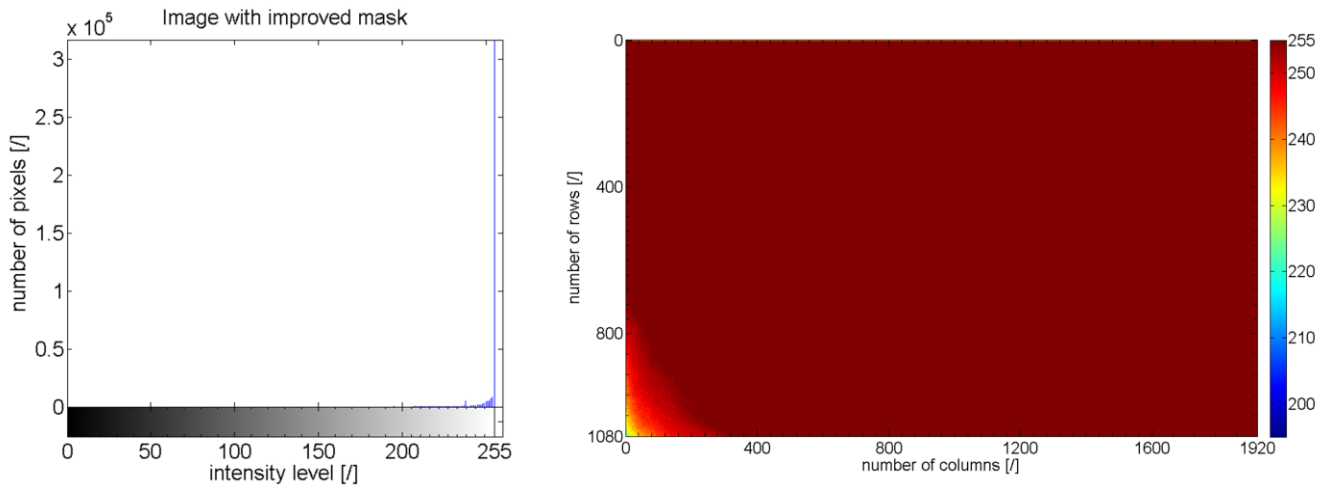


Figure 9: Image with improved mask.

## 5 Printing tests

In total four printing tests were performed to confirm the improvement in the uniformity of the DLP projector illumination. The printing objects were five cubes, placed to cover the entire working space of the 3D DLP printer. Two printing tests were performed without the mask, while the other two were performed with the improved mask (Figure 10).

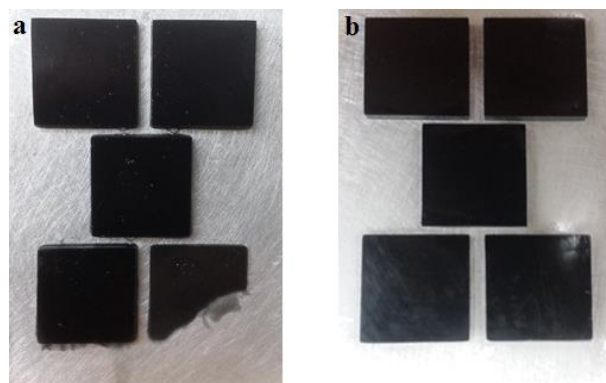


Figure 10: (a) Printing tests without mask; (b) Printing tests with improved mask.

## 6 Results and discussion

From the image analysis we concluded that the mask wasn't properly made. In the image acquisition process we didn't isolate the ambient light correctly from our projected image. That influenced the image from which the mask was created. In the process of the mask improvement the problem was solved.

The improvement in DLP projector uniformity can be seen from the images and histograms of the DLP projector's illumination without the mask (Figure 7) and with the improved mask (Figure 9). To additionally confirm the improvement we have written a program in Matlab that loads the images and counts the number of pixels with the highest intensity level (255) on each image. We came to the conclusion that with the improved mask the uniformity of illumination has increased by 87 % (Figure 11).

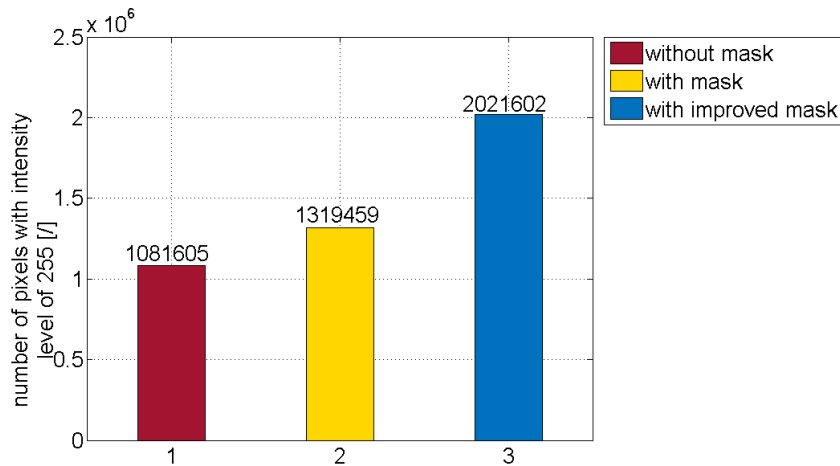


Figure 11: Number of pixels with intensity level of 255 for each illumination image.

The printing tests once more confirmed that the improved mask worked properly. The image on Figure 10(a) shows that the test pieces, printed on the area where the illumination intensity was lower are missing some layers. The reason for that is an insufficient curing time for such intensity level. The other test pieces, printed on the area with higher illumination intensity were printed successfully. In the second printing test without the mask the results were similar.

All the test pieces printed with the improved mask (Figure 10(b)) were printed successfully. The second test with the mask applied gave similar results. The results of the printing tests show that the uniformity of the DLP projector's illumination was successfully improved. The test pieces printed with the improved mask had sharp edges, while the edges of the test pieces printed without the mask weren't.

## 7 Conclusion

Uniform illumination allows us to take advantage of the entire printing area, which means that we can print more products at the same time and consequently reduce the time of printing. The method shown in the paper is a relatively simple method to improve the illumination uniformity of a low cost DLP projector, used for 3D printing. With this method no intervention to the components of the projector is needed.

A downside of this method is a higher curing time of the photopolymer. The reason for that is in the reduction of intensity on the entire printing area, which is caused by the mask.

The mask shown on Figure 6 is made only for the DLP projector mentioned in the article and it varies between the projectors.

## 8 References

- [1] I. Gibson, D. Rosen, and B. Stucker, Introduction and Basic Principles, in Additive Manufacturing Technologies, Springer New York, 2015, pp. 1–18.
- [2] K. V. Wong and A. Hernandez, A review of additive manufacturing, ISRN Mech. Eng., vol. 2012, 2012.
- [3] I. Gibson, D. Rosen, and B. Stucker, Vat Photopolymerization Processes, in Additive Manufacturing Technologies, Springer New York, 2015, pp. 63–106.
- [4] Uneven curing of the edges - Build Your Own SLA/SLS. Available: <http://www.buildyourownsla.com/forum/viewtopic.php?f=12&t=722>. [Accessed: 01-Sep-2016].
- [5] Mask - Build Your Own SLA/SLS. Available: <http://www.buildyourownsla.com/forum/viewtopic.php?f=5&t=2096&hilit=mask>. [Accessed: 01-Sep-2016].

# Comparison of optimal technological parameters obtained with two different nozzle sizes in hybrid manufacturing of 3D printing and milling

D. Grguraš<sup>1</sup>, D. Kramar<sup>1</sup>, D. Homar<sup>1</sup> and J. Kopač<sup>1</sup>

<sup>1</sup> *University of Ljubljana, Slovenia*

## Abstract

In this paper hybrid manufacturing of 3D printing and milling is presented. Fused deposition modeling (FDM) was used for creating a product and afterwards outer surface was improved with milling. Today's FDM systems use standard nozzle size with diameter of  $D = 0.4$  mm. In this research bigger nozzle size (diameter  $D = 1.1$  mm) was applied in order to achieve shorter time of production. Optimization of technological parameters of hybrid manufacturing according to the minimum time of production, a minimum final surface roughness and minimal usage of material was carried out. Those optimal results were compared for both standard and bigger nozzle size.

**Keywords:** hybrid manufacturing, fused deposition modelling, milling, PLA material, design of experiments, empirical modeling and optimisation

## 1 Introduction

Fused deposition modeling (FDM) is additive manufacturing process where 3D components are built, using hot nozzle to melt polymer and deposit it layer by layer on the build platform. FDM is one of the most used additive manufacturing processes because FDM machines production is inexpensive and simple. Accuracy, repeatability, surface roughness and manufacturing time of parts manufactured by FDM is very dependent on abundant process parameters. In a lot of cases, FDM products do not meet requirements of accuracy and surface roughness despite the well-selected process parameters. Characteristics of the 3D printed (FDM, 3D welding etc.) parts can be improved by machining [1, 2]. Because of that reason machine for hybrid manufacturing was developed on Faculty of Mechanical Engineering in Ljubljana, Slovenia. The concept of machine is introduced in next chapter.

Hybrid manufacturing has more meanings and definitions [3]. In our case hybrid manufacturing means that one product is done by two or more completely different production technologies. Additive manufacturing and subtractive machining were used. FDM technology was used for additive manufacturing and afterwards 3 axis CNC milling was applied. Aim of technologies combination is removing drawbacks of specific technology. Milling has limitations in the type of geometry can be manufactured because cutting tool cannot reach closed surfaces. On the other hand, FDM technology is the complete opposite. FDM and other additive technologies almost do not have limitations in product geometry shapes, but lack in surface finish. These drawbacks are minimized if both technologies are used [4, 5].

In this study, to achieve optimal technological parameters of hybrid manufacturing, i. e. 3D printing and milling parameters, response surface methodology was used.

## 2 Process principle and experimental setup of 3D printing and milling

CNC machine for hybrid manufacturing has been developed and is presented in Figure 1. Machine includes 3D printing system for material adding layer by layer and milling system for removing material with machining.

3D printing system uses FDM technique where plastic filament is led to the heating body and then is deposited through the nozzle down on a build platform.

Milling part of the system is consisting of motor 800 FME, Kress with nominal rated input power of 800W. Number of revolution per minute (spindle speed) can be set between 10.000 and 29.000  $\text{min}^{-1}$ .

In this study specimens i. e. cubes (dimensions 22 x 22 x22 mm) from PLA material were produced with FDM and then in order to achieve better outer shell surface roughness milling was used.

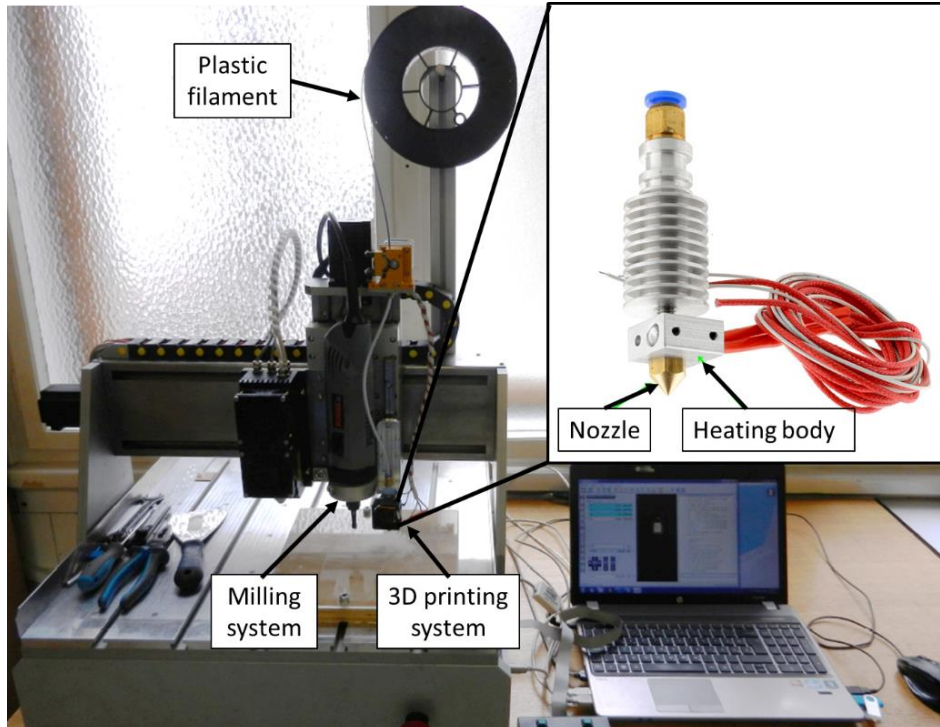


Figure 1: Hybrid manufacturing machine which includes 3D printing and milling systems [6].

### 3 Experimental approach and results

#### 3.1 Technological parameters in the hybrid manufacturing

Technological parameters of experiments, which were determined on the basis of experience and knowledge of hybrid manufacturing were:

- Spindle speed of milling tool  $n$  [ $\text{min}^{-1}$ ],
- Layer height  $h$  [mm],
- Material compensation flow  $\Phi$  [%]: the amount of material is multiplied by this value,
- Printing speed  $v$  [mm/s],
- Feed speed of milling tool  $v_f$  [mm/min],
- Milling depth  $a_p$  [mm].

For hybrid manufacturing two different nozzle sizes were used; standard ( $D = 0.4$  mm) and nonstandard ( $D = 1.1$  mm). The limit values (minimal and maximal values) of the technological parameters were determined on the basis of pilot experiments and by using the proposed values of a 3D printing computer program CURA.

#### 3.2 Design and execution of experiments

Because technological parameters for nozzle sizes  $D = 0.4$  mm and  $D = 1.1$  mm are different two separate experiment plans were created.

Each technological parameter was examined on three levels. As the level -1 minimum values of parameters were considered, and as the level +1 maximum values. Values of a mid-level 0 were get as the average between levels -1 and +1. Parameter values at each level for both nozzles are shown in the Tables 1 and 2.



Table 1: Values of technological parameters at each level for nozzle size  $D = 0.4$  mm.

		Technological parameters					
		$n$ [mm <sup>-1</sup> ]	$h$ [mm]	$\Phi$ [%]	$v$ [mm/s]	$v_f$ [mm/min]	$a_p$ [mm]
Level 1	-1	10000	0.10	55.0	15	200	0.10
Level 2	0	15500	0.20	67.5	40	400	0.20
Level 3	+1	21000	0.30	80.0	65	600	0.30

Table 2: Values of technological parameters at each level for nozzle size  $D = 1.1$  mm.

		Technological parameters					
		$n$ [min <sup>-1</sup> ]	$h$ [mm]	$\Phi$ [%]	$v$ [mm/s]	$v_f$ [mm/min]	$a_p$ [mm]
Level 1	-1	10000	0.30	60.0	10	200	0.41
Level 2	0	15500	0.55	70.0	25	400	0.55
Level 3	+1	21000	0.80	80.0	40	600	0.69

For design of experiments (DOE) with 6 technological parameters on three levels Taguchi orthogonal array  $L_{27}(3^{13})$  was applied and two different DOEs for both nozzle sizes were created. DOE for both nozzle sizes are presented in the next chapter 3.3- in Tables 4 and 6 (left of the bold line). Output parameters, which are listed down in Table 3, represent responses of hybrid manufacturing which were followed and measured.

Table 3: List of output parameters.

Output parameters	Unit	Parameter description
$Ra_h$	[ $\mu\text{m}$ ]	arithmic deviation profile in the direction perpendicularly to the loading material
$Ry_h$	[ $\mu\text{m}$ ]	maximal surface roughness in the direction perpendicularly to the loading material
$Ra_l$	[ $\mu\text{m}$ ]	arithmic deviation profile in the direction of loading material
$Ry_l$	[ $\mu\text{m}$ ]	maximal surface roughness in the direction of loading material
$MD$	[m]	material deposition - used material for FDM process in meters
$t$	[s]	time for hybrid manufacturing

### 3.3 Evaluation and analysis of results

In Tables 4 and 6 DOEs together with resulted measured values of output responses on hybrid manufacturing for both nozzle sizes  $D = 0.4$  mm and  $D = 1.1$  mm are given.

Those results were used for further analysis to study how technological parameters influence on the output responses and to obtain mathematical models for their final optimisation. Mathematical models were obtained and evaluated using a computer program Design-Expert. Program develops and analyzes regression (mathematical) models using analysis of variance (ANOVA).

Those acquired models have been evaluated (Tables 5 and 7) on the basis of F-value, coefficient of determination  $R^2$ , adjusted  $R^2$  (Adj -  $R^2$ ), predicted  $R^2$  (Pred -  $R^2$ ) and S/N ratio (*signal to noise ratio*).

Table 4: Design of experiments and results obtained using nozzle size  $D = 0.4$  mm.

	$n$ [ $\text{min}^{-1}$ ]	$h$ [mm]	$\Phi$ [%]	$v$ [mm/s]	$v_f$ [mm/min]	$a_p$ [mm]	$Ra_h$ [ $\mu\text{m}$ ]	$Ry_h$ [ $\mu\text{m}$ ]	$Ra_l$ [ $\mu\text{m}$ ]	$Ry_l$ [ $\mu\text{m}$ ]	$MD$ [m]	$t$ [s]
1	10000	0.10	55.0	15	200	0.10	5.69	47.35	4.97	44.15	1.02	8066
2	10000	0.10	67.5	40	400	0.20	5.05	42.40	6.57	48.02	1.21	7324
3	10000	0.10	80.0	65	600	0.30	5.86	45.63	6.62	50.40	1.48	7191
4	10000	0.20	55.0	40	400	0.30	3.89	45.11	5.85	47.16	1.02	3715
5	10000	0.20	67.5	65	600	0.10	2.43	22.18	4.19	37.27	1.24	3647
6	10000	0.20	80.0	15	200	0.20	5.55	40.55	5.71	43.97	1.48	4100
7	10000	0.30	55.0	65	600	0.20	1.93	25.18	2.39	23.58	1.01	2477
8	10000	0.30	67.5	15	200	0.30	5.82	41.24	6.28	44.95	1.24	2776
9	10000	0.30	80.0	40	400	0.10	4.71	50.47	5.50	38.99	1.48	2522
10	15500	0.10	55.0	40	600	0.20	5.45	48.25	5.68	46.61	1.02	7313
11	15500	0.10	67.5	65	200	0.30	3.53	27.65	4.05	29.91	1.24	7210
12	15500	0.10	80.0	15	400	0.10	5.33	45.29	5.80	41.53	1.48	8053
13	15500	0.20	55.0	65	200	0.10	7.96	82.49	5.62	48.47	1.02	3668
14	15500	0.20	67.5	15	400	0.20	5.68	45.58	5.47	41.10	1.24	4082
15	15500	0.20	80.0	40	600	0.30	6.06	46.26	6.69	52.11	1.48	3714
16	15500	0.30	55.0	15	400	0.30	6.13	50.70	6.62	47.77	1.01	2761
17	15500	0.30	67.5	40	600	0.10	5.29	42.10	5.54	45.38	1.24	2516
18	15500	0.30	80.0	65	200	0.20	5.37	41.39	5.30	40.88	1.48	2496
19	21000	0.10	55.0	65	400	0.30	5.29	42.82	5.71	44.66	1.02	7202
20	21000	0.10	67.5	15	600	0.10	6.71	48.43	6.33	45.22	1.24	8043
21	21000	0.10	80.0	40	200	0.20	2.88	26.48	2.67	19.78	148	7337
22	21000	0.20	55.0	15	600	0.20	6.20	48.38	5.76	45.69	1.02	4079
23	21000	0.20	67.5	40	200	0.30	5.37	52.67	5.58	47.86	1.24	3736
24	21000	0.20	80.0	65	400	0.10	5.14	47.09	5.44	43.72	1.48	3657
25	21000	0.30	55.0	40	200	0.10	6.56	70.75	5.61	49.68	1.01	2540
26	21000	0.30	67.5	65	400	0.20	6.26	52.78	5.52	48.43	1.23	2482
27	21000	0.30	80.0	15	600	0.30	6.27	47.76	6.93	53.11	1.48	2759

Table 5: Evaluation of regression models of hybrid manufacturing using nozzle size  $D = 0.4$  mm.

Output parameters	F-value	p-value	Regressor-influential parameter	$R^2$	Adj- $R^2$	Pred- $R^2$	S/N
			Atypical hierarchical parameter				
$Ra_h$	9.03	<0.0001	$n, n^*v_f, h^*v_f, \Phi^*v_f, n^2, h, \Phi, v_f$	0.801	0.712	0.5379	12.48
$Ry_h$	5.83	0.0011	*	0.811	0.672	0.164	10.88
$Ra_l$	8.99	<0.0001	$a_p, n^*v_f, h^*v_f, \Phi^*v_f, v_f^2, n, h, \Phi, v_f, n^*h$	0.849	0.755	0.597	12.28
$Ry_l$	12.27	<0.0001	$n, v_f, a_p, n^*h, n^*v_f, h^*v_f, \Phi^*v_f, v^2, h, \Phi, v, \phi^*v, h^2$	0.925	0.849	0.668	15.04
$MD$	39259.52	<0.0001	$\Phi$	0.999	0.999	0.999	343.19
$t$	3121.86	<0.0001	$h, v$	0.996	0.996	0.995	123.40

\*Note: useless model because Adj- $R^2$  and Pred- $R^2$  differ more than 0.2.

Table 6: Design of experiments and results obtained using nozzle size  $D = 1.1$  mm.

	$n$ [ $\text{min}^{-1}$ ]	$h$ [mm]	$\Phi$ [%]	$v$ [mm/s]	$v_f$ [mm/min]	$a_p$ [mm]	$Ra_h$ [ $\mu\text{m}$ ]	$Ry_h$ [ $\mu\text{m}$ ]	$Ra_l$ [ $\mu\text{m}$ ]	$Ry_l$ [ $\mu\text{m}$ ]	$MD$ [m]	$t$ [s]
1	10000	0.30	60.0	10	200	0.41	5.10	47.26	4.91	41.65	2.09	2330
2	10000	0.30	70.0	25	400	0.55	5.64	47.73	6.92	52.15	2.43	1977
3	10000	0.30	80.0	40	600	0.69	4.83	45.01	5.82	45.32	2.78	1901
4	10000	0.55	60.0	25	400	0.69	4.81	49.14	6.26	50.37	2.05	1102
5	10000	0.55	70.0	40	600	0.41	9.19	114.12	4.33	43.31	2.39	1061
6	10000	0.55	80.0	10	200	0.55	16.08	162.03	10.90	73.92	2.73	1312
7	10000	0.80	60.0	40	600	0.55	1.18	8.44	3.75	27.50	2.04	721
8	10000	0.80	70.0	10	200	0.69	2.24	17.52	3.64	24.02	2.38	900
9	10000	0.80	80.0	25	400	0.41	2.57	18.40	3.57	21.06	2.72	763
10	15500	0.30	60.0	25	600	0.55	4.30	33.67	4.43	33.19	2.09	1973
11	15500	0.30	70.0	40	200	0.69	24.75	198.15	9.61	75.19	2.43	1921
12	15500	0.30	80.0	10	400	0.41	7.47	61.69	8.65	57.98	2.78	2319
13	15500	0.55	60.0	40	200	0.41	14.65	171.67	5.64	40.99	2.05	1079
14	15500	0.55	70.0	10	400	0.55	7.56	55.75	8.94	60.33	2.39	1293
15	15500	0.55	80.0	25	600	0.69	9.07	120.38	6.09	54.23	2.73	1103
16	15500	0.80	60.0	10	400	0.69	2.97	26.14	5.25	38.50	2.04	882
17	15500	0.80	70.0	25	600	0.41	3.64	31.49	4.07	34.31	2.38	752
18	15500	0.80	80.0	40	200	0.55	8.98	65.07	8.11	60.07	2.72	752
19	21000	0.30	60.0	40	400	0.69	10.63	158.18	6.20	42.14	2.09	1907
20	21000	0.30	70.0	10	600	0.41	7.76	56.27	6.78	48.55	2.43	2311
21	21000	0.30	80.0	25	200	0.55	8.09	55.75	9.48	68.24	2.78	1989
22	21000	0.55	60.0	10	600	0.55	5.73	42.42	7.87	53.77	2.05	1282
23	21000	0.55	70.0	25	200	0.69	25.00	154.25	11.12	95.37	2.39	1121
24	21000	0.55	80.0	40	400	0.41	6.30	54.83	6.22	49.46	2.73	1068
25	21000	0.80	60.0	25	200	0.41	9.60	98.97	8.04	61.24	2.04	771
26	21000	0.80	70.0	40	400	0.55	3.40	43.69	7.06	48.81	2.38	730
27	21000	0.80	80.0	10	600	0.69	6.82	51.13	5.39	42.63	2.72	888

Table 7: Evaluation of regression models of hybrid manufacturing using nozzle size  $D = 1.1$  mm.

Output parameters	F-value	p-value	Regressor-influential parameter	$R^2$	Adj- $R^2$	Pred- $R^2$	S/N
			Atypical hierarchical parameter				
$Ra_h$	7.97	0.0002	$h, v_f, v^*v_f, h^2, v$	0.705	0.617	0.427	10.90
$Ry_h$	5.90	0.0012	*	0.835	0.693	0.344	9.95
$Ra_l$	12.50	<0.0001	$n, \Phi, v_f, v^*a_p, h^2, a_p^2, h, v$	0.902	0.830	0.669	12.11
$Ry_l$	14.40	<0.0001	$n, \Phi, v_f, a_p, n^*h, n^*v, \Phi^*v_f, v^*a_p, v_f^*a_p, h^2, h, v$	0.935	0.870	0.673	15.68
$MD$	246000	<0.0001	$h, \Phi, h^*\Phi, h^2, \Phi^2$	1.000	1.000	1.000	1190.27
$t$	1157.56	<0.0001	$h, v$	0.990	0.989	0.987	80.32

\*Note: useless model because Adj- $R^2$  and Pred- $R^2$  differ more than 0.2.

### 3.4 Regression models and their interpretation

In the following chapters regression models for both nozzle sizes are presented. After interpretation of equations the effects the technological parameters on output responses are given.

*Regression model for roughness  $Ra_h$ :*

$$\begin{aligned} \text{Nozzle size } D = 0.4 \text{ mm} &\rightarrow Ra_h \\ &= 12.07961 + 3.2641 \cdot 10^{-4} \cdot n + 18.38333 \cdot h - 0.15542 \cdot \phi - 0.030158 \cdot v_f \\ &\quad + 8.49242 \cdot 10^{-7} \cdot n \cdot v_f - 0.042417 \cdot h \cdot v_f + 3.67 \cdot 10^{-4} \cdot \phi \cdot v_f - 1.83104 \cdot 10^{-8} \cdot n^2 \end{aligned}$$

$$\begin{aligned} \text{Nozzle size } D = 1.1 \text{ mm} &\rightarrow \ln(Ra_h) \\ &= 0.54592 + 8.93868 \cdot h + 0.056732 \cdot v - 5.08715 \cdot 10^{-3} \cdot v_f - 1.28640 \cdot 10^{-4} \cdot v \cdot v_f \\ &\quad - 9.38239 \cdot h^2 + 8.21082 \cdot 10^{-6} \cdot v_f^2 \end{aligned}$$

Main influence on surface roughness for both nozzle sizes has layer height  $h$ . The minimal roughness  $Ra_h$  can be achieved with higher layers which allows creating products with more or less thick layers. That leads to less passages or gaps in between layers, which might be detected with tip of the stylus of measuring device for roughness. From Figures 2 and 3 by highest layer printing, printing speed  $v$  has no influence on surface roughness while feed speed of milling tool  $v_f$  is very influential. For minimal roughness maximal feed speed is optimal, otherwise in slow feeds milling tool cause material overheating, which leads to material winding on the tool.

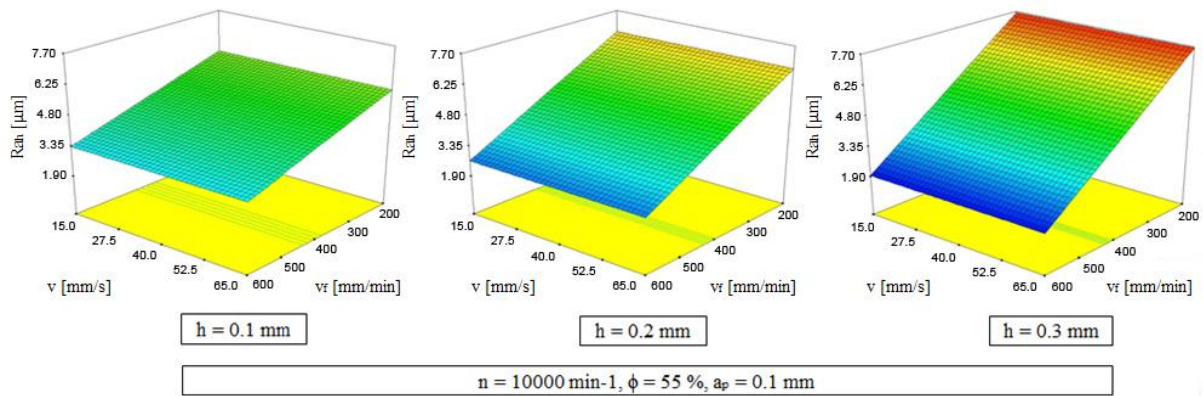


Figure 2: Influence of printing speed  $v$  and feed speed of milling tool  $v_f$  on surface roughness  $Ra_h$  by different layer heights  $h$  using nozzle size  $D = 0.4$  mm.

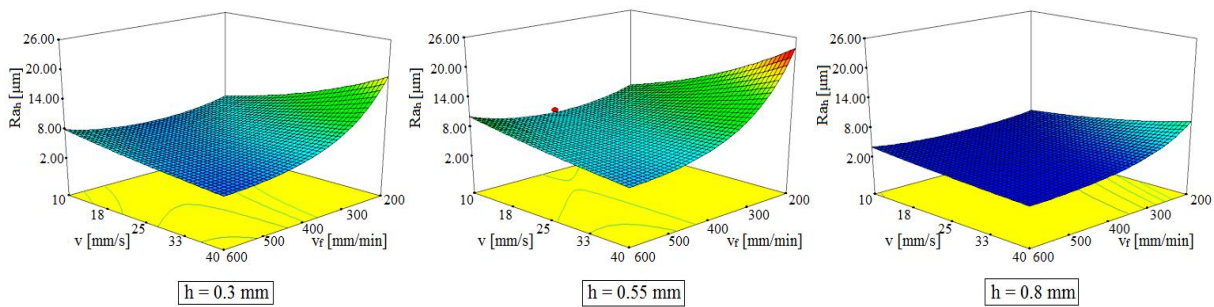


Figure 3: Influence of printing speed  $v$  and feed speed of milling tool  $v_f$  on surface roughness  $Ra_h$  by different layer heights  $h$  using nozzle size  $D = 1.1$  mm.

*Regression model for roughness  $Ra_l$ :*

$$\begin{aligned} \text{Nozzle size } D = 0.4 \text{ mm} &\rightarrow Ra_l \\ &= 10.85149 - 3.71616 \cdot 10^{-4} \cdot n + 7.16414 \cdot h - 0.082622 \cdot \phi - 7.27924 \cdot 10^{-3} \cdot v_f \\ &\quad + 2.96111 \cdot a_p + 5.80808 \cdot 10^{-4} \cdot n \cdot h + 6.75758 \cdot 10^{-7} \cdot n \cdot v_f - 0.038625 \cdot h \cdot v_f \\ &\quad + 2.33778 \cdot 10^{-4} \cdot \phi \cdot v_f - 1.25556 \cdot 10^{-5} \cdot v_f^2 \end{aligned}$$

Nozzle size  $D = 1.1\text{mm} \rightarrow Ra_l$

$$\begin{aligned}
 &= -28.06072 + 3.78833 \cdot 10^{-4} \cdot n + 49.56052 \cdot h + 0.18399 \cdot \Phi - 0.26487 \cdot v \\
 &- 7.98704 \cdot 10^{-3} \cdot v_f + 58.95257 \cdot a_p - 7.85634 \cdot 10^{-6} \cdot n \cdot v - 0.21452 \cdot h \cdot \Phi \\
 &+ 0.66534 \cdot v \cdot a_p - 31.67556 \cdot h^2 - 66.12812 \cdot a_p^2
 \end{aligned}$$

Conclusions obtained by previous regression model can be also applied by the model of surface roughness in the direction of loading material  $Ra_l$ . To achieve minimal roughness, value of spindle speed of milling tool  $n$  must be low as show in Figure 4 for the case of nozzle size  $D = 1.1$  mm. Higher values cause material overheating and similar problems with material winding as found by interpretation of feed speed  $v_f$  by previous regression model. By highest value of layer  $h$  minimal surface roughness  $Ra_l$  can be achieved using minimal material compensation flow  $\Phi$  (Figures 5 and 6).

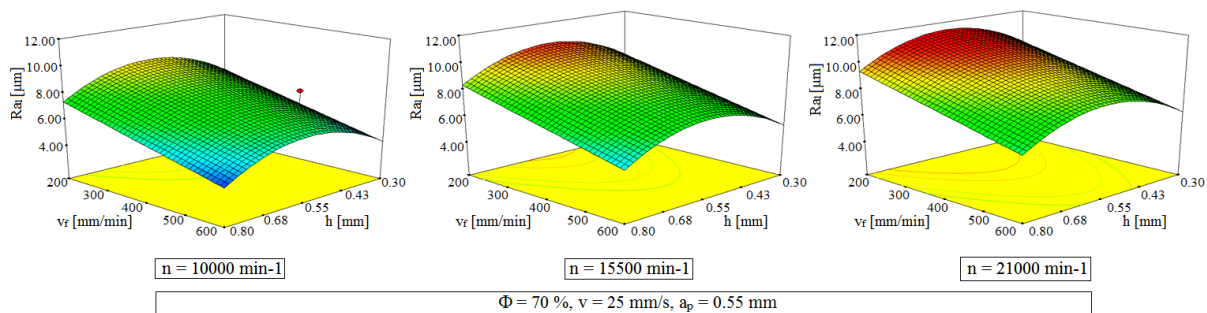


Figure 4: Influence of feed speed of milling tool  $v_f$  and layer height  $h$  on surface roughness  $Ra_l$  by different spindle speed of milling tool  $n$  using nozzle size  $D = 1.1$  mm.

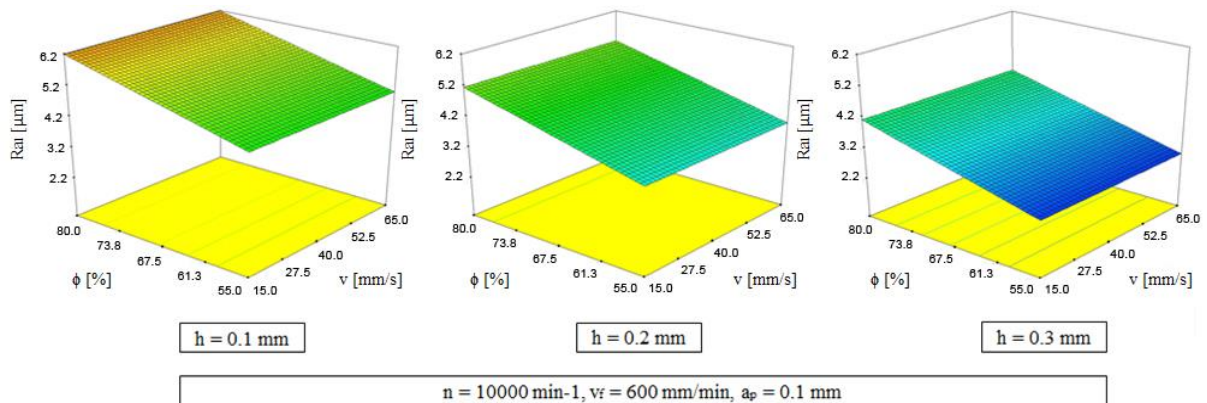


Figure 5: Influence of material compensation flow  $\Phi$  and printing speed  $v$  on surface roughness  $Ra_l$  by different layer heights  $h$  using nozzle size  $D = 0.4$  mm.

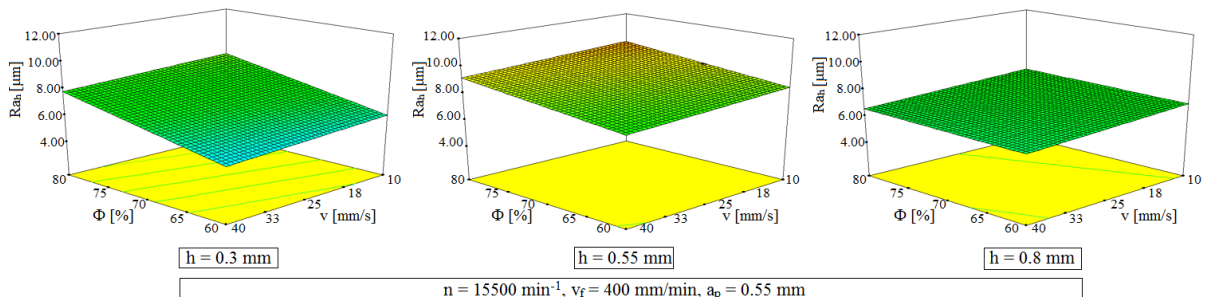


Figure 6: Influence of material compensation flow  $\Phi$  and printing speed  $v$  on surface roughness  $Ra_l$  by different layer heights  $h$  using nozzle size  $D = 1.1$  mm.

Regression model for roughness  $Ry_l$ :

Nozzle size  $D = 0.4 \text{ mm} \rightarrow Ry_l^{2.68}$

$$= 71475.11377 - 3.97046 \cdot n + 86279.98635 \cdot h - 613.28730 \cdot \phi + 1212.98635 \cdot v$$

$$- 158.1637 \cdot v_f + 22158.41371 \cdot a_p + 10.87269 \cdot n \cdot h + 5.37597 \cdot 10^{-3} \cdot n \cdot v_f$$

$$- 295.27319 \cdot h \cdot v_f - 6.99385 \cdot \phi \cdot v + 2.15472 \cdot \phi \cdot v_f - 3.08891 \cdot 10^{-5} \cdot h^2 - 8.9001$$

$$\cdot v^2$$

Nozzle size  $D = 1.1 \text{ mm} \rightarrow Ry_l$

$$= -129.23439 - 7.37746 \cdot 10^{-4} \cdot n + 265.11886 \cdot h + 2.13655 \cdot \Phi - 1.19240 \cdot v$$

$$+ 0.22008 \cdot v_f - 3.26786 \cdot a_p + 7.46030 \cdot 10^{-3} \cdot n \cdot h - 8.17239 \cdot 10^{-5} \cdot n \cdot v$$

$$- 1.26044 \cdot h \cdot \Phi - 2.44771 \cdot 10^{-3} \cdot \Phi \cdot v_f + 4.41349 \cdot v \cdot a_p - 0.19900 \cdot v_f \cdot a_p$$

$$- 270.54667 \cdot h^2$$

Applying previous conclusions and analysing diagrams in Figures 7 and 8 minimal roughness  $Ry_l$  can be achieved using minimal (level -1) to middle (level 0) values of milling depth  $a_p$ .

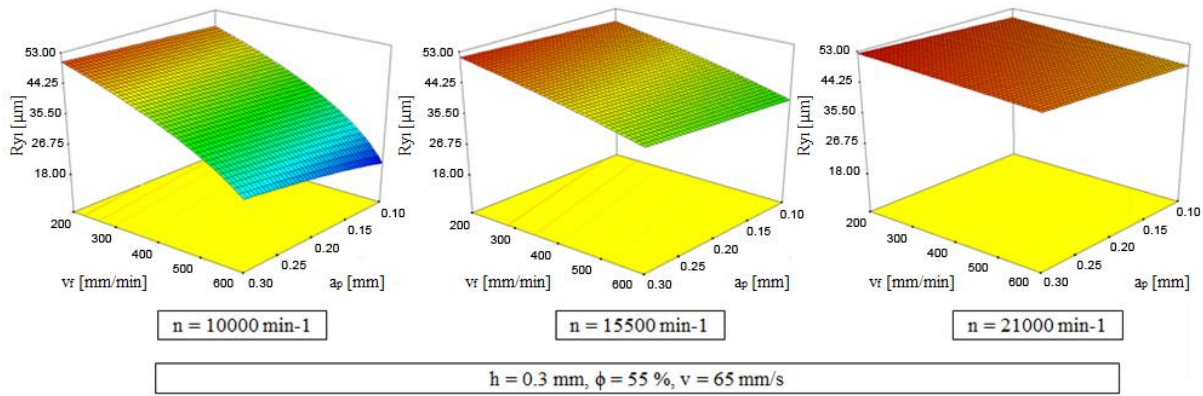


Figure 7: Influence of feed speed of milling tool  $v_f$  and milling depth  $a_p$  on surface roughness  $Ry_l$  by different spindle speed of milling tool  $n$  using nozzle size  $D = 0.4 \text{ mm}$ .

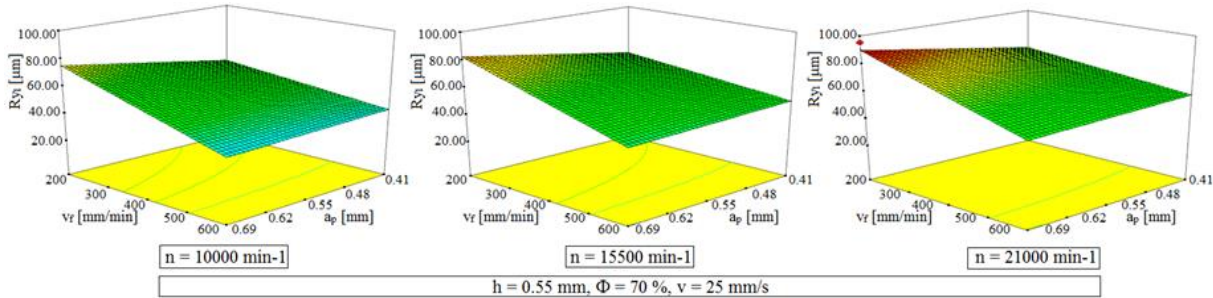


Figure 8: Influence of feed speed of milling tool  $v_f$  and milling depth  $a_p$  on surface roughness  $Ry_l$  by different spindle speed of milling tool  $n$  using nozzle size  $D = 1.1 \text{ mm}$ .

Regression model for material deposition  $MD$ :

Nozzle size  $D = 0.4 \text{ mm} \rightarrow \sqrt{MD} = 0.54968 + 8.32623 \cdot 10^{-3} \cdot \phi$

Nozzle size  $D = 1.1 \text{ mm} \rightarrow \ln(MD)$

$$= -0.53217 - 0.18252 \cdot h + 0.027546 \cdot \Phi + 2.39521 \cdot 10^{-4} \cdot h \cdot \Phi + 0.11018 \cdot h^2$$

$$- 9.53869 \cdot 10^{-5} \cdot \phi^2$$

As can be observed from equations above the main influence on material deposition  $MD$  has material compensation flow  $\Phi$ . More material flow cause more material consumption. And if the minimal material flow is used the layer height  $h$  has no big influence on material deposition. That shows graph below in Figure 9.

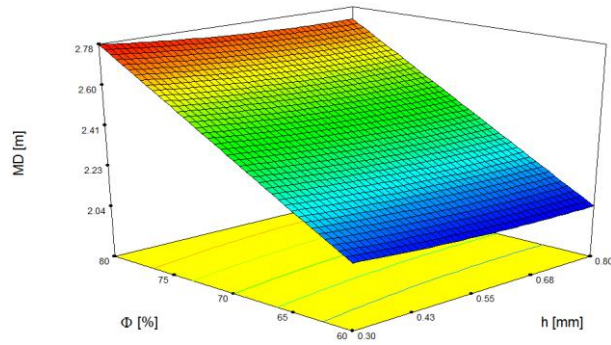


Figure 9: Influence of layer height  $h$  and material compensation flow  $\Phi$  on material deposition  $MD$  using nozzle size  $D = 1.1$  mm.

Regression model for time for hybrid manufacturing  $t$ :

$$\text{Nozzle size } D = 0.4 \text{ mm} \rightarrow \frac{1}{t} = -1.488 \cdot 10^{-5} + 1.2647 \cdot 10^{-3} \cdot h + 5.61659 \cdot 10^{-7} \cdot v$$

$$\text{Nozzle size } D = 1.1 \text{ mm} \rightarrow \frac{1}{\sqrt{t}} = 0.011849 + 0.027023 \cdot h + 9.22941 \cdot 10^{-5} \cdot v$$

Biggest influence on time for hybrid manufacturing  $t$  has layer height  $h$ . Higher layer means shorter production time and at the same time with higher layer minimal surface roughness can be achieved. This statement confirms previous conclusions. Printing speed  $v$  at maximal layer height has not big influence on time for hybrid manufacturing.

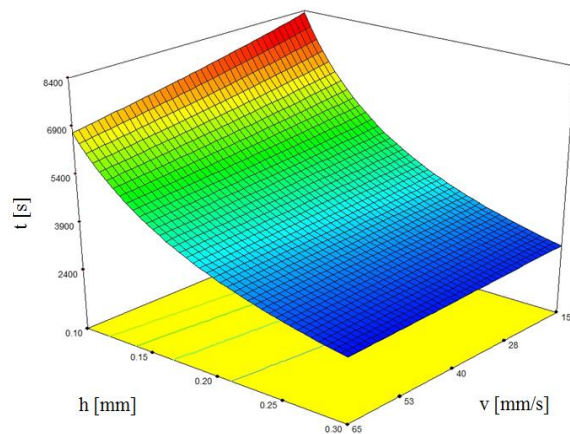


Figure 10: Influence of layer height  $h$  and printing speed  $v$  on time for hybrid manufacturing  $t$  using nozzle size  $D = 0.4$  mm.

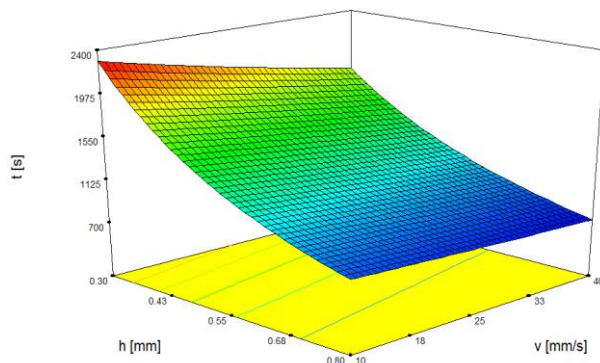


Figure 11: Influence of layer height  $h$  and printing speed  $v$  on time for hybrid manufacturing  $t$  using nozzle size  $D = 1.1$  mm.

### 3.5 Optimization of parameters in the hybrid manufacturing

Derived regression models were used for optimization of hybrid manufacturing according to three criteria: the minimal surface roughness  $Ra$  and  $Ry$  (in both directions), minimal material deposition  $MD$  and shortest production time  $t$ . Optimal technological parameters for both nozzle sizes are shown in Table 8.

Table 8: Optimal technological parameters for both nozzle sizes.

	Nozzle size	
	0.4 mm	1.1 mm
$n$ [ $\text{mm}^{-1}$ ]	10000	10000
$h$ [mm]	0.3	0.8
$\Phi$ [%]	55	60
$v$ [mm/s]	65	40
$v_f$ [mm/min]	600	600
$a_p$ [mm]	0.1	0.46

Depending on the optimization requirements optimal technological parameters are coincide with the conclusions obtained with interpretation of regression models. Nevertheless, obtained optimal parameters were checked with the confirmation test (Tables 9 and 10). As shown in tables results of output parameters measured after confirmation test matches with optimization predicted values by both nozzle sizes.

Table 9: Results of confirmation test obtained with nozzle size  $D = 0.4$  mm.

	With optimization predicted values	After confirmation test measured values
$Ra_n$ [ $\mu\text{m}$ ]	1.96	2.05
$Ry_n$ [ $\mu\text{m}$ ]	useless model	not measured
$Ra_t$ [ $\mu\text{m}$ ]	2.71	2.74
$Ry_t$ [ $\mu\text{m}$ ]	18.56	19.24
$MD$ [m]	1.02	1.01
$t$ [s]	2494	2496

Table 10: Results of confirmation test obtained with nozzle size  $D = 1.1$  mm.

	With optimization predicted values	After confirmation test measured values
$Ra_n$ [ $\mu\text{m}$ ]	2.18	2.16
$Ry_n$ [ $\mu\text{m}$ ]	useless model	not measured
$Ra_t$ [ $\mu\text{m}$ ]	2.69	2.60
$Ry_t$ [ $\mu\text{m}$ ]	18.05	18.18
$MD$ [m]	2.04	2.04
$t$ [s]	724	723

#### Comparison of optimal technological parameters obtained with two different nozzle sizes:

If comparing optimal technological parameters for nozzle sizes  $D = 0.4$  mm and  $D = 1.1$  mm the same conclusions can be applied for both of them. To achieve optimization set conditions maximal layer height  $h$ , maximal printing speed  $v$ , minimal material compensation flow  $\Phi$ , minimal spindle speed of milling tool  $n$ , maximal feed speed of milling tool  $v_f$  and milling depth  $a_p$  from minimal (level -1) to middle (level 0) should be selected.

Measured values of output parameters in confirmation tests do not differ too much from values obtained by model predictions for both nozzle sizes. In terms of minimal surface roughness, it is not important what nozzle size is used. Difference in material consumption is here not so important because of affordable material. But when the time for hybrid manufacturing is important then it is better to use bigger nozzle size  $D = 1.1$  mm which allows shortening time for factor 3.



## 4 Conclusions

A statistical approach has been applied to investigate the influence of the technological parameters on the surface roughness, material deposition and time for hybrid manufacturing.

Based on the analysis of regression models, the optimal spindle speed of the milling tool  $n$ , layer height  $h$ , material compensation flow  $\Phi$ , printing speed  $v$ , feed speed of the milling tool  $v_f$  and milling depth  $a_p$  have been identified. Conclusions obtained with optimal results by both nozzle sizes can be interpreted in the same manner:

**1. Surface roughness after hybrid manufacturing:** main influence on roughness has layer height  $h$ . By the highest layer minimal roughness ( $Ra$  and  $Ry$ ) can be achieved in both measurement directions. At this layer height material compensation flow  $\Phi$  has no influence on roughness. High spindle speed  $n$  of the milling tool can cause material winding on the milling tool so the optimal value of this parameter is selected as minimal. Feed speed of the milling tool  $v_f$  effects on roughness inversely proportional. Milling depth  $a_p$  is optimal between the values of level -1 and level 0.

**2. Material deposition in the hybrid manufacturing:** main influence on material deposition  $MD$  has material compensation flow  $\Phi$  which affects proportionally.

**3. Time for hybrid manufacturing:** influence on time needed for hybrid manufacturing  $t$  have layer height  $h$  and printing speed  $v$ . The fastest printing and higher layer is applied, the shortest hybrid manufacturing time is needed.

**Main conclusion:** using a bigger nozzle size ( $D = 1.1$  mm) same final surface roughness as with smaller (standard) nozzle size can be achieved but in much shorter (three times shorter) time.

## References

- [1] Y. – Ak. Song, S. Park, D. Choi, H. Jee: 3D welding and milling: Part I – a direct approach for freeform fabrication of metallic prototypes. International Journal of Machine Tools & Manufacture, Vol. 45, pp 1057 – 1062, 2005.
- [2] Y. – Ak. Song, S. Park, D. Choi, S. – W. Chae: 3D welding and milling: Part II – optimization of the 3D welding process using an experimental design approach. International Journal of Machine Tools & Manufacture, Vol. 45, pp 1063 – 1069, 2005.
- [3] K. Boivie, D. Homar, S. Dolinšek, V. Broetan: The hybrid manufacturing cell : an integrated solution for additive manufacturing with CNC machining. 4th International Conference on Additive Technologies iCAT2012, Maribor, Slovenia, pp 1-15, 2012.
- [4] D. Grguraš: Preparation of the CNC-code and optimization of the technological parameters in the hybrid manufacturing (in Slovenian). Master thesis, Faculty of Mechanical Engineering, Ljubljana, 2015.
- [5] Ž. Kozan: Optimization of the technological parameters in hybrid manufacturing (in Slovenian). Diploma thesis, Faculty of Mechanical Engineering, Ljubljana, 2016.
- [6] A schematic of the FDM process. Available at: <http://reprap.org/mediawiki/images/thumb/2/22/FFF.png/400px-FFF.png>, viewed: 2.6.2015.

# Comparison of stereolithography in two modes of illumination with DLP technology

A. Zupan, J. Valentinčič<sup>1</sup>, A. Lebar<sup>1</sup>, M. Jerman<sup>1</sup>

<sup>1</sup> *University of Ljubljana, Slovenia*

## Abstract

The following paper focuses on the field of additive technology, called stereolithography. Specifically it focuses on the use of DLP technology in illuminating a medium. The medium is a photopolymer or resin, which hardens when exposed to a specific wavelength of light. The technology is used to generate 3D object. We used a non-commercial 3D printer to study two methods of illuminating the photopolymer using the DLP technology. The first method concentrates on the illumination of the bottom of the vat called constrained-surface method, the second one is called free-surface method and the illumination takes place on the surface of the photopolymer. Both times, photopolymerization takes place on the exposed section. We compared both methods of illumination based on the measurements of the test products. We concluded that products created by illuminating the bottom of the vat are both dimensionally and visually superior.

**Keywords:** stereolithography, DLP technology, constrained-surface method, free-surface method.

## 1 Introduction

Additive Manufacturing (AM) is a new manufacturing technology that fabricates complex three-dimensional objects by adding materials layer upon layer [1]. Stereolithography (SLA) is one of the most important additive manufacturing. Stereolithographic processes transform a multifunctional prepolymer into a crosslinked polymer through a chain reaction initiated by reactive species (free radicals or ions) generated by light exposure [2]. The medium is called resin. The differences between the free-surface and constrained-surface based techniques are in the build orientation and method of polymer curing. In top-down or free-surface SLA process a pattern is fabricated by solidifying a thin layer of liquid resin at the free surface of the liquid using a computer controlled laser beam or a digital light projector. The layer of resin exposed to light is cured to a predetermined pattern and adheres to the platform. After a layer is cured, the platform is moved down in small increment and the liquid surface is again exposed to light and the next layer is cured. This process is repeated until the entire solid object is fabricated in a layer-by-layer fashion. In the bottom-up or constrained-surface SLA process, the light is projected from bottom allowing a thin layer of liquid in the small gap between the platform and vat to be cured. The platform along with the solidified layer (which is attached to the platform) is then pulled up some distance causing the liquid resin to smoothly flow into the gap. The platform with the attached solidified layer then moves down leaving only a thin layer of liquid between the solidified layer and the vat underneath. The thin layer of liquid is then cured and the process continues until the entire solid object is built [1].

In this paper, comparison of constrained and free-surface stereolithography process using digital light projector (DLP) is presented.

## 2 Prototype 3D DLP printer

For our research we used free-surface prototype 3D DLP printer (Figure 1). The printer was not operational entirely.

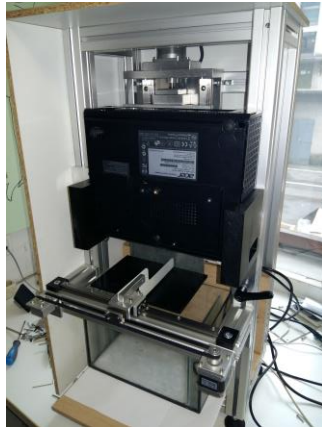


Figure 1: 3D DPL printer.

We design new components such as vat, printing table and blade for free-surface stereolithography. For constrained-surface method, we had to design entire new table for projector, table for vat, vat and printing table. Modified printer is presented on Figure 2, with both methods of illuminating the medium. To make a good comparison of methods we design a test specimen (Figure 3) and made a physically and visually comparison.

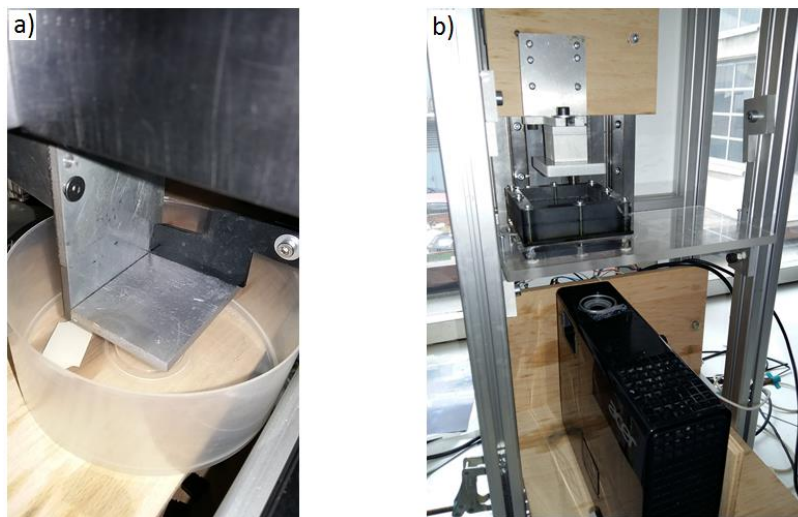


Figure 2: a) Free-surface method; b) Constrained-surface method.

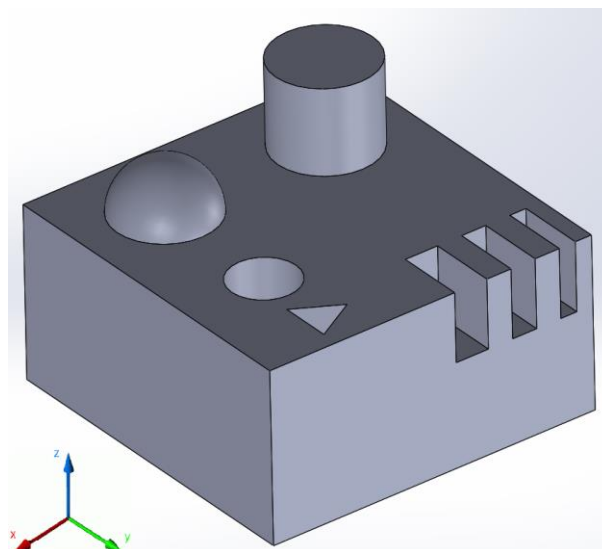


Figure 3: Test specimen.

### 3 Resin and printing parameters

We used resin of Netherlands producer FunToDo, Deep Black. According to producer, resin is suitable for both printing methods. With experiments we determined parameters using testing method. In Table 1 parameters for both methods are presented. In first trial run we used the same parameters at free surface as we used in constrain surface method. After that, we determined more appropriate parameters for free surface method. For comparison we printed five specimens for each series.

Table 1: Used parameters for printing.

Parameters	Constrained-surface	Free-surface	Free-surface
Bottom exposure (ms)	3500	3500	5500
Exposure time (ms)	2500	2500	5500
Total time(s)	2071	2071	2970
Z lift distance (mm)	6	3	3
Layer thickness (µm)	50	50	50
Lift and sequence time (ms)	4400	4400	4400
Z retract speed (mm/min)	200	200	200

### 4 Results

Result can be seen on Figure 4, that specimen of series 2 is completely inappropriate, assessed only by visually examination. But despite that fact, we made exact evaluation using measuring tools. The results are presented with diagrams including average series values with standard deviations. Figure 5 and Figure 6 present dimensions in x and y direction. From the diagrams it can be said that constrained-surface method bring much better results. As the measured average is close to dimensions 3D model, also standard deviation is much smaller at mentioned method. We noticed one important characteristic. Features such as valve, cupola have undersize dimensions, while hole has oversize dimensions.

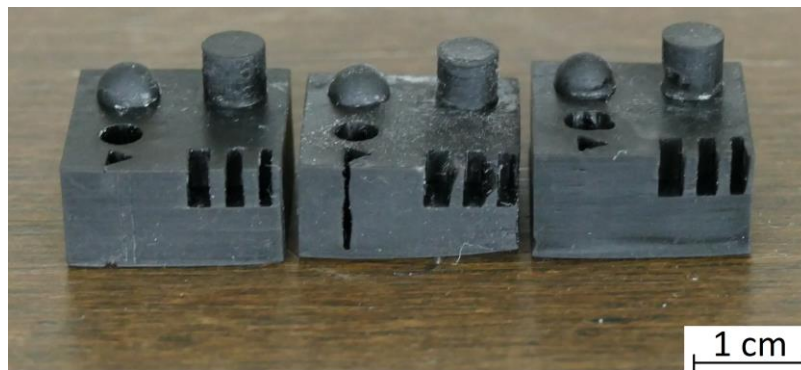


Figure 4: First test specimen from all series.

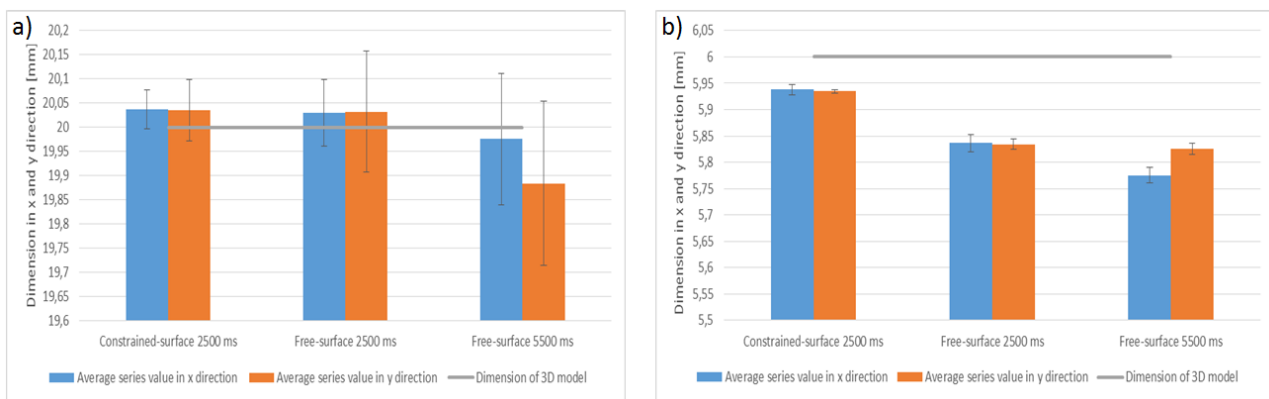


Figure 5: a) Outside dimensions; b) Cupola.

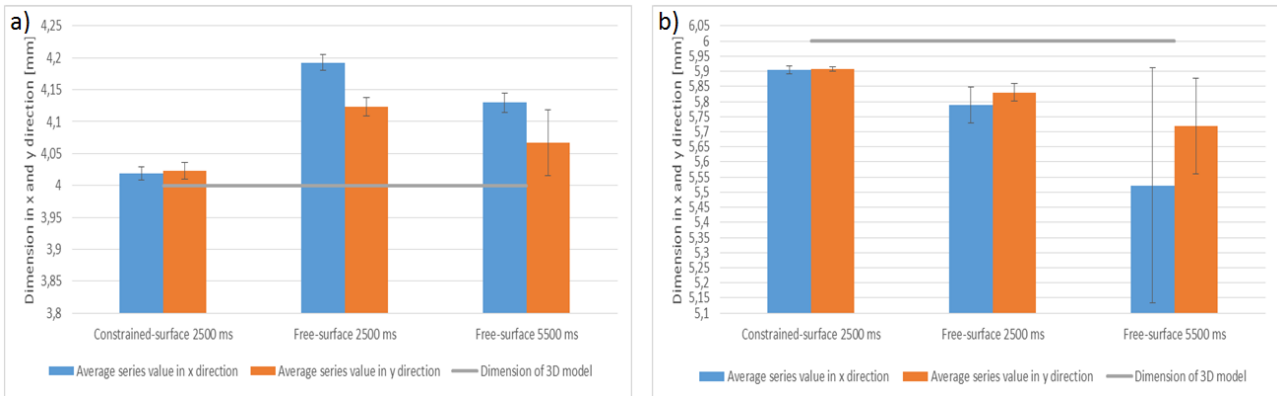


Figure 6: a) Hole; b) Valve.

Dimensions in z direction are presented in Figure 7. Figure 7 presents the height of basic cube. It is clearly that constrained-surface method is better also to achieve excellent and accurate results in vertical direction. Average measurement of specimens made with constrained-surface method is 0,01 mm smaller than dimension of 3D model. Also range of standard deviation is small. Adjustment of printer is easier at constrained-surface method.

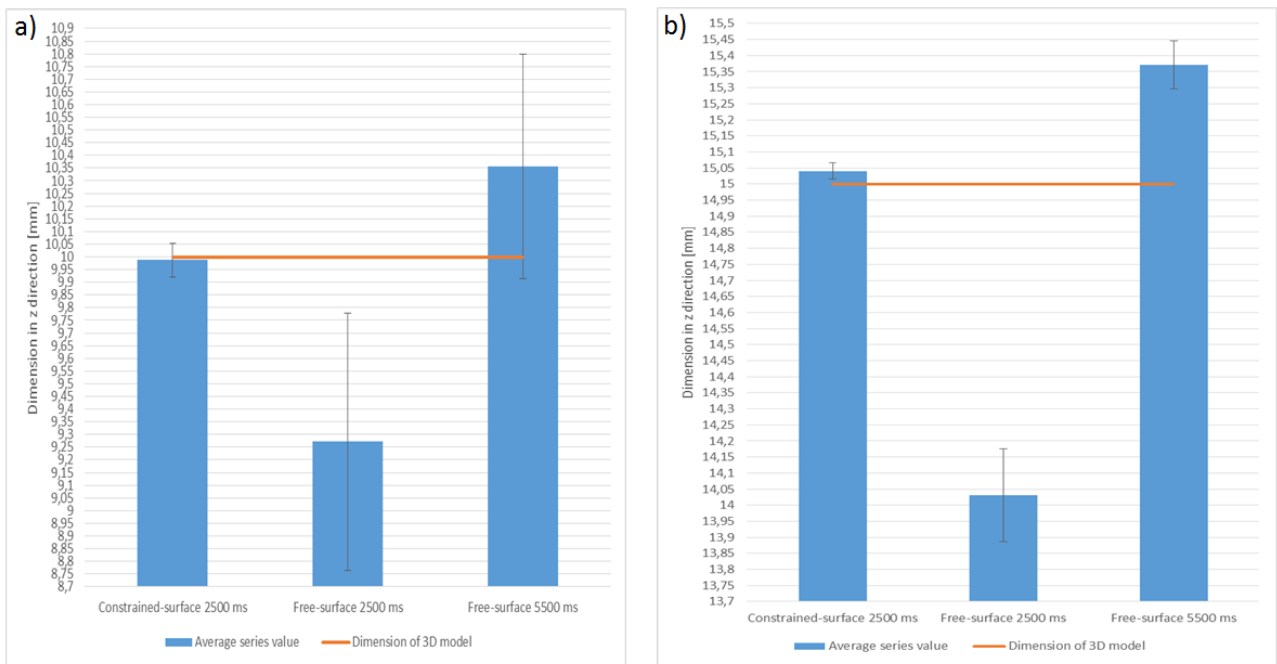


Figure 7: a) Height of basic cube; b) Height of entire specimens.

## 5 Conclusions

Constrained-surface method is more appropriate. Test specimens made by this method are dimensional more accurate. Repeatability using this method is better. Exposure time is smaller comparing to free-surface method. Also smaller amount of resin is needed for constrained-surface method. From that perspective is economically more suitable choice. Similar opinion was noticed in stated article [1].

## References

- [1] F. Liravi, S. Das, in C. Zhou: Separation force analysis and prediction based on cohesive element model for constrained-surface Stereolithography processes. *Comput.-Aided Des.*, let. 69, str. 134–142, Dec. 2015.
- [2] P. J. Bártolo: *Stereolithography: Materials, Processes and Applications*. Springer Science & Business Media, 2011.